POLITECNICO DI TORINO

Master of Science in Aerospace and Astronautic Engineering

Thesis

HIGH LIFT SYSTEMS FOR PLANETARY DESCENT AND LANDING

with

Jet Propulsion Laboratory
California Institute of Technology

Candidate
Jasmine Rimani
Politecnico di Torino

Academic Supervisor
Prof. Dr. Nicole Viola
Politecnico di Torino

Mentor
Dr. Marco B. Quadrelli
Jet Propulsion Laboratory, California Institute of Technology

October 2018

This research was carried out at the Jet Propulsion Laboratory, California Institute of Technology, and was sponsored by JVSRP (JPL Visiting Student Research Program) and the National Aeronautics and Space Administration.

TABLE OF CONTENTS

LIST OF FIGURES

LIST OF TABLES

LIST OF ABBREVIATIONS

AGU	Airborne Guidance Unit
AR	Aspect Ratio
CFD	Computational Fluid Dynamics
CG	Center of Gravity
CONOPs	Concept of Operations
DOF	Degree of Freedom
GNC	Guidance, Navigation and Control
GPS	Global Positioning System
IMU	Inertial Measurement Unit
INS	Inertial Navigation System
JPL	Jet Propulsion Laboratory
PADs	Precision Aerial Delivery System
PID	Proportional-Integral-Derivative
Sys	System
TE	Trailing Edge
TRN	Terrain Relative Navigation

ACKNOWLEDGEMENTS

The work presented in this thesis was developed at the Jet Propulsion Laboratory, California Institute of Technology, under the JVSRP (JPL Visiting Student Research Program) program.

I would like to thank my mentor at JPL, Dr. Marco B. Quadrelli, who guided me throughout all my study and taught me how to organize and write about scientific research.

A special thanks goes to my academic supervisor, Prof. Dr. Nicole Viola, for her strong support during this last university year and her useful advices.

I am grateful to all of those that I have meet in those months, for their aid and for all the beautiful experiences that made great this journey.

I want to express my profound gratitude to my parents, who encouraged me and helped me from far away.

ABSTRACT

In this thesis, I present a summary of the work performed in five months at the JPL (Jet Propulsion Laboratory) on the dynamics of autonomous parafoils and other autonomous flight solutions.

The growing interest in our solar system icy moons is pushing towards innovative solutions for planetary exploration that can enable missions towards difficult targets on this alien satellites. From this point of view, the analysis of high-efficiency gliding systems (i.e., high lift over drag systems) can identify new and more efficient solutions for terminal descent. The present work follows this trend by studying the advantages of a parafoil for autonomous precision delivery of a probe in the Titan environment.

The previous successful mission to Titan, the Huygens probe, used a series of drag-only parachutes to drop the payload (low lift to drag parachute). However, this solution provides a limited maneuverability to negotiate the not well-known environmental conditions (air density and winds) and the possibility of targeting different landing sites of scientific interest, shaping the trajectory accordingly. With a ram-air system (a parafoil) one can fly over different interesting sites, map them ahead of time, and even allow the re-planning of the trajectory to land near the most desirable sites.

To analyze all these possibilities, dynamics models of the PADs (Precision Aerial Delivery System), with different degrees of freedom, had to be developed and tested. Three degree-of-freedom models focused on the trajectory development. Six degree-of-freedom models were needed to evaluate the parafoil-payload system overall behavior. Seven to nine degree-of-freedom models were needed to determine the payload-canopy interaction. These models were tested in the relevant environmental conditions on Titan, from the aerodynamics to the wind effect to a noisy sensor reading. As a consequence, the performance of the system trying to follow a trajectory in the uncertain atmosphere was evaluated.

To realize these tasks, we relied on the methodologies derived from dynamics system modelling for the related equations of motion, from the aerodynamics to investigate the effect of the forces that enable the descent on Titan, from the GN&C (Guidance, Navigation and Control) to determine the requirements posed by autonomy. Consequently, the aim of this work was to provide a system modeling and simulation framework to ultimately allow the development of a complete GN&C system that will lead to a feasible system design, and which advantages these high lift solutions can bring to future missions to Titan.

1 INTRODUCTION

In the last decade the interest in oceans world as Titan, Enceladus and Europa has grown due to the possibilities of outstanding scientific discoveries in different disciplines: from geology to meteorology and, maybe, even biology. This enthusiasm brought up different projects and proposals on disparate CONOPs (Concept of Operations). Riding this wave, the five months that I spent at JPL where focused on the development, verification and modelling of the dynamics of Titan high-lift delivery systems. Following this trend, we developed models of parafoil, hang-glider and a wingsuit to understand their capabilities in other atmospheres different from the known Earth one.

The beginning point of every project is the compliance with some high-level requirements that will shape the project path to follow. In our case we can design our framework based on the Titan parafoil proposal (on-going work).

- Starting conditions:
  - ❖ Starting altitude of 40 km over land. The target altitude and longitude are still to be decided. The polar regions can give access to some interesting hydrocarbon lakes. Moreover, the equatorial lands are characterized by hydrocarbon sand-like dunes. Both sites can be of interest, however the systems presented in this thesis exploit a wind model built for the polar regions exploration [1].
  - ❖ Starting speed on 22 m/s (speed of the probe before parafoil deployment.)
- Payload:
  - ❖ 200 kg, with a front surface drag of 0.1 m^2 .
- Preferred environment:
  - ❖ Titan, Saturn's moon.

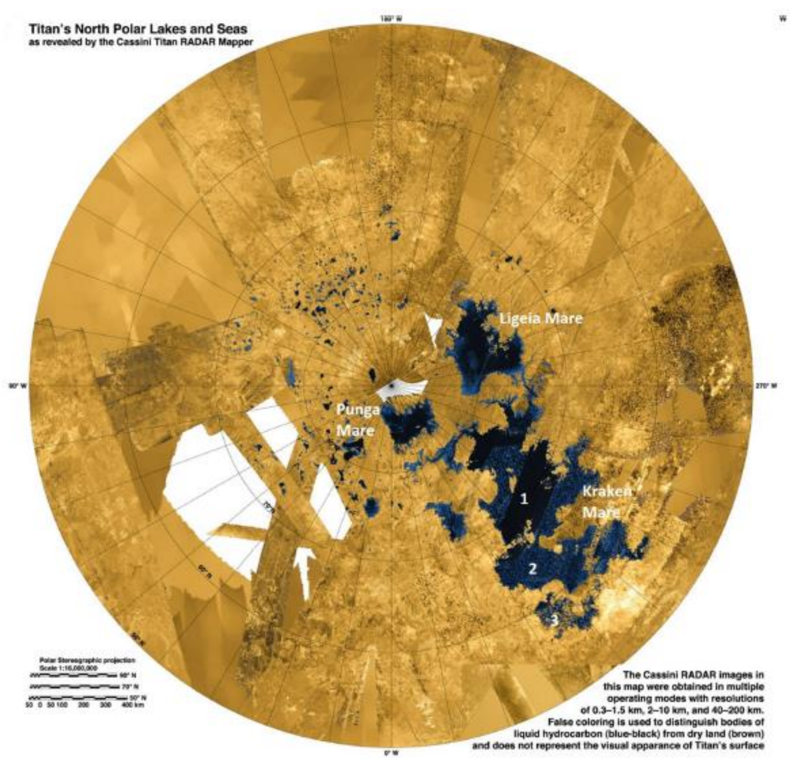

Figure 1: Titan's northern polar regions as reconstructed from Cassini radar. [2]

1.1 TITAN

The alien environment of our interest is Titan, the largest Saturn's moon. It has the silver medal as largest satellite in our solar system: Ganymede (Jupiter) keeps the record, even if it is just 2% larger than Titan.

Titan is interesting for scientists because it is the only known moon in our solar system with an earth-like cycle of liquids (methane, ethane and other hydrocarbons), but with surface temperatures around -179 °C. Moreover, it is thought that on Titan a subsurface ocean of water could be present. We are almost certain that rivers and lakes of methane and ethane exist on the moon surface.

Another peculiarity of Titan is the thick atmosphere (five times greater than Earth): the descent of Huygens from 40 km to the surface took up to 2.5 hours, there is plenty of time for control as well as for disturbance to act.

The atmosphere is mostly nitrogen (95%) with some methane and other carbon-rich compounds (5%).

Table 1: Titan Characteristics.

Distance from Saturn	$1.226 * 10^6\ km$
Density from 40 km to surface	0.7-5.43 $\mathrm{kg/m^3}$
Mean Density	$1.881\ \mathrm{g/cm^3}$
Mean gravity acceleration	$1.352\ \mathrm{m/s^2}$
Equatorial Radius	2575 km
Mass	1.346×10^3
Surface Pressure	147 kPa
Mean Surface Temperature	-179 °C
Atmospheric Constituents	N_2 , CH_4
Sound Speed at 0 km	195 m/s

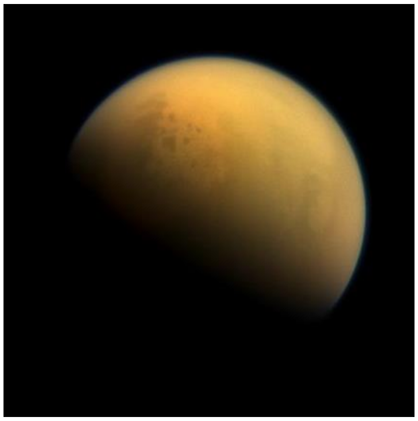

Figure 2: Titan image from Cassini-Huygens mission. The blurred effect is due to the thick moon atmosphere [2]

On Titan we would face various challenges during descent: the atmosphere, the gravity field, the winds will all affect the high efficiency delivery system.

- The aerodynamic performance will be different between Earth and Titan.
- Large dispersions in the entry point and parafoil deployment point may occur for the high intensity winds at high altitudes.

- The winds can vary unpredictably, we still lack a complete knowledge of the moon atmosphere.
- Terrain relative navigation, a camera-based navigation, needs an unfluctuating platform. The camera will be attached to the payload that should be as stable as possible.

1.2 PRECISION AERIAL DELIVERY SYSTEM

On Earth the problem to deliver a payload safely to a well-known target autonomously has been addressed in different ways, one of which is of our interest: autonomous parafoil for precision delivery system. The PADs (Precision Aerial Delivery System) is guided to an ideal trajectory to land on the spot or, in the worst-case scenario, near it: the guidance will accommodate wind estimator, density estimator, GPS and all the possible tools that can enable a successful mission.

The atmosphere of our planet is well known and the slight uncertainties that hit the mission (like wind gust) can be overcome with maneuvers of no more than 20s-30s. If we fly in a foreign environment, with little knowledge on winds and density, without GPS or other earthling autonomous guidance systems, how can we plan the right trajectory to land where we need?

A feasible strategy can be to set more than one target, enter the atmosphere, identify the interesting zones and, then, among them set a landing site. In this scenario the guidance, navigation and control (GNC) system will plan a first reference trajectory and be ready to re-plan the path to accommodate any kind of uncertainties. Hence, the motion planning will be performed online, as we descend in the atmosphere.

In this thesis the focus will be on parafoils, to fulfil some studies on a possible mission on Titan with an autonomous parafoil. However, models of 6 DOF of hang-glider and wingsuit will be presented as well to enable a comparison study: we would like to have a wide vision on the possibilities the different high lift system can give us.

New possible scientific targets like Titans can be the right candidates to understand the potentiality of those systems.

This project workflow can be summarized as:

- Understand what has been published in literature on the PADs (Precision Aerial Delivery System) dynamics modelling.
    - ❖ Geometrical parameters estimation.
    - ❖ Aerodynamic coefficients estimation.
    - ❖ Mathematical dynamics modelling.
- Built the literature models, improve them (some assumption that are usually made on the well-known Earth atmosphere should be relaxed on Titan) and verify the results with the established models. In this thesis only the most significant plots will be reported to not make the reading too cumbersome.
    - ❖ Wind environment simulations.
    - ❖ Gust model simulations.
    - ❖ Steady state simulations to study the equilibrium parameters.
    - ❖ Symmetrical control simulations.
    - ❖ Asymmetrical control simulations.
    - ❖ Models Validation.
- Test the system maneuverability in following a reference trajectory building a simplified GNC system.
    - ❖ Motion planning with a 3 DOF model.
    - ❖ Wind and density estimation.
    - ❖ Proportional control to follow the trajectory.
- Compare the different high lift systems for planetary applications.
    - ❖ Built a 6 DOF model for the hang-gliders.
    - ❖ Compare the models in the nominal Titan atmosphere conditions.

❖ Built a wingsuit model inspired by the northern flying squirrel and test its capabilities, like the vertical landing.

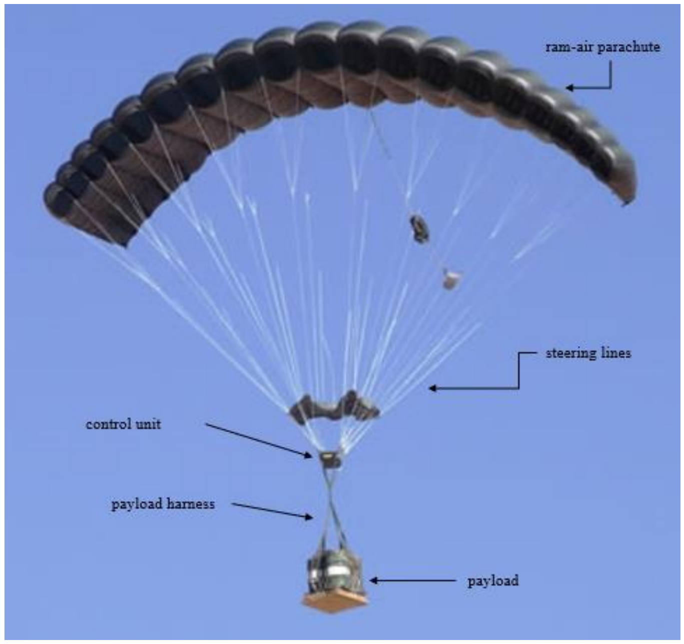

Figure 3: Parafoil main components. [5]

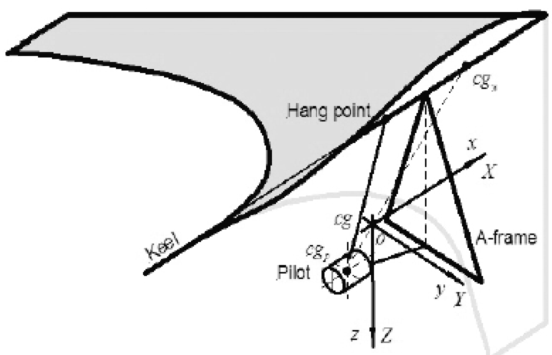

Figure 4: Schematic representation of a hang glider. [6]

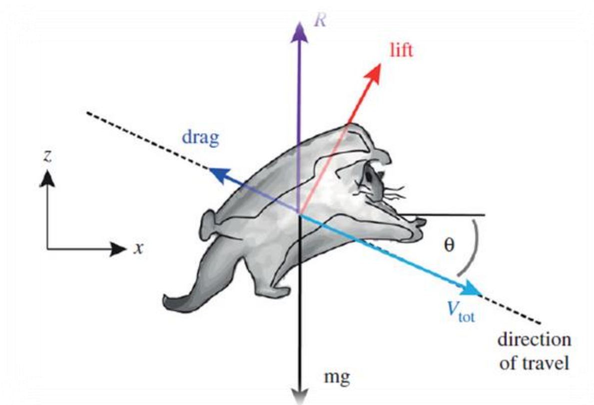

Figure 5: Northern flying squirrel force model. [7]

Table 2: Project Outline

TOPIC	WHERE?	REMARKS
Environment	Section 2.1	• Environmental models
Aerodynamics	Sections 2.2 0	• Lifting line theory • Panel method • Titan aerodynamics estimation
Parafoil Dynamics Models	Chapters 3 4 5 6	• 6 Degree of freedom with simulations and validation. • 7 Degree of freedom with simulations and validation. • 8 Degree of freedom with simulations and validation. • 9 Degree of freedom with simulations and validation.
Hang Glider Dynamics Models	Chapter 7	• 6 Degree of freedom with simulations
Wingsuit Dynamics Models	Chapter 8	• 6 Degree of freedom with simulations
Guidance, Navigation and Control (Parafoil)	Chapter 9	• Wind and density estimation from inaccurate sensor readings. • Motion planning with a 3 DOF of freedom model. • Control in time domain

2 ENVIRONMENT AND HIGH LIFT SYSTEMS AERODYNAMICS

To understand the study performed, we need to introduce some background information on the environment and aerodynamics challenges that we will probably face. This will be an introductive chapter where we will briefly contextualize the research framework.

2.1 ENVIRONMENT

To simulate the Titan environment some models has been developed throughout the years, however after Cassini-Huygens mission we had the luck to gain a better understanding of the conditions we will probably face.

"Lorenz et al" formulate an exponential wind model in [1] that can describe the atmosphere of the poles in late summer. The climate can change abruptly with latitude and season: this model could lose in validity at different seasons or latitudes. However, we will use that wind formulation in all the simulations reported in this thesis as a reference wind disturbance model to develop and test our models. The wind is divided by zonal wind and meridian wind: the first is a high intensity wind that can heavily affect the trajectory, the latter is a disturbance wind around 1-2 m/s.

- Zonal wind:
  - ❖ The zonal wind model (west-east direction) is realized for a latitude of 80°.

$$W = \frac{W_{300}}{1 + e^{\frac{z_0 - z}{L}}} \quad \mathrm{m/s} \tag{2.1}$$

  - ❖ W_{300} : speed of wind at 300 km.
  - ❖ z_0: reference altitude.
  - ❖ z: altitude at which we are evaluating the wind.
  - ❖ L: length scale.

Table 3: Parameters for zonal wind estimation [1]

Wind Profile	$U_{300}\ [m/s]$	$z_0\ [km]$	$L\ [km]$
Nominal	22	35	8
Maximum	50	38	11
Minimum	-3	0	1

From [1] we can derive the wind environment as well as density and gravity from the surface up to 170 km. The density and gravity of Lorenz et all is derived from [3], usually referred as the "Yelle model".

$$\rho = 5.43 * e^{\frac{-0.512 * h}{1000}} \quad kg/m^3 \tag{2.2}$$

Model wind profile and relevant descent parameters at representative heights. Atmospheric density is from the nominal Yelle model. Note that the nominal meridional speed *V*nom is zero throughout—the minimum and maximum are given by $\pm|V|_{max}$.

Altitude (km)	Density (kg/m^3)	Gravity (m/s^2)	U_{min} (m/s)	$U_{nominal}$ (m/s)	U_{max} (m/s)	$\lvert V\rvert_{max}$ (m/s)
170	0.0030	1.19	−3.0	22.0	50.0	3.3
150	0.0051	1.21	−3.0	22.0	50.0	3.1
130	0.0088	1.22	−3.0	22.0	50.0	3.0
110	0.02	1.24	−3.0	22.0	49.9	2.8
90	0.03	1.26	−3.0	22.0	49.6	2.6
80	0.05	1.27	−3.0	21.9	48.9	2.5
70	0.08	1.28	−3.0	21.7	47.4	2.4
60	0.18	1.29	−3.0	21.1	44.0	2.3
50	0.36	1.30	−3.0	19.1	37.4	2.2
44	0.52	1.31	−3.0	16.6	31.7	2.1
38	0.76	1.31	−3.0	13.0	25.0	2.1
32	1.1	1.32	−3.0	9.0	18.3	2.0
26	1.55	1.32	−3.0	5.4	12.6	1.9
20	2.16	1.33	−3.0	2.9	8.1	1.8
18	2.4	1.33	−3.0	2.3	7.0	1.7
16	2.65	1.33	−3.0	1.9	6.0	1.7
14	2.93	1.34	−3.0	1.5	5.1	1.6
12	3.24	1.34	−3.0	1.2	4.3	1.6
10	3.56	1.34	−3.0	0.9	3.6	1.5
8	3.91	1.34	−3.0	0.7	3.1	1.5
6	4.27	1.34	−3.0	0.6	2.6	1.4
5	4.46	1.34	−3.0	0.5	2.4	1.4
4	4.67	1.35	−2.9	0.4	2.2	1.3
3	4.86	1.35	−2.9	0.4	2.0	1.3
2	5.05	1.35	−2.6	0.3	1.8	1.2
1	5.24	1.35	−2.2	0.3	1.7	1.2

Figure 6:Lorenz et all atmospheric model specification. [2]

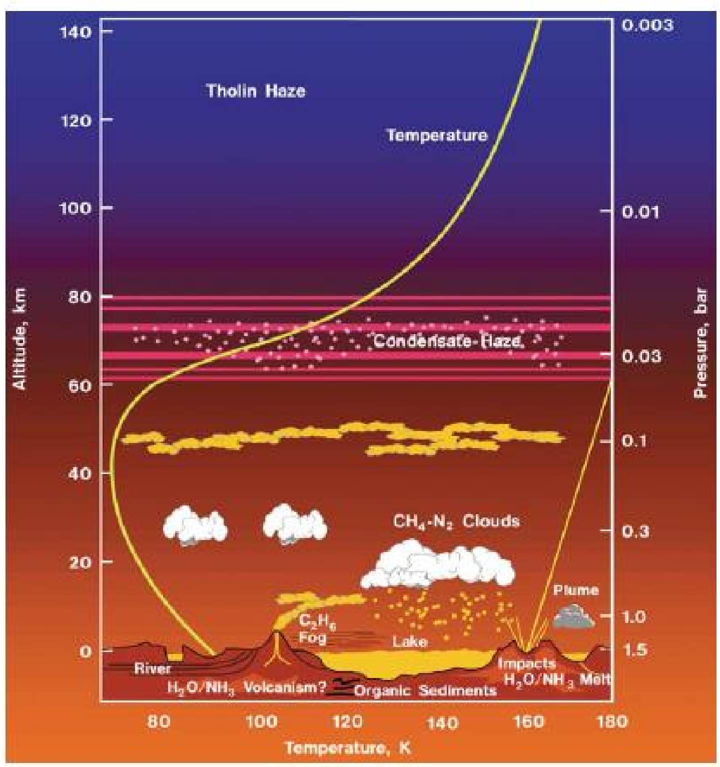

Figure 7: Titan atmosphere [4]

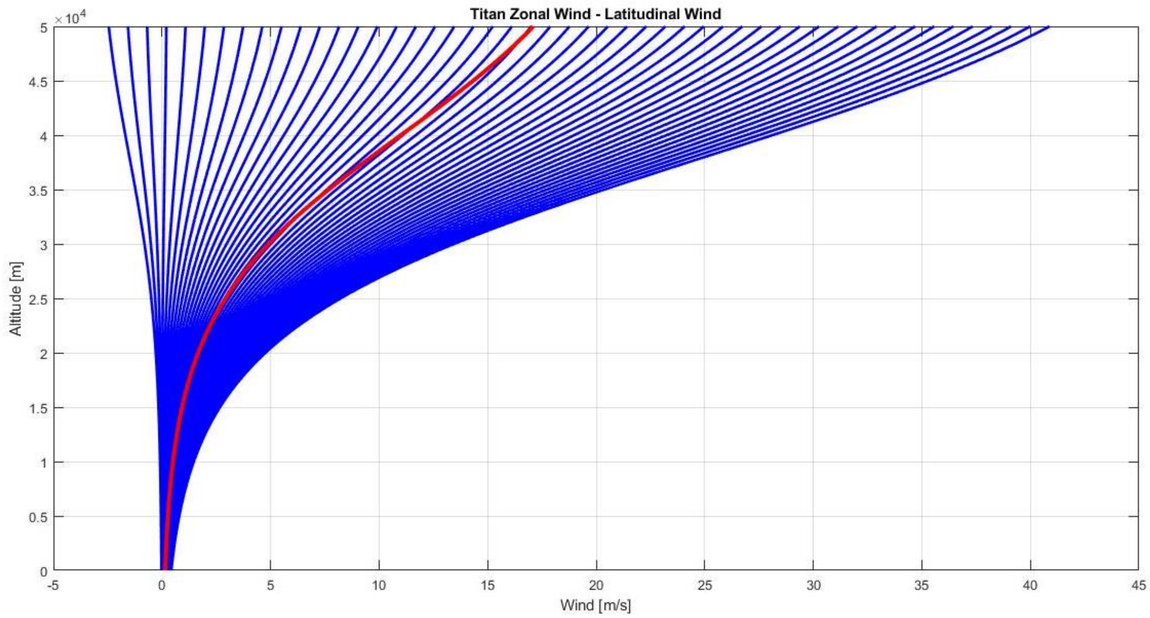

Figure 8: Titan zonal wind model from minimum to maximum wind expected.
The red line represents the nominal wind profile.

2.2 High Efficiency Systems Aerodynamics

Titan has a different density, different gravity and different "air" composition: the aerodynamic performances will be different than on Earth. We should find a way to evaluate them, so the simulations can gain more reliability. It can help us to understand towards which direction we should enhance our system (changing the wing shape, surface, etc.) The overall efficiency of the system shouldn't be affected on Titan, but we can experience an anticipated stall or a decreased latero-directional stability.

To find the aerodynamics of the parafoil on Titan environment it is advisable to compute the required database from a CFD analysis. However, in this preliminary phase of the project, we should find an easiest and more straightforward way to obtain the aerodynamic coefficients. We can compute the coefficients on Earth environment and then scale them for Titan atmosphere.

From [8] we can derive the values of force coefficients of the parafoil from the lifting line theory: unfortunately, that method overestimated the lift and underestimated the drag (the estimation is based only on the wing profile). The mathematical expressions from [8] become very useful if we aim to estimate the control derivatives for the ram-air $\{C_{L_{ds}}, C_{D_{ds}}, C_{m_{ds}}, C_{n_{da}}, C_{l_{da}}\}$.

To estimate the aerodynamic coefficients of a certain wing-shape we can use a panel method: we will obtain a consistent set dependent on the angle of attack and on the airspeed. The tool "Tornado" [9] enables to analyze different wings with different profiles: for the parafoil an usual profile is the CLARK-Y.

However, the drag data obtained from the method must be uploaded with some value typical of the parafoil system. The parafoil profile is cut to form an inlet that permits to inflate the canopy: inside the ram-air is trapped an air mass called added mass. The associated drag is called inlet drag.

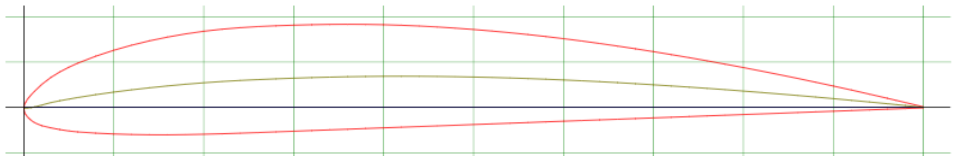

Figure 9: Clark-Y from Airfoil Tool.

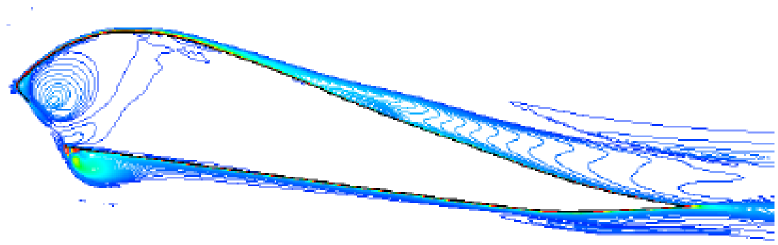

Figure 10: Parafoil profile with inlet cut [10]

Table 4: Additional Drag terms for a small parafoil

$C_{D_{inlet}} = 0.5 * h/c$	Inlet drag (c=profile chord, h=inlet height)
$C_{D_{lines}} = 0.019$	Drag relative to the rise lines for a small parafoil.
$C_{D_{roughness}} = 0.004$	Drag relative to the parafoil surface roughness

After the evaluation on Earth environment we can rescale the values for Titan: the scaling is quite a rough approximation but can provide a reasonable behavior of the system in the alien atmosphere. We assume to flight in a subsonic flux so that the aerodynamic coefficients can be assumed to be independent from the Mach number. The coefficients are then rescaled based on the Reynold number. For Titan we have the Reynolds associated to the Huygens parachute: from that values, keeping into account the different reference length, we can roughly find the Reynold for the Titan Parafoil. In Earth environment we can estimate the Reynolds or use tabulated value of flight test of similar parafoil from high altitude.

$$Re = \frac{u * L}{\nu} \tag{2.3}$$

$$C_{f_{TITAN}} = C_{f_{EARTH}} * \frac{Re_{TITAN}}{Re_{EARTH}} \tag{2.4}$$

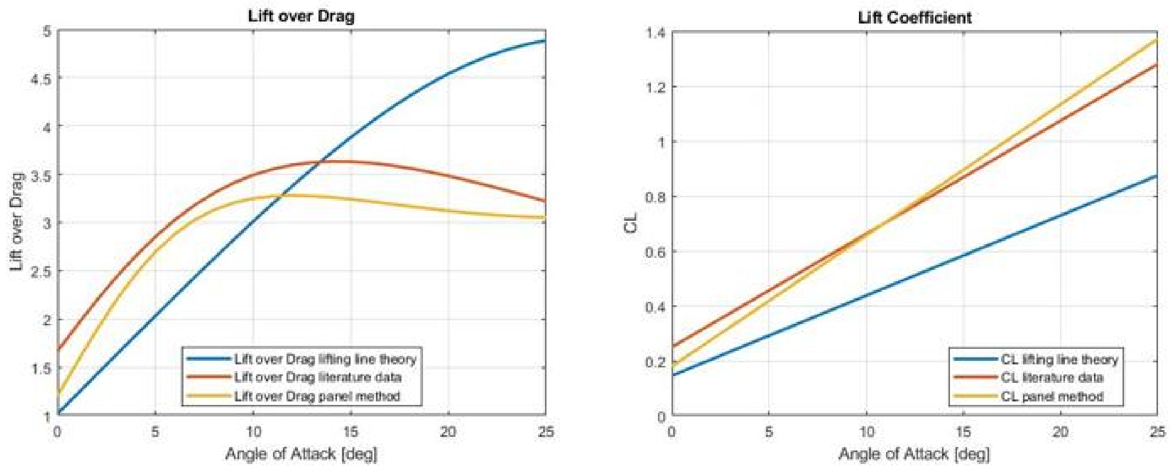

Figure 11: Comparison between the results of the different methods to obtain an aerodynamic dataset.

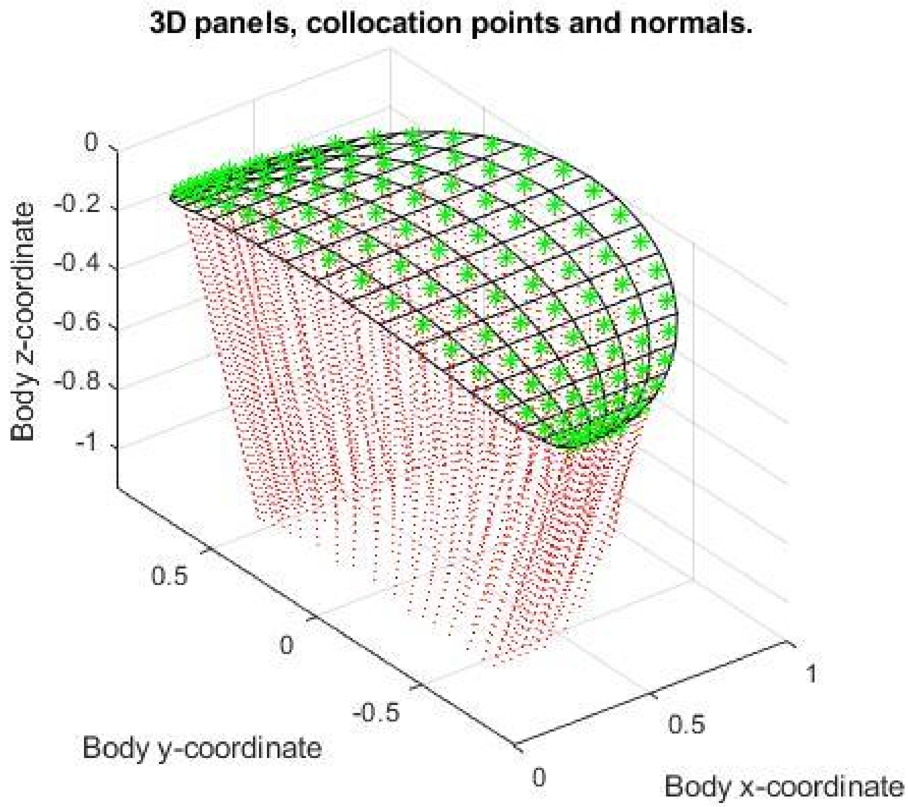

Figure 12: Graphical result from Tornado applied to a possible parafoil wing shape. The lengths are expressed in meters.

If we compare the data set given in [8] and the one derived from the panel method (even without a dense discretization and the lack of knowledge of the used aerodynamic profile), we can find a good match with the data.

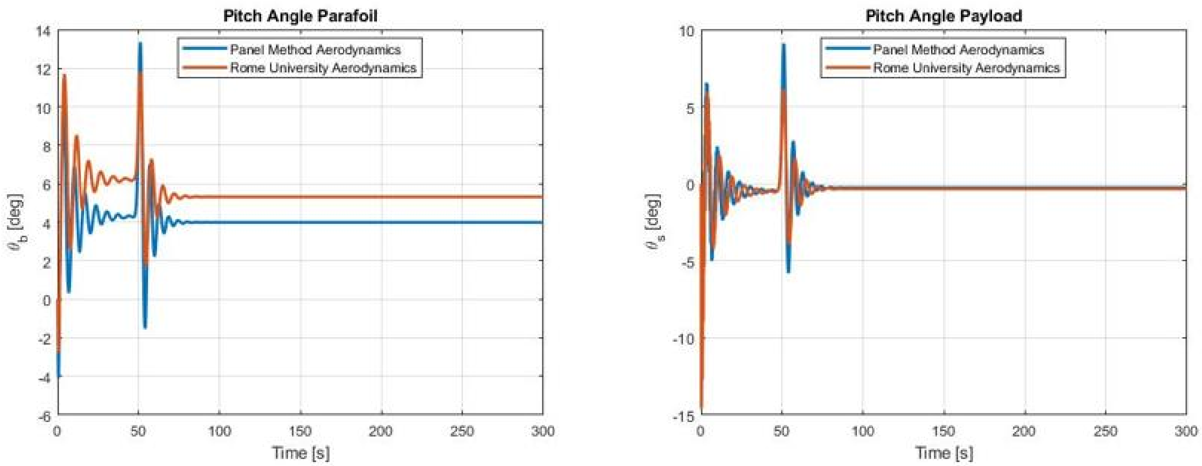

Figure 13: Comparison between the data set from [8] and the panel method.

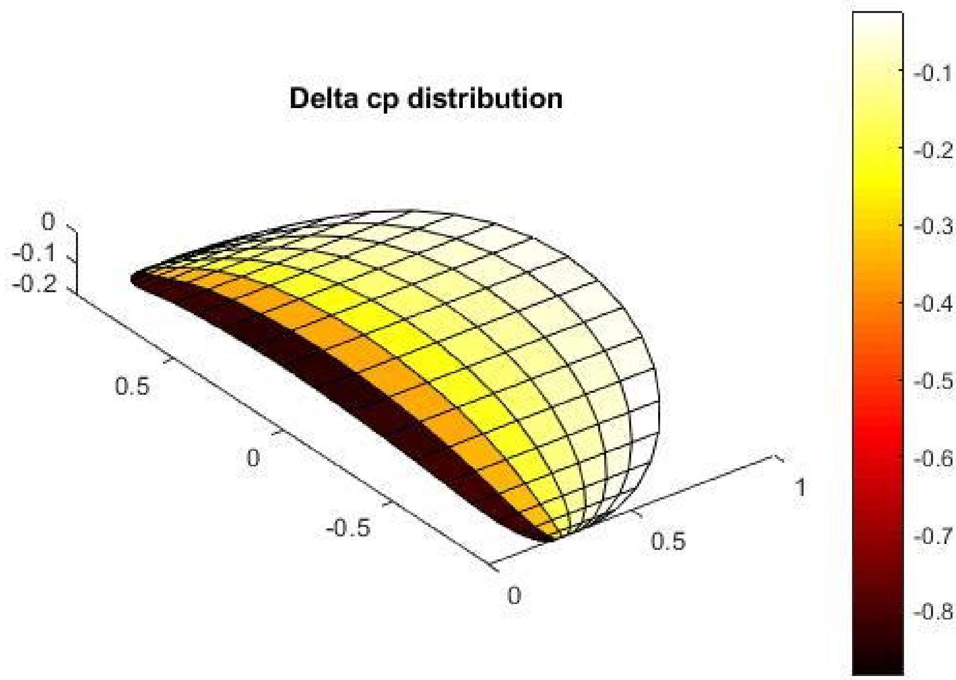

Figure 14: Pressure coefficient distribution on the wing.

2.3 APPARENT MASSES AND INERTIAS

The model considers the apparent mass and inertia tensors. When a body is moving in a fluid, it sets the fluid into motion. Thus, the motion generates a pressure field around the body that we call apparent mass pressure. For every moving body in fluid, we can define a mass ratio between the mass of the system and the air mass shifted by the vehicle. For an airplane the apparent mass is negligible, for a parafoil the apparent mass heavily characterizes the dynamic of the ram-air. To evaluate the entity of the apparent mass, we usually use a formulation similar to the one in equation (2.5).

$$M_r = \frac{m}{\rho * S^{\frac{2}{3}}} \tag{2.5}$$

The ratio is usually in the order of 0.8 on Earth environment and around 7 for a PADs flying in Titan atmosphere (data from Airborne). If the parafoil is thought as inflated, the apparent mass tensor $\boldsymbol{M_f}$ and the apparent inertia tensor $\boldsymbol{I_f}$ are defined as [11]:

$$\boldsymbol{M_f} = \begin{bmatrix} A & 0 & 0 \\ 0 & B & 0 \\ 0 & 0 & C \end{bmatrix} \tag{2.6}$$

$$\boldsymbol{I_f} = \begin{bmatrix} I_a & 0 & 0 \\ 0 & I_b & 0 \\ 0 & 0 & I_c \end{bmatrix} \tag{2.7}$$

Where:

$$A = 0.666 * \rho * \left(1 + \frac{8}{3} * a^{*2}\right) * t^2 * b \tag{2.8}$$

$$B = 0.267 * \rho * \left(1 + 2 * \frac{a^{*2}}{t^{*2}} * AR * (1 - t^{*2})\right) * t^2 * c \tag{2.9}$$

$$C = 0.785 * \rho * \sqrt{1 + 2 * a^{*2} * (1 - t^{*2})} * \frac{AR}{1 + AR} * c^2 * b \tag{2.10}$$

$$I_a = 0.055 * \rho * \frac{AR}{1 + AR} * c^2 * b^3 \tag{2.11}$$

$$I_b = 0.0308 * \rho * \frac{AR}{1 + AR} * [1 + \frac{\pi}{6} * (1 + AR) * AR * a^{*2} * t^{*2}] * c^4 * b \tag{2.12}$$

$$I_c = 0.0555 * \rho * (1 + 8 * a^{*2}) * t^2 * b^3 \tag{2.13}$$

$$AR = \frac{b}{c} \quad t^* = \frac{t}{c} \quad a^* = \frac{a}{b} \tag{2.14}$$

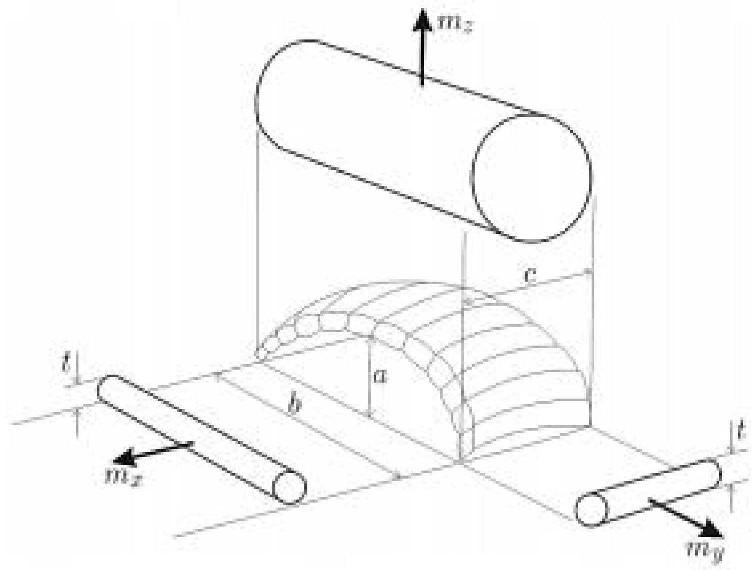

Figure 15: Apparent masses representation for an inflated canopy [11].

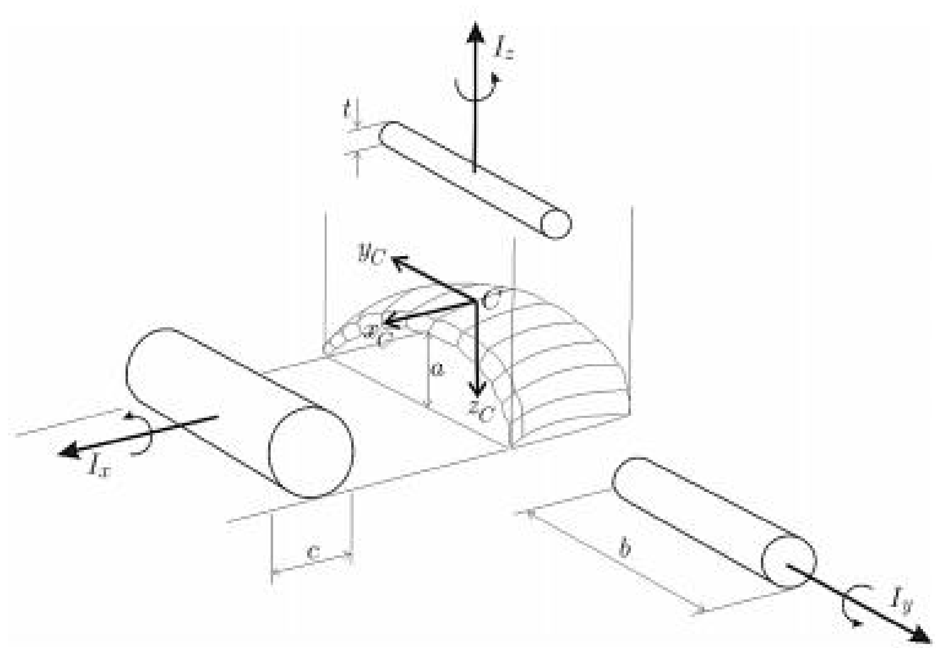

Figure 16: Apparent inertias representation for an inflated canopy [11].

For the hang glider and the wing suit model the apparent masses and inertias are evaluated for a flat wing [8]. In general, those terms in the apparent matrices can be written as:

$$A = k_a * \rho * \frac{\pi}{4} * t^2 * b; \quad \mathrm{B} = \mathrm{k_b} * \rho * \frac{\pi}{4} * t^2 * c; \quad C = k_c * \rho * \frac{\pi}{4} * c^2 * b \tag{2.15}$$

$$I_a = k'_a * \rho * \frac{\pi}{48} * c^2 * b^3; I_b = k'_b * \rho * \frac{4}{48*\pi} * c^4 * b;\ I_c = k'_c * \rho * \frac{\pi}{48} * t^2 * b^3 \tag{2.16}$$

With the parameters $k_a, k_b, k_c, k'_a, k'_b, k_c{}'$ that fluctuate for the different wing configurations. For all those high $\frac{L}{D}$ unpropelled systems the apparent masses could not be neglected.

Table 5: Flat wing apparent masses and inertias coefficients [8]

$k_a = 0.899$	$k_b = 0.34$	$k_c = 0.766$
$k'_a = 0.63$	$k'_b = 0.874$	$k'_c = 1$

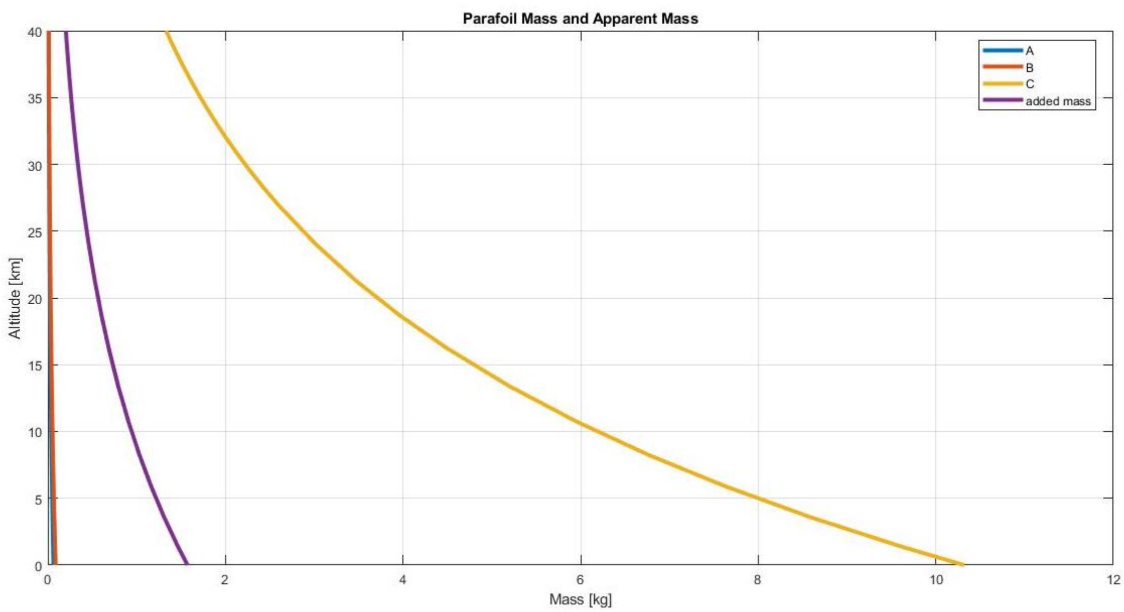

Figure 17: Apparent masses entity during Titan descent for a small parafoil.

2.4 KINEMATICS

Before introducing the equations of motion, we will present a quick review of the reference frames used for all the thesis. The frames are or right-handed cartesian coordinate systems or polar systems in terms of latitude and longitude.

Principal reference systems:

- The body frame {b} located in the system (parafoil plus payload scheme) center of mass.

- The X-axis lays on the plane of symmetry of the PADs, positive along the parafoil wing chord pointing to the leading edge.
    - The Z-axis is positive pointing down and perpendicular to the X-axis.
    - The Y-axis completes the right-handed cartesian reference system.
- The canopy fixed frame {p} with origin in the apparent mass center (the three axes are defined as in {b}).
- The parafoil body frame $\{b_p\}$ with origin in the parafoil center of mass and the right-handed triad defined as {p}.
- The payload fixed frame {s} with origin in the payload mass center (the three axes are defined as in {b}).
- The NED (North-East-Down) refence frame{I} with origin in the perpendicular projection of the vehicle on the planet surface at the beginning of the simulation.
    - The X-axis lays in a plane parallel to the one tangent the planet surface at zero altitude and aims at the true North.
    - The Z-axis points to down with the same direction of the system (parafoil and payload) gravity acceleration vector.
    - The Y-axis completes the right-handed cartesian reference system pointing eastward.
- The navigation frame {n} parallel to {I} with origin in the PADs center of gravity or in the conjunction point in the 9 DOF model.
- The wind frame {w} with origin in the center of mass of the PADs (in the 6 DOF model) and in the center of mass of the canopy in the higher fidelity models.
    - The X-axis is aligned to the direction of the airspeed and positive pointing towards parafoil's leading edge.
    - The Z-axis is perpendicular to the X-axis, it lays on the plane on symmetry of the PADs, pointing down.
    - The Y-axis completes he right-handed cartesian reference system.

To switch from one system to the other, we use rotation matrices:

- The transformation matrix from {b} to {p} is a one-axis rotation due to the rigging angle μ:

$$\boldsymbol{R_{pb}} = \begin{bmatrix} \cos(\mu) & 0 & -\sin(\mu) \\ 0 & 1 & 0 \\ \sin(\mu) & 0 & \cos(\mu) \end{bmatrix} \tag{2.17}$$

- The rotation matrix from {n} to {b} is defined by the trio of Euler angles: roll angle φ, pitch angle θ and yaw angle ψ. In this case the rotation matrix could be expressed as:

$$\boldsymbol{R_{bn}} = \begin{bmatrix} \cos(\psi) * \cos(\theta) & \sin(\psi) * \cos(\theta) & -\sin(\theta) \\ \cos(\psi) * \sin(\theta) * \sin(\phi) - \sin(\psi) * \cos(\phi) & \sin(\psi) * \sin(\theta) * \sin(\phi) + \cos(\psi) * \cos(\phi) & \cos(\theta) * \sin(\phi) \\ \cos(\psi) * \sin(\theta) * \cos(\phi) + \sin(\psi) * \sin(\phi) & \sin(\psi) * \sin(\theta) * \cos(\theta) - \cos(\psi) * \sin(\theta) & \cos(\theta) * \cos(\phi) \end{bmatrix} \tag{2.18}$$

- The rotation matrix from {n} to {w} is given in terms of bank angle ϕ_a, flight path angle γ_a and heading angle χ_a in a fashion similar to ${}^{b}_{n}R$. However, this transformation is used only during guidance and control.

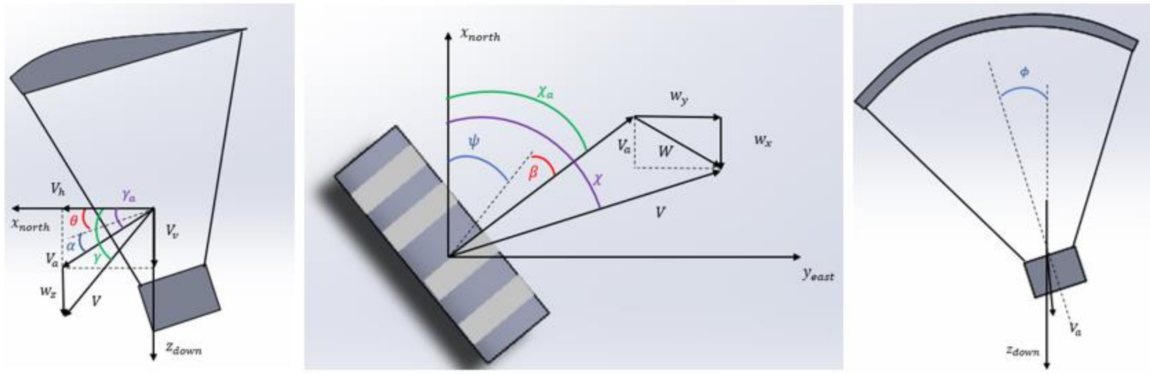

Figure 18: Views of parafoil. [8]

3 PADs LOW FIDELITY MODEL: 6 DOF

The 6 degrees of freedom model is usually used to develop and test Guidance, Navigation and Control algorithms: the parafoil-payload system is a rigid 3D body with linear velocities, attitude and angular rates resulting from the motion of the two main components. In our case this approximation of the true dynamics can be useful to study the system characteristics with few inputs on the parafoil size, shape and dimension.

Different models have different kinds of simplified assumptions made on Earth environment: in our case the more inclusive the model the better. We are not sure on what we will face on Titan. However, all those established and published examples can help us verify and validate our design on Earth and on the moon of Saturn environment.

Table 6: Small ram-air wing design parameters [8].

$AR = 2.5$	Aspect Ratio
$b = \sqrt{S * AR}$	Parafoil Wingspan
$c = \sqrt{S/AR}$	Parafoil Chord
$h = 0.14 * c$	Parafoil height
$R/b = 0.6 \div 0.8$	Line-length-to-span ratio
$\epsilon = b/2/R$	Anhedral angle

3.1 EQUATIONS OF MOTION

The 6 DOF model developed for the JPL relies on those assumptions:

- The parafoil is considered to be a fixed shape once it has been completely inflated.
- The angular rates and the relative Euler angles are written in body frame {b} in respect to the external {I} reference frame.
- The linear velocities are written in the {I} reference frame.
- The apparent masses and inertia acts in the parafoil system frame {p}. They generate forces and moments concentrated in the apparent mass center M: the distance, $\boldsymbol{r_{BM}}$, between the center of the body fixed frame {b} and M is a crucial parameter for the following equations.

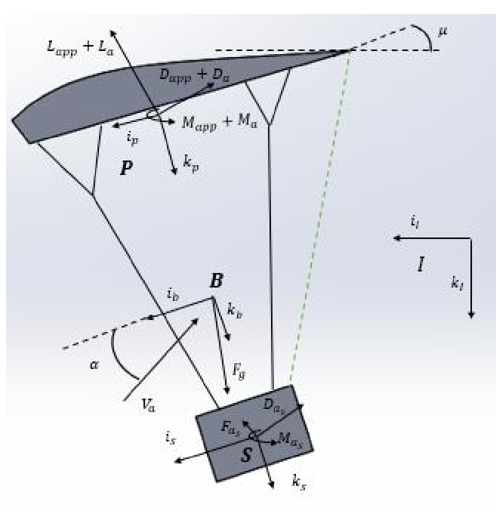

Figure 19: 6 DOF parafoil model, side view.

The equations of motion can be written as:

$$\begin{bmatrix} (m+m_e)*\boldsymbol{I_{3x3}}+\boldsymbol{M_f}' & -\boldsymbol{M}_f'*\boldsymbol{S}(\boldsymbol{r_{BM}}) \\ \boldsymbol{S}(\boldsymbol{r_{BM}})*\boldsymbol{M_f}' & \boldsymbol{I}+\boldsymbol{I}_f'-\boldsymbol{S}(\boldsymbol{r_{BM}})*\boldsymbol{M}_f'*\boldsymbol{S}(\boldsymbol{r_{BM}}) \end{bmatrix} * \begin{bmatrix} \dot{u} \\ \dot{v} \\ \dot{w} \\ \dot{p} \\ \dot{q} \\ \dot{r} \end{bmatrix} = \begin{bmatrix} \boldsymbol{F} \\ \boldsymbol{M} \end{bmatrix} \tag{3.1}$$

$$\begin{gathered} \boldsymbol{F} = \boldsymbol{F_a^p} + \boldsymbol{F_a^s} + \boldsymbol{F_g} + \boldsymbol{F_b^p} - (m+m_e)*\boldsymbol{S}(\boldsymbol{\omega})*\begin{bmatrix} u \\ v \\ w \end{bmatrix} - \boldsymbol{S}(\boldsymbol{\omega})*\boldsymbol{M}_f' \\ *\left(\begin{bmatrix} u \\ v \\ w \end{bmatrix} - \boldsymbol{S}(\boldsymbol{r_{BM}})*\begin{bmatrix} p \\ q \\ r \end{bmatrix}\right) + \boldsymbol{S}(\boldsymbol{\omega})*\boldsymbol{M}_f'*\boldsymbol{R_{bn}}*\boldsymbol{W} \end{gathered} \tag{3.2}$$

$$\begin{gathered} \boldsymbol{M} = \boldsymbol{M_a} + \boldsymbol{M_b^p} + \boldsymbol{S}(\boldsymbol{r_{BM}})*\boldsymbol{F_a^p} + \boldsymbol{S}(\boldsymbol{r_{BS}})*\boldsymbol{F_a^s} - \boldsymbol{S}(\boldsymbol{\omega})*\boldsymbol{I}*\begin{bmatrix} p \\ q \\ r \end{bmatrix} - \boldsymbol{S}(\boldsymbol{\omega})*\boldsymbol{I}_f'*\begin{bmatrix} p \\ q \\ r \end{bmatrix} \\ - \boldsymbol{S}(\boldsymbol{r_{BM}})*\boldsymbol{S}(\boldsymbol{\omega})*\boldsymbol{M}_f'*\left(\begin{bmatrix} u \\ v \\ w \end{bmatrix} - \boldsymbol{S}(\boldsymbol{r_{BM}})*\begin{bmatrix} p \\ q \\ r \end{bmatrix} - \boldsymbol{R_{bn}}*\boldsymbol{W}\right) \end{gathered} \tag{3.3}$$

$$\begin{bmatrix} \dot{\phi} \\ \dot{\theta} \\ \dot{\psi} \end{bmatrix} = \begin{bmatrix} 1 & \sin(\phi)*\dfrac{\sin(\theta)}{\cos(\theta)} & \cos(\phi)*\dfrac{\sin(\theta)}{\cos(\theta)} \\ 0 & \cos(\phi) & -\sin(\phi) \\ 0 & \sin(\phi)*\dfrac{1}{\cos(\theta)} & \cos(\phi)*\dfrac{1}{\cos(\theta)} \end{bmatrix} * \begin{bmatrix} p \\ q \\ r \end{bmatrix} \tag{3.4}$$

$$\begin{bmatrix} \dot{x} \\ \dot{y} \\ \dot{z} \end{bmatrix} = \boldsymbol{R'_{bn}} * \begin{bmatrix} u \\ v \\ w \end{bmatrix} \tag{3.5}$$

Where:

- “m” is the overall system mass:

$$m = m_{payload} + m_{parafoil} + m_{suspension\ lines} \tag{3.6}$$

- “m_e” is the added mass: the mass trapped inside the inflated parafoil. There are different expressions to evaluate it and they heavily depend on the parafoil shape. In our model, the added mass, is defined as in [12] using the profile area “$0.09 * c^2$ “.

$$m_e = 0.09 * c^2 * b * \rho \tag{3.7}$$

- “$\boldsymbol{M_f}'$” is the parafoil apparent mass tensor rotated by the rigging angle:

$$\boldsymbol{M}_f' = \boldsymbol{R'_{pb}} * \boldsymbol{M_f} * \boldsymbol{R_{pb}} \tag{3.8}$$

- "$\boldsymbol{I_f}'$" is the parafoil apparent inertia tensor rotated by the rigging angle:

$$\boldsymbol{I}'_{\boldsymbol{f}} = \boldsymbol{R'}_{\boldsymbol{pb}} * \boldsymbol{I}_{\boldsymbol{f}} * \boldsymbol{R}_{\boldsymbol{pb}} \tag{3.9}$$

- "**W**" is the wind vector expressed in the navigation frame {n}.

$$\boldsymbol{V}_{\boldsymbol{ground}} = \boldsymbol{V}_{\boldsymbol{airspeed}} - \boldsymbol{W} \tag{3.10}$$

- "$\boldsymbol{S}(\boldsymbol{r}_{\boldsymbol{BM}})$" is the skew-symmetric matrix that replace the vector product $\boldsymbol{r}_{\boldsymbol{BM}} \times$

$$\boldsymbol{S}(\boldsymbol{r}_{\boldsymbol{BM}}) = \begin{bmatrix} 0 & -z_{BM} & y_{BM} \\ z_{BM} & 0 & -x_{BM} \\ -y_{BM} & x_{BM} & 0 \end{bmatrix} \tag{3.11}$$

Where $\boldsymbol{r}_{\boldsymbol{BM}}$ is the vector that points from the origin of the body reference frame to the apparent mass center of gravity of the parafoil. In our model it is evaluated as:

$$\boldsymbol{r}_{\boldsymbol{BM}} = \boldsymbol{R'}_{\boldsymbol{pb}} * [\,0\;0\;z_{BM}] \tag{3.12}$$

- "$\boldsymbol{S}(\boldsymbol{r}_{\boldsymbol{BS}})$" is the skew-symmetric matrix that replace the vector product $\boldsymbol{r}_{\boldsymbol{BS}} \times$:

$$\boldsymbol{S}(\boldsymbol{r}_{\boldsymbol{BS}}) = \begin{bmatrix} 0 & -z_{BS} & y_{BS} \\ z_{BS} & 0 & -x_{BS} \\ -y_{BS} & x_{BS} & 0 \end{bmatrix} \tag{3.13}$$

Where $\boldsymbol{r}_{\boldsymbol{BS}}$ is the vector that points from the origin of the body reference frame to the payload mass center. In our model it is evaluated as:

$$\boldsymbol{r}_{\boldsymbol{BS}} = [0\;0\;z_{BS}] \tag{3.14}$$

- "$S(\boldsymbol{\omega})$" is the skew-symmetric matrix of the system rates:

$$\boldsymbol{S}(\boldsymbol{\omega}) = \begin{bmatrix} 0 & -r & q \\ r & 0 & -p \\ -q & p & 0 \end{bmatrix} \tag{3.15}$$

- "$\boldsymbol{F}_{\boldsymbol{a}}^{\boldsymbol{p}}$" is the parafoil aerodynamic force vector expressed as:

$$\boldsymbol{F_a^p} = \frac{1}{2} * \rho * V_{ap}^2 * S_p * \boldsymbol{R'_{pb}} * \boldsymbol{R_{pw}} * \begin{bmatrix} -(CL_0 + CL_{alpha} * \alpha + CL_{ds} * \overline{\delta_s}) \\ CY_{beta} * \beta \\ -(CD_0 + CD_{a2} * \alpha^2 + CD_{ds} * \overline{\delta_s}) \end{bmatrix} \tag{3.16}$$

Where

- "$\boldsymbol{R'_{pb}}$" is the rotation matrix between parafoil reference frame {p} and body reference frame {b}. The forces and the moments on the parafoil are all written in {p} and expressed in {b}.
- "$\boldsymbol{R_{pw}}$" is the rotation matrix between the wind frame {w} and parafoil body frame {p}. The matrix is expressed in terms of angle of attach, α, and sideslip angle, β.

$$\boldsymbol{R_{pw}} = \boldsymbol{R_\alpha} * \boldsymbol{R_\beta} = \begin{bmatrix} \cos(\alpha) & 0 & -\sin(\alpha) \\ 0 & 1 & 0 \\ \sin(\alpha) & 0 & \cos(\alpha) \end{bmatrix} * \begin{bmatrix} \cos(\beta) & \sin(\beta) & 0 \\ -\sin(\beta) & \cos(\beta) & 0 \\ 0 & 0 & 1 \end{bmatrix} \tag{3.17}$$

$$\alpha = \tan^{-1}\left(\frac{w_p}{u_p}\right) \tag{3.18}$$

$$\beta = \tan^{-1}\left(\frac{v_p}{\sqrt{u_p^2 + w_p^2}}\right) \tag{3.19}$$

$$\boldsymbol{V_p} = \boldsymbol{R'_{pb}} * \left(\begin{bmatrix} u \\ v \\ w \end{bmatrix} + \boldsymbol{S(\omega)} * \boldsymbol{r_{BM}} - \boldsymbol{R_{bn}} * \boldsymbol{W}\right) = \boldsymbol{R'_{pb}} * (\boldsymbol{V} + \boldsymbol{S(\omega)} * \boldsymbol{r_{BM}}) \tag{3.20}$$

$$V_{ap} = \sqrt{u_p^2 + v_p^2 + w_p^2} \tag{3.21}$$

- "$\boldsymbol{M_a^p}$" is the parafoil aerodynamic moment vector expressed as:

$$\boldsymbol{M_a^p} = \frac{1}{2} * \rho * V_{ap}^2 * S_p * \boldsymbol{R'_{pb}} * \begin{bmatrix} b(C_{l\beta} * \beta + \frac{b}{2 * V_a} * C_{lr} * r + \frac{b}{2 * V_a} * C_{lp} * p + C_{l\delta_a} * \overline{\delta_a}) \\ \bar{c} * (C_{m0} + C_{m\alpha} * \alpha + \frac{b}{2 * V_a} * C_{mq} * q) \\ b(C_{n\beta} * \beta + \frac{b}{2 * V_a} * C_{np} * p + \frac{b}{2 * V_a} * C_{nr} * r + C_{n\delta_a} * \overline{\delta_a} \end{bmatrix} \tag{3.22}$$

- "$\boldsymbol{F_a^s}$" is the payload aerodynamic force vector expressed as:

$$\boldsymbol{F_a^s} = \frac{1}{2} * \rho * V_{as}^2 * S_s * \boldsymbol{R_{sw}} * \begin{bmatrix} -CD_s \\ 0 \\ 0 \end{bmatrix} \tag{3.23}$$

❖ "$\boldsymbol{R_{sw}}$" is the rotation matrix between the wind frame {w} and payload body frame {s}. The matrix has the same expression as the one for the parafoil, but with the angle of attack and the sideslip angle expressed with the parafoil linear velocities.

$$\boldsymbol{V_s} = \left(\begin{bmatrix} u \\ v \\ w \end{bmatrix} + \boldsymbol{S(\omega)} * \boldsymbol{r_{BC}} - \boldsymbol{R_{bn}} * \boldsymbol{W} \right) \tag{3.24}$$

$$V_{as} = \sqrt{u_s^2 + v_s^2 + w_s^2} \tag{3.25}$$

The aerodynamic moment of the payload is usually neglected: however, if the payload has some lifting characteristics, we should include it.

- "$\boldsymbol{F_g}$" is the system weight force expressed in body frame as:

$$\boldsymbol{F_g} = \left(m_{parafoil} + m_e + m_{payload}\right) * g * \begin{bmatrix} -\sin(\theta) \\ \cos(\theta) * \sin(\phi) \\ \cos(\theta) * \cos(\phi) \end{bmatrix} \tag{3.26}$$

- "$\boldsymbol{F_b^p}$" is the buoyancy force, upward force given by the parafoil added mass. It is small, but it can contribute to the overall balance of moments due to the large distance between the canopy mass center and the overall body center of gravity.

$$\boldsymbol{F_b^p} = -(m_{added}) * \begin{bmatrix} -\sin(\theta) \\ \cos(\theta) * \sin(\phi) \\ \cos(\theta) * \cos(\phi) \end{bmatrix} \tag{3.27}$$

$$\boldsymbol{M_b^p} = \boldsymbol{S(r_{BM})} * \boldsymbol{F_b^p} \tag{3.28}$$

- The apparent masses and inertias generate a set of forces and moments that can be expressed as:

$$\begin{aligned} \boldsymbol{F_{app}} = -\boldsymbol{R'_{pb}} * \Bigg\{ & \left[\boldsymbol{M_f} * \boldsymbol{R_{pb}} * \left(\begin{bmatrix} \dot{u} \\ \dot{v} \\ \dot{w} \end{bmatrix} - \boldsymbol{S(r_{BM})} * \begin{bmatrix} \dot{p} \\ \dot{q} \\ \dot{r} \end{bmatrix} \right) \right] \\ & + \Bigg[\boldsymbol{R_{pb}} * \boldsymbol{S(\omega)} * \boldsymbol{R'_{pb}} * \boldsymbol{M_f} * \boldsymbol{R_{pb}} \\ & * \left(\begin{bmatrix} u \\ v \\ w \end{bmatrix} - \boldsymbol{S(r_{BM})} * \begin{bmatrix} p \\ q \\ r \end{bmatrix} - \boldsymbol{R_{bn}} * \boldsymbol{W} \right) \Bigg] \Bigg\} \end{aligned} \tag{3.29}$$

$$M_{app} = -R'_{pb} * \left(M_f * R_{pb} * \begin{bmatrix} \dot{p} \\ \dot{q} \\ \dot{r} \end{bmatrix} + R_{pb} * S(\omega) * R'_{pb} * M_f * R_{pb} * \begin{bmatrix} p \\ q \\ r \end{bmatrix} \right) + S(r_{BM}) * F_{app} \tag{3.30}$$

3.1.1 CONTROL

The control is modelled as deflections of brake lines that modify the shape of the parafoil, hence its aerodynamics. This deformation of the arm-air wing is associated to the aerodynamic coefficients $C_{D_{\delta_s}}$, $C_{L_{\delta_s}}$, $C_{n\delta a}$, $C_{l_{\delta_a}}$ multiplied by a "normalized" brake deflection:

- Normalized asymmetric brake deflection for latero-directional control:
$$\overline{\delta_a} = \delta_a/\delta_{max}$$
- Normalized symmetric brake deflection for longitudinal control:
$$\overline{\delta_s} = \delta_s/\delta_{max}$$

In some models more aerodynamic coefficients are taken into account. It is evaluated the effect of the symmetric and asymmetric deflection on the pitching moment coefficients C_m, on the lateral force coefficients C_Y. The number of those aerodynamic coefficients associated with control depends on the aerodynamic data set used during the simulations. We are using system identification derived parameters: they have been expressed for the Earth environment. However, with some assumptions we can extended them to Titan atmosphere for this first steps in the mission design. The aerodynamics is discussed and analyzed in section 2.2

3.1.2 AERODYNAMICS

The aerodynamic used in the simulations of all parafoil models, it is based on a set of aerodynamic coefficients arranged as in equations (3.16) and (3.22):

Table 7: Aerodynamic coefficients used in the parafoil simulations [8].

$C_{D0} = 0.25$	$C_{D\alpha} = 0.12$		
$C_{Y\beta} = -0.23$			
$C_{L0} = 0.091$	$C_{L\alpha} = 0.90$		
$C_{m0} = 0.35$	$C_{m\alpha} = -0.72$	$C_{mq} = -1.49$	
$C_{l\beta} = -0.036$	$C_{lp} = -0.84$	$C_{lr} = -0.082$	$C_{l\delta_a} = -0.0035$
$C_{n\beta} = -0.0015$	$C_{np} = -0.082$	$C_{nr} = -0.27$	$C_{n\delta_a} = 0.0215$
$C_{D_{payload}} = 0.4$			

Those coefficients are given for a wing with an aspect ratio of $\frac{b}{c} = 2$ and a glide ratio $\frac{L}{D} = 2$ of a SNOWFLAKE parafoil. The wing we would like to use on Titan environment has the same glide ratio but a bit different aspect ratio $\left(\frac{b}{c} = 3\right)$: the following simulations catch the dynamics of the system, probably the true aerodynamic of the PADs will enhance the system performances. We kept this aerodynamics definition because it was able to match the results from Airborne, JPL's contractors for the analysis of the parafoil characteristics on Titan environment.

3.2 PARAFOIL AND PAYLOAD GEOMETRY, MASS AND INERTIA

In the 6 DOF model all the equations of motion are referred to a body mass center, that takes into account parafoil and payload masses and their relative position at the beginning of the simulations. The geometrical characteristics of the parafoil-payload are well explained in [12] and in [8], where, thanks to system identification, a plausible parafoil geometry can be derived knowing the surface and the aspect ratio of the wing.

3.2.1 PAYLOAD

The load is modelled as a cube of height $z_b = 0.5$, $x_b = 0.5$, $y_b = 0.5$ and of mass of 200 kg. The payload centre of mass coincides with the geometric centre of the box. The moment of inertia of the payload can be written as:

Table 8: Payload geometrical inputs.

$z_s = 0.5\ m$	Payload height
$x_s = 0.5\ m$	Payload length
$y_s = 0.5\ m$	Payload width
$m_s = 200\ kg$	Payload mass

$$I_{xs} = \frac{m_l}{12} * (z_s^2 + y_s^2) \tag{3.31}$$

$$I_{ys} = \frac{m_l}{12} * (z_s^2 + y_s^2) \tag{3.32}$$

$$I_{zs} = \frac{m_l}{12} * (z_s^2 + y_s^2) \tag{3.33}$$

3.2.2 PARAFOIL

The parafoil is assumed to be a parallelepiped of dimensions b, c h_{mean}. The h_{mean} is an "apparent thickness" that keeps into account parafoil mean thickness "t" and the parafoil chamber. To evaluate the h_{mean}, the canopy volume, v_{vol}, must be evaluated using the profile area (defined as $0.09 * c^2$ [12]).

Table 9: Parafoil geometrical inputs.

$b = 3.07\ m$	Parafoil wingspan
$c = 1.02\ m$	Parafoil aerodynamic chord
$t = 0.075$	Parafoil thickness
$a = 0.164\ m$	Parafoil height
$R = 1.84\ m$	Parafoil line length (from parafoil to confluence point)
$\mu = -12\ deg$	Rigging angle

$\epsilon = 47.74\ deg$	Anhedral angle
$l_{ha} = 1\ m$	Harness length
$m_p = 1.4\ m$	Parafoil mass
$\sigma = 0.45$	Sigma aerial density
$\delta_{max} = 0.16\ m$	Maximum trailing edge deflection

$$\epsilon = \frac{b}{2 * R} \tag{3.34}$$

$$b_{inflated} = 2 * R * \sin(\epsilon) \tag{3.35}$$

$$v_{vol} = 0.09 * c^2 * b \tag{3.36}$$

$$h_{mean} = \frac{v_{vol}}{c_{chord} * b_{inflated}} \tag{3.37}$$

$$I_{xp} = \left(\frac{v_{vol} * \rho + m_p}{12}\right) * (b_{inflated}^2 + h_{mean}^2) \tag{3.38}$$

$$I_{yp} = \left(\frac{v_{vol} * \rho + m_p}{12}\right) * (c^2 + h_{mean}^2) \tag{3.39}$$

$$I_{zp} = \left(\frac{v_{vol} * \rho + m_p}{12}\right) * (b_{inflated}^2 + c^2) \tag{3.40}$$

The parafoil is inclined by the rigging angle μ: the inertia moment should be transformed from the parafoil reference frame {p} to the body frame {b}.

$$I_{xp_b} = I_{xp} * \cos^2(\mu) + I_{zp} * \sin^2(\mu) \tag{3.41}$$

$$I_{yp_b} = I_{yp} \tag{3.42}$$

$$I_{zp_b} = I_{xp} * sin^2(\mu) + I_{zp} * cos^2(\mu) \tag{3.43}$$

$$I_{xzp_b} = \frac{1}{2} * \left(I_{xp} - I_{zp}\right) * \sin(2 * \mu) \tag{3.44}$$

3.2.3 PARAFOIL AND PAYLOAD SYSTEM

After the single man subsystems analysis, we can now define the position of the system center of mass, the mass of the system the total inertia of the system and the positions of parafoil and payload relative to the body center of mass. The system total mass can be expressed as:

$$m_t = m_s + m_p \tag{3.45}$$

The distance between the parafoil center of mass, M, and the payload body center, S, can be expressed using the distance between parafoil and the confluence point C, l_{cgp}:

$$l_z = \frac{z_b}{2} + l_{ha} + l_{cgp} \tag{3.46}$$

$$l_{cgp} = \frac{2}{3} * \frac{(l_s + t_{mean})^3 - l_s^3}{(l_s + t_{mean})^2 - l_s^2} * \frac{\sin(\epsilon)}{\epsilon} \tag{3.47}$$

$$t_{mean} = \frac{v_{vol}}{S_p} \tag{3.48}$$

The vectors from the body center of mass and parafoil center of mass, r_{BM}, and the vector from the body center of mass and the payload center of mass, r_{BS} can be defined as:

$$\boldsymbol{r_{BS}} = [0\ 0\ z_{BS}];\ z_{BS} = l_z * \frac{m_p + v_{vol} * \rho}{m_p + m_s} \tag{3.49}$$

$$\boldsymbol{r_{BM}} = [0\ 0\ z_{BM}];\ \ z_{BM} = z_{BS} - l_z \tag{3.50}$$

The system inertia tensor can be expressed as:

$$I_x = I_{xp_b} + I_{xs} + \left(m_p + \rho * v_{vol}\right) * z_{BM}^2 + m_s * z_{BS}^2 \tag{3.51}$$

$$I_y = I_{yp_b} + I_{xs} + \left(m_p + \rho * v_{vol}\right) * z_{BM}^2 + m_s * z_{BS}^2 \tag{3.52}$$

$$I_z = I_{zp_b} + I_{zs} \tag{3.53}$$

$$I_{xz} = I_{xz_b} \tag{3.54}$$

$$\boldsymbol{I} = \begin{bmatrix} I_x & 0 & I_{xz} \\ 0 & I_y & 0 \\ I_{xz} & 0 & I_z \end{bmatrix} \tag{3.55}$$

3.3 SIMULATION PLOTS RESULTS

To analyze the PADs dynamics, we performed a series of simulations: we will report only the important results. The following simulations are performed on Titan environment.

- Steady-State Simulation: those first results show the stable equilibrium conditions of the descending parafoil without introducing gust disturbance. Than we will analyze what happens introducing the gust: the system is intrinsically stable and tends to return to unperturbed equilibrium configuration.

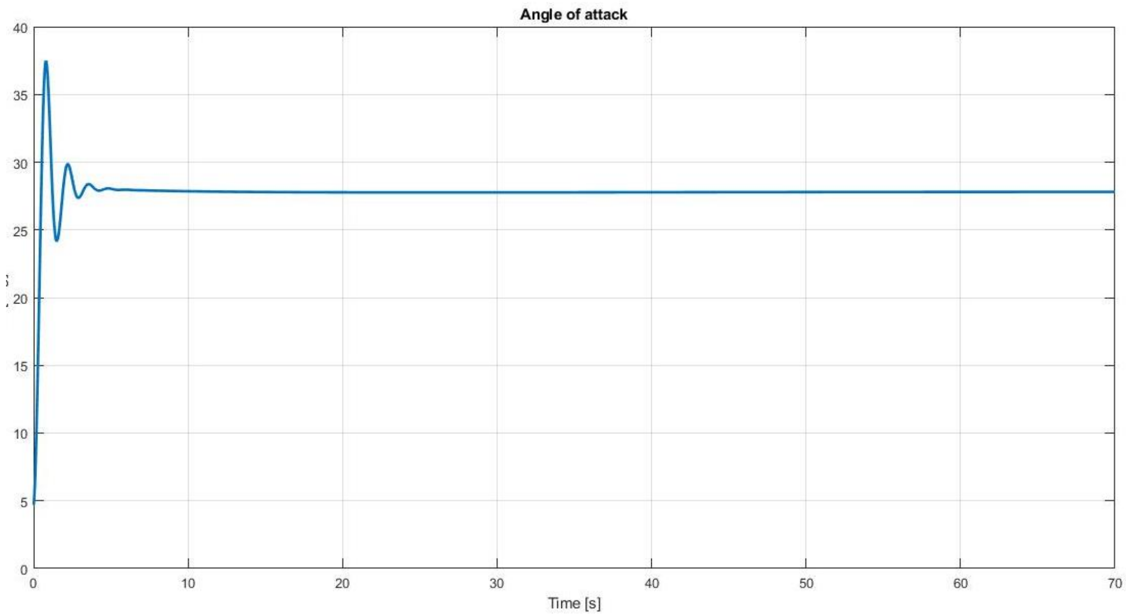

Figure 20:Angle of Attack during a steady state simulation without gust.

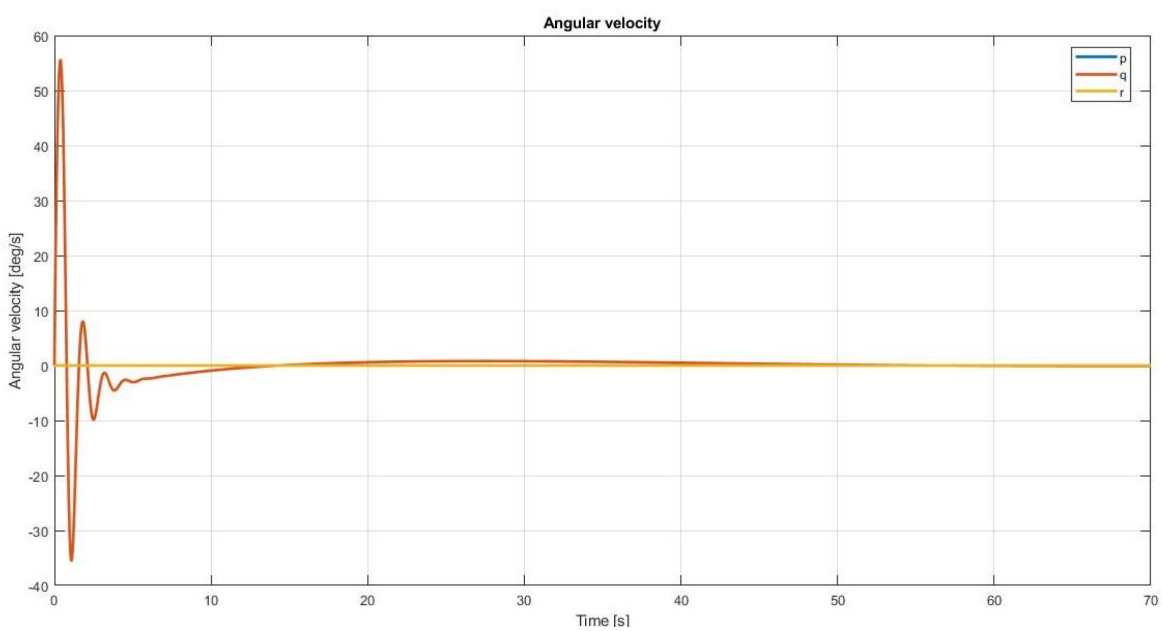

Figure 21: Angular velocity during a steady state simulation without gust

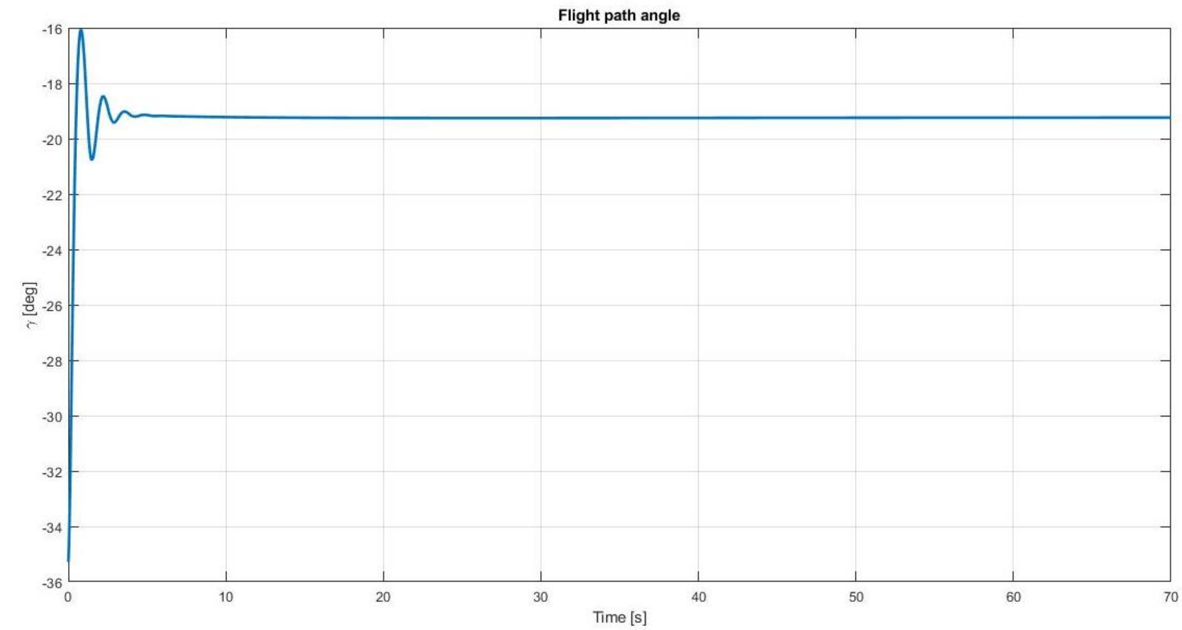

Figure 22: Flightpath angle during a steady state simulation without gust.

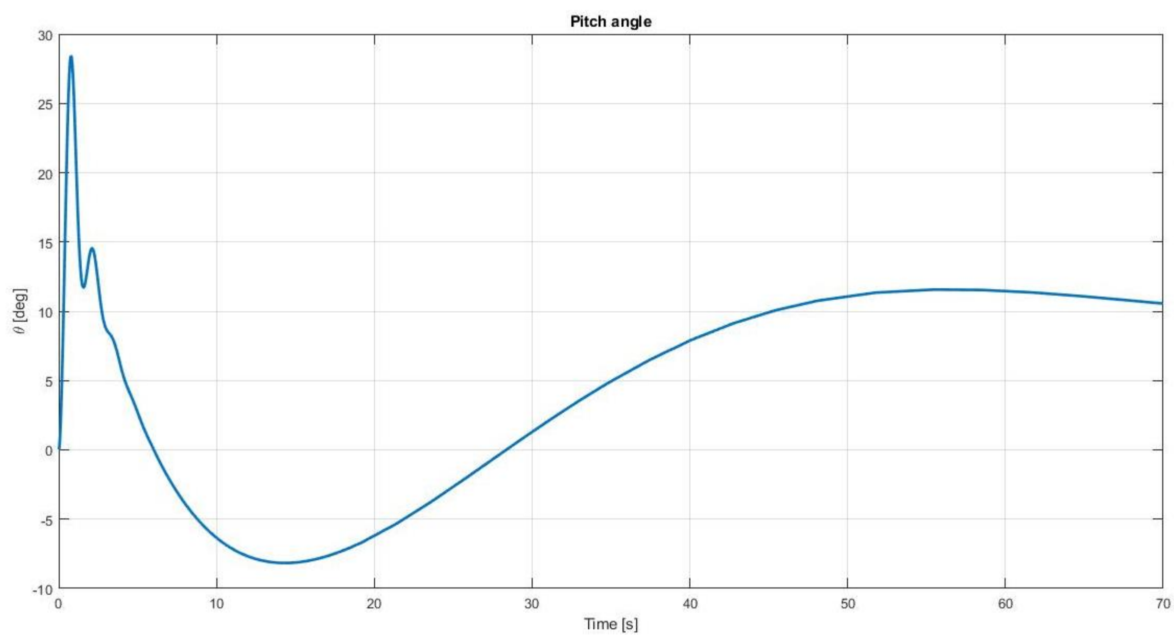

Figure 23: Pitch angle during a steady state simulation without gust.

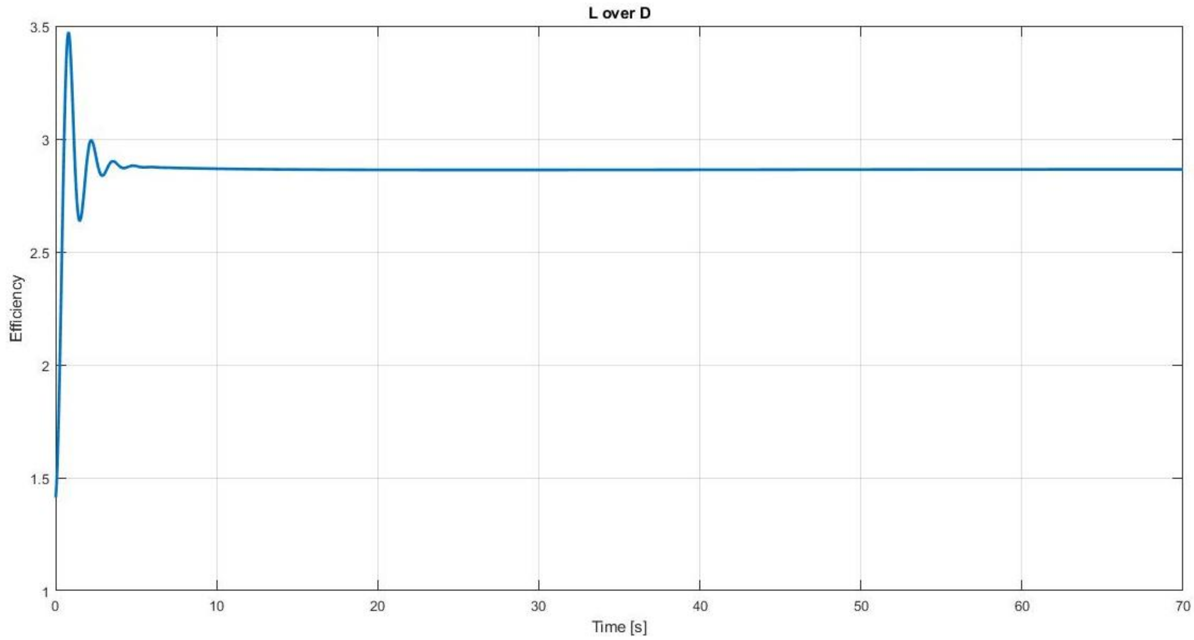

Figure 24: Aerodynamic Efficiency during a steady state simulation without gust.

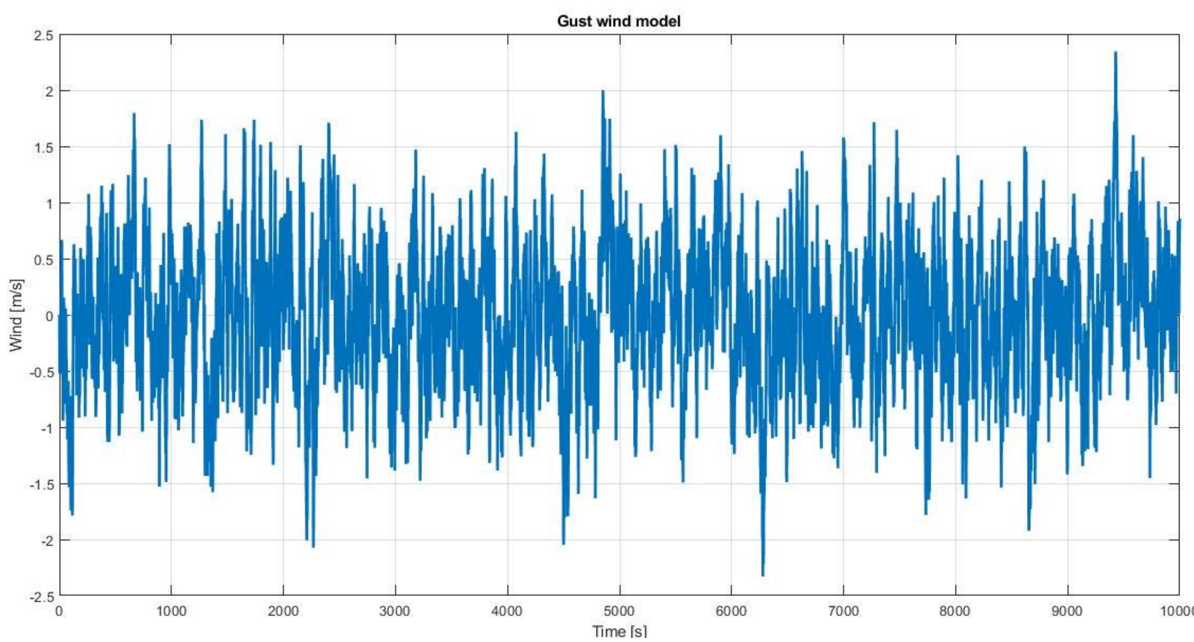

Figure 25: Example of a gust wind model.

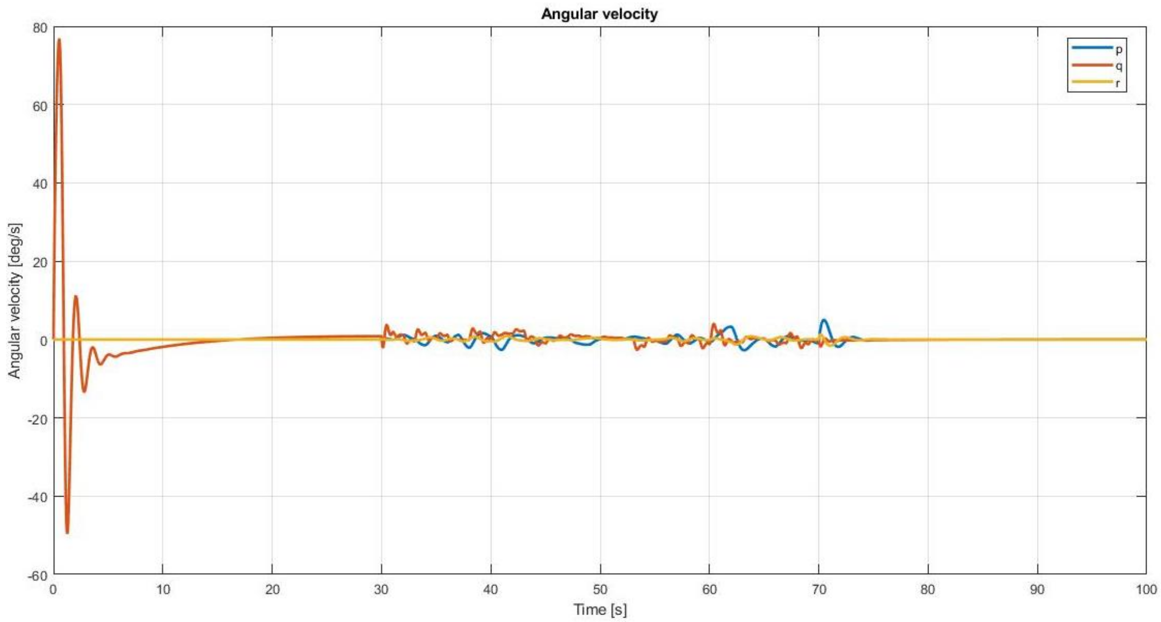

Figure 26: Angular velocity during a steady state descent affected by a 40s gust wind.

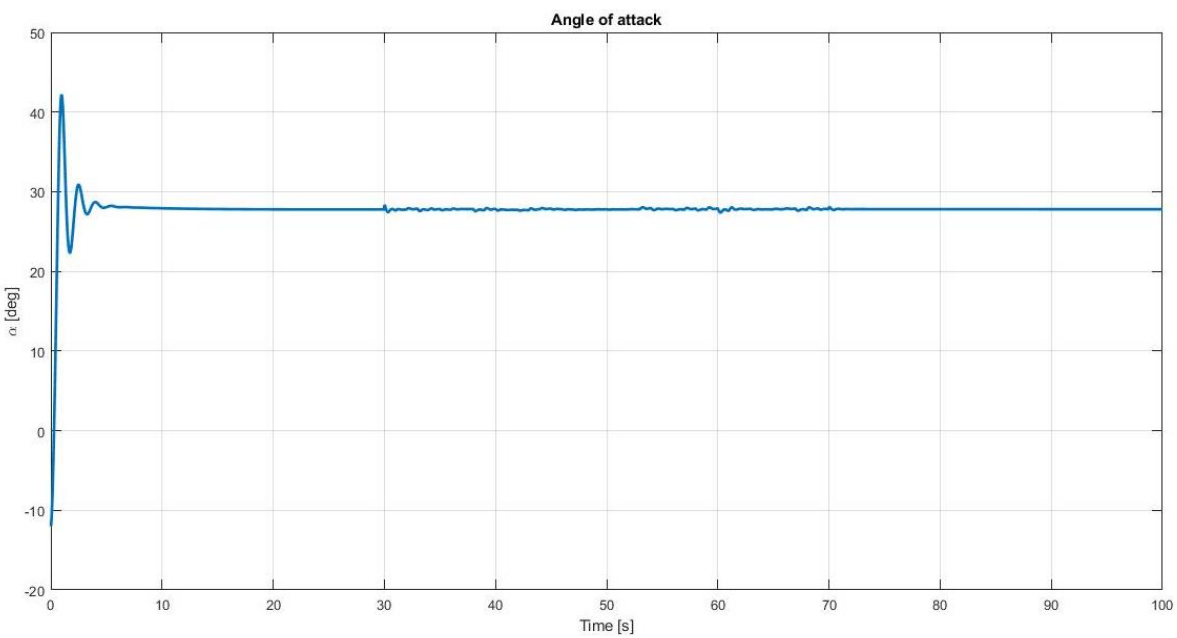

Figure 27: Angle of attack during a steady state descent affected by a 40s gust wind.

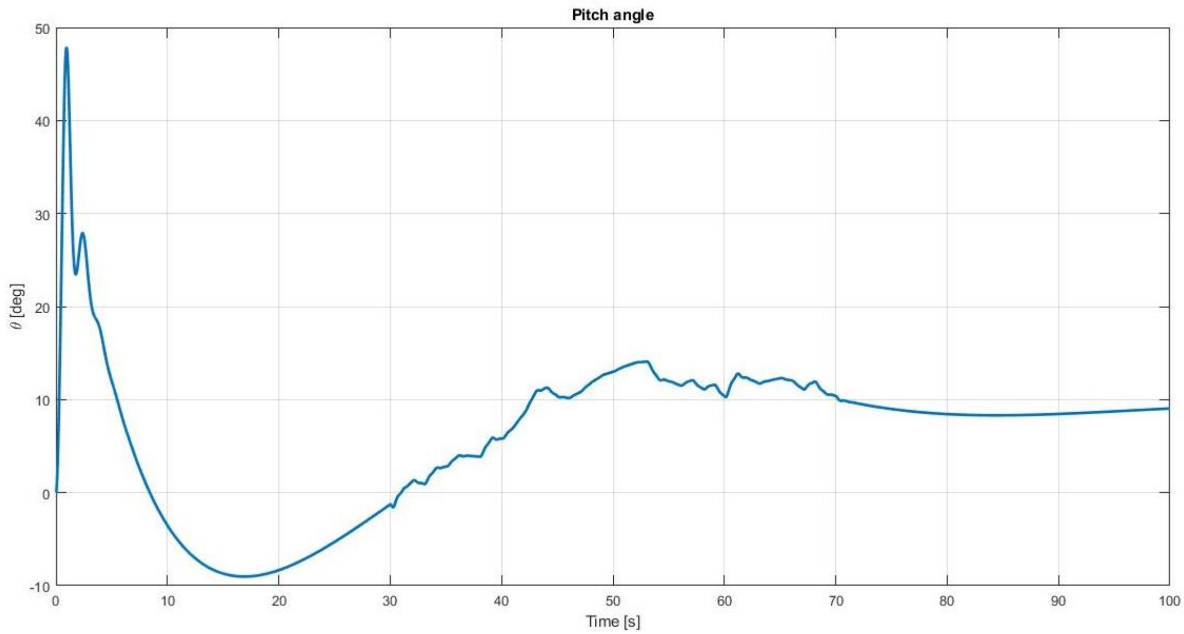

Figure 28: Pitch angle during a steady state descent affected by a 40s gust wind.

- Symmetrical deflection of the trailing edge (TE): the flare maneuver consists in the symmetric deflection of the parafoil brake. The control enables to boost the downrange increasing the angle of attack.

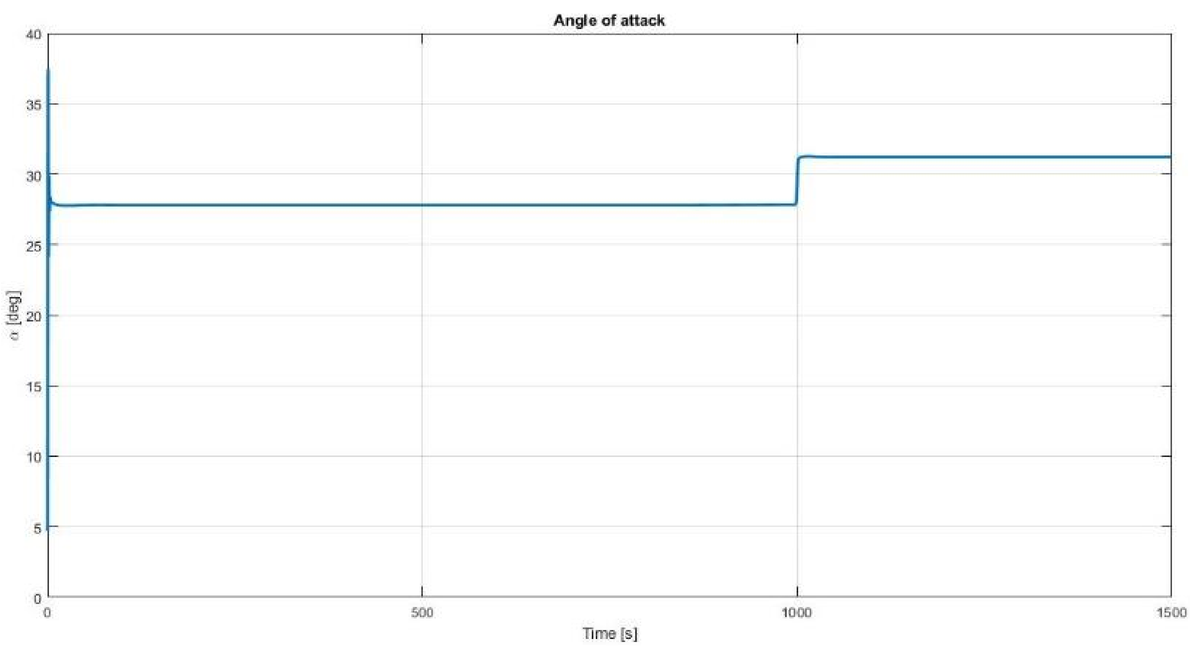

Figure 29: Angle of attack with symmetric trailing edge deflection ($\delta_s = 0.5 * delta_{max}$).

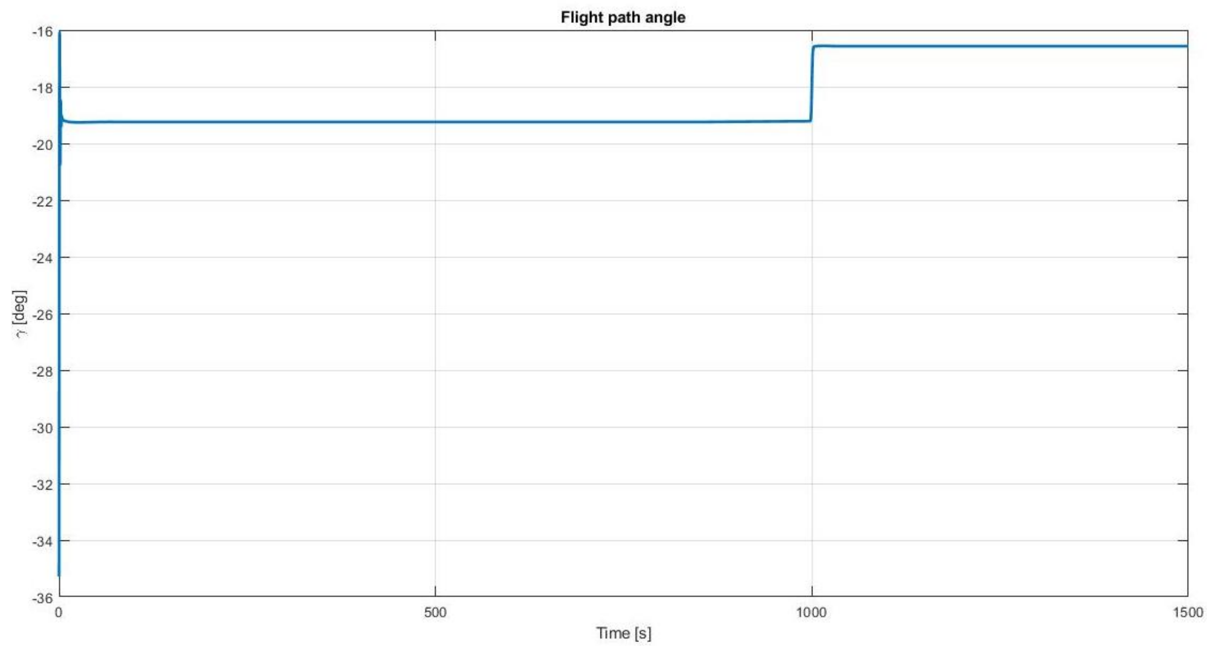

Figure 30: Flight-path angle with symmetric trailing edge deflection ($\delta_s = 0.5 * delta_{max}$).

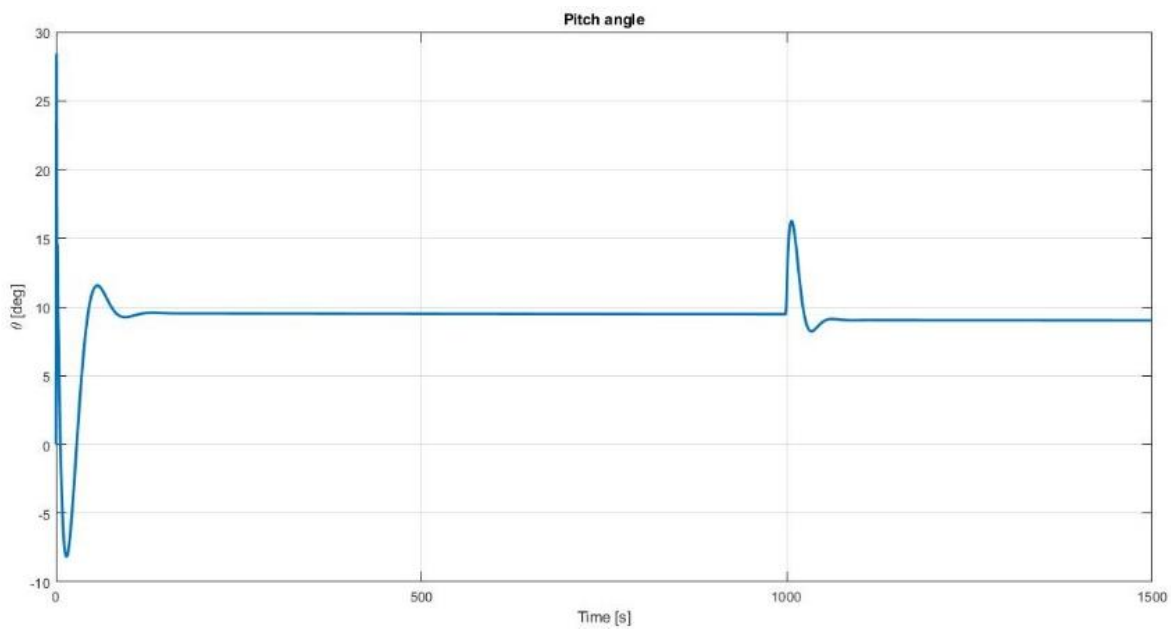

Figure 31: Pitch angle with symmetric trailing edge deflection ($\delta_s = 0.5 * delta_{max}$).

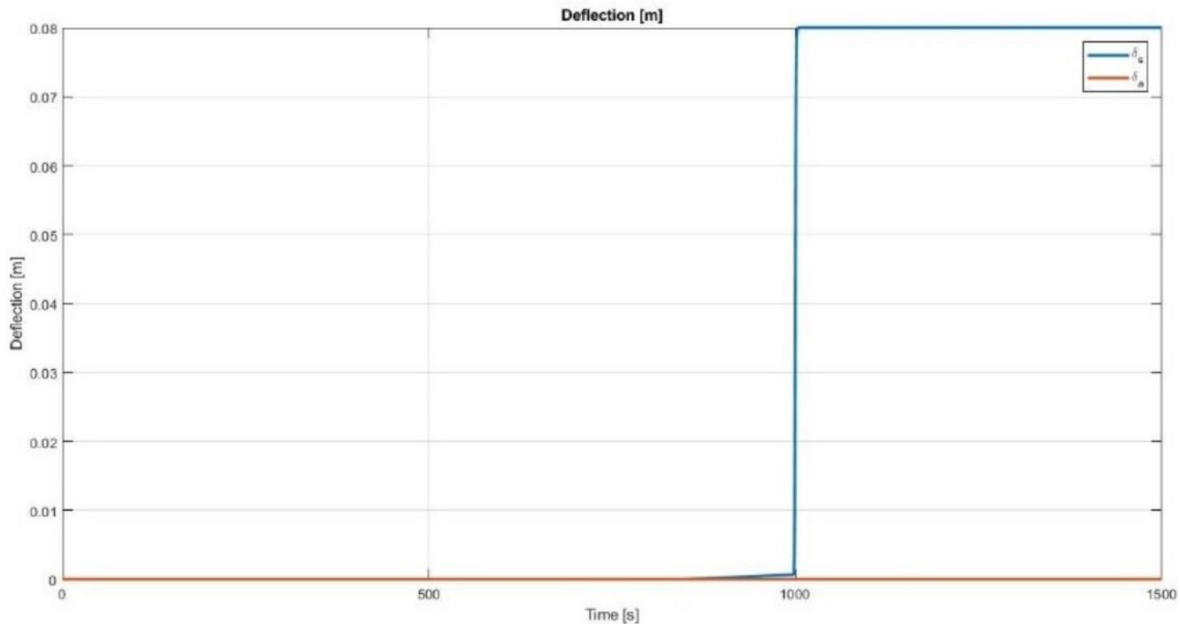

Figure 32: Trailing edge symmetric deflection.

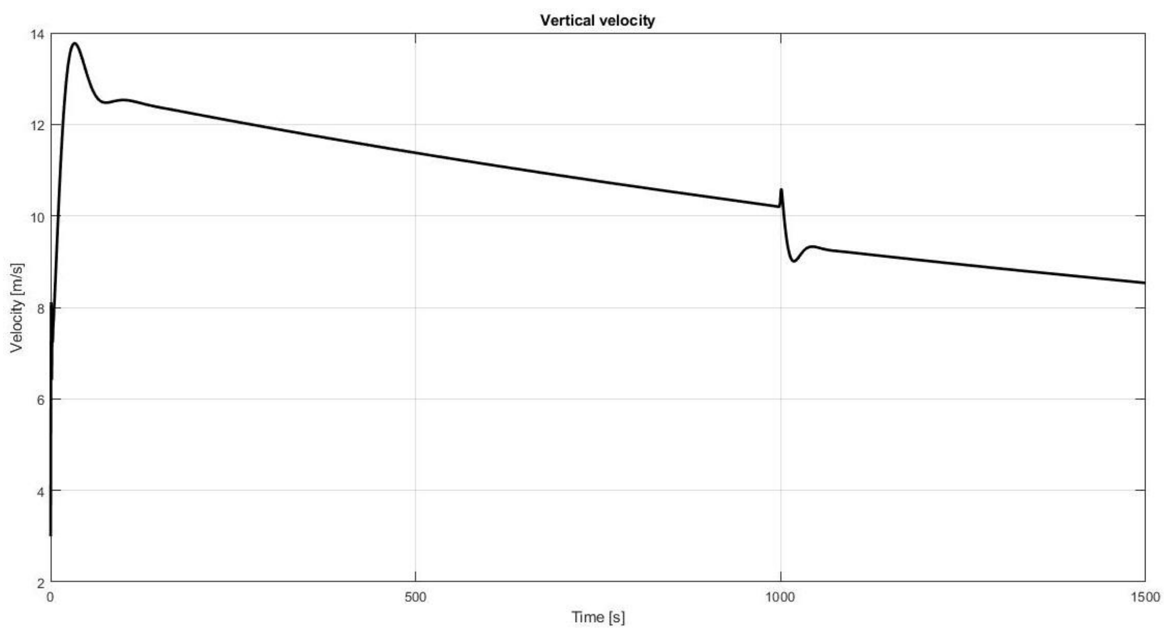

Figure 33: Vertical velocity with symmetric trailing edge deflection ($\delta_s = 0.5 * delta_{max}$).

- Asymmetric trailing edge deflection: in those simulations a long asymmetric control is given to the parafoil. The result is a stable descending spiral. During a true control the command is small in time (few seconds) to adjust the trajectory. However, sometimes one or two spiral envelopes are needed during the energy management phase. Therefore, it is important to study the characteristics of a long TE δ_a command.

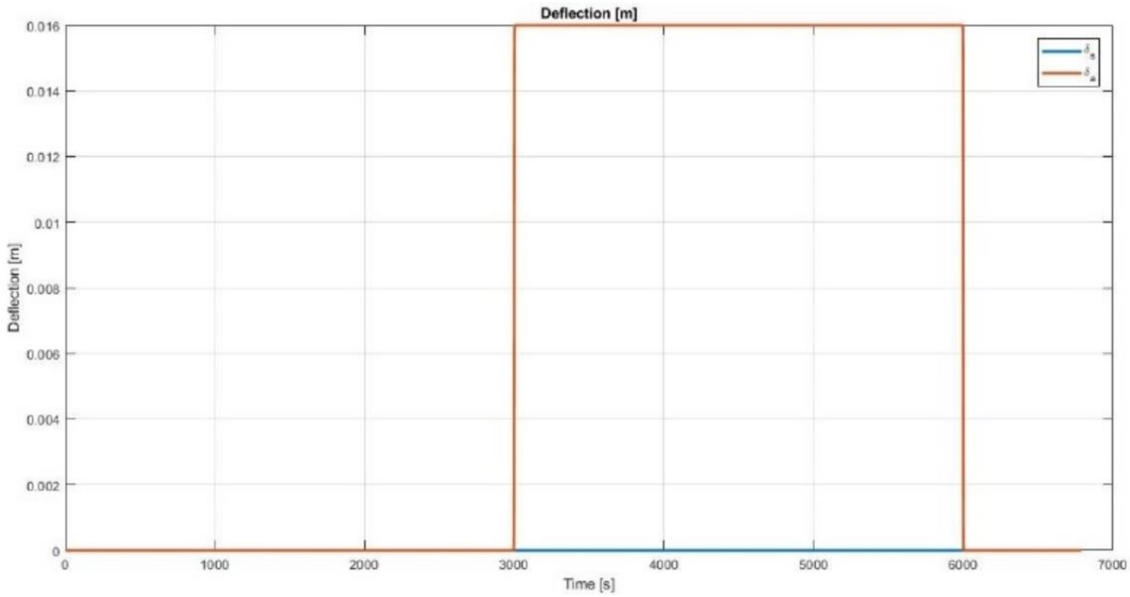

Figure 34: Small and long-time-duration asymmetric deflection ($\delta_a = 0.1 * delta_{max}$)

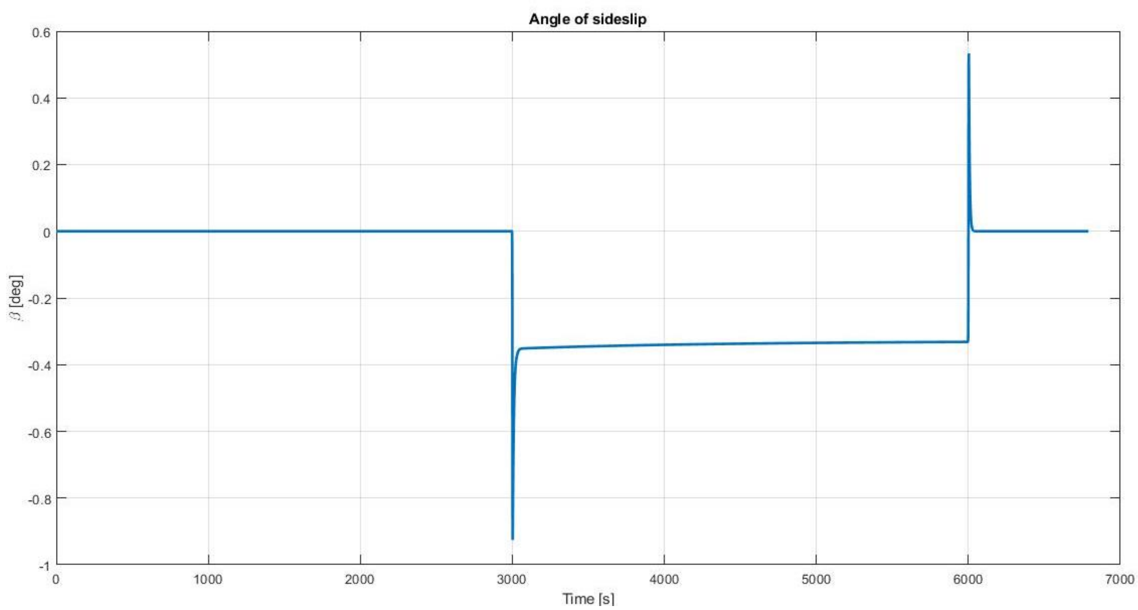

Figure 35: Angle of sideslip during an asymmetric TE deflection.

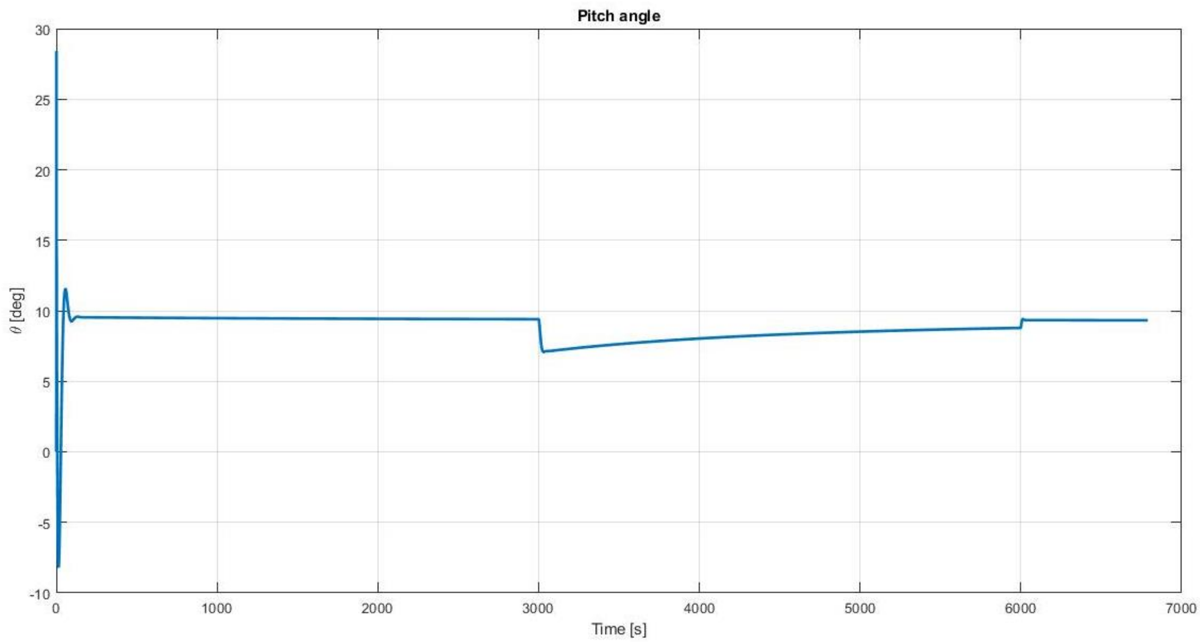

Figure 36: Pitch angle during an asymmetric TE deflection.

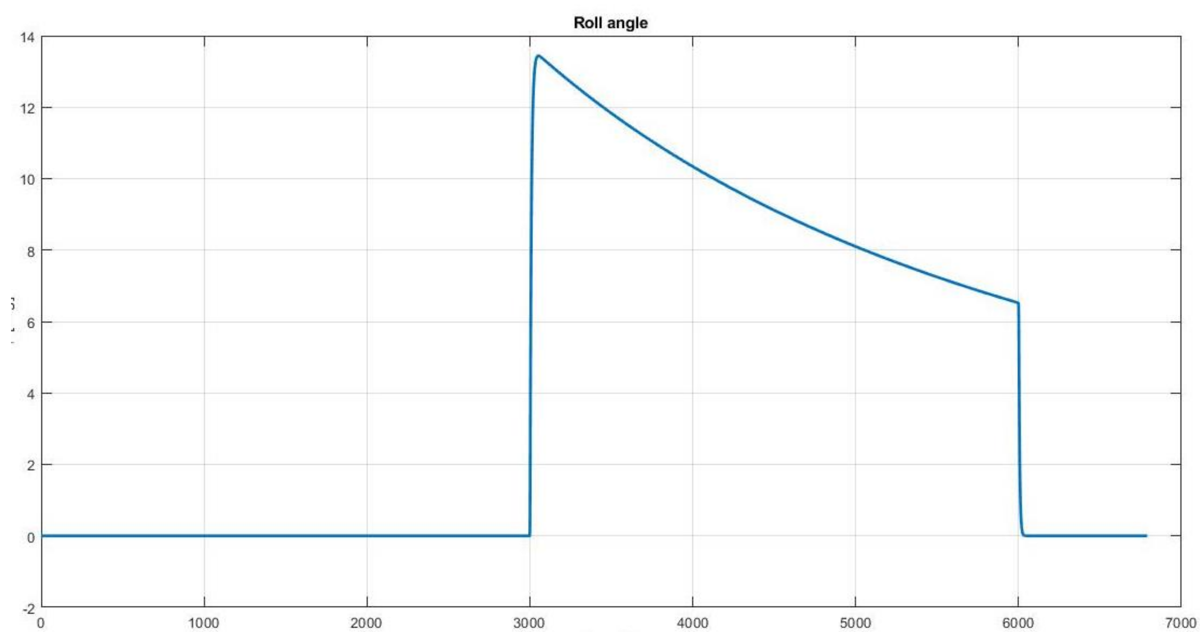

Figure 37: Roll angle during an asymmetric TE deflection.

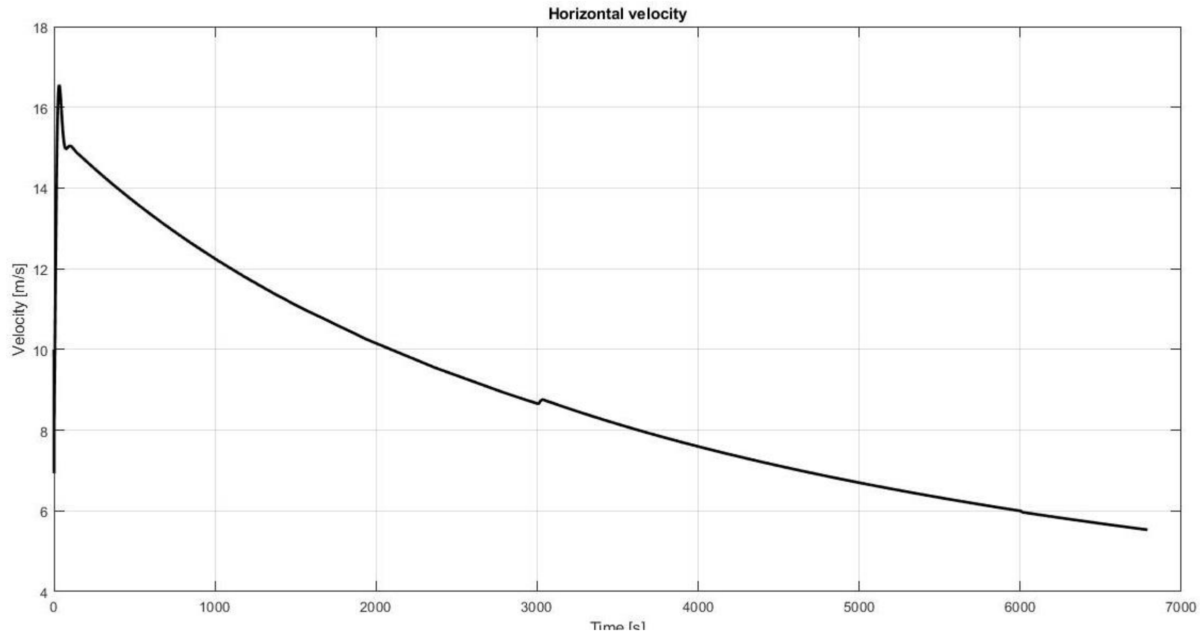

Figure 38: Horizontal velocity during an asymmetric TE deflection.

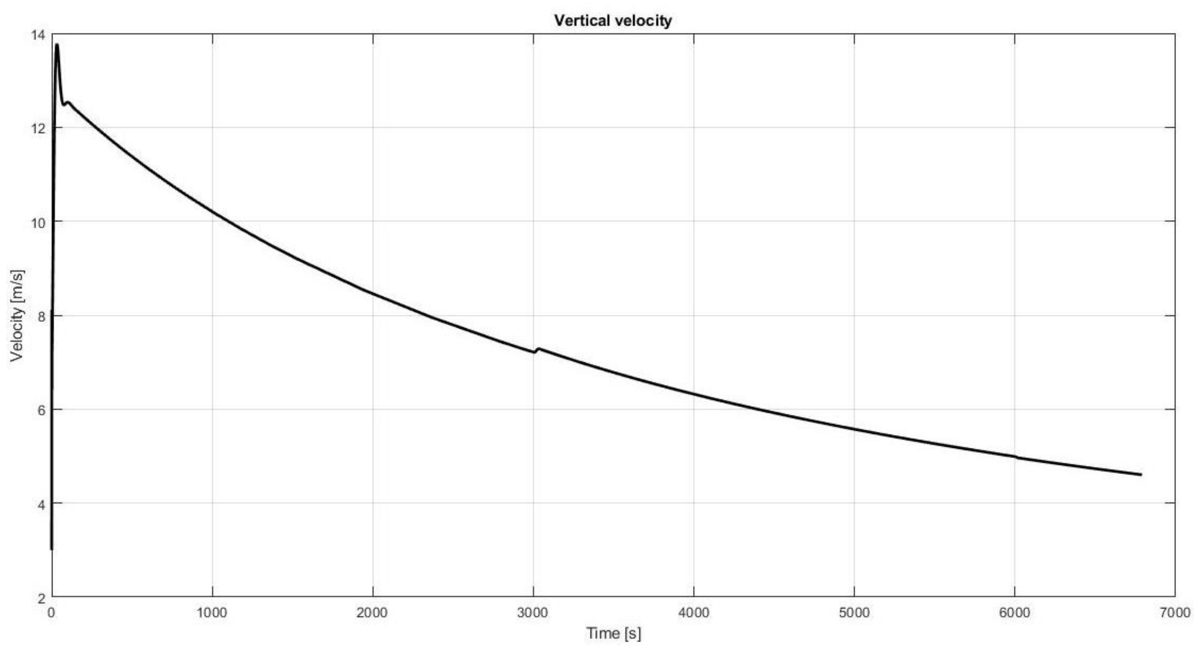

Figure 39: vertical velocity during an asymmetric TE deflection.

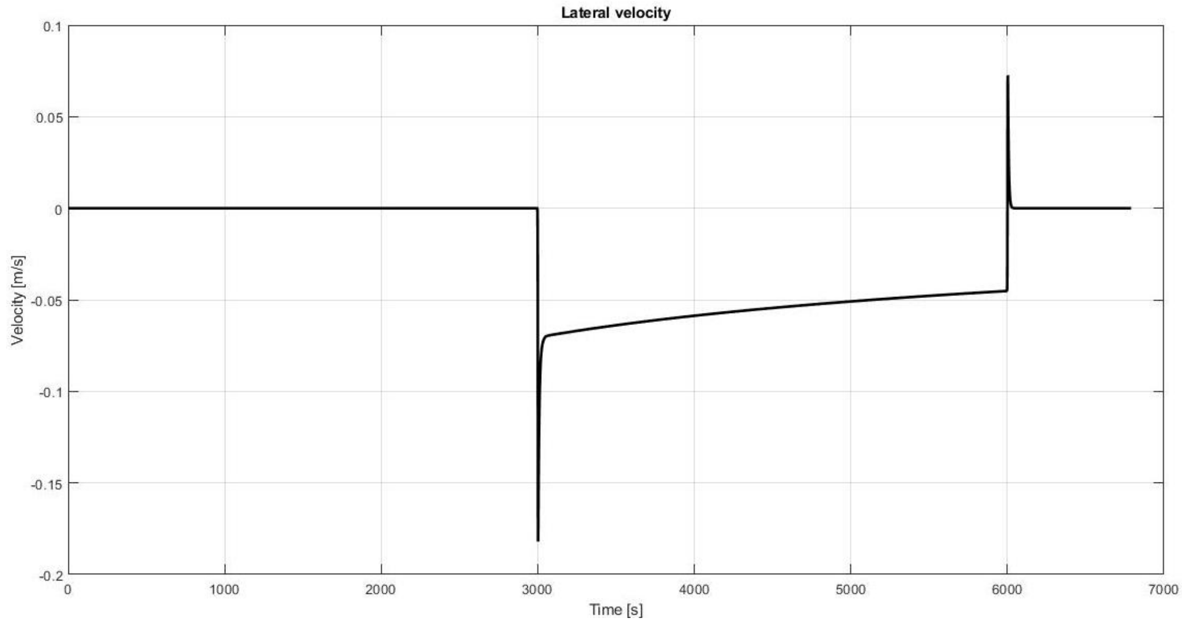

Figure 40: Lateral velocity during an asymmetric TE deflection.

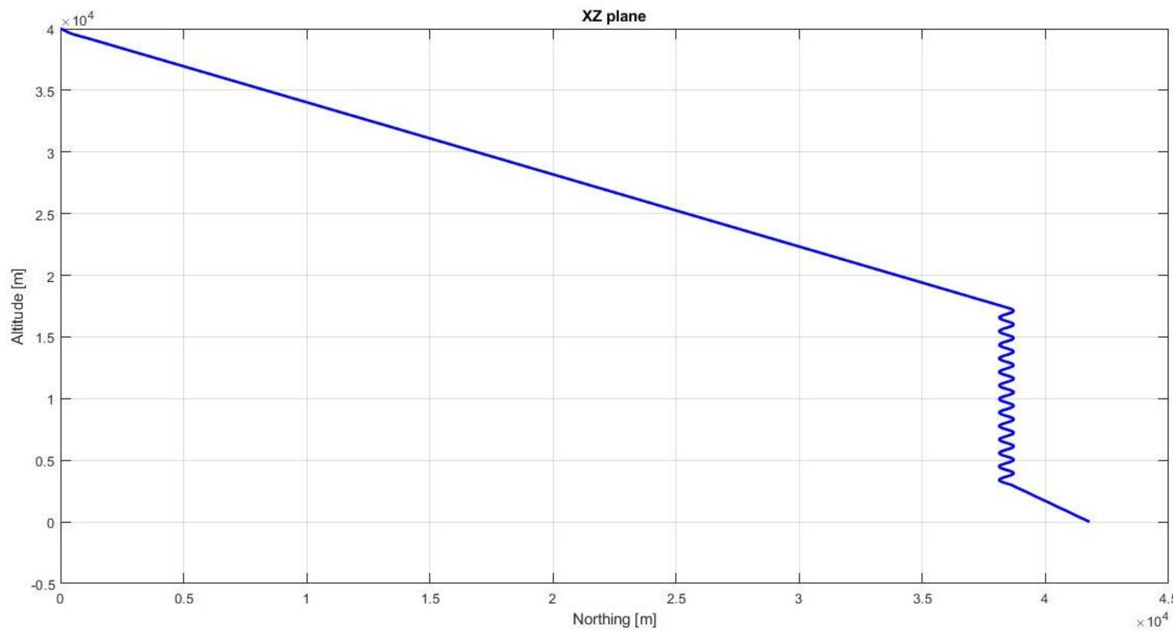

Figure 41: Descending parafoil trajectory during an asymmetric TE deflection.

- An S-maneuver is a typical control given to the parafoil, hence those more realistic results will be presented. In this last case the simulation will start at 1000 m to analyze the maneuver in a high-density atmosphere ($\rho_{Titan\ surface} \cong 5.43\ kg/m^3$)

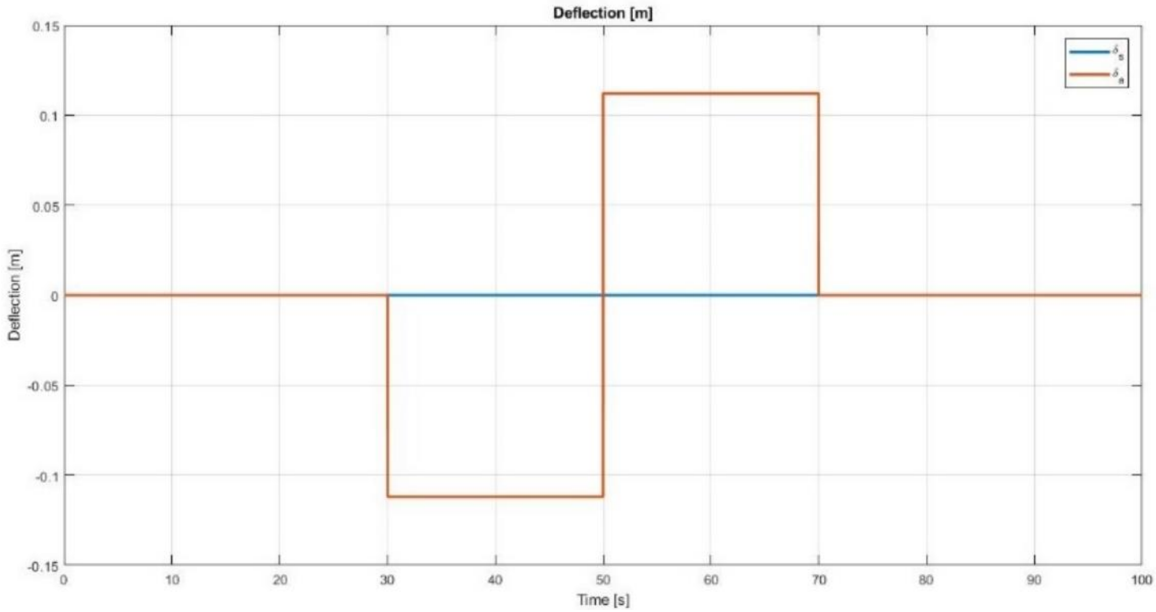

Figure 42: S-maneuver asymmetric TE deflection ($\delta_a = \pm 0.7 * delta_{max}$)

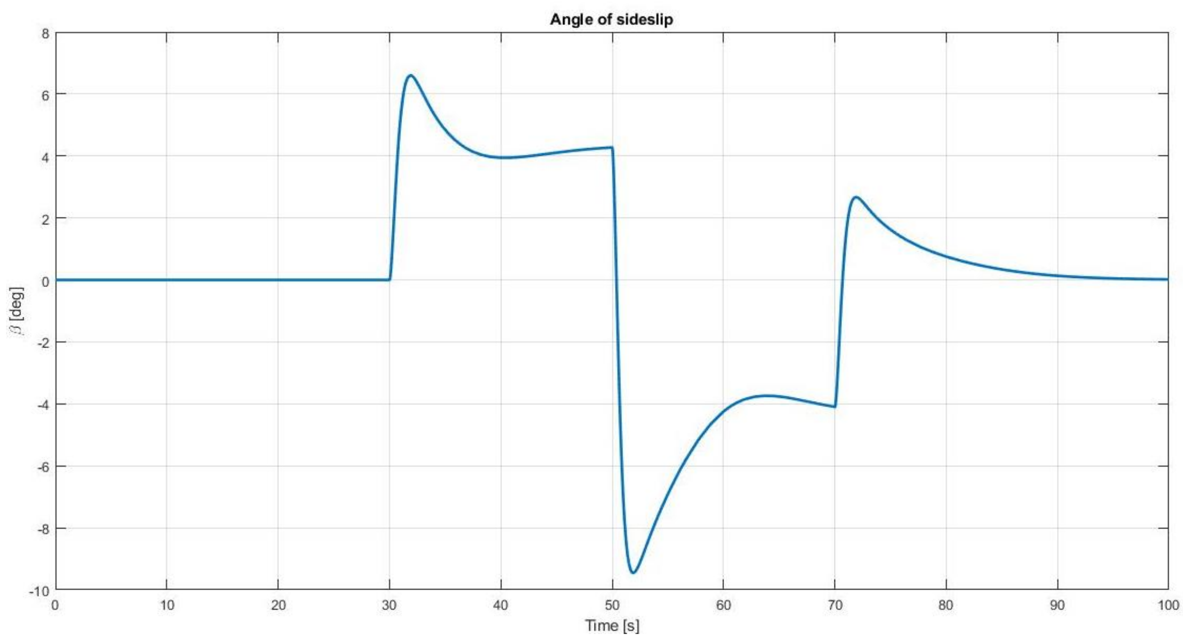

Figure 43: Angle of sideslip during the S-maneuver.

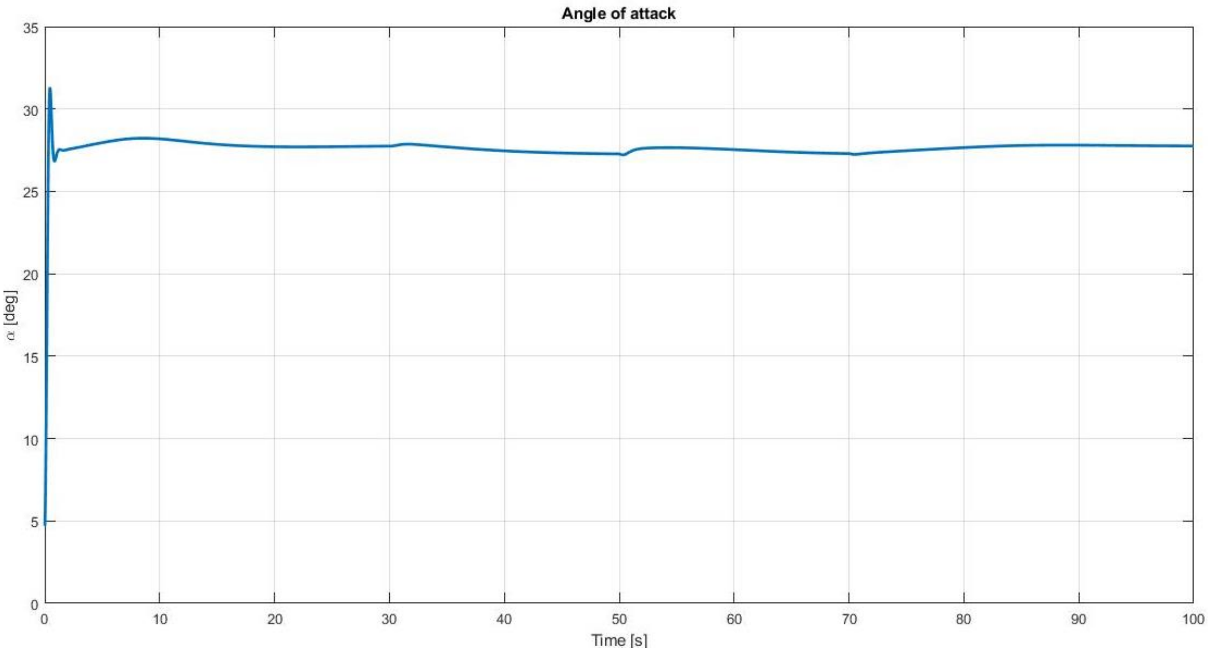

Figure 44: Angle of attack during the S-maneuver.

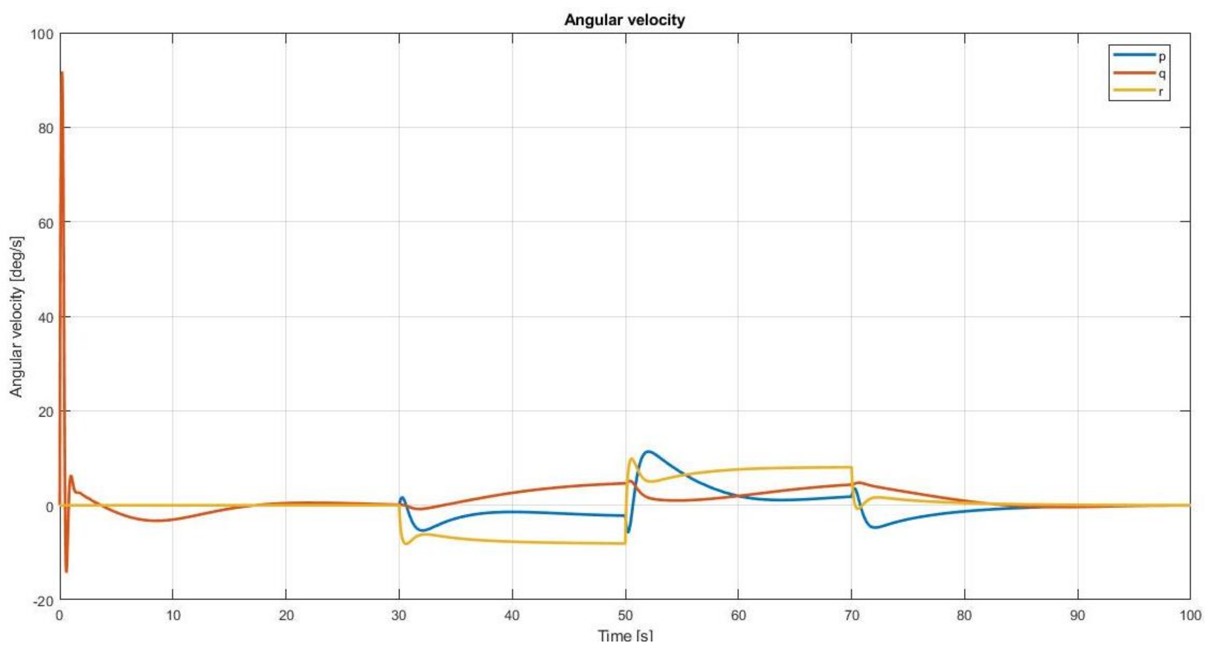

Figure 45: Angular velocity during an S-maneuver.

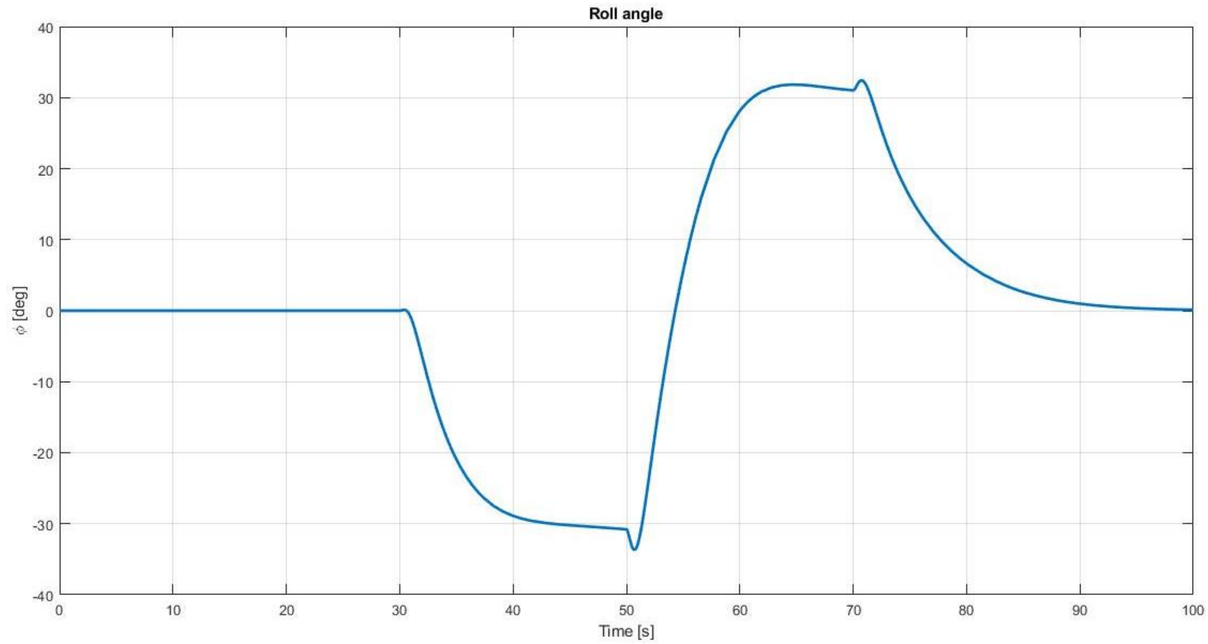

Figure 46: Roll angle during an S-maneuver.

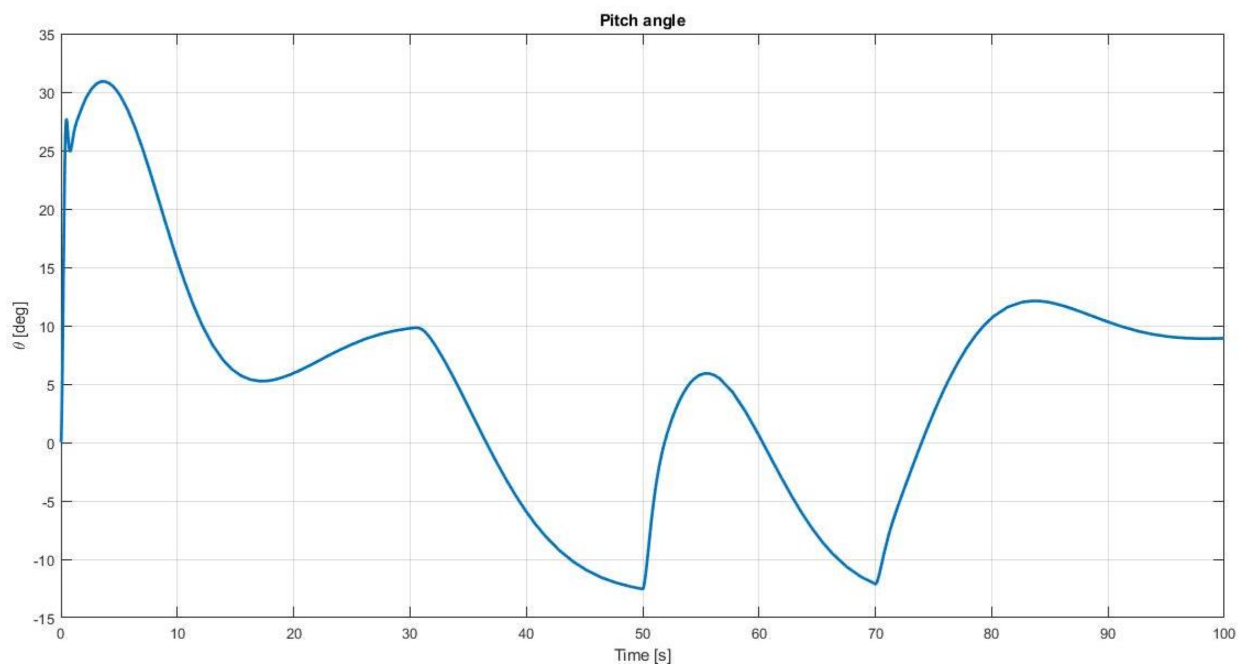

Figure 47: Pitch angle during an S-maneuver.

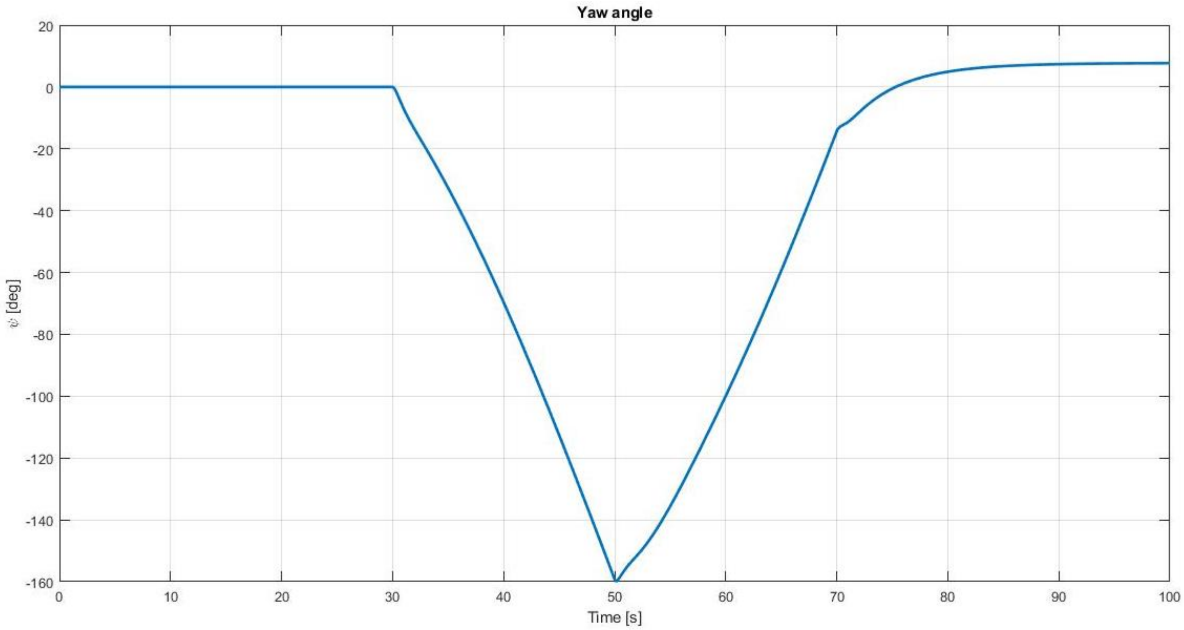

Figure 48: Yaw angle during an S-maneuver.

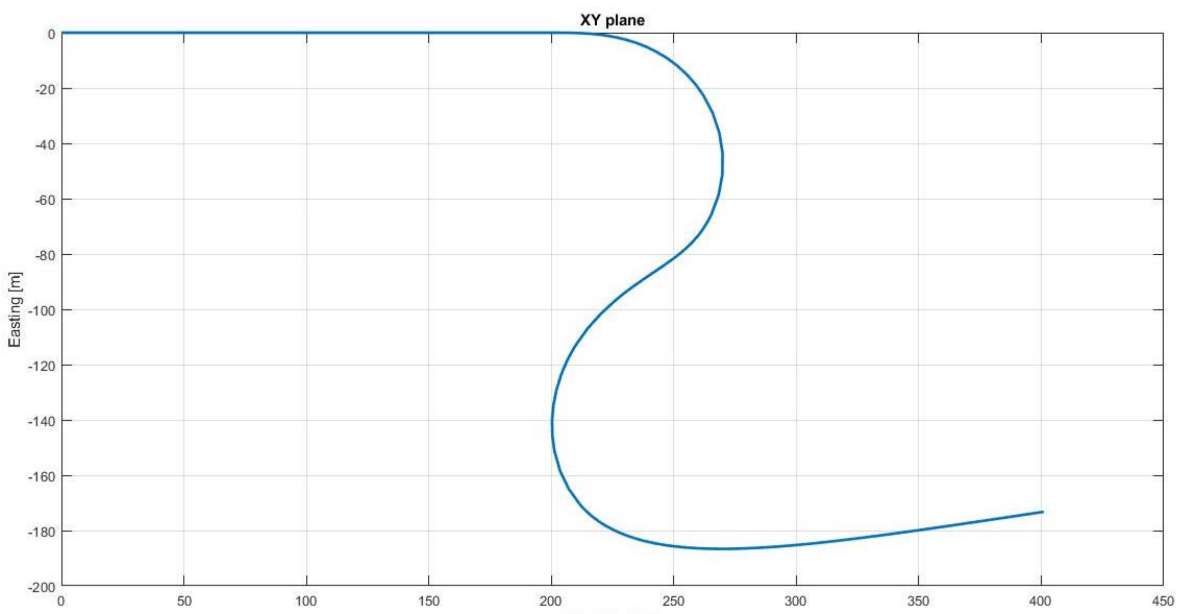

Figure 49: On-plane trajectory during an S-maneuver.

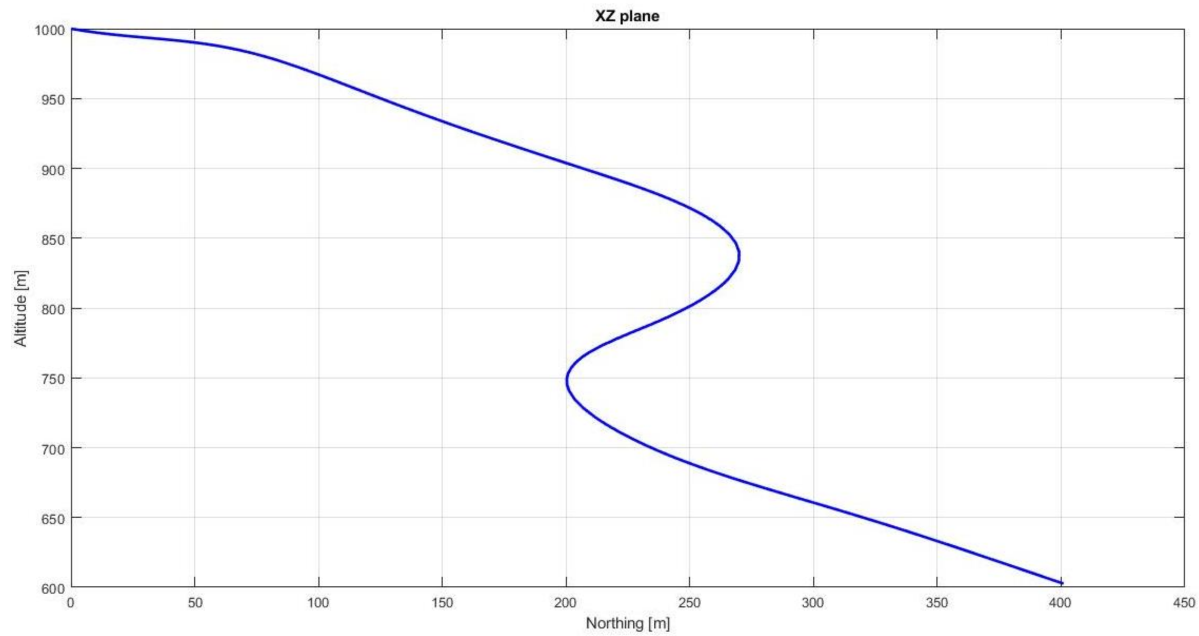

Figure 50: Descending trajectory during an S-maneuver.

3.4 PADs STABILITY

The parafoils is an inherently stable system, both longitudinal and latero-directional modes are stable, negative real part of the state matrix eigenvalues. Usually they don't need any stability augmentation system, their dynamics is slow and winds disturbance is kept in account during the motion planning. To study the stability of a system we need to linearize the equation of motion and express them in steady-state form:

$$\{\dot{\boldsymbol{x}}\} = [\boldsymbol{A}]\{\boldsymbol{x}\} + [\boldsymbol{B}]\{\boldsymbol{u}\} \qquad \{\boldsymbol{y}\} = [\boldsymbol{C}]\{\boldsymbol{x}\} \tag{3.56}$$

Where $\{\boldsymbol{x}\} = \{u, v, w, p, q, r\}'$ is the state vector, $[\boldsymbol{A}]_{\boldsymbol{6x6}}$ is the state matrix, $\{\boldsymbol{u}\} = \{\delta_s, \delta_a\}'$ is the control input vector, $[\boldsymbol{B}]_{\boldsymbol{6x2}}$ is the control matrix, $\{\boldsymbol{y}\}$ is the output vector and $[\boldsymbol{C}]_{\boldsymbol{3x6}}$ is the output matrix. The linearization has been performed evaluating the state and control matrices during trimmed steady state condition (trim point).
For the equilibrium

$$\{\dot{\boldsymbol{x}}\} = \boldsymbol{f}(\boldsymbol{x}, \boldsymbol{u}) = \boldsymbol{f}(\boldsymbol{x_0}, \boldsymbol{u_0}) = \boldsymbol{0} \tag{3.57}$$

Introducing the small perturbation theory and the Jacobian matrix, we can write:

$$\{\boldsymbol{\delta\dot{x}}\} = \boldsymbol{f}_{,\boldsymbol{x}}(\boldsymbol{x_0}, \boldsymbol{u_0}) * \{\boldsymbol{\delta x}\} + \boldsymbol{f}_{,\boldsymbol{u}}(\boldsymbol{x_0}, \boldsymbol{u_0}) * \{\boldsymbol{\delta u}\} = [\boldsymbol{A}]\{\boldsymbol{x}\} + [\boldsymbol{B}]\{\boldsymbol{u}\} \tag{3.58}$$

$$
\boldsymbol{f}_{,\boldsymbol{x}} = \begin{bmatrix} \frac{\partial f_1}{\partial x_1} & \cdots & \frac{\partial f_1}{\partial x_n} \\ \vdots & \ddots & \vdots \\ \frac{\partial f_n}{\partial x_1} & \cdots & \frac{\partial f_n}{\partial x_n} \end{bmatrix} \tag{3.59}
$$

The output matrix is usually built at doc for the performance we want to analyze. For the stability analysis only the state equation is needed. The linearization is performed with MATLAB symbolic toolbox.

The analysis is performed at a trim condition at 30 km from ground with a density of $1.2\ \mathrm{kg/m^3}$: to compare the results from the PADs that fly on Earth environment we need a comparable density. At ground level, where $\rho = 5.43\ \mathrm{kg/m^3}$ the phugoid mode disappears.

$$
\begin{gathered}
\{\boldsymbol{x_0}\} = \{u_0\ v_0\ w_0\ p_0\ q_0\ r_0\} = \{13.5\ 0\ 7.5\ 0\ 0\ 0\} \\
\{\boldsymbol{u_0}\} = \{\delta_s, \delta_a\} = \{0, 0\}\ (steady\ state\ performance) \\
\{\phi_0\ \theta_0\ \psi_0\ \} = \{0 - 3\deg\ 0\}
\end{gathered} \tag{3.60}
$$

Usually we split the longitudinal plane from the latero-directional plane to study the performance. The eigenvalues of **[A]** define the system dynamics properties:

Table 10: Parafoil dynamics proprieties on Titan.

Motion Mode	Eigenvalues	Period T [s]	Damping Ratio ξ
Short Period	-2.61±4.7i	1.3	0.49
Phugoid	-0.0855±0.004i	11	~1
Dutch Roll	-0.0715±0.145i	14	0.44
Roll Subsidence	-4.7	0.3	-
Spiral Mode	-3.8	0.2	-

The phugoid mode is highly damped: it depends on the exchange of potential and kinetic energy. The high damping can be related to the high altitude (30 km) and the relatively small airspeed velocity $V_a = 15\ m/s$ at that altitude. Lowering the altitude, the velocity keeps decreasing until the disappearance of the phugoid mode: we have two real values instead of two complex conjugates. This can be related to both the tiny pitch angle and modest velocity [13].

$$
m * g * h + \frac{1}{2} * m * v^2 = E_{tot} \tag{3.61}
$$

The linearize model can be used in the control analysis: we can define a transfer function and shape the signal to obtain the desired control. The only problem in our case is that the trajectory is very long (from 40 km to land) and the PADs will encounter different scenarios with a density changing from $0.7\ kg/m^3$ to $5.43\ kg/m^3$. We should create a routine that will continuously linearize the model based on the external conditions: however, the MATLAB toolbox can take up to 5/7 minutes to linearize around one point. An idea could be linearizing analytically the equations, but that takes time and can be tricky due to all the apparent mass terms to keep into account. In this preliminary study a simple proportional control is implemented in time domain without linearization.

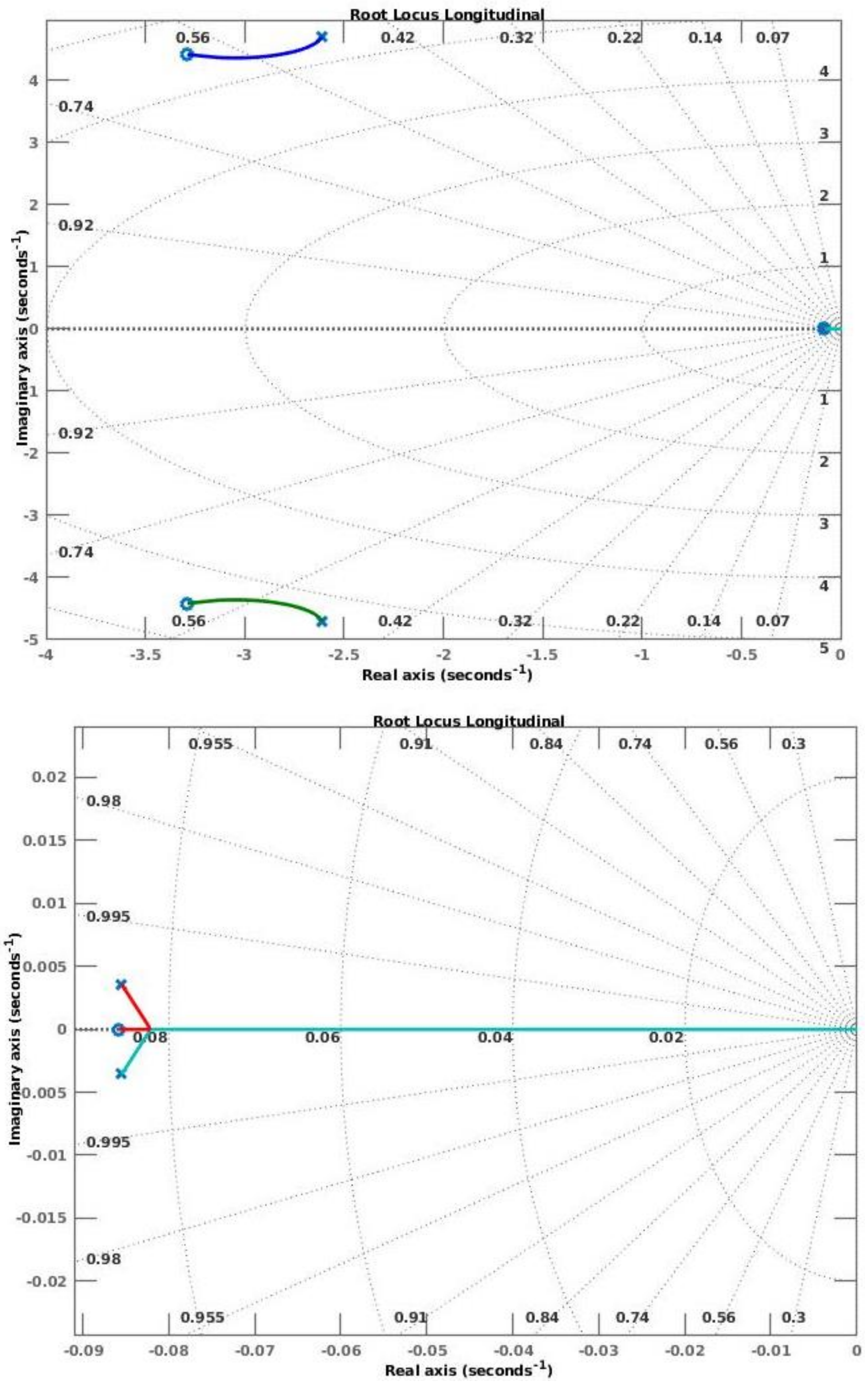

Figure 51: Longitudinal root locus with phugoid mode highlight

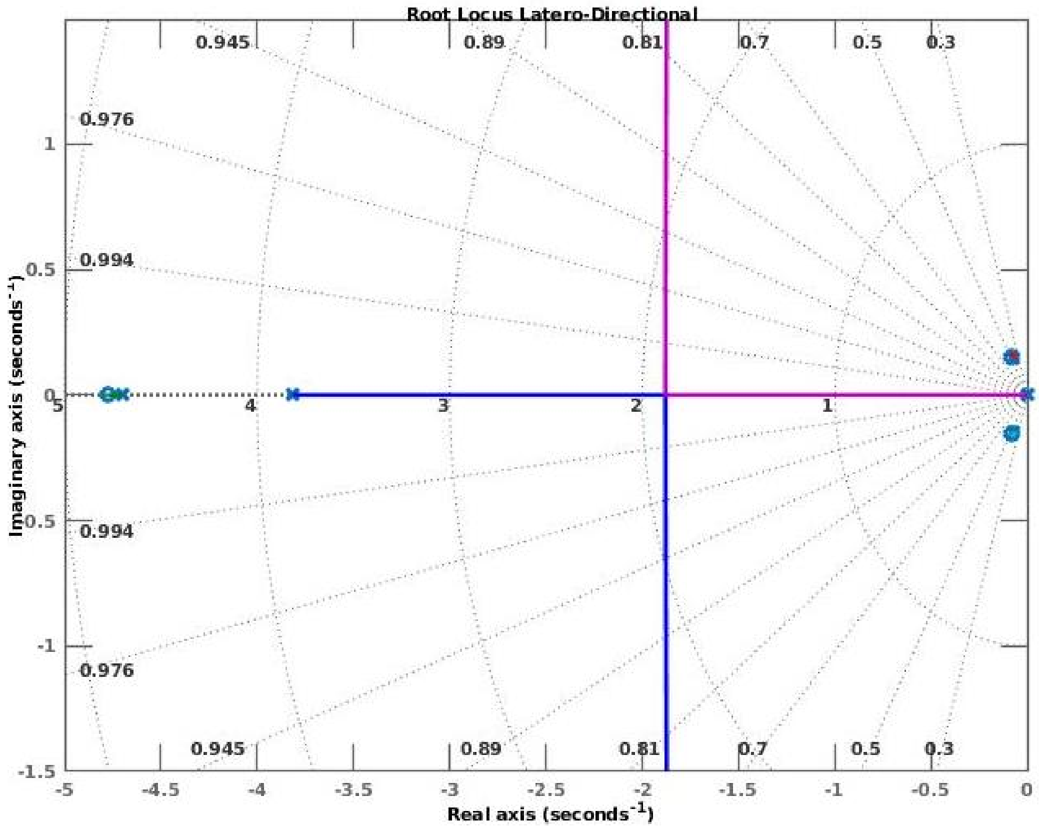

Figure 52: Lateral-directional root locus

3.5 MODEL VALIDATION

The model had been validated with Airborne data on Titan atmosphere and with the university “La Sapienza” (Rome) simulations on Earth environment. The Airborne data match quite perfectly with the 6 DOF results for a PADs with an efficiency $\left(\frac{L}{D}\right)$ of 2.1 with a steady state flight (Airborne is a JPL’s contractor for Titan mission, specialized in parafoils development).

We can match the trend of the data from [14], however we lack the knowledge of their initial conditions, so we can’t replicate the data exactly. Moreover, their control relies on the deflection angle of an ideal flap that simulate the parafoil bending at the trailing edge.

The simplified 6 DOF developed by [14] is not of our interest: to build it they have assumed apparent masses and inertias and aerodynamic force moments negligible. It will be reported just to draw analogous plots.

- Airborne Data

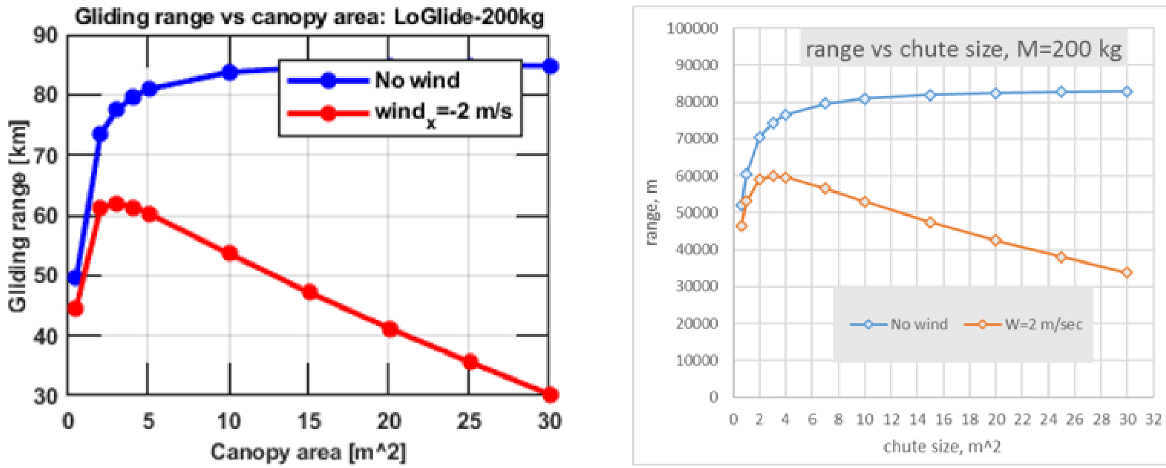

Figure 53: Airborne data comparison on Titan for a steady state descent with an efficiency of 2.1.

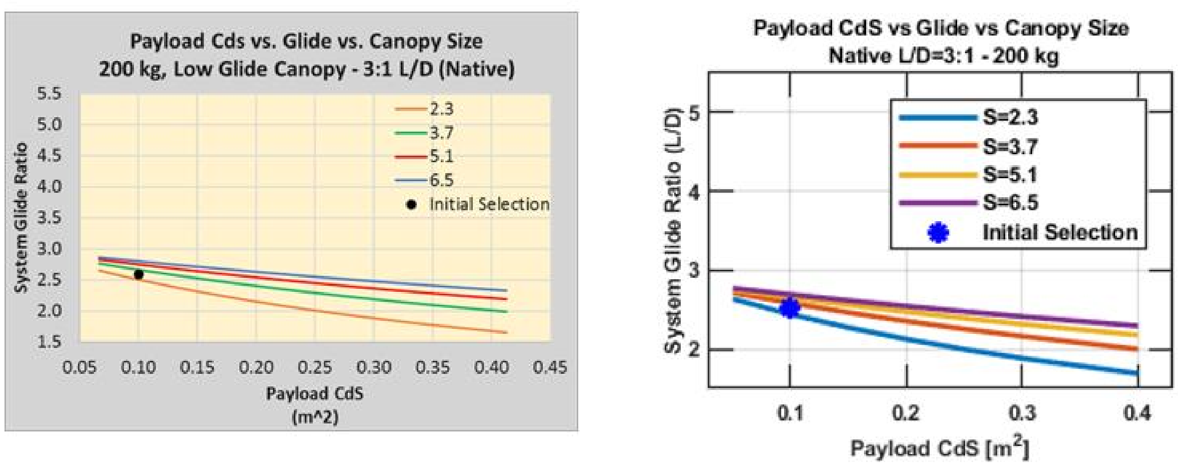

Figure 54: Payload drag surface vs efficiency vs canopy surface.

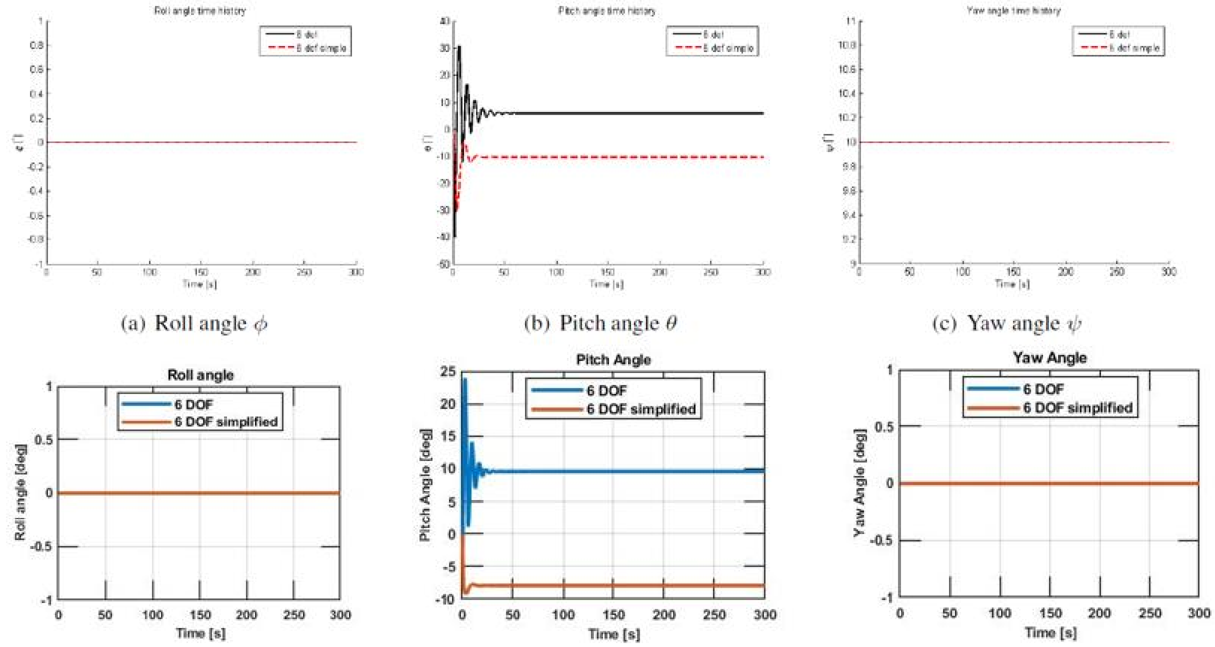

Figure 55: Results from "la Sapienza" (up) and from the JPL model (bottom).

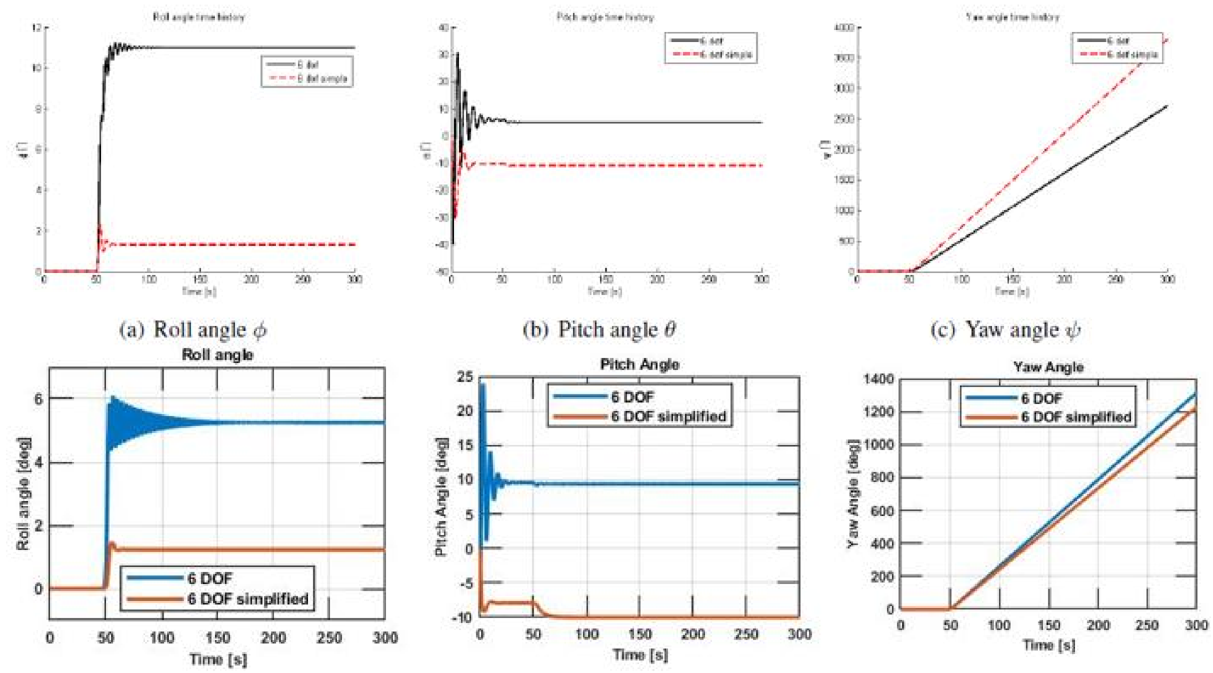

Figure 56: Results from "la Sapienza" (up) and from the JPL model (bottom).

4 PADs HIGH-FIDELITY MODEL: 7 DOF

The six degrees of freedom model could be used to simulate the overall dynamics of the PADs intended as parafoil and payload together. However, for many applications, like attitude control, it is important to understand the relative dynamics between parafoil and payload.

The number of degrees of freedom of this high-fidelity models varies with the type of rising connection between payload and parafoil. The 7 DOF model has the two PADs components linked in a fashion that permit only one relative degree of freedom for the payload, a relative yaw. This relative yaw creates disturbs on the other two angular relative motions, pitch and roll, that can be seen in the plots in the simulation section.

We have created all the range of possible high-fidelity models to ensure us a good understanding of each possible higher fidelity model that Airborne can develop. Studies are still performed to adapt the high-fidelity models to a “multibody dynamics” as defined in Kane’s “Dynamics: Theory and Application”. The study performed for the 7, 8, 9 DOF is derived from [8]: the equations of motion follow the “rigid-body” formulation. In the “connection point” the parafoil and payload exchange forces and moments that are modelled in the equations of motions. This formulation permits to detach the payload motion in respect of the parafoil one and analyze its typical oscillator behavior. The mathematical definition will be fully reported because there are some differences and improvements from [8].

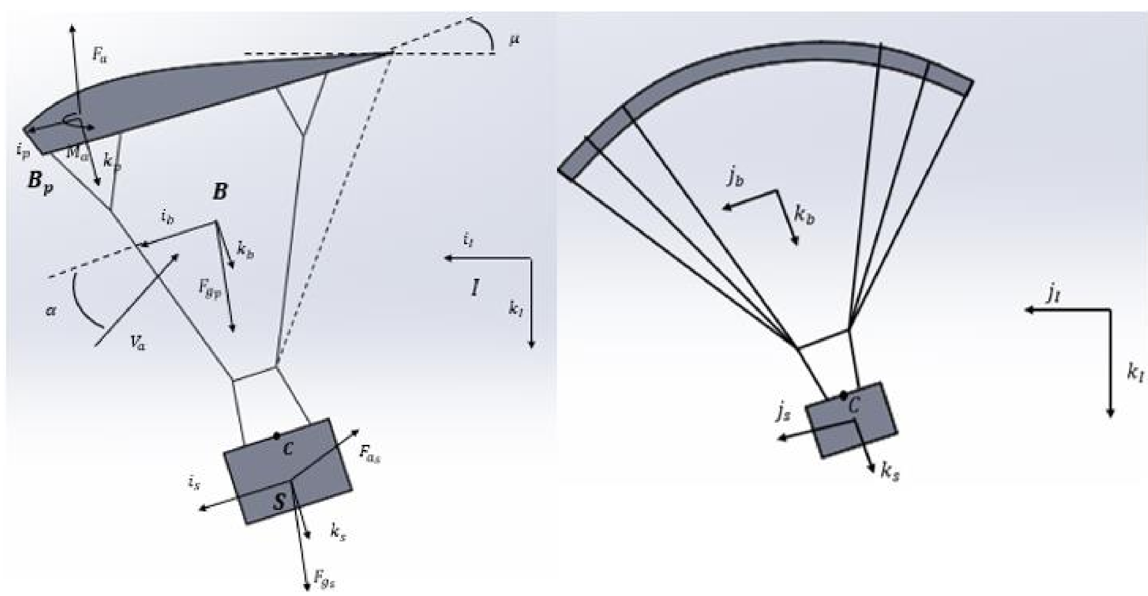

Figure 57: 7 DOF parafoil-payload connection.

4.1 PAYLOAD CONSTRAINED ROTATIONAL KINEMATICS

The relative angular motion of the payload in respect of the parafoil $\omega^s_{s/b}$, expressed in the parafoil reference system {s}, can be written as:

$$\boldsymbol{\omega^s_{s/b}} = \boldsymbol{\omega^s_s} - \boldsymbol{R_{sb}} * \boldsymbol{\omega_p} = \boldsymbol{R_{\psi_s}} * \begin{bmatrix} 0 \\ 0 \\ \dot{\psi}_s \end{bmatrix} = \begin{bmatrix} \cos(\psi_s) & \sin(\psi_s) & 0 \\ -\sin(\psi_s) & \cos(\psi_s) & 0 \\ 0 & 0 & 1 \end{bmatrix} * \begin{bmatrix} 0 \\ 0 \\ \dot{\psi}_s \end{bmatrix} \tag{4.1}$$

$$\boldsymbol{\omega_s} = \begin{bmatrix} p_s \\ q_s \\ r_s \end{bmatrix}; \boldsymbol{\omega_p} = \begin{bmatrix} p_p \\ q_p \\ r_p \end{bmatrix} \tag{4.2}$$

$$\boldsymbol{R_{sb}} = \begin{bmatrix} \cos(\psi_s) * \cos(\theta_s) & \sin(\psi_s) * \cos(\theta_s) & -\sin(\theta_s) \\ \cos(\psi_s) * \sin(\theta_s) * \sin(\phi_s) - \sin(\psi_s) * \cos(\phi_s) & \sin(\psi_s) * \sin(\theta_s) * \sin(\phi_s) + \cos(\psi_s) * \cos(\phi_s) & \cos(\theta_s) * \sin(\\ \cos(\psi_s) * \sin(\theta_s) * \cos(\phi_s) + \sin(\psi_s) * \sin(\phi_s) & \sin(\psi_s) * \sin(\theta_s) * \cos(\theta_s) - \cos(\psi_s) * \sin(\theta_s) & \cos(\theta_s) * \cos(\end{bmatrix} \tag{4.3}$$

With R_{sb} is the rotation matrix from parafoil body $\{b_p\}$ system of reference to payload {s} frame defined by three Euler angles ϕ_s, θ_s, ψ_s. The payload has one "free" relative yaw motion.

$$\begin{bmatrix} 0 \\ 0 \\ r_s \end{bmatrix} - \boldsymbol{R_{sb}} * \begin{bmatrix} p_p \\ q_p \\ r_p \end{bmatrix} = \begin{bmatrix} -1 & 0 & 0 \\ 0 & -1 & 0 \\ 0 & 0 & 1 \end{bmatrix} * \begin{bmatrix} p_s \\ q_s \\ r_s \end{bmatrix} \tag{4.4}$$

$$\begin{bmatrix} p_s \\ q_s \\ r_s \end{bmatrix} = \begin{bmatrix} 0 \\ 0 \\ \dot{\psi}_s \end{bmatrix} + \begin{bmatrix} \cos(\psi_s) & \sin(\psi_s) & 0 \\ -\sin(\psi_s) & \cos(\psi_s) & 0 \\ 0 & 0 & 1 \end{bmatrix} * \begin{bmatrix} p_p \\ q_p \\ r_p \end{bmatrix} \tag{4.5}$$

$$\begin{bmatrix} \dot{p}_s \\ \dot{q}_s \\ \dot{r}_s \end{bmatrix} = G + K_1 * \dot{r}_s + K_2 * \begin{bmatrix} \dot{p}_p \\ \dot{q}_p \\ \dot{r}_p \end{bmatrix} \tag{4.6}$$

$$\boldsymbol{G} = (r_s - r_p) * \begin{bmatrix} -\sin(\psi_s) & \cos(\psi_s) & 0 \\ -\cos(\psi_s) & -\sin(\psi_s) & 0 \\ 0 & 0 & 0 \end{bmatrix} * \begin{bmatrix} p \\ q \\ r \end{bmatrix} \tag{4.7}$$

$$\boldsymbol{K_1} = \begin{bmatrix} 0 \\ 0 \\ 1 \end{bmatrix} \tag{4.8}$$

$$\boldsymbol{K_2} = \begin{bmatrix} \cos(\psi_s) & \sin(\psi_s) & 0 \\ -\sin(\psi_s) & \cos(\psi_s) & 0 \end{bmatrix} \tag{4.9}$$

4.2 EQUATIONS OF MOTION

With equations (4.5) and (4.6), the 7 DOF model equations of motion can be written in a fashion similar to the 6 DOF ones (Chapter 3.1).

In the 7 DOF and 8 DOF models the moment acting on the parafoil-payload connection lines can be expressed as:

$$\boldsymbol{M_C} = \begin{bmatrix} 0 \\ 0 \\ M_{CZ} \end{bmatrix} + \boldsymbol{R_{sb}} * \begin{bmatrix} M_{CX} \\ M_{CY} \\ 0 \end{bmatrix} = \begin{bmatrix} 0 \\ 0 \\ M_{CZ} \end{bmatrix} + \boldsymbol{R_{sb}} * \begin{bmatrix} 1 & 0 \\ 0 & 1 \\ 0 & 0 \end{bmatrix} * \begin{bmatrix} M_{CX} \\ M_{CY} \end{bmatrix} = \begin{bmatrix} 0 \\ 0 \\ M_{CZ} \end{bmatrix} + \boldsymbol{R_{sb}} * \boldsymbol{E} * \begin{bmatrix} M_{CX} \\ M_{CY} \end{bmatrix} \tag{4.10}$$

$$M_{CZ} = -K_{\psi}(\psi_s) * \psi_s + K_r(\psi_s) * \dot{\psi}_s \tag{4.11}$$

The twisting moment M_{CZ} is modelled as a spring and damper mechanism, in which the coefficients K_{ψ} *and* K_r can widely vary from PADs to PADs. Sometimes a simplified line induced moment linked to the rising lines is introduced in the 9 DOF model as well, with a similar fashion of the one in equation (4.11) [15]. M_{CY} *and* M_{CX} are usually unknown and are introduced in the equation of motions: they are expressed in the parafoil body reference frame $\{b_p\}$. As well the forces exchanged between payload and parafoil ($\boldsymbol{F_c} = [F_{CX}, F_{CY}, F_{CZ}]'$) are expressed in the parafoil body reference frame.

The overall linear velocities are expressed in NED ($[\dot{x}\ \dot{y}\ \dot{z}]'$), they are derived in the parafoil-payload connection point C: $\boldsymbol{V_c} = [u_c\ v_c\ w_c]'$.

The parafoil angular velocities are expressed in the parafoil body reference frame $\{b_p\}$, the payload relative angular velocities are expressed in the payload reference frame {s}.

The first two equations are related to the parafoil motion, the last two to the payload relative motion.

The parafoil canopy is considered already inflated at the beginning of the simulation and it is considered as a rigid body with a certain inclination (rigging angle μ) and fixed distances ($\boldsymbol{r_{CB}}, \boldsymbol{r_{BM}}, \boldsymbol{r_{CS}}, \boldsymbol{r_{BA}}, \boldsymbol{r_{CM}}$).

The equations of motion for the 7 DOF can be written as:

$$\boldsymbol{A_{4x12}} * \boldsymbol{b_{12x1}} = \begin{bmatrix} \boldsymbol{F_p} \\ \boldsymbol{M_p} \\ \boldsymbol{F_s} \\ \boldsymbol{M_s} \end{bmatrix} \tag{4.12}$$

$$\boldsymbol{A_{4x12}} =$$

$$\begin{bmatrix} (m_p + m_e) * \boldsymbol{I_{3x3}} + \boldsymbol{M_f}' & -\boldsymbol{M}'_f * \boldsymbol{S}(\boldsymbol{r_{CM}}) - (m_p + m_e) * \boldsymbol{S}(\boldsymbol{r_{CB}}) & \boldsymbol{0_{3x1}} & -\boldsymbol{I_{3x3}} & \boldsymbol{0_{3x2}} \\ \boldsymbol{S}(\boldsymbol{r_{BM}}) * \boldsymbol{M}'_f & \boldsymbol{I_p} + \boldsymbol{I_f} - \boldsymbol{S}(\boldsymbol{r_{BM}}) * \boldsymbol{M}'_f * \boldsymbol{S}(\boldsymbol{r_{CM}}) & \boldsymbol{0_{3x1}} & \boldsymbol{S}(\boldsymbol{r_{CB}}) & \boldsymbol{E} \\ m_s * \boldsymbol{R_{sb}} & -m_s * \boldsymbol{S}(\boldsymbol{r_{CS}}) * \boldsymbol{K_2} & -m_s * \boldsymbol{S}(\boldsymbol{r_{CS}}) * \boldsymbol{K_1} & \boldsymbol{R_{sb}} & \boldsymbol{0_{3x2}} \\ \boldsymbol{0_{3x3}} & \boldsymbol{I_s} * \boldsymbol{K_2} & \boldsymbol{I_s} * \boldsymbol{K_1} & -\boldsymbol{S}(\boldsymbol{r_{CS}}) * \boldsymbol{R_{sb}} & -R_{sb} * E \end{bmatrix} \tag{4.13}$$

$$\boldsymbol{b}_{\boldsymbol{12x1}} = [\dot{u}_c \ \dot{v}_c \ \dot{w}_c \ \dot{p}_p \ \dot{q}_p \ \dot{r}_p \ \dot{r}_s \ F_{CX} \ F_{CY} \ F_{CZ} \ M_{CX} \ M_{CY}]' \tag{4.14}$$

$$\begin{aligned}\boldsymbol{F_p} &= \boldsymbol{F_a^p} + \boldsymbol{F_b^p} + \boldsymbol{F_g^p} \\ &-\boldsymbol{S}(\boldsymbol{\omega_p}) * \left[(m + m_e)\boldsymbol{I_{3x3}} + \boldsymbol{M_f'}\right] * \begin{bmatrix} u_c \\ v_c \\ w_c \end{bmatrix} + \boldsymbol{S}(\boldsymbol{\omega_p}) * \boldsymbol{M_f'} * \boldsymbol{S}(\boldsymbol{r_{CM}}) * \begin{bmatrix} p_p \\ q_p \\ r_p \end{bmatrix} + \boldsymbol{S}(\boldsymbol{\omega_p}) \\ &* \boldsymbol{M_f'} * \boldsymbol{R_{bn}} * \boldsymbol{W} - (m_p + m_e) * \boldsymbol{S}(\boldsymbol{\omega_p}) * \boldsymbol{S}(\boldsymbol{\omega_p}) * \boldsymbol{r_{CB}}\end{aligned} \tag{4.15}$$

$$\begin{aligned}\boldsymbol{M_p} &= \boldsymbol{M_a} + \boldsymbol{M_b^p} + \boldsymbol{S}(\boldsymbol{r_{BA}}) * \boldsymbol{F_a^p} - \begin{bmatrix} 0 \\ 0 \\ M_{CZ} \end{bmatrix} \\ &- \left[\boldsymbol{S}(\boldsymbol{\omega_p}) * (\boldsymbol{I_p} + \boldsymbol{I_f'}) - \boldsymbol{S}(\boldsymbol{r_{BM}}) * \boldsymbol{S}(\boldsymbol{\omega_p}) * \boldsymbol{M_f'} * \boldsymbol{S}(\boldsymbol{r_{CM}})\right] * \begin{bmatrix} \boldsymbol{p_p} \\ \boldsymbol{q_p} \\ \boldsymbol{r_p} \end{bmatrix} \\ &- \boldsymbol{S}(\boldsymbol{r_{BM}}) * \boldsymbol{S}(\boldsymbol{\omega_p}) * \boldsymbol{M_f'} * \begin{bmatrix} u_c \\ v_c \\ w_c \end{bmatrix} + \boldsymbol{S}(\boldsymbol{r_{BM}}) * \boldsymbol{S}(\boldsymbol{\omega_p}) * \boldsymbol{M_f'} * \boldsymbol{R_{bn}} * \boldsymbol{W}\end{aligned} \tag{4.16}$$

$$\begin{aligned}\boldsymbol{F_s} &= \boldsymbol{F_a^s} + \boldsymbol{F_g^s} + m_s * \boldsymbol{S}(\boldsymbol{r_{CS}}) * \boldsymbol{G} - m_s * \boldsymbol{R_{bs}} * \boldsymbol{S}(\boldsymbol{\omega_p}) * \begin{bmatrix} u_c \\ v_c \\ w_c \end{bmatrix} - m_s * \boldsymbol{S}(\boldsymbol{\omega_s}) \\ &* \boldsymbol{S}(\boldsymbol{\omega_s}) * \boldsymbol{r_{CS}}\end{aligned} \tag{4.17}$$

$$\boldsymbol{M_s} = -\boldsymbol{I_s}\boldsymbol{G} + \boldsymbol{R_{sb}} * \boldsymbol{M_c} - \boldsymbol{S}(\boldsymbol{\omega_s}) * \boldsymbol{I_s} * \begin{bmatrix} p_s \\ q_s \\ r_s \end{bmatrix} \tag{4.18}$$

$$\begin{bmatrix} \dot{\phi}_p \\ \dot{\theta}_p \\ \dot{\psi}_p \end{bmatrix} = \begin{bmatrix} 1 & \sin(\phi_p) * \dfrac{\sin(\theta_p)}{\cos(\theta_p)} & \cos(\phi_p) * \dfrac{\sin(\theta_p)}{\cos(\theta_p)} \\ 0 & \cos(\phi_p) & -\sin(\phi_p) \\ 0 & \sin(\phi_p) * \dfrac{1}{\cos(\theta_p)} & \cos(\phi_p) * \dfrac{1}{\cos(\theta_p)} \end{bmatrix} * \begin{bmatrix} p_p \\ q_p \\ r_p \end{bmatrix} \tag{4.19}$$

$$\begin{aligned}\begin{bmatrix} \dot{\phi}_s \\ \dot{\theta}_s \end{bmatrix} &= \begin{bmatrix} 1 & \sin(\phi_p) * \dfrac{\sin(\theta_p)}{\cos(\theta_p)} & \cos(\phi_p) * \dfrac{\sin(\theta_p)}{\cos(\theta_p)} \\ 0 & \cos(\phi_p) & -\sin(\phi_p) \end{bmatrix} * \begin{bmatrix} p_s \\ q_s \\ r_s \end{bmatrix} \\ \dot{\psi}_s &= r_s - r\end{aligned} \tag{4.20}$$

$$\begin{bmatrix}\dot{x}\\ \dot{y}\\ \dot{z}\end{bmatrix} = \boldsymbol{R'_{bn}} * \begin{bmatrix}u\\ v\\ w\end{bmatrix} \tag{4.21}$$

Almost all the formulas are explained in section 3.1 however we should describe some new entries:

"$\boldsymbol{r_{CM}}$" is the vector from the parafoil apparent mass center to the connection point C.
"$\boldsymbol{r_{CS}}$" is the vector from the payload mass centre to the connection point C.
"$\boldsymbol{r_{CB}}$" is the vector from the parafoil centre of gravity to the connection point C.
"$\boldsymbol{r_{BA}}$" is the vector from parafoil center of gravity to the parafoil aerodynamic center.
"$\boldsymbol{F_g^p}$" and "$\boldsymbol{F_g^s}$" are the parafoil and payload weight forces:

$$F_g = \left(m_{parafoil} + m_e\right) * g * \begin{bmatrix}-\sin(\theta)\\ \cos(\theta) * \sin(\phi)\\ \cos(\theta) * \cos(\phi)\end{bmatrix} \tag{4.22}$$

$$F_g = \left(m_{payload}\right) * g * \boldsymbol{R_{sb}} * \begin{bmatrix}-\sin(\theta)\\ \cos(\theta) * \sin(\phi)\\ \cos(\theta) * \cos(\phi)\end{bmatrix} \tag{4.23}$$

The data used for simulations are the same as in section 3.1 and 3.2 The damping coefficient and the system stiffness can vary from system to system, we have used:

$$K_\psi = 0.2\ N * \frac{m}{rad}\ ; K_r = 0\ N * \frac{m}{rad} \tag{4.24}$$

In this model the inertias of parafoil and payload are included in $\boldsymbol{I_p}$ *and* $\boldsymbol{I_s}$ **,** respectively as:

$$\begin{aligned} I_{xp} &= \left(\frac{v_{vol} * \rho + m_p}{12}\right) * (b^2 + t^2) \\ I_{yp} &= \left(\frac{v_{vol} * \rho + m_p}{12}\right) * (c^2 + t^2) \\ I_{zp} &= \left(\frac{v_{vol} * \rho + m_p}{12}\right) * (b^2 + c^2) \end{aligned} \tag{4.25}$$

$$\begin{gathered} I_{xp_b} = I_{xp} * \cos^2(\mu) + I_{zp} * \sin^2(\mu) \\ I_{yp_b} = I_{yp} \\ I_{zp_b} = I_{xp} * sin^2(\mu) + I_{zp} * cos^2(\mu) \\ I_{xzp_b} = \frac{1}{2} * \left(I_{xp} - I_{zp}\right) * \sin(2 * \mu) \end{gathered} \tag{4.26}$$

$$
\boldsymbol{I_p} = \begin{bmatrix} I_{xp_b} & 0 & I_{xzp_b} \\ 0 & I_{yp_b} & 0 \\ I_{xzp_b} & 0 & I_{z_{pb}} \end{bmatrix} \tag{4.27}
$$

$$
\begin{aligned}
I_{xs} &= \frac{m_l}{12} * (z_s^2 + y_s^2) \\
I_{ys} &= \frac{m_l}{12} * (z_s^2 + y_s^2) \\
I_{zs} &= \frac{m_l}{12} * (z_s^2 + y_s^2)
\end{aligned} \tag{4.28}
$$

$$
\boldsymbol{I_s} = \begin{bmatrix} I_{xs} & 0 & 0 \\ 0 & I_{ys} & 0 \\ 0 & 0 & I_{zs} \end{bmatrix} \tag{4.29}
$$

4.3 SIMULATIONS

The 7 DOF is the preferred candidate for the mission: we want to have a stable payload for terrain relative navigation (TRN). Less degree of freedom can be linked to less cargo oscillations. Moreover, with a 7 DOF we can still perfectly match the data from Airborne. The system validation will be performed using both Airborne data and [8] plots.

However, the probe will probably still be spinning when the parafoil will be deployed: the 9 DOF solution may become a good alternative to solve this problem. Before taking a definitive decision, we must understand the entity of the spinning and how it can afflict the parafoil deployment.

4.3.1 TITAN SIMULATIONS

The simulations will focus on a S-maneuver to highlight the constrained oscillations of the payload. The simulations are made for a parafoil with L/D of 2.1 and deployment altitude of 4000 m.

The model keeps into account a more complex geometrical parameters definition from [8] a more complex iteration between payload and parafoil: the aerodynamic definition must be different from the 6 DOF model (derived from a set from [8]) to respect the requirement on the efficiency. When the true aerodynamic of the vehicle will be computed with CFD analysis, the guideline parameters should come from the definitive parafoil configuration (7,8 or 9 DOF).

The load swing highlight in the payload yaw plot it’s a relative motion between the payload and the parafoil, the systems moves accordingly to the ram-air wing. On the pitch and roll plots the payload detached dynamics is highly damped through the link structure and the lines damping and stiffness: we can catch an oscillatory behavior linked to the load yaw motion. Even with a strong link the probe will have some relative motion: the 7 DOF model is not usually used on Earth because at the equilibrium conditions the parafoil and the load tend to have a differential pitch angle, positive for the first and negative for the latter.

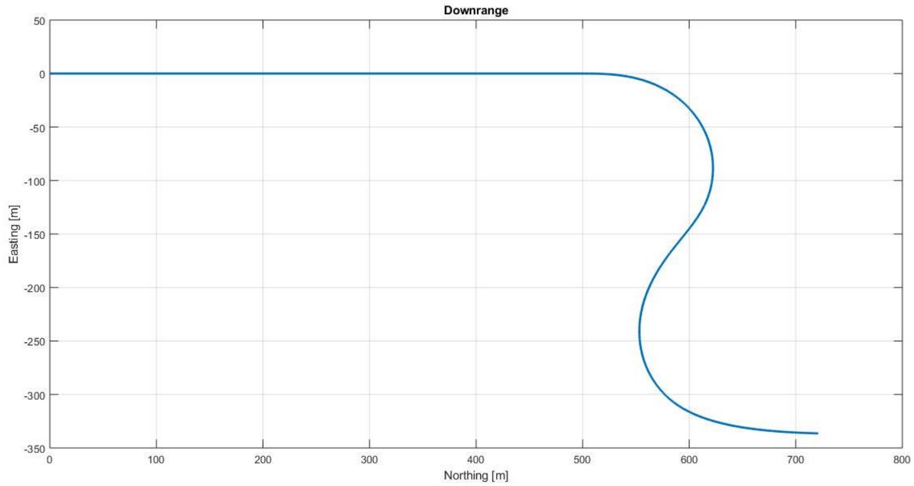

Figure 58: On-plane 7 DOF S-maneuver.

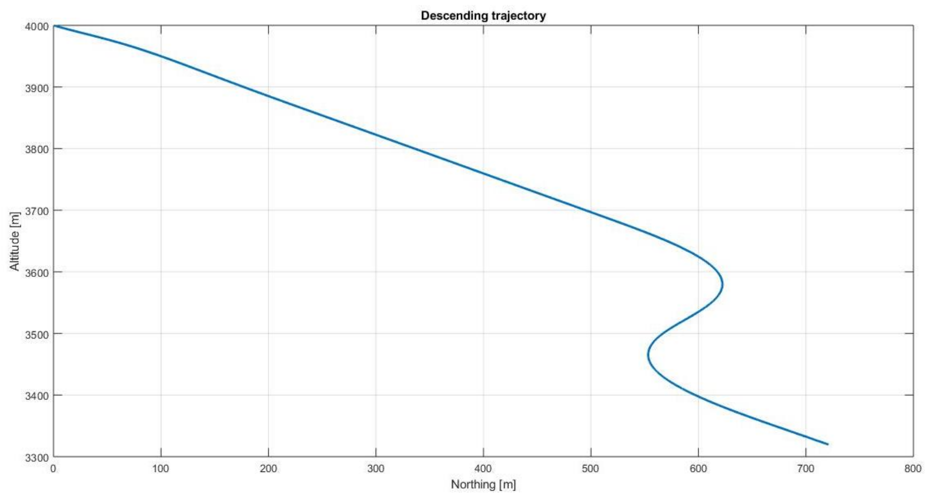

Figure 59: Altitude vs Downrange for 7 DOF.

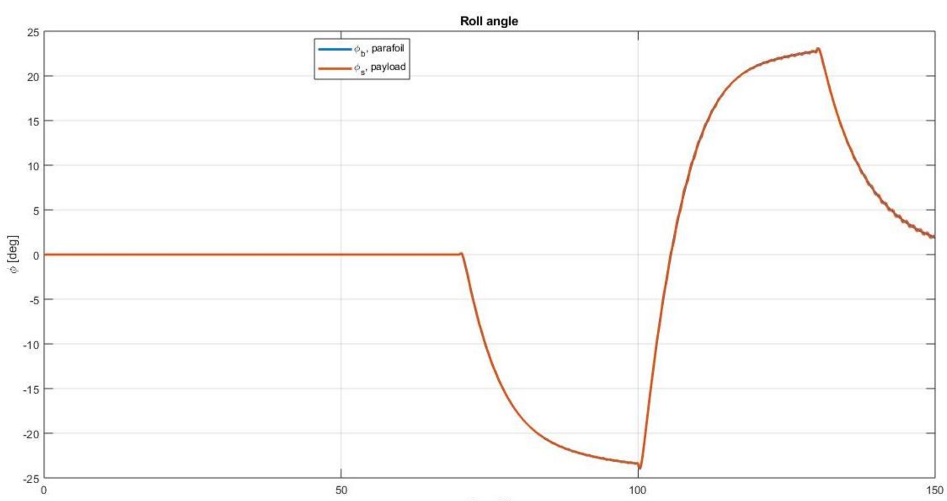

Figure 60: Roll angle S-maneuver 7 DOF.

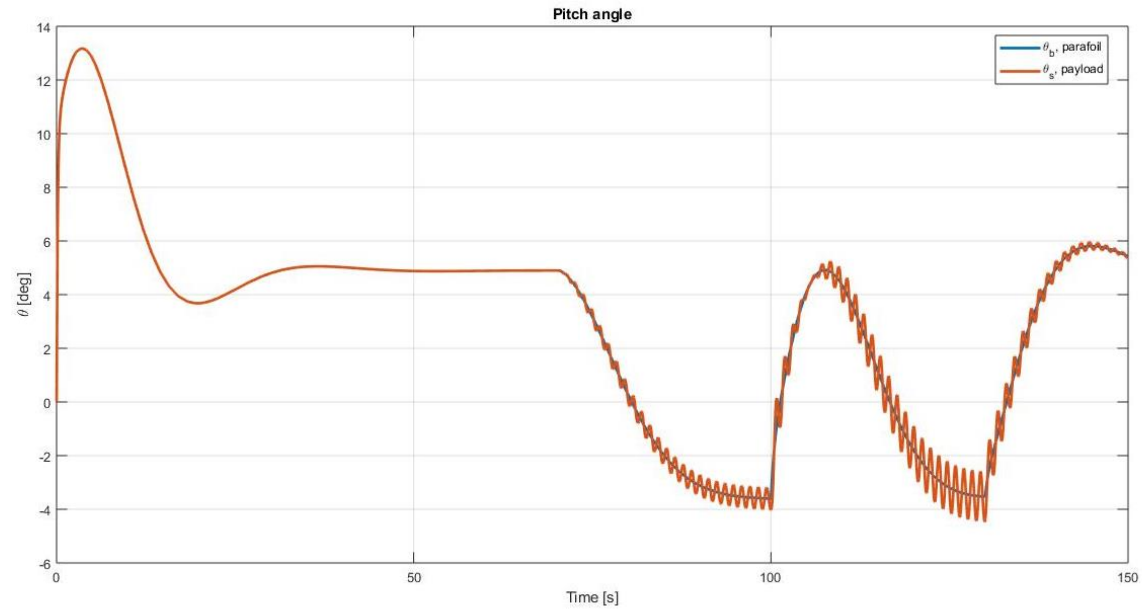

Figure 61: Pitch angle S-maneuver 7 DOF.

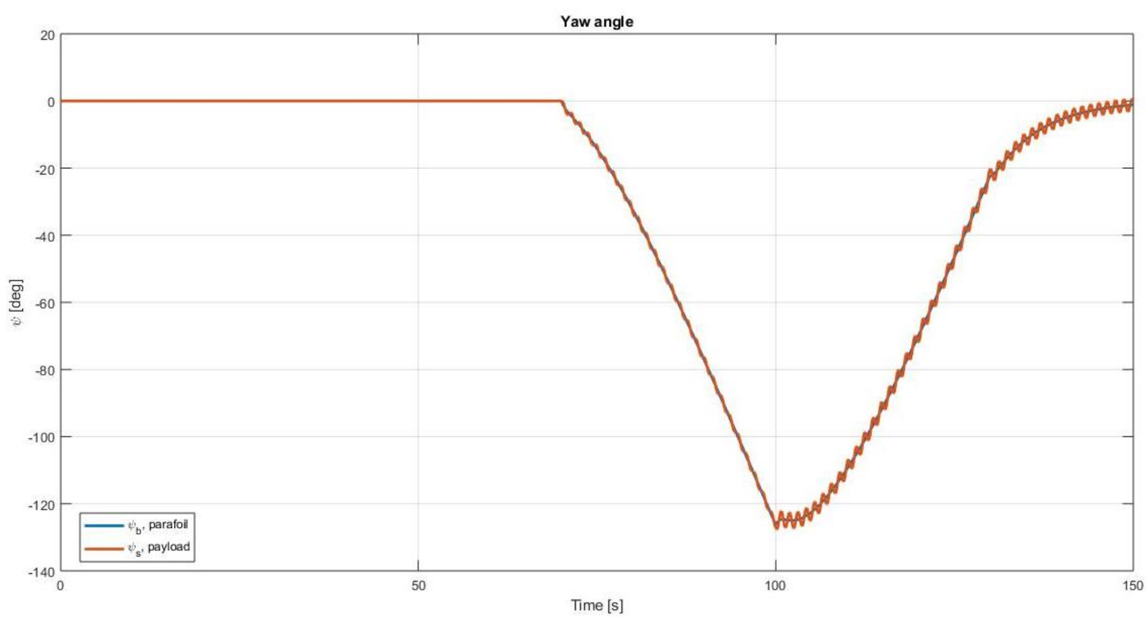

Figure 62: Yaw angle S-maneuver 7 DOF

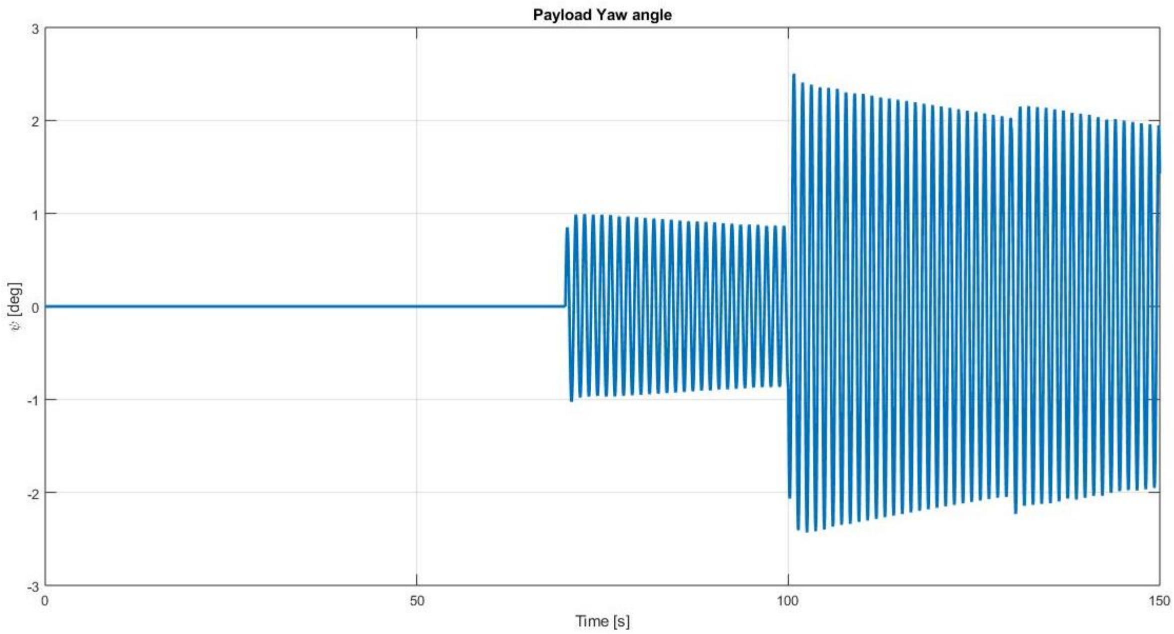

Figure 63: Payload yaw motion S-maneuver 7 DOF

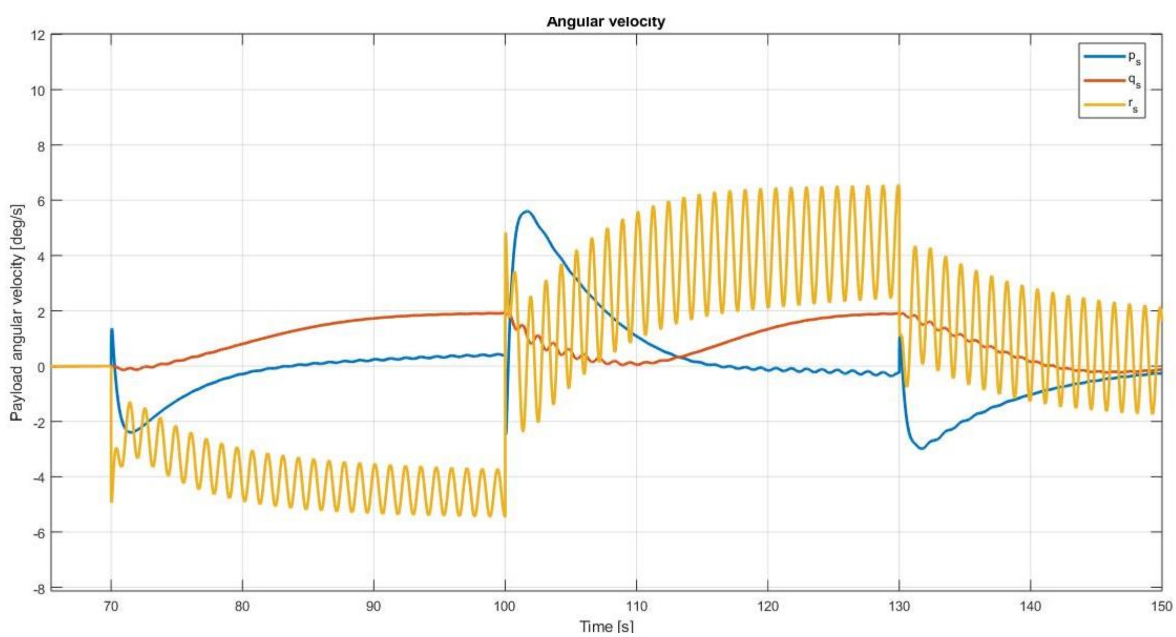

Figure 64: Payload angular velocities S-maneuver 7 DOF (highlight on the control response behavior).

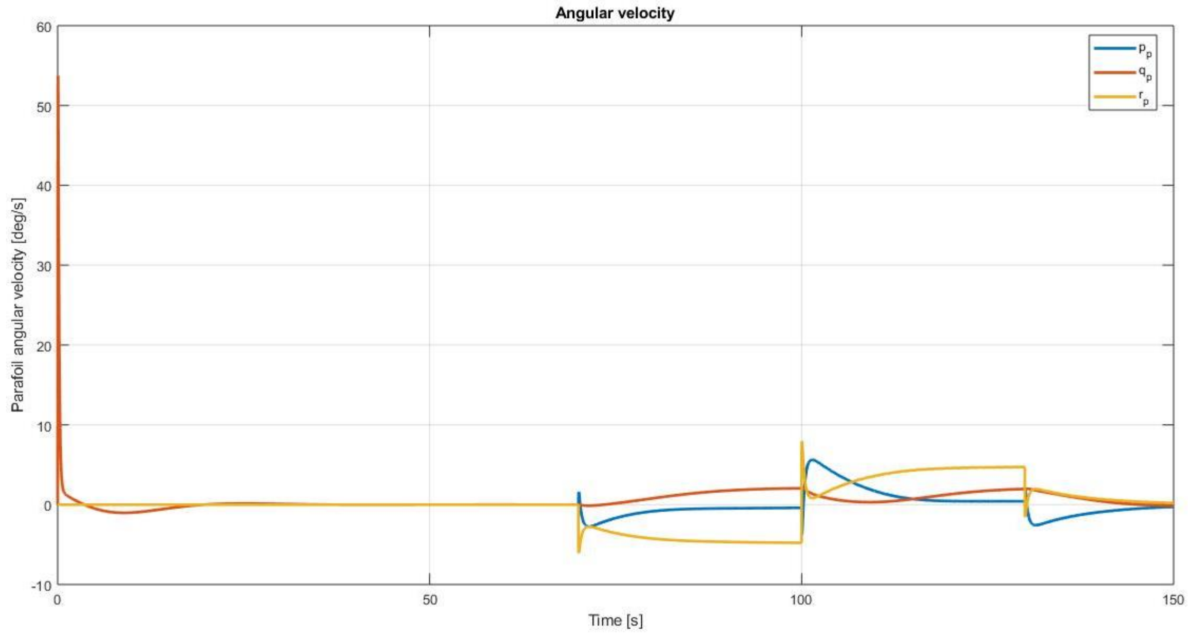

Figure 65: Parafoil angular velocities S-maneuver 7 DOF.

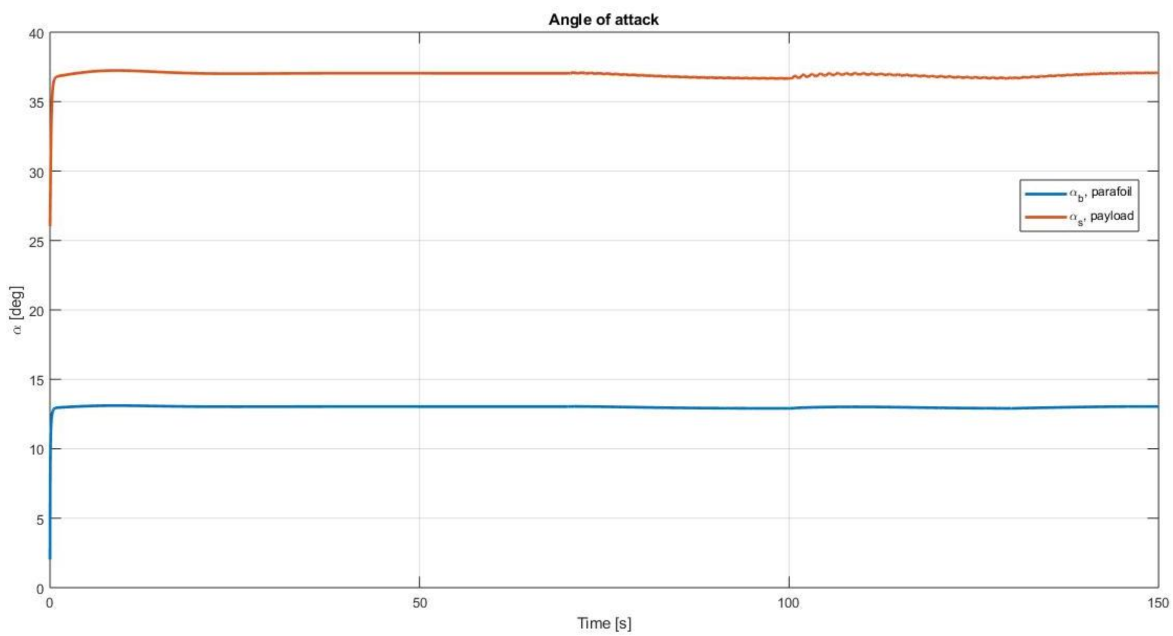

Figure 66: Angle of attack S-maneuver 7 DOF.

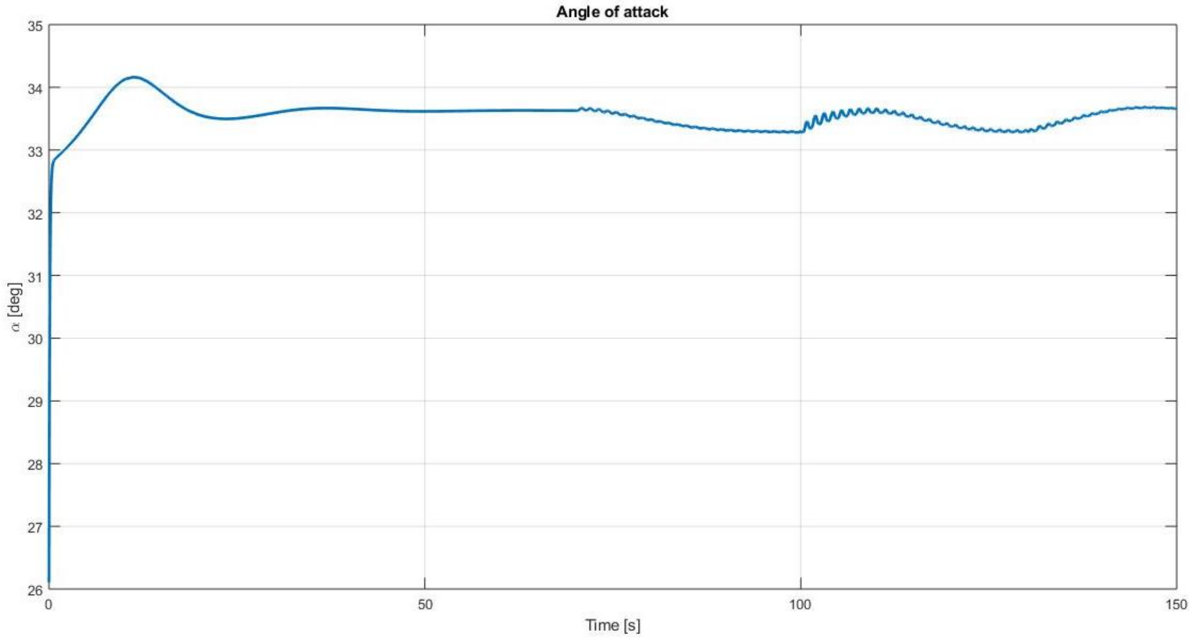

Figure 67: Angle of attack of total system S-maneuver 7 DOF.

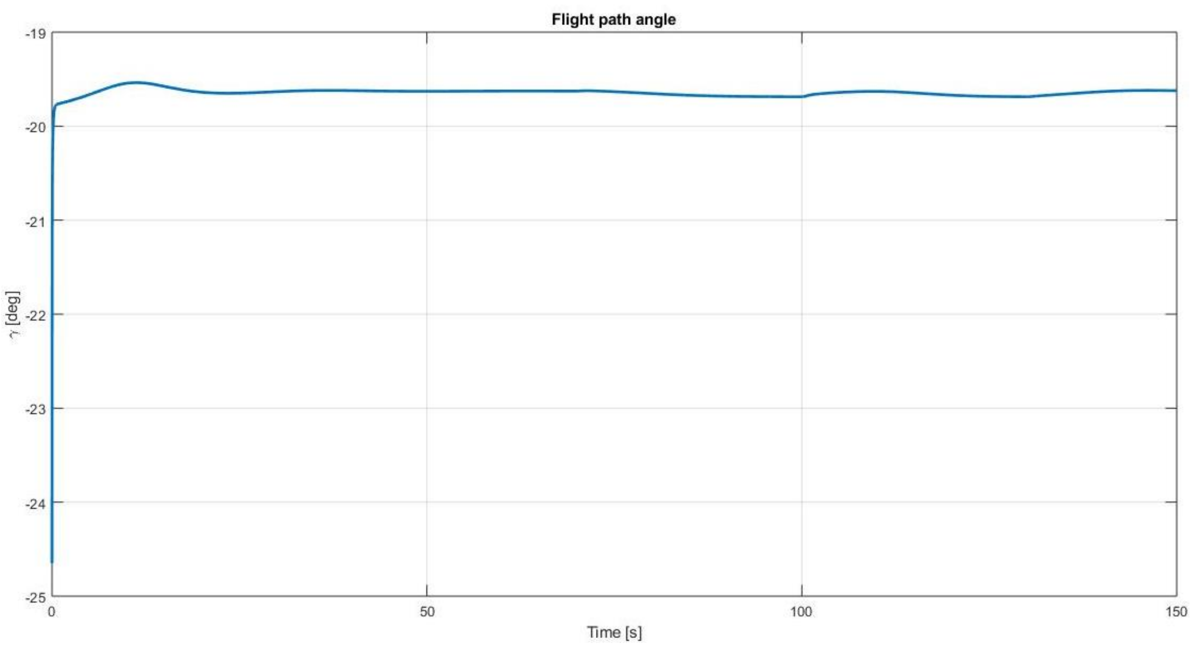

Figure 68: Flightpath angle S-maneuver 7 DOF.

4.3.2 AIRBORNE VALIDATION

The model is again validated with Airborne data on Titan with a low glide system $\left(\frac{L}{D} = 2.1\right)$ and a high glide system $(\frac{L}{D} = 4)$. This last simulation can catch the overall trend but not match perfectly with Airborne data: we don't have their full aerodynamic but just an indication on the efficiency they have used for those simulations. We assumed the aerodynamic of a system of similar characteristics, however the difference can be easily spotted in the simulation with wind. The cause can be the different pitching moment: if they use an aerodynamic profile different from ours then the behavior against the wind will be different.

$$\frac{L}{D} = 2.1$$

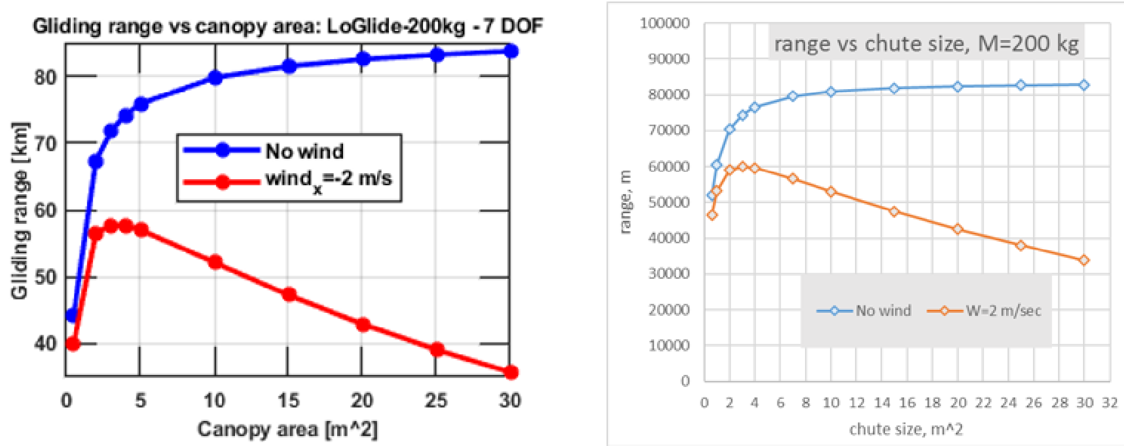

Figure 69: Low-glide steady state Titan descent.

$$\frac{L}{D} = 4$$

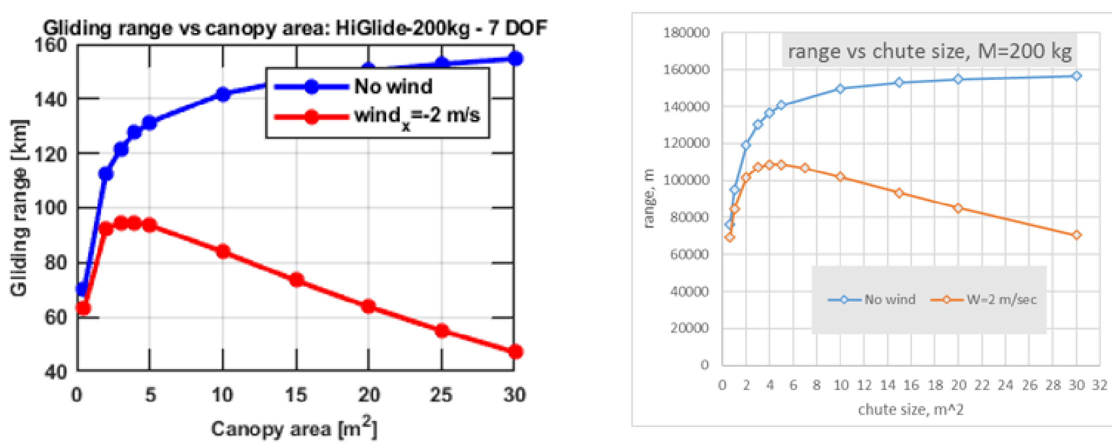

Figure 70:High glide steady state Titan descent.

4.3.3 EARTH ENVIRONMENT VALIDATION

The simulation is performed on Earth environment (see [16]) at 400 m with payload and parafoil pitch angles of 1.8 deg and 1 deg respectively. The control performs an S-maneuver with $V_i = \{8.6,0,4.2\}\ \ m/s$.

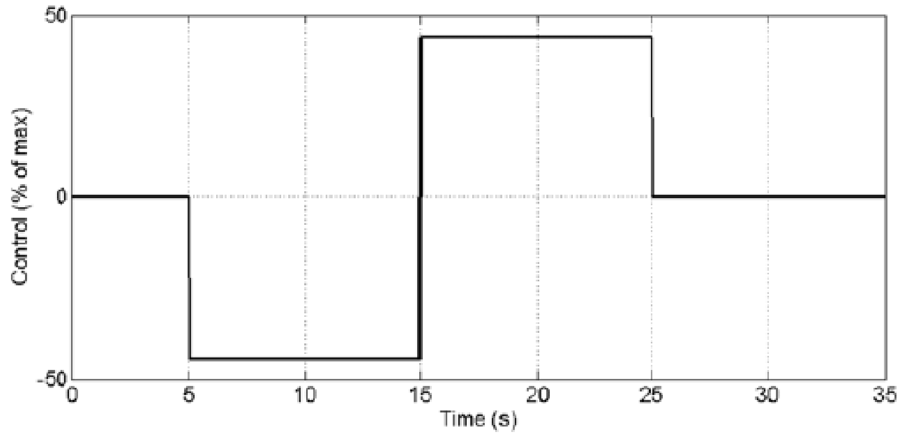

Figure 71: Control maneuver history [16].

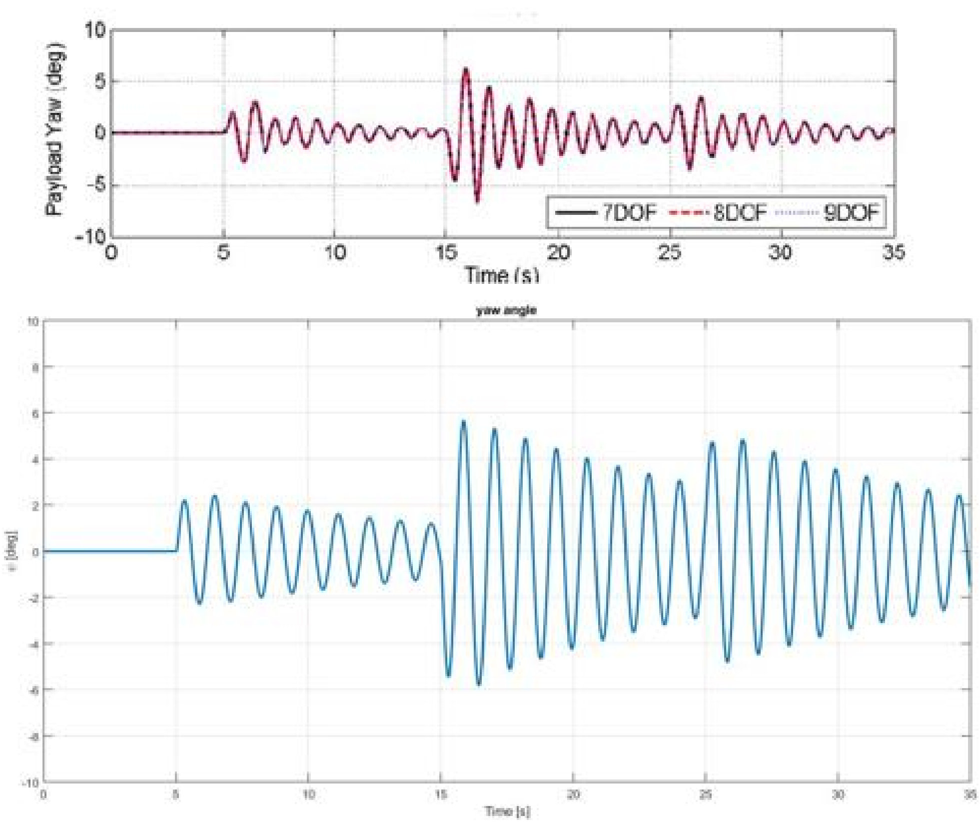

Figure 72: Yaw angle oscillations [16]

5 PADs HIGH FIDELITY MODEL: 8 DOF

The 8 DOF model is very similar to the 7 DOF in its formulation: however, the payload gains one degree of freedom more, a relative pitch. The major part of the autonomous PADs is connected as an 8 DOF: unfortunately, the model is highly sensible to the inputs as aerodynamics, the rotation damping and stiffness of the risers. The geometry of the parafoil should be already well defined: a wrong geometry definition will make the computation highly instable. Moreover, the entity of the apparent masses (and of the related moments) on Titan enhance the instabilities in the computation.

The rising lines fashion does not seem appropriate for Titan: the pitch oscillation can be quite intense, it is not the best solution for a TRN system on the load. However, the model is reported to complete the rose of the available high-fidelity examples.

The 7 DOF,8 DOF and complete 9 DOF should be used after a clear definition of the PADs parameters to exploit their functionalities. The alien environment and the possible position of the AGU (Airborne Guidance Unit) on the payload complicates the modelling.

For the simulations the same data of sections 3.1 and 3.2 will be used. The parafoil canopy is already fully inflated at the beginning of the simulations and it is considered as a 3D rigid body.

All the quantities used in this chapter have already been explained in chapters 04

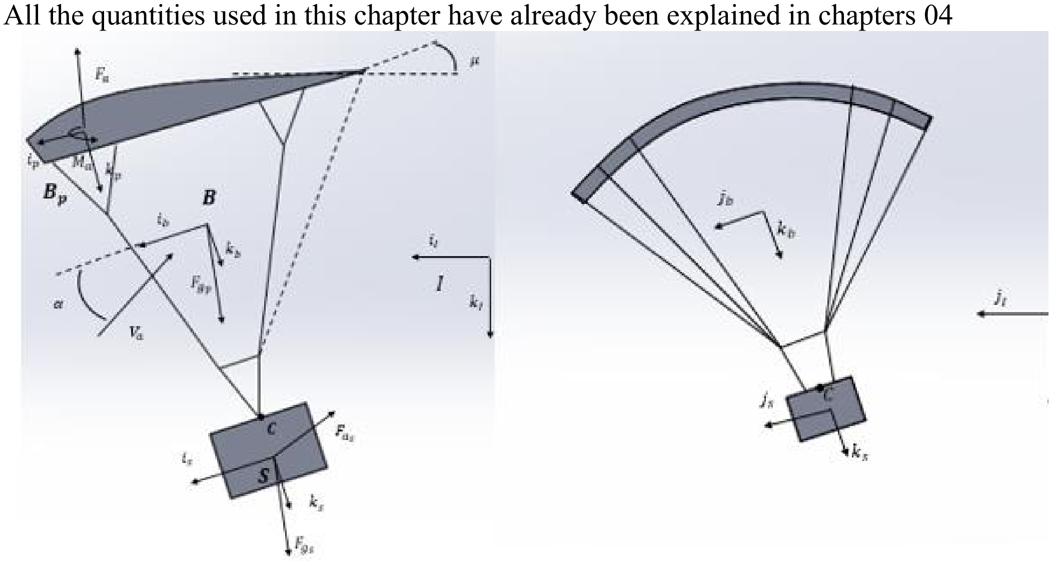

Figure 73: 8 DOF model parafoil-payload connection.

5.1 EQUATIONS OF MOTION

As in the 7 DOF model the payload has a relative motion in respect of the parafoil that can be expressed as:

$$\boldsymbol{\omega}_{\frac{s}{b}}^{s} = \boldsymbol{\omega}_{s}^{s} - \boldsymbol{R}_{sb} * \boldsymbol{\omega}_{p} = \boldsymbol{R}_{\theta_s} * \begin{bmatrix} 0 \\ \dot{\theta}_s \\ 0 \end{bmatrix} + \boldsymbol{R}_{\theta_s} * \boldsymbol{R}_{\psi_s} * \begin{bmatrix} 0 \\ 0 \\ \dot{\psi}_s \end{bmatrix} \tag{5.1}$$

$$\boldsymbol{R}_{\boldsymbol{\theta}_s} = \begin{bmatrix} \cos(\theta_s) & 0 & -\sin(\theta_s) \\ 0 & 1 & 0 \\ \sin(\theta_s) & 0 & \cos(\theta_s) \end{bmatrix} \tag{5.2}$$

$$\boldsymbol{R}_{\boldsymbol{\psi}_s} = \begin{bmatrix} \cos(\psi_s) & \sin(\psi_s) & 0 \\ -\sin(\psi_s) & \cos(\psi_s) & 0 \\ 0 & 0 & 1 \end{bmatrix} \tag{5.3}$$

$$\begin{bmatrix} p_s \\ \dot{\theta}_s \\ \dot{\psi}_s \end{bmatrix} = \begin{bmatrix} 0 & -\tan(\theta_s) \\ 1 & 0 \\ 0 & \dfrac{1}{\cos(\theta_s)} \end{bmatrix} * \begin{bmatrix} q_s \\ r_s \end{bmatrix} +$$
$$\begin{bmatrix} \dfrac{\cos(\psi_s)}{\cos(\theta_s)} & \dfrac{\sin(\psi_s)}{\cos(\theta_s)} & 0 \\ \sin(\psi_s) & -\cos(\psi_s) & 0 \\ -\cos(\psi_s) * \tan(\theta_s) & -\sin(\psi_s) * \tan(\theta_s) & 1 \end{bmatrix} * \begin{bmatrix} p_p \\ q_p \\ r_p \end{bmatrix} \tag{5.4}$$

$$\begin{bmatrix} p_s \\ q_s \\ r_s \end{bmatrix} = R_{sb} * \begin{bmatrix} p_p \\ q_p \\ r_p \end{bmatrix} + \begin{bmatrix} 0 & 0 & -\sin(\theta_s) \\ 0 & 1 & 0 \\ 0 & 0 & \cos(\theta_s) \end{bmatrix} * \begin{bmatrix} 0 \\ \dot{\theta}_s \\ \dot{\psi}_s \end{bmatrix}$$

$$\begin{bmatrix} \dot{p}_s \\ \dot{q}_s \\ \dot{r}_s \end{bmatrix} = G + K_1 * \begin{bmatrix} \dot{q}_s \\ \dot{r}_s \end{bmatrix} + K_2 * \begin{bmatrix} \dot{p}_p \\ \dot{q}_p \\ \dot{r}_p \end{bmatrix} \tag{5.5}$$

$$G = \begin{bmatrix} -sin(\psi_s) * (r_s - r_p) * p_p + cos(\psi_s) * (r_s - r_p) * q_p \\ -cos(\psi_s) * (r_s - r_p) * p_p - \sin(\psi_s) * (r_s - r_p) * q_p \\ 0 \end{bmatrix} \tag{5.6}$$

$$K_1 = \begin{bmatrix} 0 & \tan(\theta_s) \\ 1 & 0 \\ 0 & 1 \end{bmatrix} \tag{5.7}$$

$$K_2 = \begin{bmatrix} \dfrac{\cos(\psi_s)}{\cos(\theta_s)} & \dfrac{\sin(\psi_s)}{\cos(\theta_s)} & 0 \\ 0 & 0 & 0 \\ 0 & 0 & 0 \end{bmatrix} \tag{5.8}$$

The connection point moment M_c in 8 DOF model is expressed as:

$$\boldsymbol{M_C} = \begin{bmatrix} 0 \\ 0 \\ M_{CZ} \end{bmatrix} + \boldsymbol{R_{sb}} * \begin{bmatrix} M_{CX} \\ 0 \\ 0 \end{bmatrix} = \begin{bmatrix} 0 \\ 0 \\ M_{CZ} \end{bmatrix} + \boldsymbol{R_{sb}} * \begin{bmatrix} 1 \\ 0 \\ 0 \end{bmatrix} * [M_{CX}] \\ = \begin{bmatrix} 0 \\ 0 \\ M_{CZ} \end{bmatrix} + \boldsymbol{R_{sb}} * \boldsymbol{E} * [M_{CX}] \tag{5.9}$$

$$M_{CZ} = -K_{\psi}(\psi_s) * \psi_s + K_r(\psi_s) * \dot{\psi}_s \tag{5.10}$$

The equations of motion for the 8 DOF can be written as:

$$\boldsymbol{A_{4x12}} * \boldsymbol{b_{12x1}} = \begin{bmatrix} \boldsymbol{F_p} \\ \boldsymbol{M_p} \\ \boldsymbol{F_s} \\ \boldsymbol{M_s} \end{bmatrix} \tag{5.11}$$

$$\boldsymbol{A_{4x12}} = \\ \begin{bmatrix} (m_p + m_e) * \boldsymbol{I_{3x3}} + \boldsymbol{M_f}' & -\boldsymbol{M'_f} * \boldsymbol{S}(\boldsymbol{r_{CM}}) - (m_p + m_e) * \boldsymbol{S}(\boldsymbol{r_{CB}}) & \boldsymbol{0_{3x2}} & -\boldsymbol{I_{3x3}} & \boldsymbol{0_{3x1}} \\ \boldsymbol{S}(\boldsymbol{r_{BM}}) * \boldsymbol{M'_f} & \boldsymbol{I_p} + \boldsymbol{I_f} - \boldsymbol{S}(\boldsymbol{r_{BM}}) * \boldsymbol{M'_f} * \boldsymbol{S}(\boldsymbol{r_{CM}}) & \boldsymbol{0_{3x2}} & \boldsymbol{S}(\boldsymbol{r_{CB}}) & \boldsymbol{E} \\ m_s * \boldsymbol{R_{sb}} & -m_s * \boldsymbol{S}(\boldsymbol{r_{CS}}) * \boldsymbol{K_2} & -m_s * \boldsymbol{S}(\boldsymbol{r_{CS}}) * \boldsymbol{K_1} & \boldsymbol{R_{sb}} & \boldsymbol{0_{3x1}} \\ \boldsymbol{0_{3x3}} & \boldsymbol{I_s} * \boldsymbol{K_2} & \boldsymbol{I_s} * \boldsymbol{K_1} & -\boldsymbol{S}(\boldsymbol{r_{CS}}) * \boldsymbol{R_{sb}} & -R_{sb} * E \end{bmatrix} \tag{5.12}$$

$$\boldsymbol{b_{12x1}} = [\dot{u}_c \;\; \dot{v}_c \; \dot{w}_c \;\; \dot{p}_p \;\; \dot{q}_p \;\; \dot{r}_p \;\; \dot{q}_s \;\; \dot{r}_s \;\; F_{CX} \;\; F_{CY} \;\; F_{CZ} \;\; M_{CX}]' \tag{5.13}$$

$$\boldsymbol{F_p} = \boldsymbol{F_a^p} + \boldsymbol{F_b^p} + \boldsymbol{F_g^p} \\ -\boldsymbol{S}(\boldsymbol{\omega_p}) * [(m + m_e)\boldsymbol{I_{3x3}} + \boldsymbol{M'_f}] * \begin{bmatrix} u_c \\ v_c \\ w_c \end{bmatrix} + \boldsymbol{S}(\boldsymbol{\omega_p}) * \boldsymbol{M'_f} * \boldsymbol{S}(\boldsymbol{r_{CM}}) * \begin{bmatrix} p_p \\ q_p \\ r_p \end{bmatrix} + \boldsymbol{S}(\boldsymbol{\omega_p}) \\ * \boldsymbol{M'_f} * \boldsymbol{R_{bn}} * \boldsymbol{W} - (m_p + m_e) * \boldsymbol{S}(\boldsymbol{\omega_p}) * \boldsymbol{S}(\boldsymbol{\omega_p}) * \boldsymbol{r_{CB}} \tag{5.14}$$

$$\boldsymbol{M_p} = \boldsymbol{M_a} + \boldsymbol{M_b^p} + \boldsymbol{S}(\boldsymbol{r_{BA}}) * \boldsymbol{F_a^p} \\ -[\boldsymbol{S}(\boldsymbol{\omega_p}) * (\boldsymbol{I_p} + \boldsymbol{I'_f}) - \boldsymbol{S}(\boldsymbol{r_{BM}}) * \boldsymbol{S}(\boldsymbol{\omega_p}) * \boldsymbol{M'_f} * \boldsymbol{S}(\boldsymbol{r_{CM}})] * \begin{bmatrix} \boldsymbol{p_p} \\ \boldsymbol{q_p} \\ \boldsymbol{r_p} \end{bmatrix} - \\ \boldsymbol{S}(\boldsymbol{r_{BM}}) * \boldsymbol{S}(\boldsymbol{\omega_p}) * \boldsymbol{M'_f} * \begin{bmatrix} u_c \\ v_c \\ w_c \end{bmatrix} + \boldsymbol{S}(\boldsymbol{r_{BM}}) * \boldsymbol{S}(\boldsymbol{\omega_p}) * \boldsymbol{M'_f} * \boldsymbol{R_{bn}}\boldsymbol{W} - \begin{bmatrix} 0 \\ 0 \\ M_{CZ} \end{bmatrix} \tag{5.15}$$

$$\boldsymbol{F_s} = \boldsymbol{F_a^s} + \boldsymbol{F_g^s} + m_s * \boldsymbol{S}(\boldsymbol{r_{CS}}) * \boldsymbol{G} - m_s * \boldsymbol{R_{bs}} * \boldsymbol{S}(\boldsymbol{\omega_p}) * \begin{bmatrix} u_c \\ v_c \\ w_c \end{bmatrix} - m_s * \boldsymbol{S}(\boldsymbol{\omega_s}) * \boldsymbol{S}(\boldsymbol{\omega_s}) * \boldsymbol{r_{CS}} \tag{5.16}$$

$$\boldsymbol{M_s} = -\boldsymbol{I_s G} + \boldsymbol{R_{sb}} * \boldsymbol{M_c} - \boldsymbol{S}(\boldsymbol{\omega_s}) * \boldsymbol{I_s} * \begin{bmatrix} p_s \\ q_s \\ r_s \end{bmatrix} \tag{5.17}$$

$$\begin{bmatrix} \dot{\phi}_p \\ \dot{\theta}_p \\ \dot{\psi}_p \end{bmatrix} = \begin{bmatrix} 1 & \sin(\phi_p) * \frac{\sin(\theta_p)}{\cos(\theta_p)} & \cos(\phi_p) * \frac{\sin(\theta_p)}{\cos(\theta_p)} \\ 0 & \cos(\phi_p) & -\sin(\phi_p) \\ 0 & \sin(\phi_p) * \frac{1}{\cos(\theta_p)} & \cos(\phi_p) * \frac{1}{\cos(\theta_p)} \end{bmatrix} * \begin{bmatrix} p_p \\ q_p \\ r_p \end{bmatrix} \tag{5.18}$$

$$[\dot{\phi}_s] = \begin{bmatrix} 1 & \sin(\phi_p) * \frac{\sin(\theta_p)}{\cos(\theta_p)} & \cos(\phi_p) * \frac{\sin(\theta_p)}{\cos(\theta_p)} \end{bmatrix} * \begin{bmatrix} p_s \\ q_s \\ r_s \end{bmatrix}$$

$$\dot{\theta}_s = q_s + \sin(\psi_s) * p - \cos(\psi_s) * q \tag{5.19}$$

$$\dot{\psi}_s = \frac{1}{\cos(\theta_s)} * r_s - \cos(\psi_s) * \tan(\theta_s) * p - \sin(\psi_s) * \tan(\theta_s) * q - r$$

$$\begin{bmatrix} \dot{x} \\ \dot{y} \\ \dot{z} \end{bmatrix} = \boldsymbol{R'_{bn}} * \begin{bmatrix} u \\ v \\ w \end{bmatrix} \tag{5.20}$$

Almost all the formulas are explained in section 3.1 and 4.2 The position vectors are similar to those in the 7 DOF.

"$\boldsymbol{r_{CM}}$" is the vector from the parafoil apparent mass centre to the connection point C.

"$\boldsymbol{r_{CS}}$" is the vector from the payload mass centre to the connection point C.

"$\boldsymbol{r_{CB}}$" is the vector from the parafoil centre of gravity to the connection point C.

"$\boldsymbol{r_{BA}}$" is the vector from parafoil centre of gravity to the parafoil aerodynamic center.

The data used for simulations are the same as in section 3.1 and 3.2 The damping coefficient and the system stiffness vary from the 7 DOF: there is a different kind of connection between payload and parafoil.

$$K_\psi = 0.09\, N * \frac{m}{rad}\ ; K_r = 0.005\, N * \frac{m * s}{rad} \tag{5.21}$$

5.2 SIMULATIONS

The simulations are similar to those of the 7 DOF. For the validation we lack knowledge of the stiffness and damping of the risers used in the models in [16]: in the paper the data for the 7 DOF are reported. Nevertheless, we can match the overall trends: that is our main focus. The Airborne comparison is neglected on the 8 DOF, was computationally demanding and, for now, this shouldn't be the definitive parafoil configuration.

5.2.1 TITAN SIMULATION

As for the 7 DOF of freedom the simulation follows an S-maneuver that starts at 4000 m $\left(u_c = 8.6\frac{m}{s}\ \ v_c = 0\frac{m}{s}\ \ w_c = 4.2\frac{m}{s}\right)$ with an overall efficiency of 2.

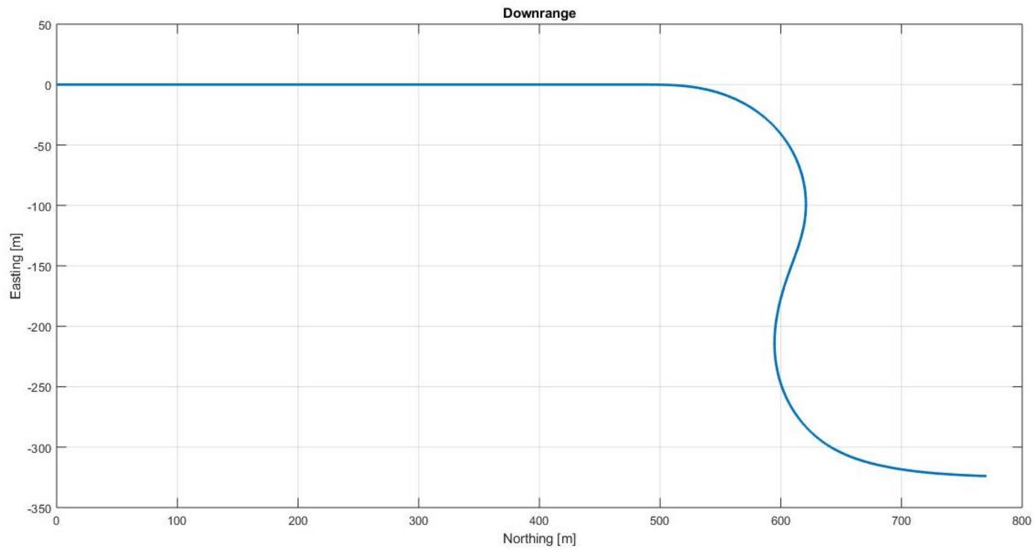

Figure 74: Downrange 8 DOF.

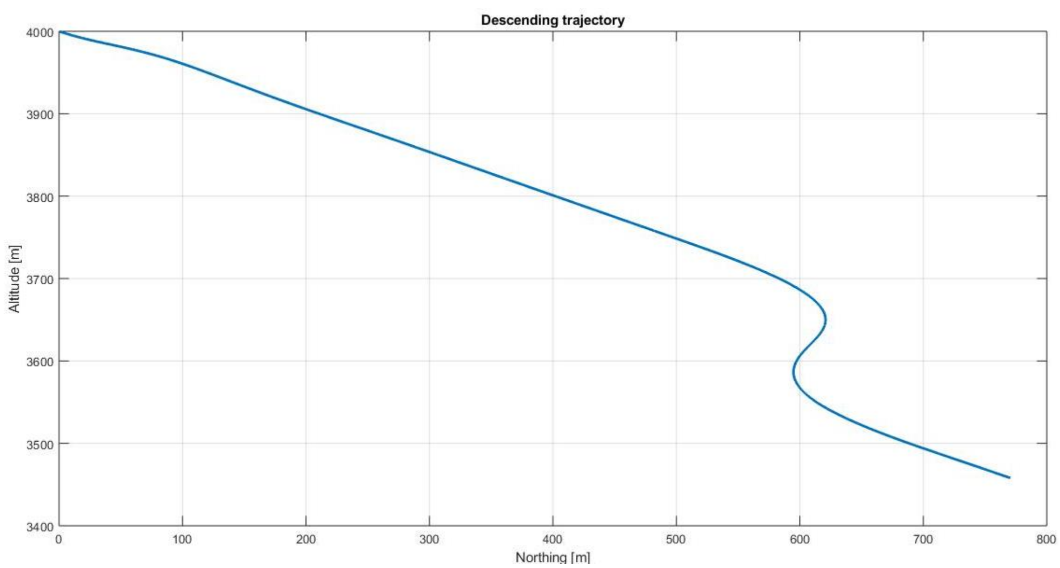

Figure 75: Descending Trajectory 8 DOF.

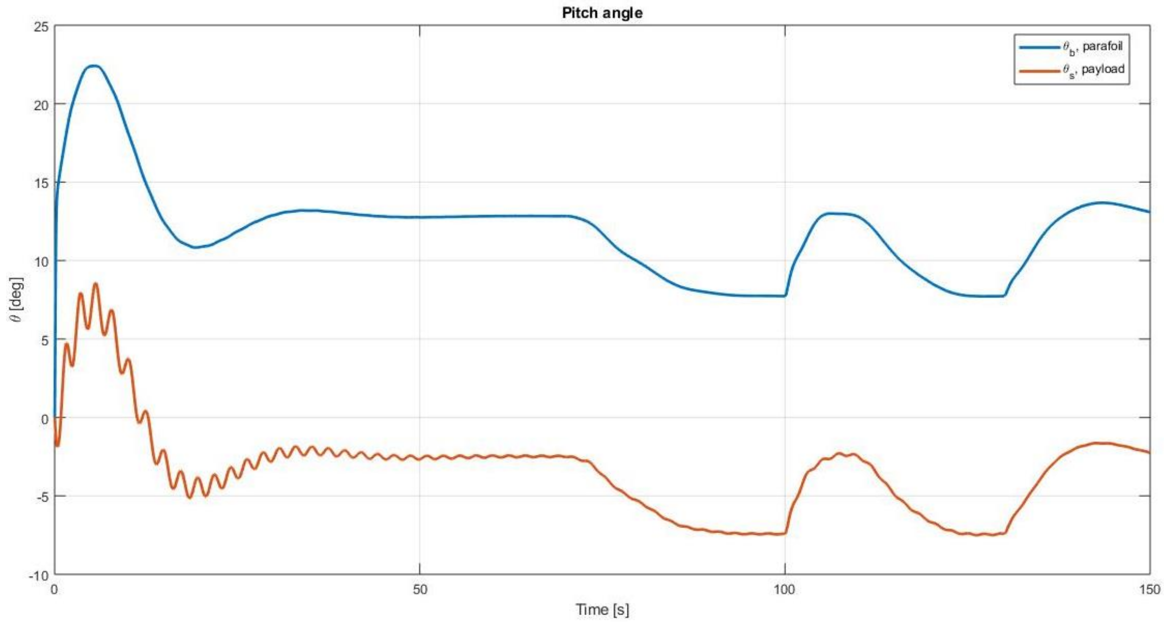

Figure 76: Pitch angle 8 DOF.

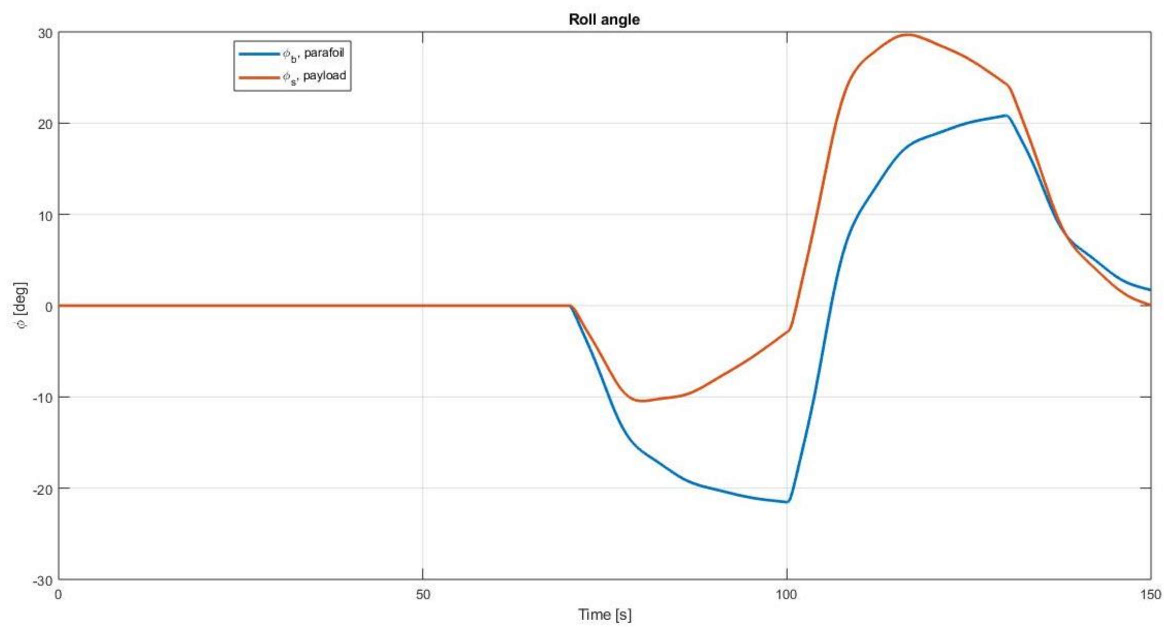

Figure 77: Roll angle 8 DOF.

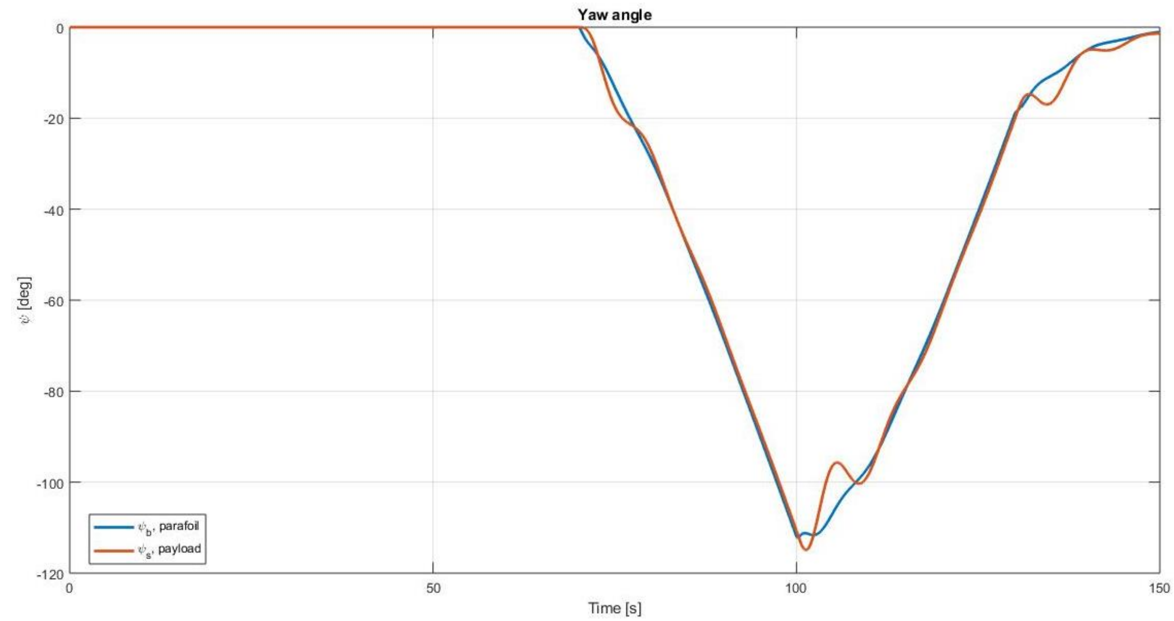

Figure 78: Yaw angle 8 DOF.

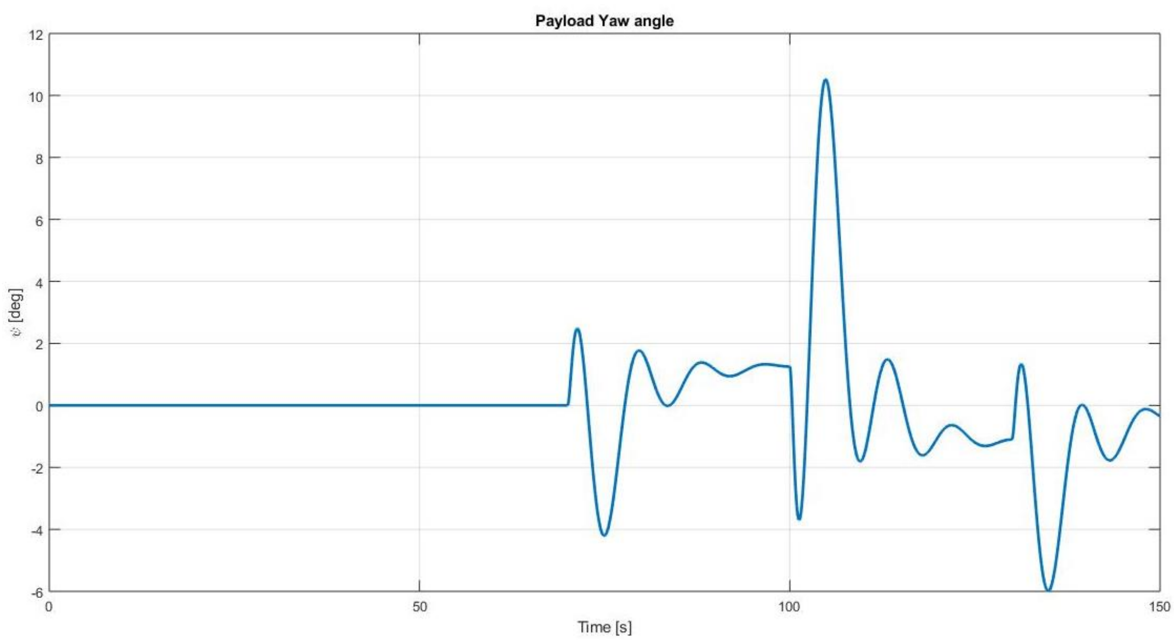

Figure 79: Payload yaw motion 8 DOF (the oscillation is damped).

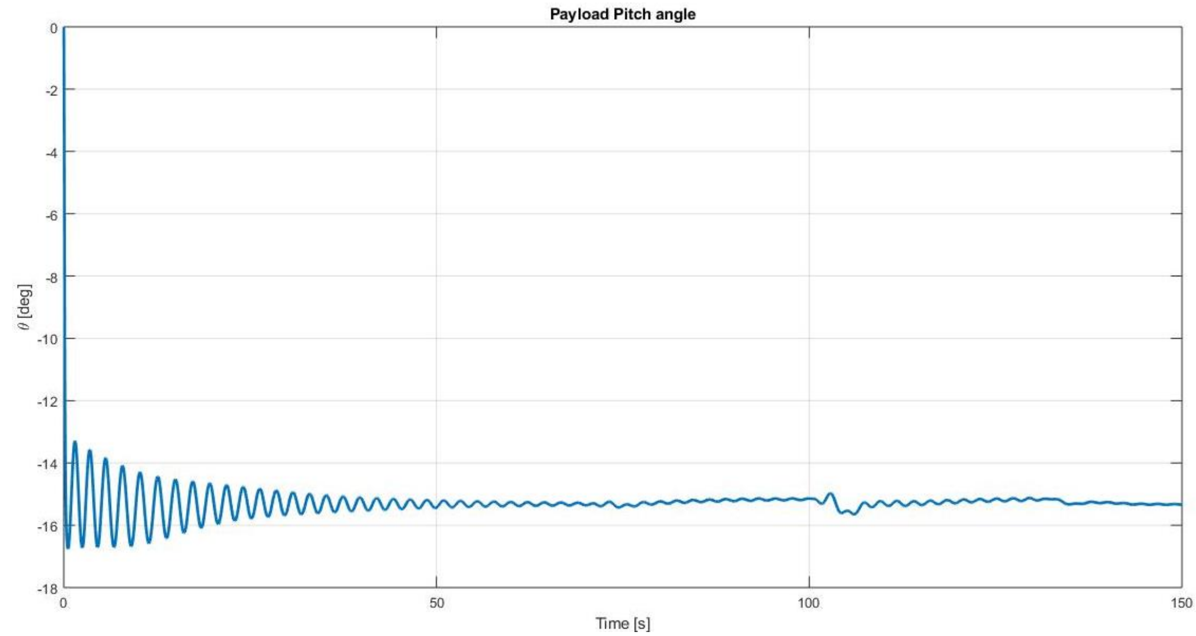

Figure 80: Payload pitch motion 8 DOF.

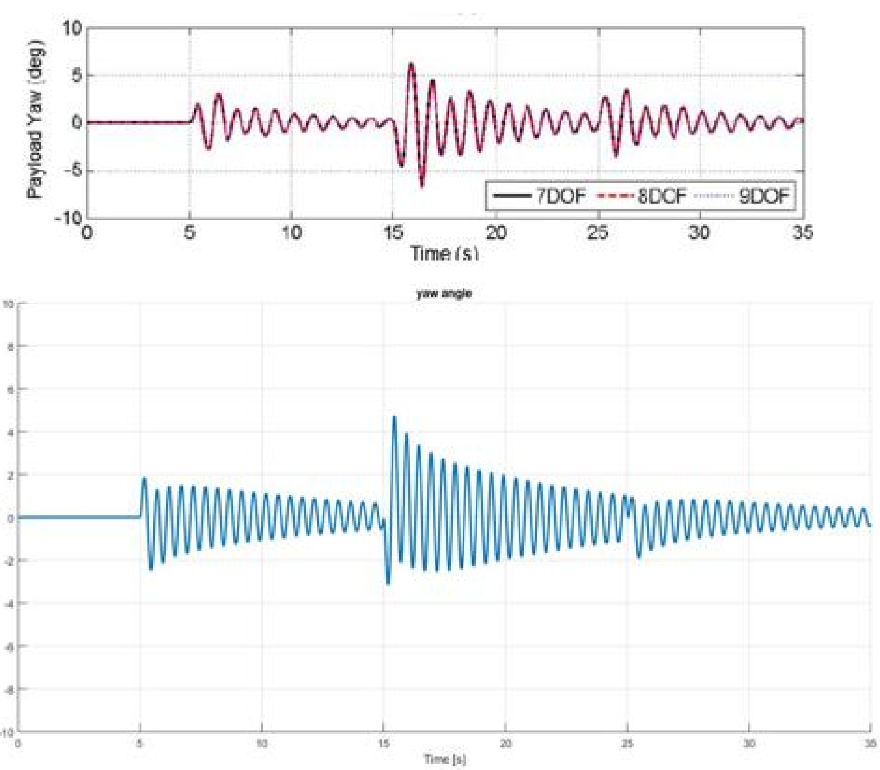

Figure 81: Yaw angle comparison 8 DOF. The parameters and aerodynamics used in [16] are not well reported, so we couldn't match the data. This model is highly sensible to the line stiffness and damping, without the true values used in the simulations is difficult even to reply the trend.

6 PADs HIGH FIDELITY MODEL: 9 DOF

The 9 DOF models represents a parafoil and payload linked in one point: the motion of the two system is joined through the vector of forces $\boldsymbol{F_c}$, put in the connection point C.

The simplified model captures the peculiarity of this PADs configuration with a small computational cost. The major part of the 9 DOF in literature ([14], [17], [18]) use “simplified models”: they are robust to computation and few geometrical information are needed.

However, those models detached the sideslip angle β, the rigging angle μ of the parafoil and they don’t give clarifying explanation of how the wind is accommodate, if accommodate in the equations. For the rigging angle an annotation must be made: the simplified 9 DOF model consider the equation of motion written in the $\{b_p\}$ reference system frame. The rigging angle enters in the computation when the distance between the connection point C and the parafoil center of mass is evaluated. All the quantities for the parafoil, comprising the apparent mass and inertia affect, are written in $\{b_p\}$: that simplified the formulations. Moreover, this formulation resembles more how we would test the PADs for system identification. We evaluate the parafoil characteristics as a solo system, then we analyze the load peculiarity and, at the end, the system characteristics will be computed.

The model develop for the JPL, takes into account those aspects keeping the computation and the equation of motion simple in their input requirements but affective in their modelling.

We still have few information on the Titan parafoil real geometry and aerodynamic: less guesses are given, less uncertainties are introduced.

6.1 SIMPLIFIED MODEL

The model is more similar to 6 DOF described in section 3.1 for its intrinsically simplicity, but payload and parafoil are two distinct systems. The main difference from the others high-fidelity models described before lays in the payload angular motions. They are described respect the external system of reference in the {s} frame and not as a parafoil relative rotations.

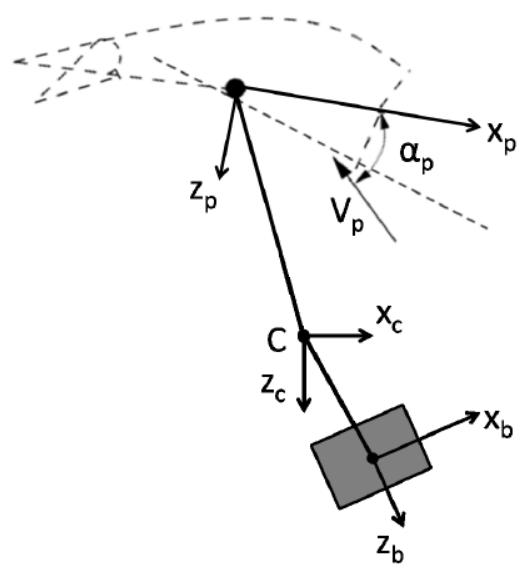

Figure 82: Simplified 9 DOF model representation [14].

6.1.1 Equations of Motion

The simplified model equations of motion can be written as:

$$\boldsymbol{A_{4x12}} * \boldsymbol{b_{12x1}} = \begin{bmatrix} \boldsymbol{F_s} \\ \boldsymbol{F_p} \\ \boldsymbol{M_s} \\ \boldsymbol{M_p} \end{bmatrix} \tag{6.1}$$

$$\boldsymbol{A_{4x12}} =$$

$$\begin{bmatrix} -m_s * \boldsymbol{I_{3x3}} * \boldsymbol{S}(\boldsymbol{r_{CS}}) & \boldsymbol{0_{3x3}} & m_s * \boldsymbol{I_{3x3}} * \boldsymbol{T_{sn}} & \boldsymbol{R_{sn}} \\ \boldsymbol{0_{3x3}} & -\left(m_p * \boldsymbol{I_{3x3}} + \boldsymbol{M_f}\right) * \boldsymbol{S}(\boldsymbol{r_{CP}}) & \left(\boldsymbol{m_p} * \boldsymbol{I_{3x3}} + \boldsymbol{M_f}\right) * \boldsymbol{T_{bn}} & -\boldsymbol{T_{bn}} \\ \boldsymbol{I_s} & \boldsymbol{0_{3x3}} & \boldsymbol{0_{3x3}} & -\boldsymbol{S}(\boldsymbol{r_{CB}}) * \boldsymbol{T_{sn}} \\ \boldsymbol{0_{3x3}} & \boldsymbol{I_p} + \boldsymbol{I_f} & \boldsymbol{0_{3x3}} & \boldsymbol{S}(\boldsymbol{r_{CP}}) * \boldsymbol{T_{bn}} \end{bmatrix} \tag{6.2}$$

$$\boldsymbol{b_{12x1}} = [\dot{p_s} \;\; \dot{q_s} \;\; \dot{r_s} \; \dot{p_p} \;\; \dot{q_p} \;\; \dot{r_p} \;\; \dot{u_c} \;\; \dot{v_c} \; \dot{w_c} \; F_{CX} \;\; F_{CY} \;\; F_{CZ} \,]' \tag{6.3}$$

$$\boldsymbol{F_p} = \boldsymbol{F_a^p} + \boldsymbol{F_b^p} + \boldsymbol{F_g^p} \\ -\boldsymbol{S}\left(\boldsymbol{\omega_p}\right) * \left(m_p * \boldsymbol{I_{3x3}} + \boldsymbol{M_f}\right) * \boldsymbol{S}\left(\boldsymbol{\omega_p}\right) * \boldsymbol{r_{CP}} - \boldsymbol{S}(\boldsymbol{\omega}) * \boldsymbol{M_f} * (\boldsymbol{R_{bn}} * \boldsymbol{V_c} + \boldsymbol{S}(\boldsymbol{\omega}) \\ * \boldsymbol{r_{CP}}) \tag{6.4}$$

$$\boldsymbol{M_p} \\ = \boldsymbol{M_a} + \boldsymbol{M_b^p} - \boldsymbol{R_{bn}} * \boldsymbol{R'_{sn}} * \boldsymbol{M_c} - \boldsymbol{S}(\boldsymbol{\omega}) * \left(\boldsymbol{I_p} + \boldsymbol{I_s}\right) * \boldsymbol{\omega_p} - \boldsymbol{\Xi} * \boldsymbol{M_f} * \boldsymbol{V_p} \tag{6.5}$$

$$\boldsymbol{F_s} = \boldsymbol{F_a^s} + \boldsymbol{F_g^s} - m_s * \boldsymbol{S}(\boldsymbol{\omega_s}) * \boldsymbol{S}(\boldsymbol{\omega_s}) * \boldsymbol{r_{CS}} \tag{6.6}$$

$$\boldsymbol{M_s} = \boldsymbol{M_a^s} + \boldsymbol{M_c} - \boldsymbol{S}(\boldsymbol{\omega_s}) * \boldsymbol{I_s} * \begin{bmatrix} p_s \\ q_s \\ r_s \end{bmatrix} \tag{6.7}$$

$$\begin{bmatrix} \dot{\phi_p} \\ \dot{\theta_p} \\ \dot{\psi_p} \end{bmatrix} = \begin{bmatrix} 1 & \sin(\phi_p) * \dfrac{\sin(\theta_p)}{\cos(\theta_p)} & \cos(\phi_p) * \dfrac{\sin(\theta_p)}{\cos(\theta_p)} \\ 0 & \cos(\phi_p) & -\sin(\phi_p) \\ 0 & \sin(\phi_p) * \dfrac{1}{\cos(\theta_p)} & \cos(\phi_p) * \dfrac{1}{\cos(\theta_p)} \end{bmatrix} * \begin{bmatrix} p_p \\ q_p \\ r_p \end{bmatrix} \tag{6.8}$$

$$\begin{bmatrix} \dot{\phi}_s \\ \dot{\theta}_s \\ \dot{\psi}_s \end{bmatrix} = \begin{bmatrix} 1 & \sin(\phi_s) * \frac{\sin(\theta_s)}{\cos(\theta_s)} & \cos(\phi_s) * \frac{\sin(\theta_s)}{\cos(\theta_s)} \\ 0 & \cos(\phi_s) & -\sin(\phi_s) \\ 0 & \sin(\phi_s) * \frac{1}{\cos(\theta_s)} & \cos(\phi_s) * \frac{1}{\cos(\theta_s)} \end{bmatrix} * \begin{bmatrix} p_s \\ q_s \\ r_s \end{bmatrix} \tag{6.9}$$

$$\begin{bmatrix} \dot{x} \\ \dot{y} \\ \dot{z} \end{bmatrix} = \begin{bmatrix} u \\ v \\ w \end{bmatrix} \tag{6.10}$$

$$\boldsymbol{M_C} = \begin{bmatrix} 0 \\ 0 \\ M_{CZ} \end{bmatrix} = \begin{bmatrix} 0 \\ 0 \\ K_{psi} * \left(\overline{\psi_p} - \overline{\psi_s}\right) + K_r * \left(\dot{\overline{\psi_p}} - \dot{\overline{\psi_s}}\right) \end{bmatrix} \tag{6.11}$$

$K_\psi = 0.07\ N * \frac{m}{rad}$; K_r =0.005 $N * \frac{m*s}{rad}$;

$$\overline{\psi_p} = \tan^{-1}\left(\frac{\sin(\phi_p) * \sin(\theta_p) * \cos(\psi_p) - \cos(\phi_p) * \sin(\psi_p)}{\cos(\theta_p) * \cos(\psi_p)}\right) \tag{6.12}$$

$$\overline{\psi_s} = \tan^{-1}\left(\frac{\sin(\phi_s) * \sin(\theta_s) * \cos(\psi_s) - \cos(\phi_s) * \sin(\psi_s)}{\cos(\theta_s) * \cos(\psi_s)}\right) \tag{6.13}$$

$$\dot{\overline{\psi_p}} = -\cos(\overline{\psi_p}) * \mathrm{t}_{\overline{\theta_p}} * p_p + \sin(\overline{\psi_p}) * \mathrm{t}_{\overline{\theta_p}} * q_p + r_p \tag{6.14}$$

$$\dot{\overline{\psi_s}} = -\cos(\overline{\psi_s}) * \mathrm{t}_{\overline{\theta_s}} * p_s + \sin(\overline{\psi_s}) * \mathrm{t}_{\overline{\theta_s}} * q_s + r_s \tag{6.15}$$

$$\mathrm{t}_{\overline{\theta_p}} = \frac{\cos(\phi_p) * \sin(\theta_p) * \cos(\psi_p) + \sin(\phi_p) * \sin(\psi_p)}{\cos(\theta_p) * cos(\psi_p)} * \cos(\overline{\psi_p}) \tag{6.16}$$

$$\mathrm{t}_{\overline{\theta_s}} = \frac{\cos(\phi_s) * \sin(\theta_s) * \cos(\psi_s) + \sin(\phi_s) * \sin(\psi_s)}{\cos(\theta_s) * cos(\psi_s)} * \cos(\overline{\psi_s}) \tag{6.17}$$

Where:

- "M_{CZ}" is the twisting moments between parafoil and payload, its definition is slightly different from the one given for the 7 DOF and 8 DOF model. This definition is explained in [18].
- "$\boldsymbol{r_{CP}}$" is the vector from the parafoil centre of mass to the connection point C:

$$\boldsymbol{r_{CP}} = [R_p * \sin(\mu) \;\; 0 \;\; R_p * \cos(\mu)]' \tag{6.18}$$

- "$\boldsymbol{r_{CS}}$" is the vector from the payload centre of mass to the connection point C:

$$\boldsymbol{r_{CS}} = \left[0 \;\; 0 \;\; \frac{z_S}{2}\right]' \tag{6.19}$$

- "$\boldsymbol{\Xi}$" is the skew matrix formed by parafoil velocity:

$$\boldsymbol{S}(\boldsymbol{V_p}) = \begin{bmatrix} 0 & -V_z & V_y \\ V_z & 0 & -V_x \\ -V_y & V_x & 0 \end{bmatrix} \tag{6.20}$$

6.2 SIMULATIONS

We have performed a series of simulations for the simplified 9 DOF: only the most significant ones will be reported. As for the 6 DOF steady state, spiral maneuver, S-maneuver and validation simulations will be reported. From the steady state, we can catch the system equilibrium values. The other simulations will highlight how the computation handle long control and a more realistic control. The apparent masses and inertias relative terms can create problems on the stability of the simulations: on Titan environment this problem enhance.

- Steady state simulations: from 40 km of altitude with initial speed vector $\{u_c, v_c, w_c\} = \{8.6 \; 0 \; 4.2\}$.

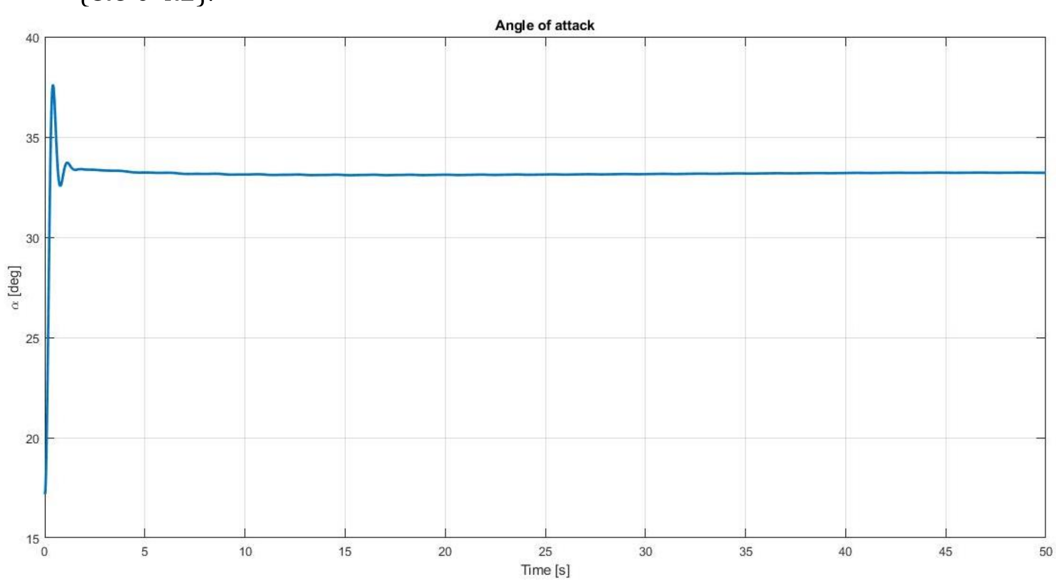

Figure 83: Angle of attack simplified 9 DOF.

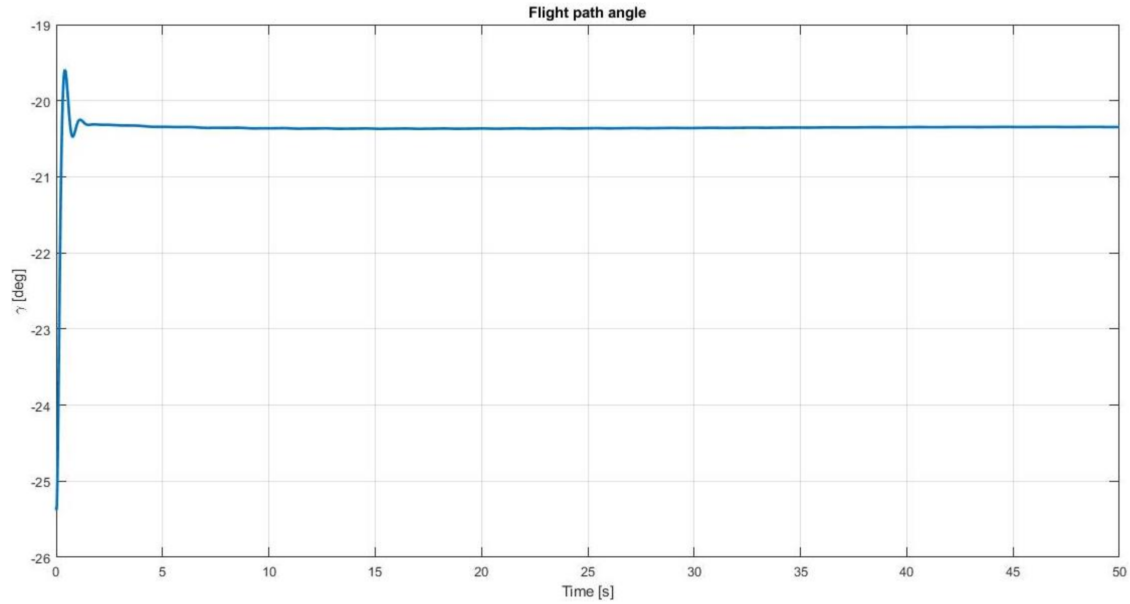

Figure 84: Flight-path angle simplified 9 DOF.

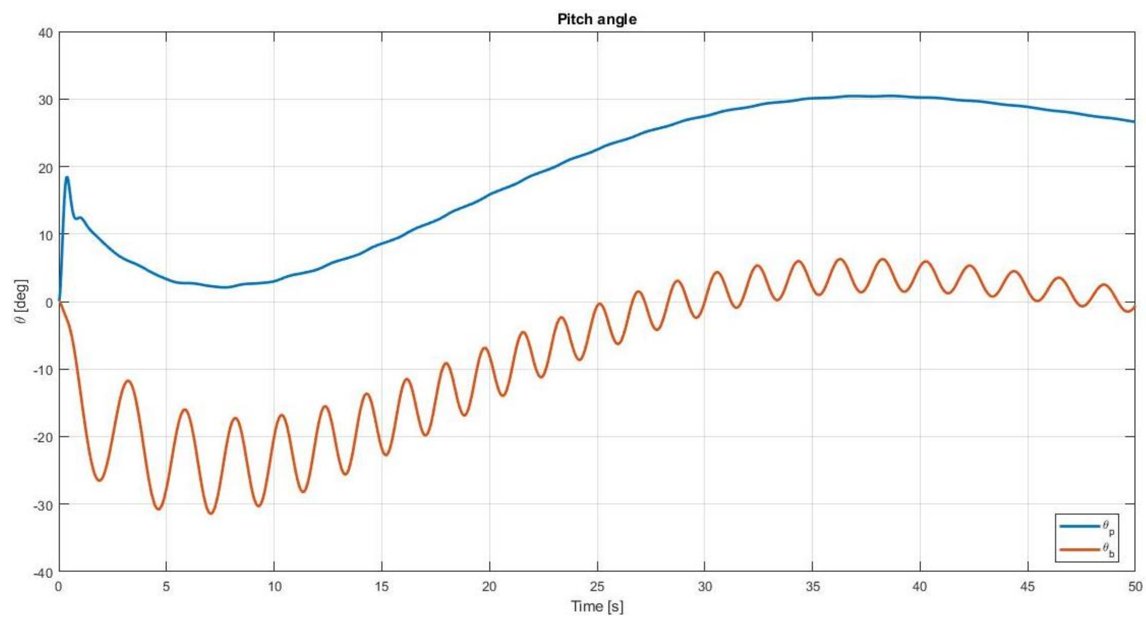

Figure 85: Pitch angle simplified 9 DOF.

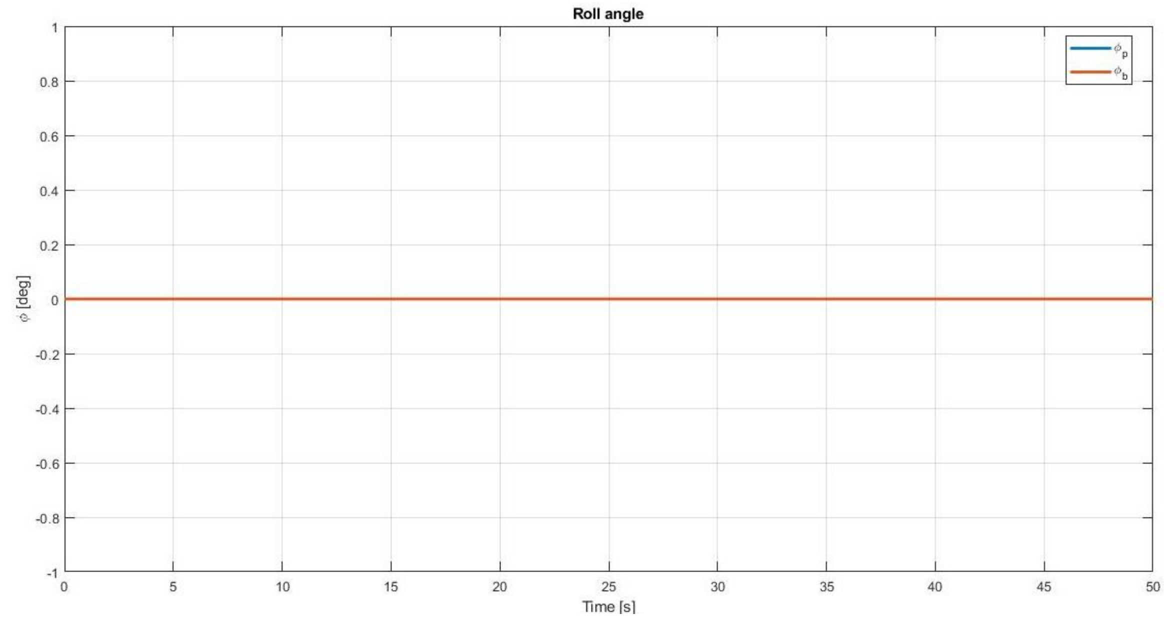

Figure 86: Roll angle simplified 9 DOF

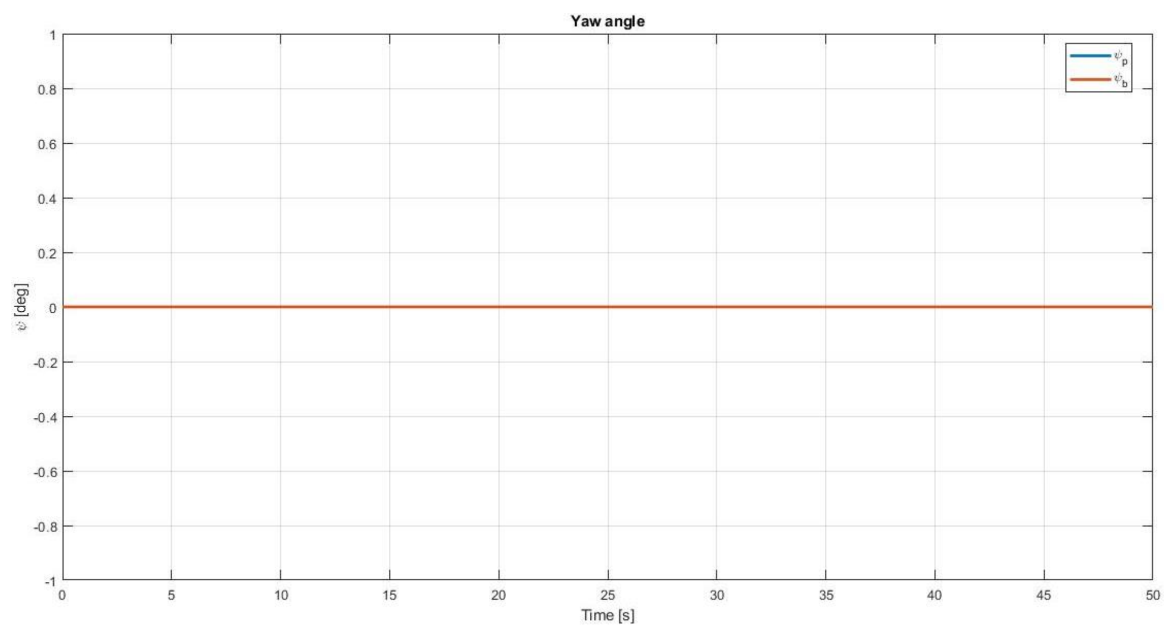

Figure 87: Yaw angle simplified 9 DOF.

- Spiral control simulations: from 40 km of altitude with initial speed vector $\{u_c, v_c, w_c\} = \{8.6\ 0\ 4.2\}\ m/s$.

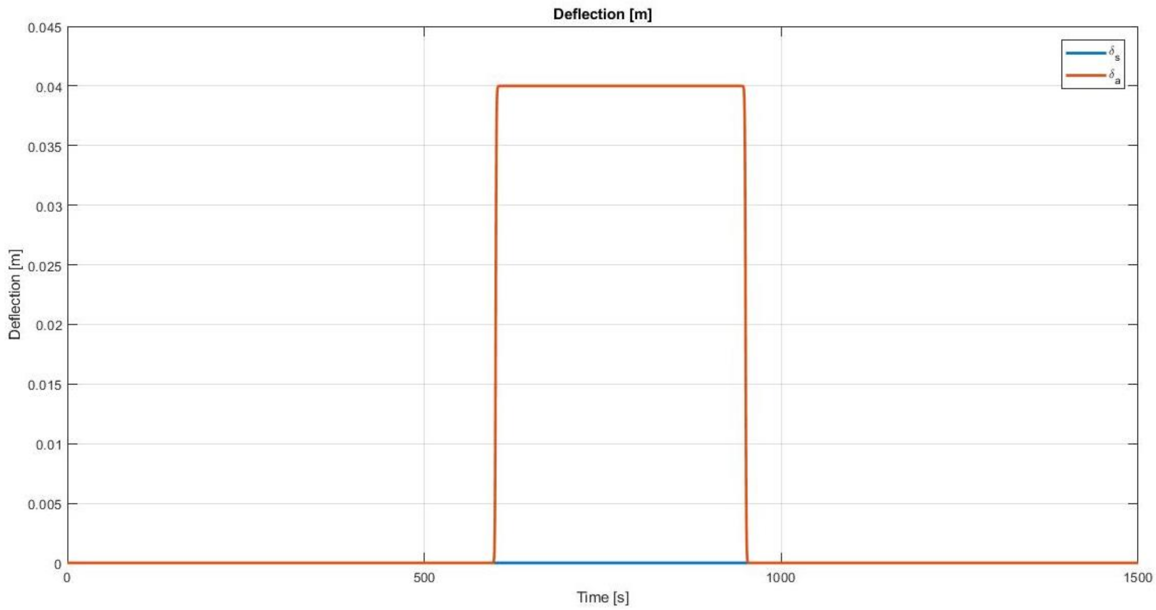

Figure 88: Spiral maneuver deflection. simplified 9 DOF.

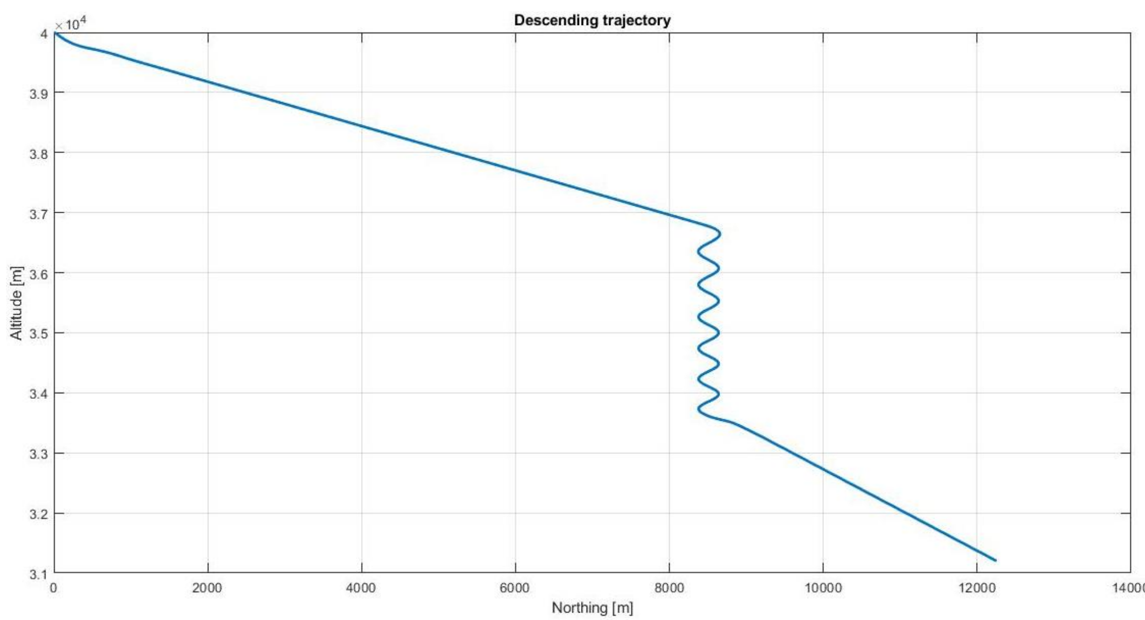

Figure 89: Descending trajectory spiral maneuver simplified 9 DOF.

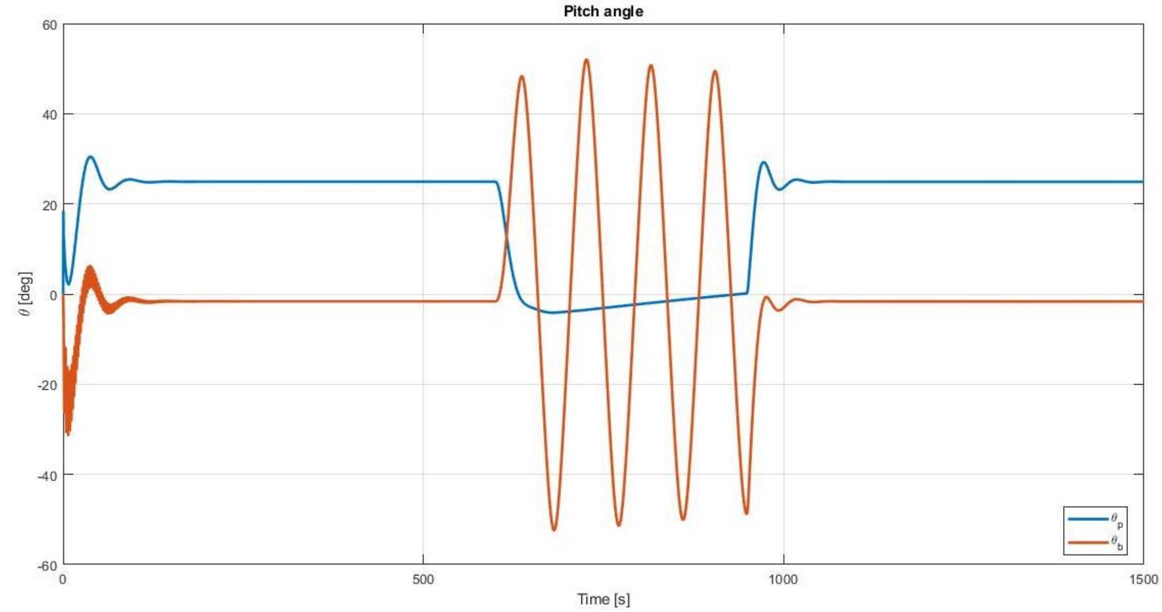

Figure 90: Pitch angle spiral maneuver simplified 9 DOF.

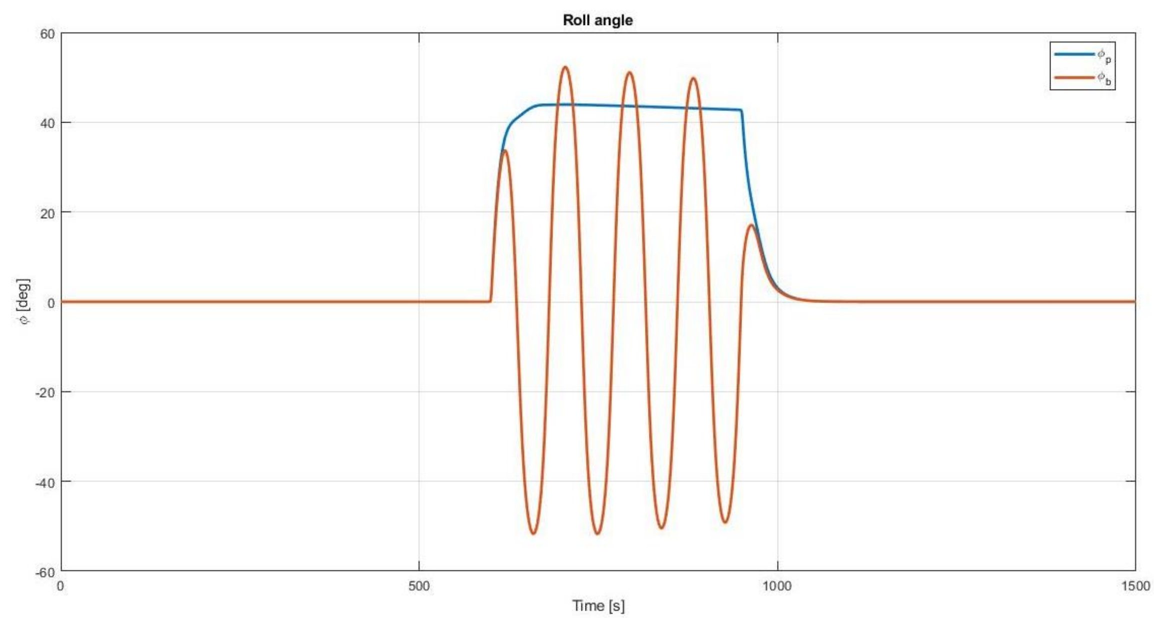

Figure 91: Roll angle spiral maneuver simplified 9 DOF.

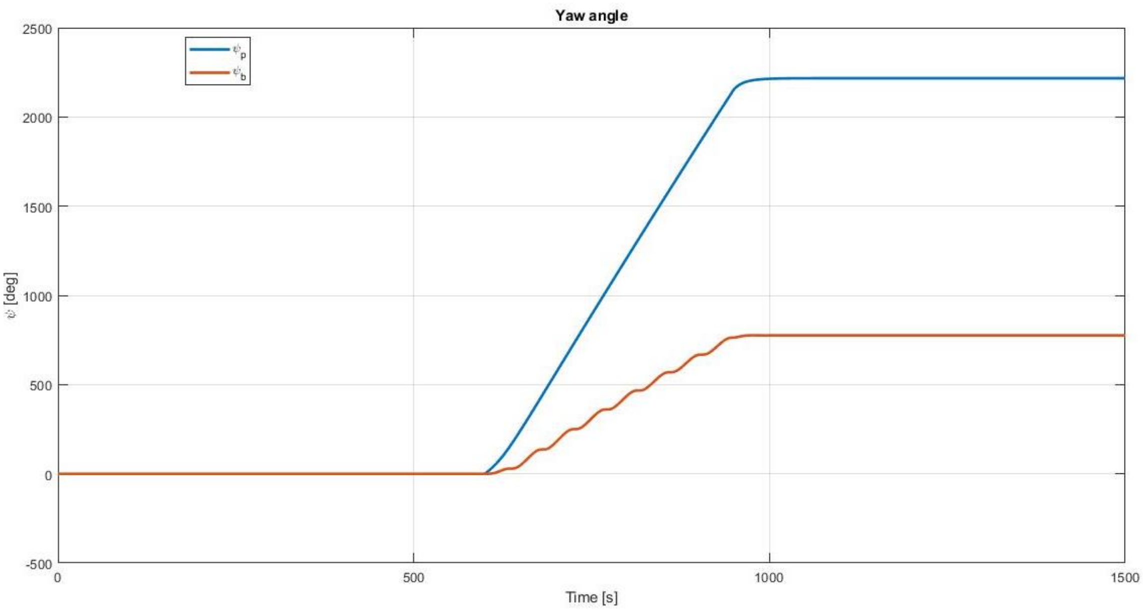

Figure 92: Yaw angle spiral maneuver simplified 9 DOF.

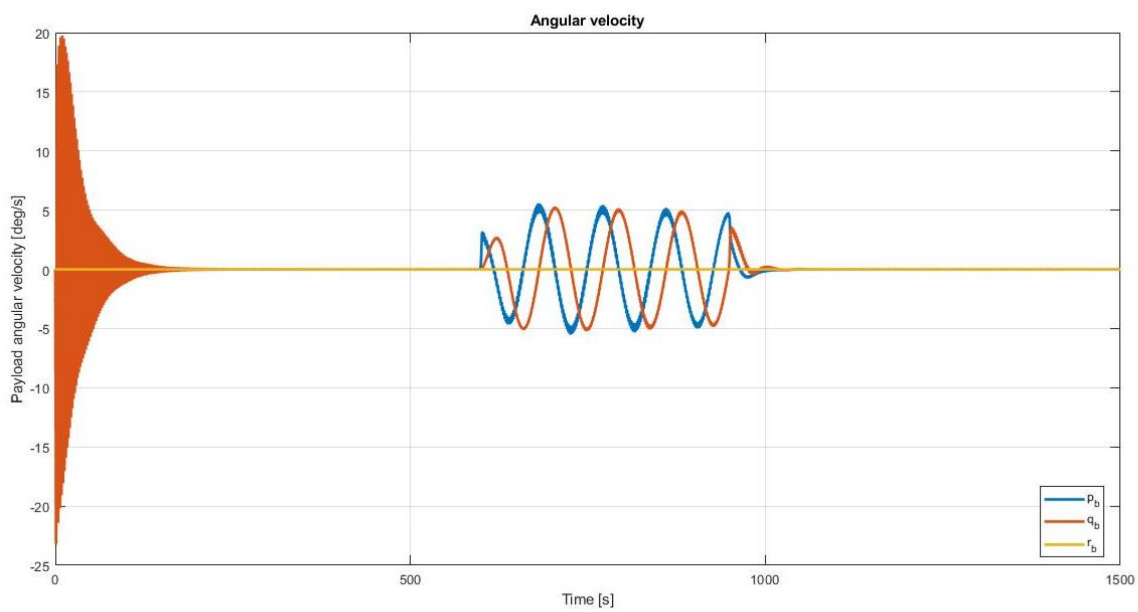

Figure 93: Payload angular velocity spiral maneuver simplified 9 DOF.

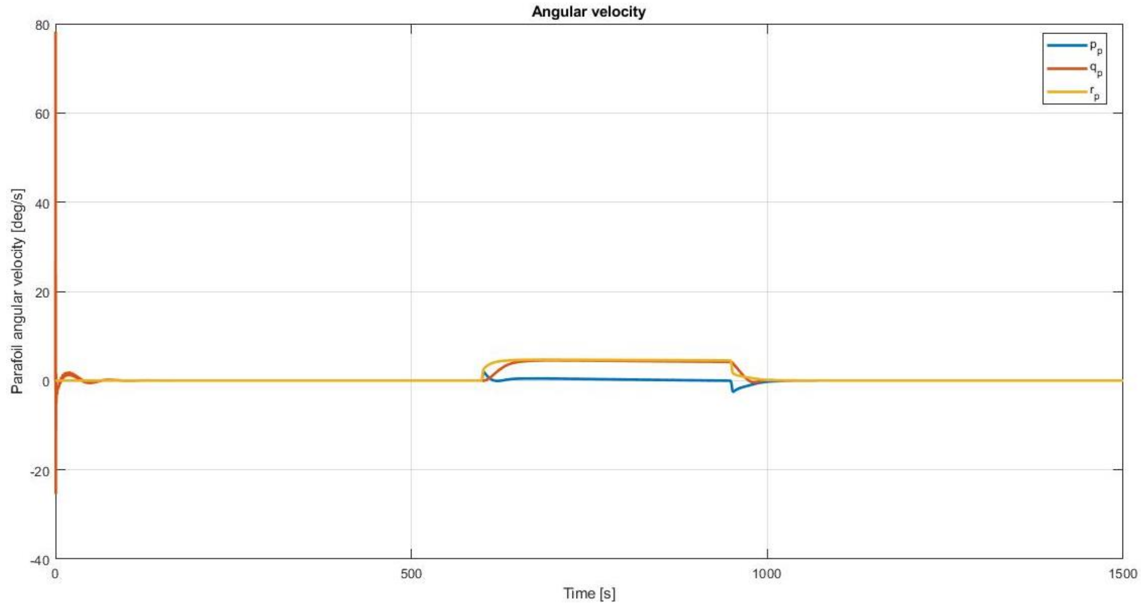

Figure 94: Parafoil Angular velocity spiral maneuver simplified 9 DOF.

- S-maneuver simulations: from 4 km with initial speed vector $\{u_c, v_c, w_c\} = \{8.6\ 0\ 4.2\}\ m/s$.

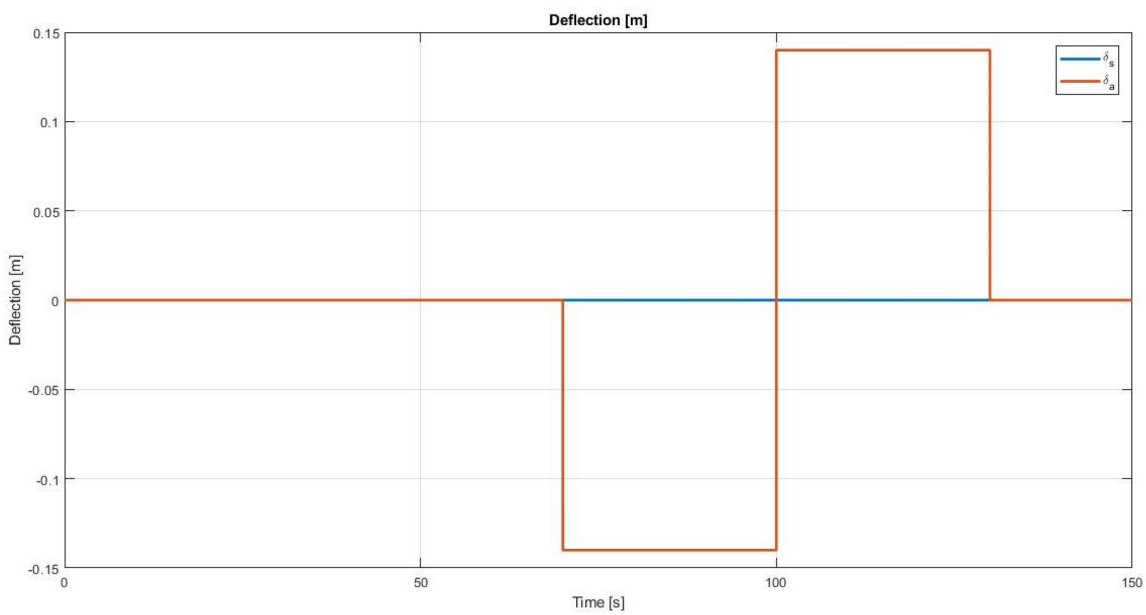

Figure 95: Control deflection S-maneuver.

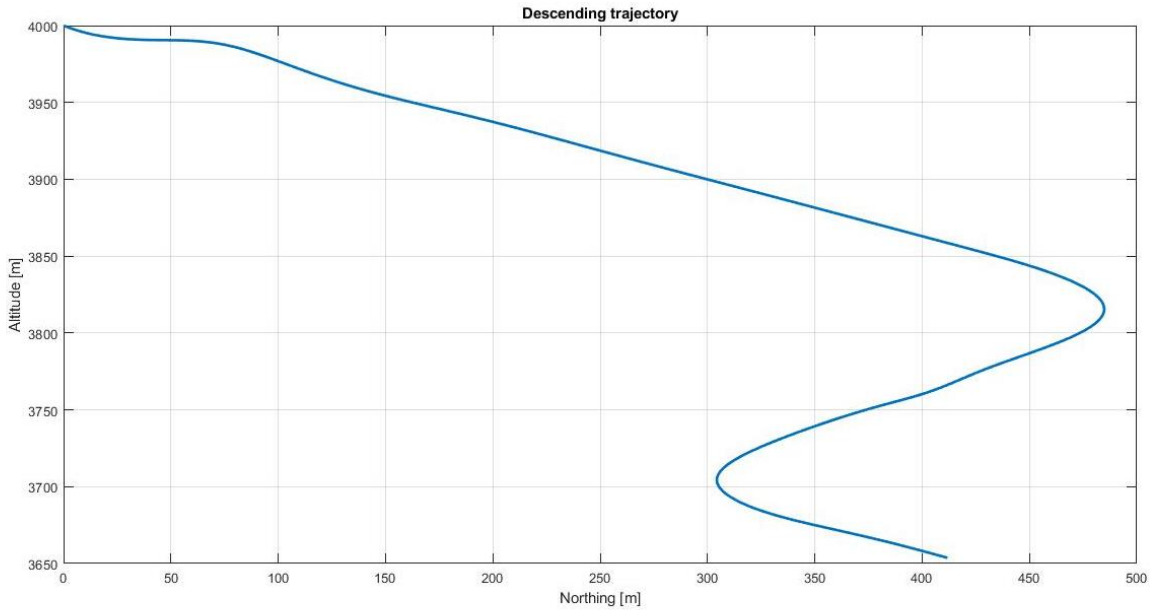

Figure 96: Descending trajectory S-maneuver.

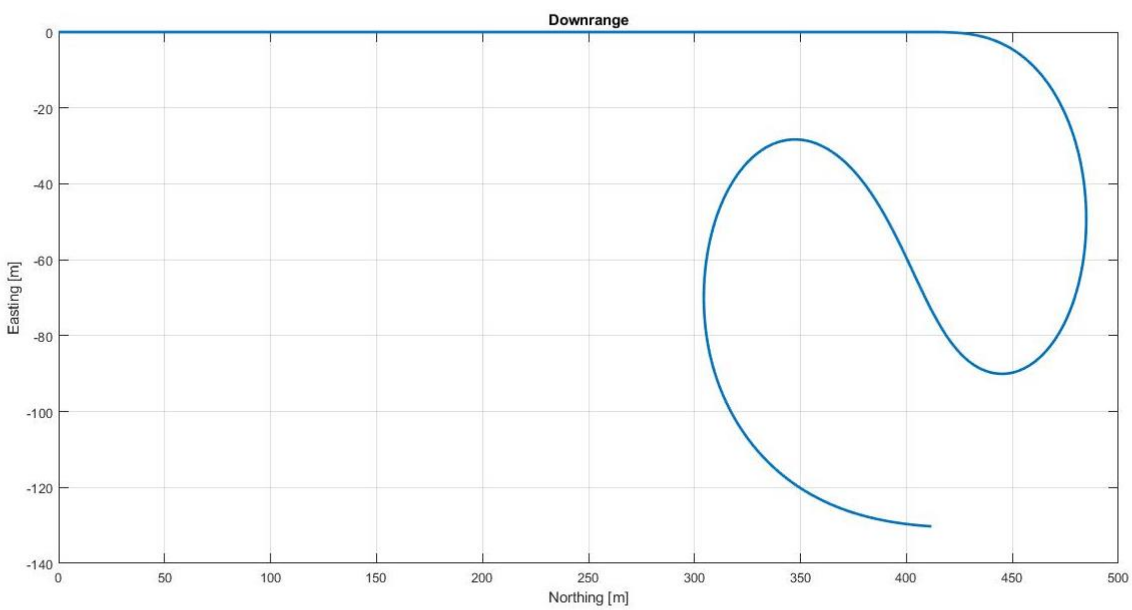

Figure 97: Downrange trajectory S-maneuver.

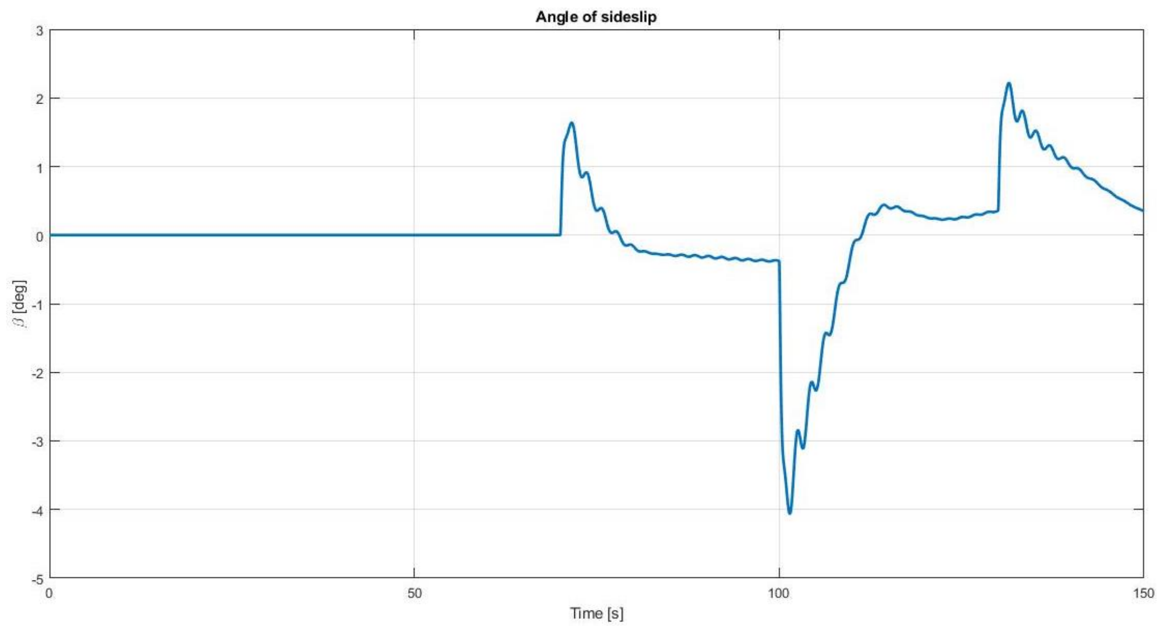

Figure 98: Sideslip angle S-maneuver.

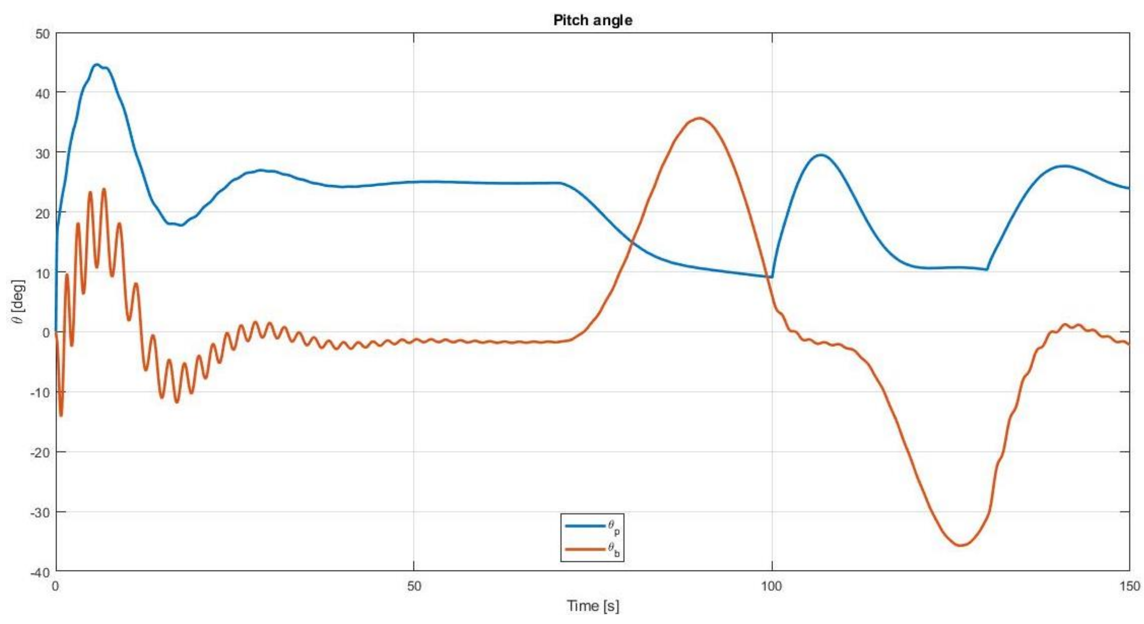

Figure 99: Pitch angle S-maneuver.

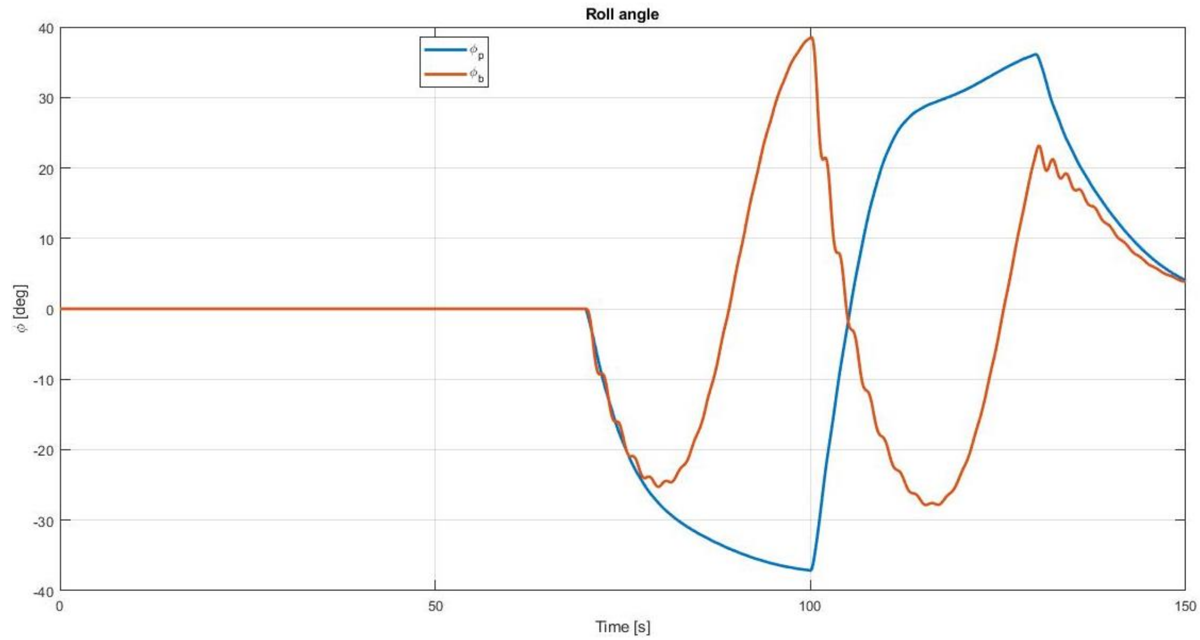

Figure 100: Roll angle S-maneuver.

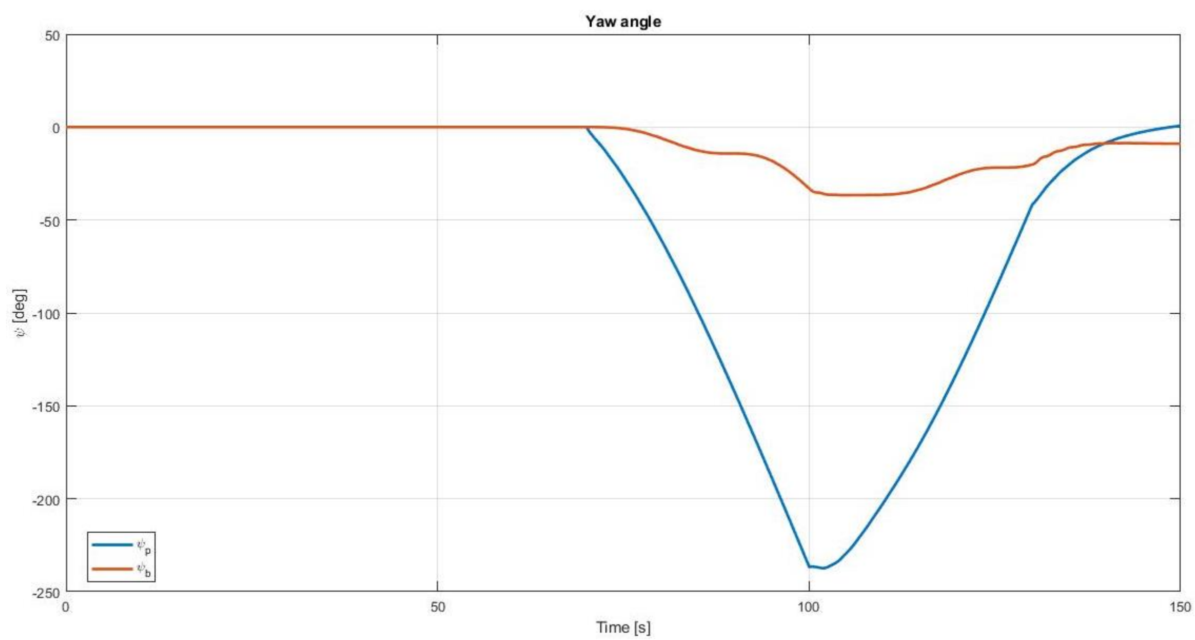

Figure 101: Yaw angle S-maneuver.

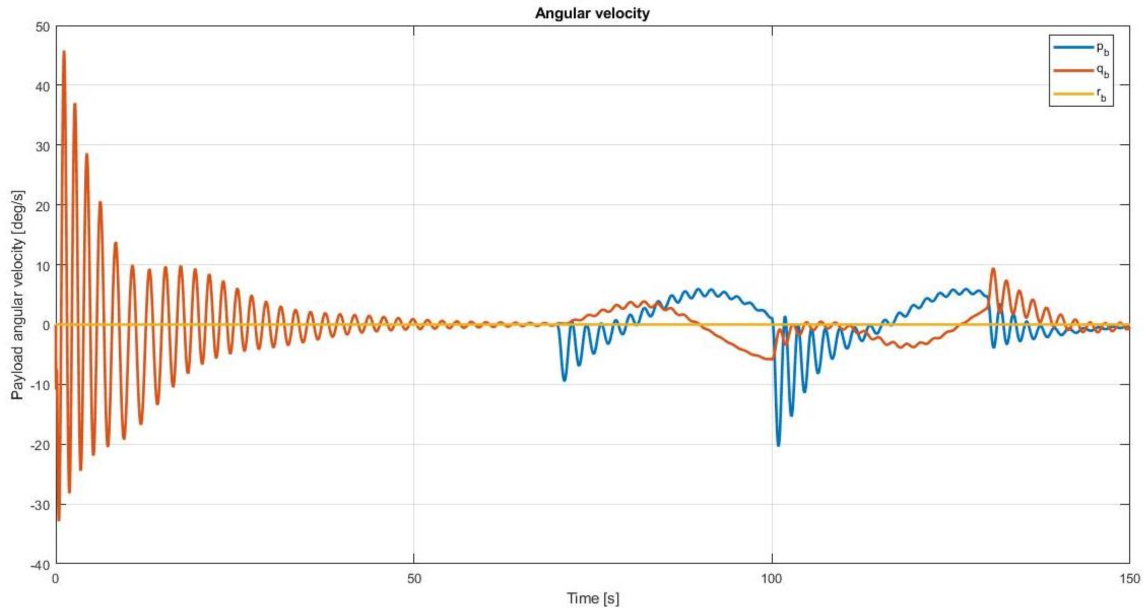

Figure 102: Payload angular velocities S-maneuver.

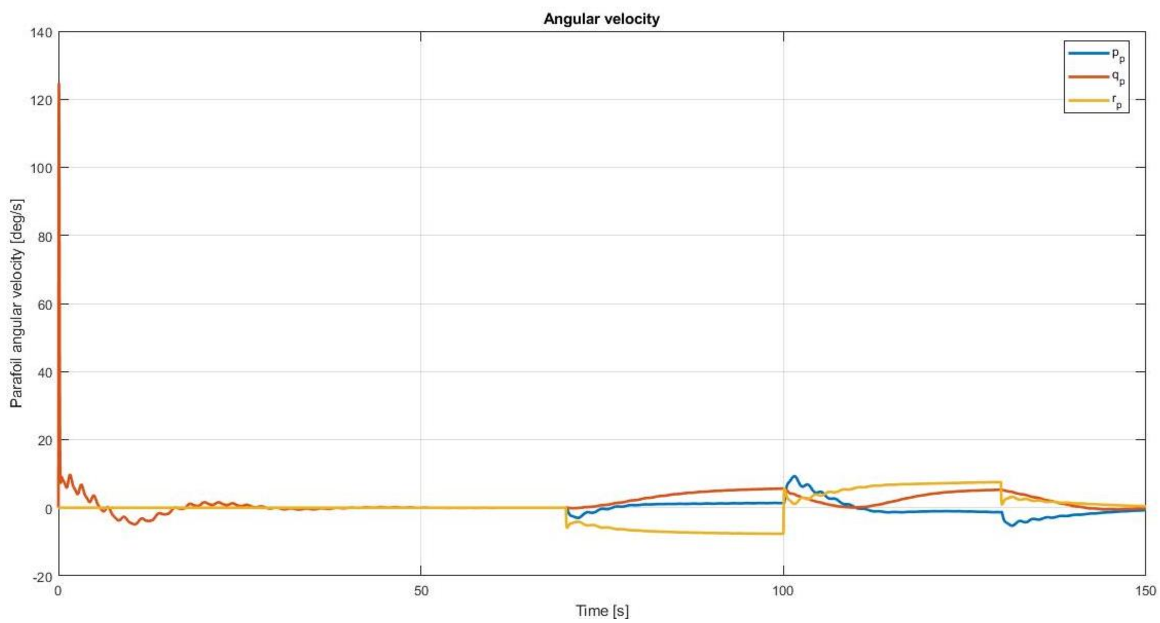

Figure 103: Parafoil angular velocities S-maneuver.

- University of Rome, “La Sapienza” validation: the control in [14] is defined as angle deflection, in our model is defined as a normalized length that refers to how much of brake is pulled.

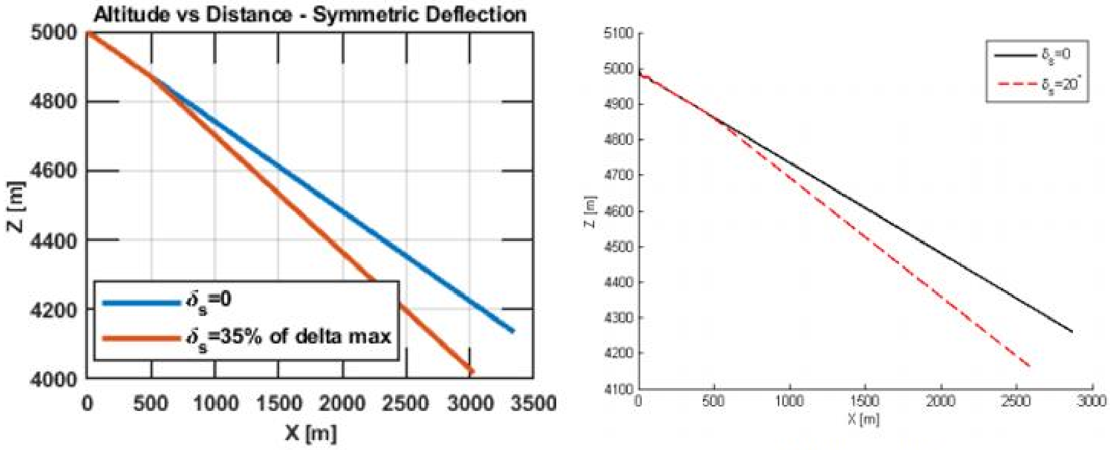

(b) Altitude *vs* Distance

Figure 104: XZ-plane symmetric deflection comparison.

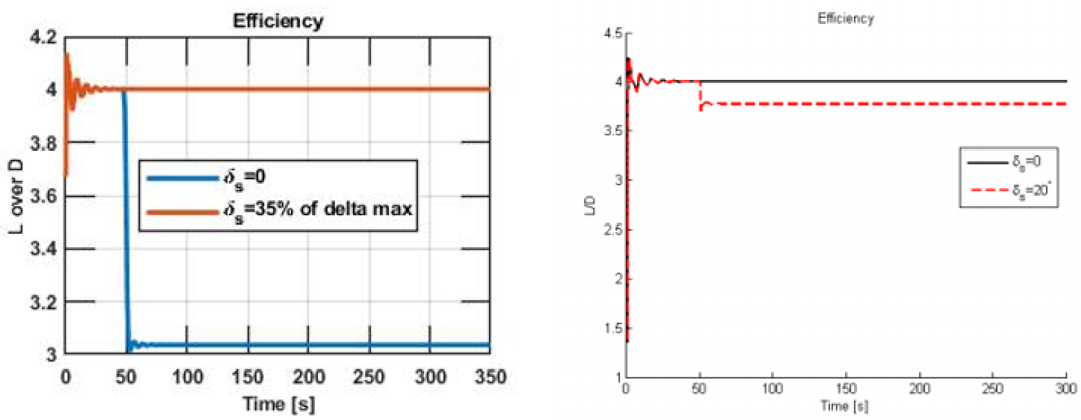

(a) Efficiency

Figure 105: Efficiency symmetric deflection comparison.

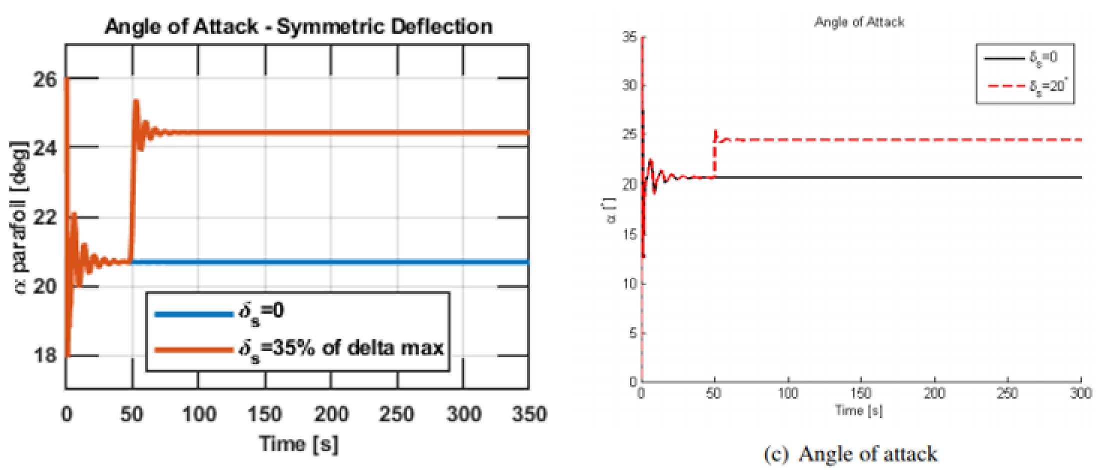

(c) Angle of attack

Figure 106: Angle of attack symmetric deflection comparison.

6.3 COMPLETE MODEL

The 9 DOF "complete model" differs from the simplified one because it takes into account some apparent masses effects and payload-parafoil relative motion that are not specified in the other models. However, to be able to use this model we need a more accurate geometry parameters identification (the number of position vectors is equal to those for the 7 and 8 DOF) and a consistent aerodynamic.

This model can be useful if we want to isolate the motion of the payload in respect of the parafoil: but the computation time and the number of needed information for the model increase. More about this model can be find in [8].

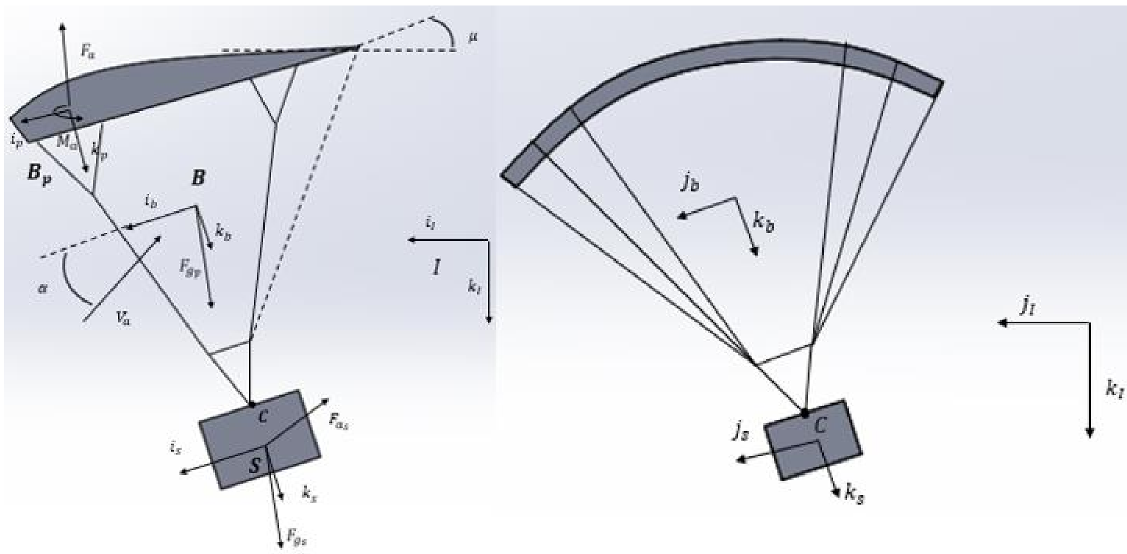

Figure 107: 9 DOF schematic representation.

6.3.1 EQUATIONS OF MOTION

The 9 DOF complete model equations of motion are very similar to those in sections 4.2 and 5.1 However, in the original model the lines twisting moment is not considered: a successive version of the model tries to insert the line contribution to the overall dynamics [15].

$$\boldsymbol{A}_{4x12} * \boldsymbol{b}_{12x1} = \begin{bmatrix} \boldsymbol{F}_p \\ \boldsymbol{M}_p \\ \boldsymbol{F}_s \\ \boldsymbol{M}_s \end{bmatrix} \tag{6.21}$$

$$\boldsymbol{A_{4x12}} = \begin{bmatrix} (m_p+m_e)*\boldsymbol{I_{3x3}}+\boldsymbol{M_f}' & -\boldsymbol{M_f'}*\boldsymbol{S(r_{CM})}-(m_p+m_e)*\boldsymbol{S(r_{CB})} & \boldsymbol{0_{3x3}} & -\boldsymbol{I_{3x3}} \\ \boldsymbol{S(r_{BM})}*\boldsymbol{M_f'} & \boldsymbol{I_p}+\boldsymbol{I_f}-\boldsymbol{S(r_{BM})}*\boldsymbol{M_f'}*\boldsymbol{S(r_{CM})} & \boldsymbol{0_{3x3}} & \boldsymbol{S(r_{CB})} \\ m_s*\boldsymbol{R_{sb}} & \boldsymbol{0_{3x3}} & -m_s*\boldsymbol{S(r_{CS})} & \boldsymbol{R_{sb}} \\ \boldsymbol{0_{3x3}} & \boldsymbol{0_{3x3}} & \boldsymbol{I_s} & -\boldsymbol{S(r_{CS})}*\boldsymbol{R_{sb}} \end{bmatrix} \tag{6.22}$$

$$\boldsymbol{b_{12x1}} = [\dot{u}_c \;\; \dot{v}_c \; \dot{w}_c \;\; \dot{p}_p \;\; \dot{q}_p \;\; \dot{r}_p \;\; \dot{p}_s \;\; \dot{q}_s \;\; \dot{r}_s \;\; F_{CX} \;\; F_{CY} \;\; F_{CZ}\;]' \tag{6.23}$$

$$\boldsymbol{F_p} = \boldsymbol{F_a^p}+\boldsymbol{F_b^p}+\boldsymbol{F_g^p} - \boldsymbol{S(\omega_p)}*\left[(m+m_e)\boldsymbol{I_{3x3}}+\boldsymbol{M_f'}\right]*\begin{bmatrix}u_c\\v_c\\w_c\end{bmatrix}+\boldsymbol{S(\omega_p)}*\boldsymbol{M_f'}*\boldsymbol{S(r_{CM})}*\begin{bmatrix}p_p\\q_p\\r_p\end{bmatrix}+\boldsymbol{S(\omega_p)} *\boldsymbol{M_f'}*\boldsymbol{R_{bn}}*\boldsymbol{W}-(m_p+m_e)*\boldsymbol{S(\omega_p)}*\boldsymbol{S(\omega_p)}*\boldsymbol{r_{CB}} \tag{6.24}$$

$$\boldsymbol{M_p} = \boldsymbol{M_a}+\boldsymbol{M_b^p}+\boldsymbol{S(r_{BA})}*\boldsymbol{F_a^p}-\begin{bmatrix}0\\0\\M_{CZ}\end{bmatrix} - \left[\boldsymbol{S(\omega_p)}*(\boldsymbol{I_p}+\boldsymbol{I_f'})-\boldsymbol{S(r_{BM})}*\boldsymbol{S(\omega_p)}*\boldsymbol{M_f'}*\boldsymbol{S(r_{CM})}\right]*\begin{bmatrix}\boldsymbol{p_p}\\\boldsymbol{q_p}\\\boldsymbol{r_p}\end{bmatrix} - \boldsymbol{S(r_{BM})}*\boldsymbol{S(\omega_p)}*\boldsymbol{M_f'}*\begin{bmatrix}u_c\\v_c\\w_c\end{bmatrix}+\boldsymbol{S(r_{BM})}*\boldsymbol{S(\omega_p)}*\boldsymbol{M_f'}*\boldsymbol{R_{bn}}*\boldsymbol{W} \tag{6.25}$$

$$\boldsymbol{F_s} = \boldsymbol{F_a^s}+\boldsymbol{F_g^s}+m_s*\boldsymbol{S(r_{CS})}*\boldsymbol{G}-m_s*\boldsymbol{R_{bs}}*\boldsymbol{S(\omega_p)}*\begin{bmatrix}u_c\\v_c\\w_c\end{bmatrix}-m_s*\boldsymbol{S(\omega_s)} *\boldsymbol{S(\omega_s)}*\boldsymbol{r_{CS}} \tag{6.26}$$

$$\boldsymbol{M_s} = \boldsymbol{M_a^s}+\boldsymbol{R_{sb}}*\boldsymbol{M_c}-\boldsymbol{S(\omega_s)}*\boldsymbol{I_s}*\begin{bmatrix}p_s\\q_s\\r_s\end{bmatrix} \tag{6.27}$$

$$\begin{bmatrix} \dot{\phi}_p \\ \dot{\theta}_p \\ \dot{\psi}_p \end{bmatrix} = \begin{bmatrix} 1 & \sin(\phi_p) * \frac{\sin(\theta_p)}{\cos(\theta_p)} & \cos(\phi_p) * \frac{\sin(\theta_p)}{\cos(\theta_p)} \\ 0 & \cos(\phi_p) & -\sin(\phi_p) \\ 0 & \sin(\phi_p) * \frac{1}{\cos(\theta_p)} & \cos(\phi_p) * \frac{1}{\cos(\theta_p)} \end{bmatrix} * \begin{bmatrix} p_p \\ q_p \\ r_p \end{bmatrix} \tag{6.28}$$

$$\begin{bmatrix} \dot{\phi}_s \\ \dot{\theta}_s \\ \dot{\psi}_s \end{bmatrix} = \begin{bmatrix} 1 & \sin(\phi_s) * \frac{\sin(\theta_s)}{\cos(\theta_s)} & \cos(\phi_s) * \frac{\sin(\theta_s)}{\cos(\theta_s)} \\ 0 & \cos(\phi_s) & -\sin(\phi_s) \\ 0 & \sin(\phi_s) * \frac{1}{\cos(\theta_s)} & \cos(\phi_s) * \frac{1}{\cos(\theta_s)} \end{bmatrix} * \begin{bmatrix} p_s \\ q_s \\ r_s \end{bmatrix} \tag{6.29}$$

$$\begin{bmatrix} \dot{x} \\ \dot{y} \\ \dot{z} \end{bmatrix} = \boldsymbol{R'}_{\boldsymbol{bn}} * \begin{bmatrix} u \\ v \\ w \end{bmatrix} \tag{6.30}$$

$$\boldsymbol{M_C} = \begin{bmatrix} 0 \\ 0 \\ M_{CZ} \end{bmatrix} ; K_\psi = 0.07\ N * \frac{m}{rad} ; K_r = 0.005\ N * \frac{m*s}{rad}; \tag{6.31}$$

6.4 Complete 9 DOF Simulations

In this section the results of a S-maneuver are presented. Fewer simulation has been made for this model: there is still a limited application in the projects view. The simplified 9 DOF can for now satisfy our requirements for this preliminary phase. If the 9 DOF will be the chosen configuration more analysis can be performed with this last implemented model.

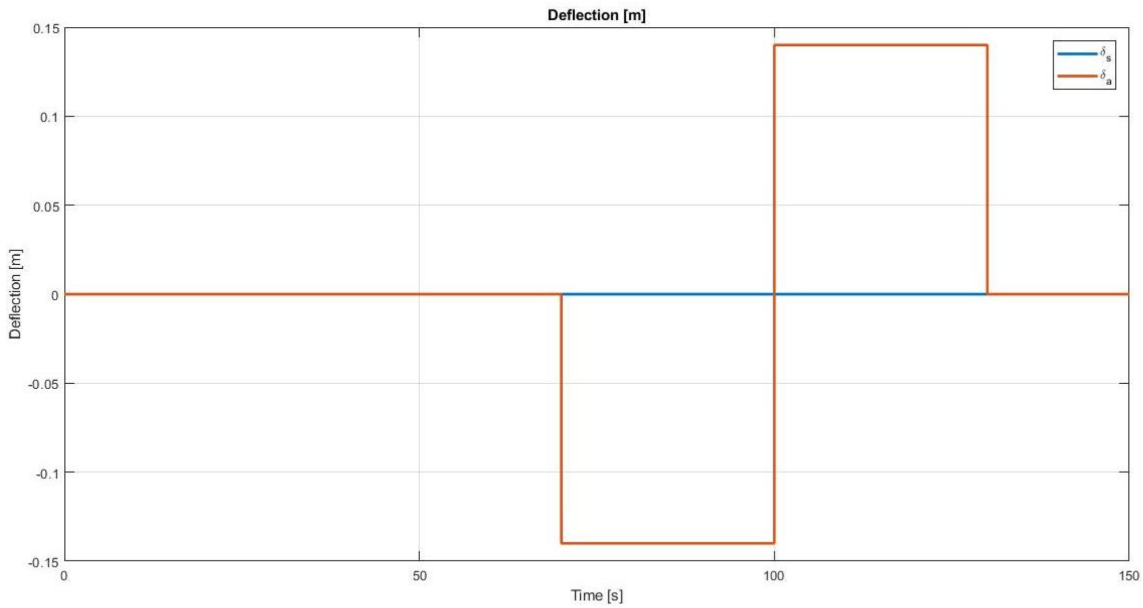

Figure 108: Control deflection complete 9 DOF.

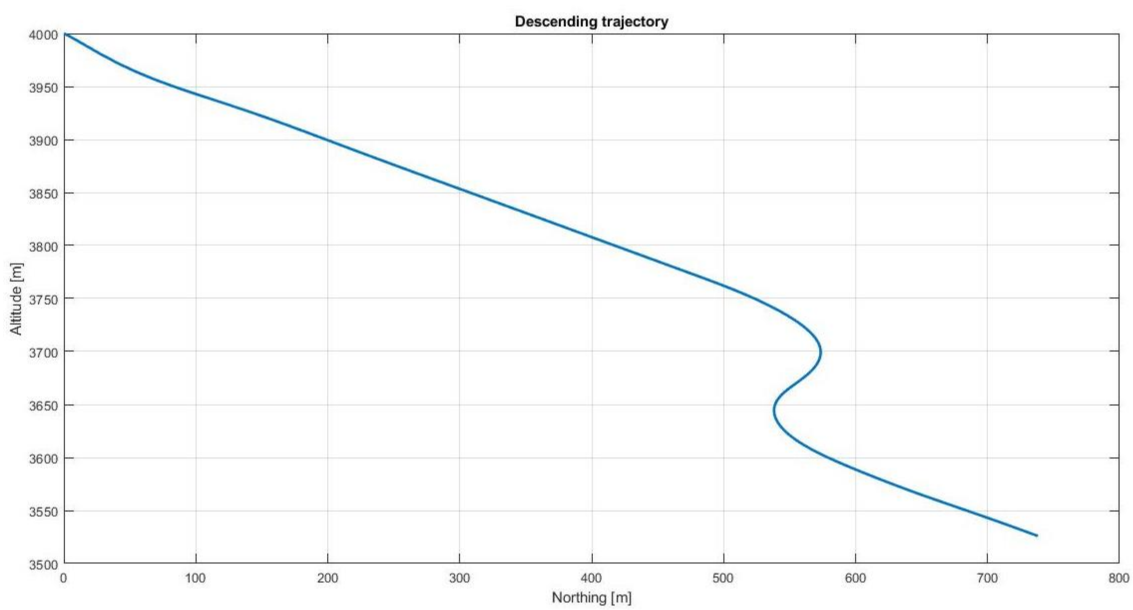

Figure 109: Descending trajectory complete 9 DOF.

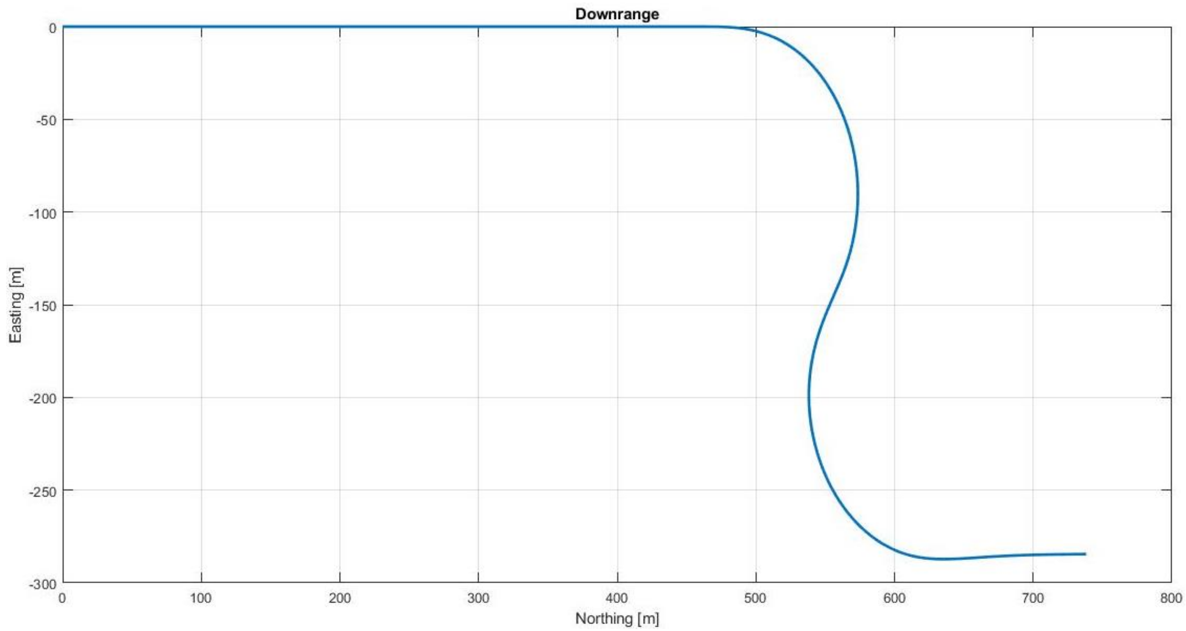

Figure 110: Downrange trajectory complete 9 DOF.

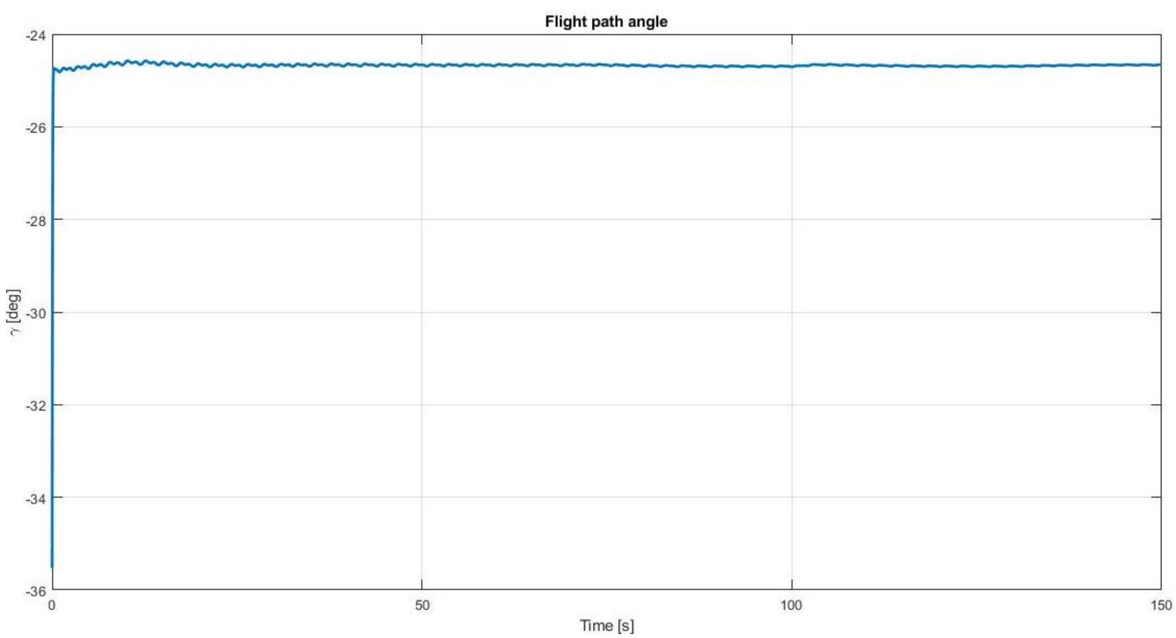

Figure 111: Flight-path angle complete 9 DOF.

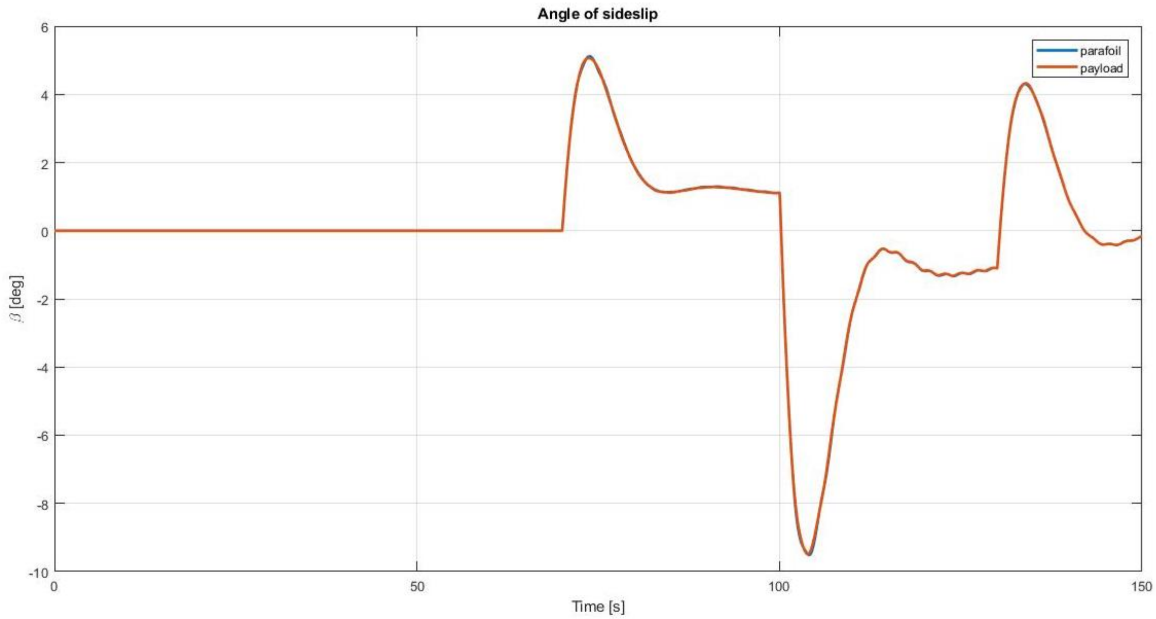

Figure 112: Sideslip angle complete 9 DOF.

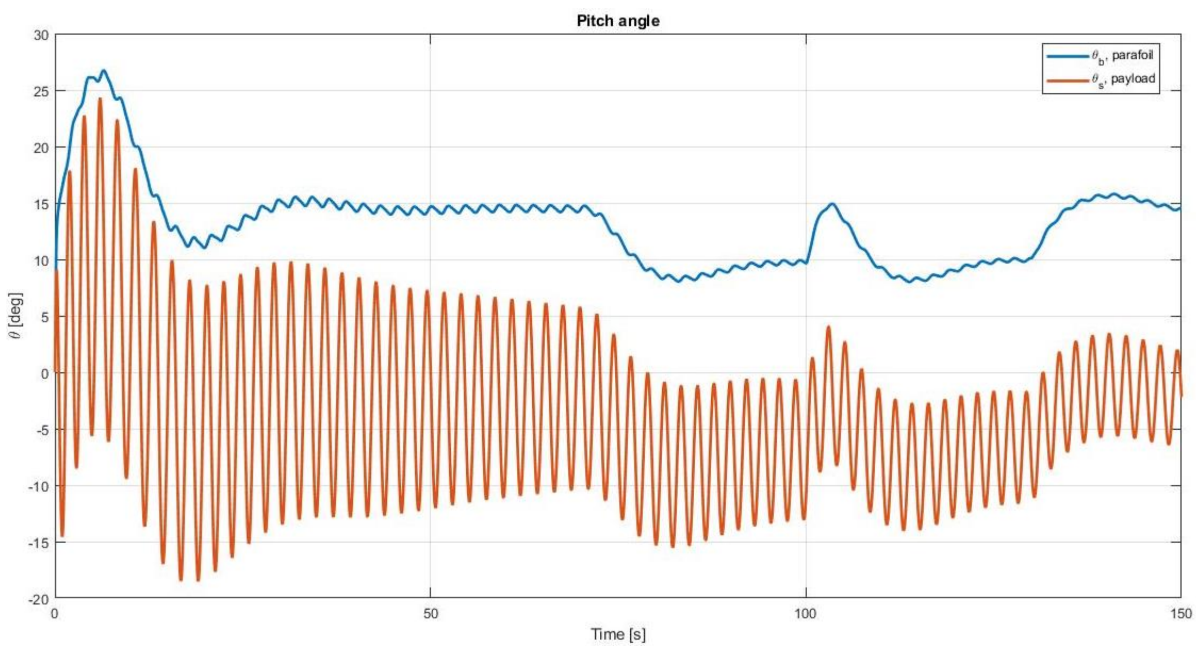

Figure 113: Pitch angle complete 9 DOF.

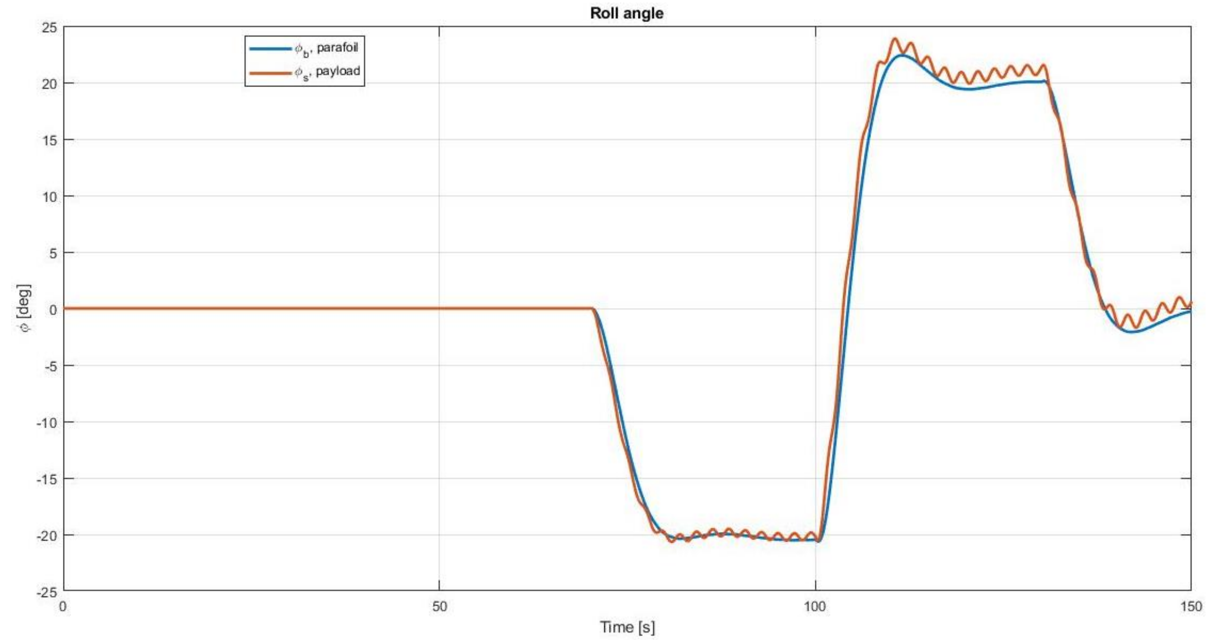

Figure 114: Roll angle complete 9 DOF.

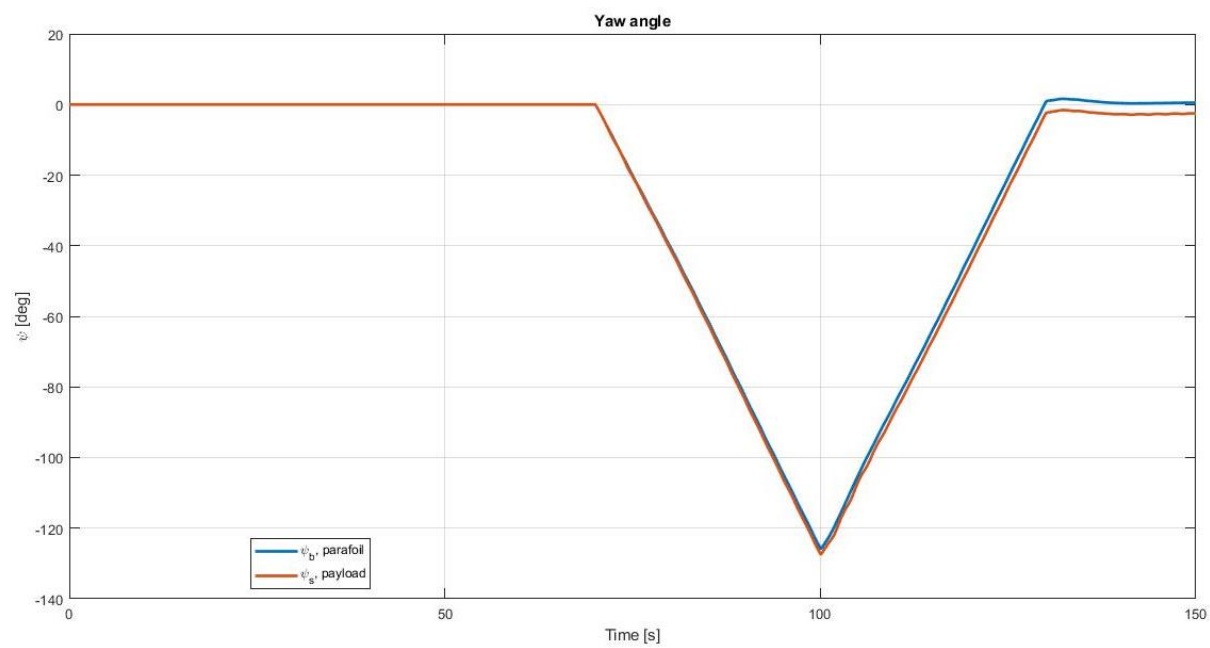

Figure 115: Yaw angle complete 9 DOF.

- Validation: we tried to match the trend of the plots in [18], unfortunately we lack their exact inputs parameters. The simulation is made on Earth environment.

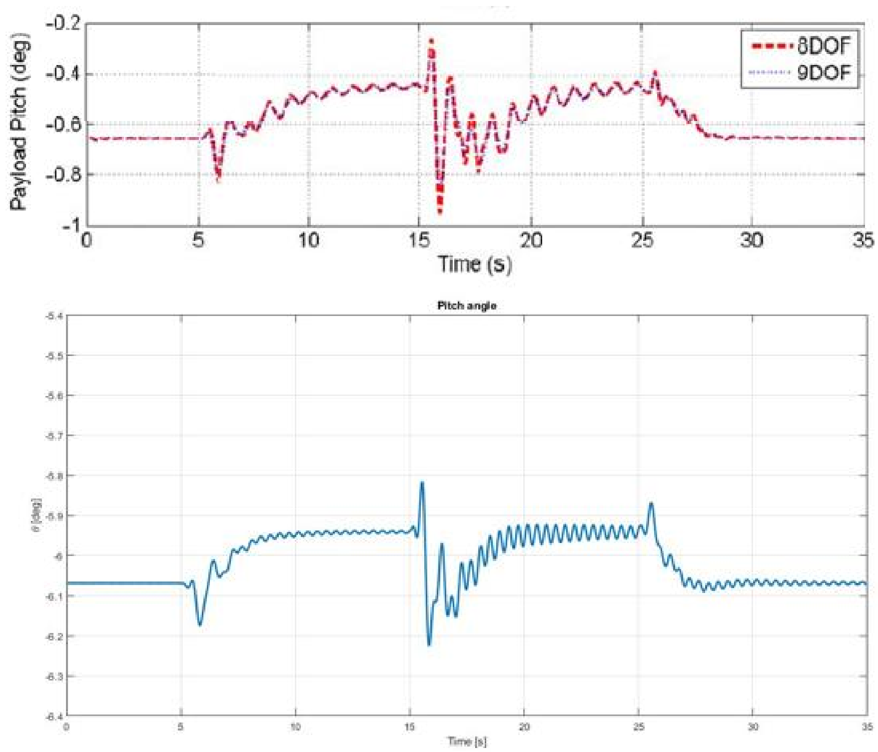

Figure 116: Pitch angle trend comparison.

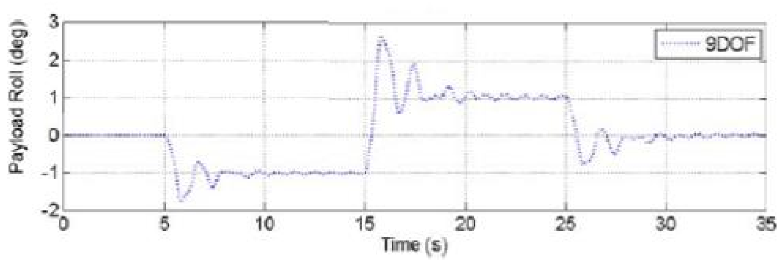

Fig. 22 Parafoil and Payload Roll.

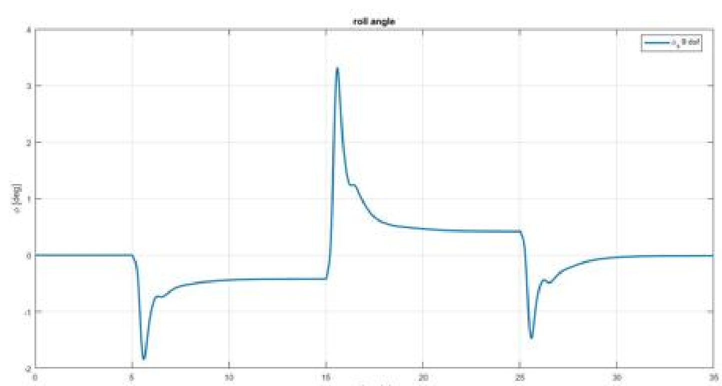

Figure 117: Roll angle trend comparison.

7 HANG GLIDER LOW FIDELITY MODEL: 6 DOF

We project to use a steerable system to deliver safely the payload to a landing site: the hang glider can give even more maneuverability and a wider range, it can be able to reach interesting landing sites with a better control authority. Small shifts of the loads can origin complex patterns, fulfil many different trajectories and, maybe, reach difficult landing sites. The issue that we would have to face is how to deploy a hang glider from a spinning probe: the complexity lays in both the unfolding maneuver and the rotation of the payload. We would need to de-spin the load and then find a way to open the glider or we can deploy the system after the parafoil on a lower altitude. We could than enhance the motion planning capabilities of all the probe or of one particular scientific payload.

To understand the capability of the system, we developed a 6 DOF model of the hang glider. In literature, some models can be find: most of them are already linearized ([19], [20], [6]) or have higher degrees of freedom, usually 9 ([21], [22]). The main aim of this model is to capture the dynamics of the glider. However, we want to keep the equations simple with few inputs that can be well-known even in this preliminary phase of the project.

The model recalls the one of the parafoil in chapter 3 the main differences are:

- No rigging angles
- Flat wing for the glider (the apparent masses and inertias are evaluated in respect to a flat wing, see section 0).
- The control of the glider is given displacing the load to generate maneuvering moments to shape the trajectory.

The hang glider wing reference frame will be called {p} as for the parafoil, the direction of the axis and characteristics are the same just with a quite different wing shape. In the formulas the quantities related to the hang glider will be label with a "g" as apex.

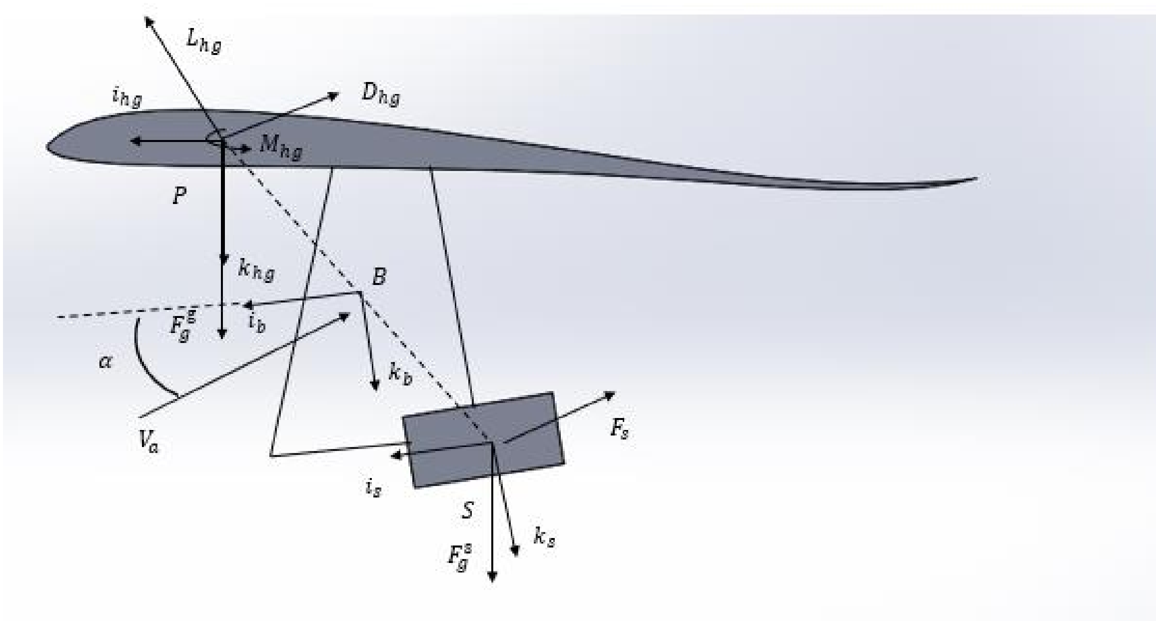

Figure 118: Hang glider side view.

7.1 EQUATIONS OF MOTION

The equations of motion can be written as:

$$\begin{bmatrix} m * \boldsymbol{I_{3x3}} + \boldsymbol{M_f} & -\boldsymbol{M_f} * \boldsymbol{S}(\boldsymbol{r_{BM}}) \\ \boldsymbol{S}(\boldsymbol{r_{BM}}) * \boldsymbol{M_f} & \boldsymbol{I} + \boldsymbol{I_f} - \boldsymbol{S}(\boldsymbol{r_{BM}}) * \boldsymbol{M_f} * \boldsymbol{S}(\boldsymbol{r_{BM}}) \end{bmatrix} * \begin{bmatrix} \dot{u} \\ \dot{v} \\ \dot{w} \\ \dot{p} \\ \dot{q} \\ \dot{r} \end{bmatrix} = \begin{bmatrix} \boldsymbol{F} \\ \boldsymbol{M} \end{bmatrix} \tag{7.1}$$

$$\begin{aligned} \boldsymbol{F} = {} & \boldsymbol{F_a^g} + \boldsymbol{F_a^s} + \boldsymbol{F_g^g} + \boldsymbol{F_g^s} - m * \boldsymbol{S}(\boldsymbol{\omega}) * \begin{bmatrix} u \\ v \\ w \end{bmatrix} - \boldsymbol{S}(\boldsymbol{\omega}) * \boldsymbol{M_f} * \left(\begin{bmatrix} u \\ v \\ w \end{bmatrix} - \boldsymbol{S}(\boldsymbol{r_{BM}}) * \begin{bmatrix} p \\ q \\ r \end{bmatrix} \right) \\ & + \boldsymbol{S}(\boldsymbol{\omega}) * \boldsymbol{M_f} * \boldsymbol{R_{bn}} * \boldsymbol{W} \end{aligned} \tag{7.2}$$

$$\begin{aligned} \boldsymbol{M} = {} & \boldsymbol{M_a^g} + \boldsymbol{S}(\boldsymbol{r_{BM}}) * \boldsymbol{F_a^g} + \boldsymbol{S}(\boldsymbol{r_{BM}}) * \boldsymbol{F_g^g} + \boldsymbol{S}(\boldsymbol{r_{BS}}) * \boldsymbol{F_a^s} + \boldsymbol{S}(\boldsymbol{r_{BS}}) * \boldsymbol{F_g^s} - \boldsymbol{S}(\boldsymbol{\omega}) * \boldsymbol{I} \\ & * \begin{bmatrix} p \\ q \\ r \end{bmatrix} - \boldsymbol{S}(\boldsymbol{\omega}) * \boldsymbol{I_f} * \begin{bmatrix} p \\ q \\ r \end{bmatrix} - \boldsymbol{S}(\boldsymbol{r_{BM}}) * \boldsymbol{S}(\boldsymbol{\omega}) * \boldsymbol{M_f} \\ & * \left(\begin{bmatrix} u \\ v \\ w \end{bmatrix} - \boldsymbol{S}(\boldsymbol{r_{BM}}) * \begin{bmatrix} p \\ q \\ r \end{bmatrix} - \boldsymbol{R_{bn}} * \boldsymbol{W} \right) \end{aligned} \tag{7.3}$$

$$\begin{bmatrix} \dot{\phi} \\ \dot{\theta} \\ \dot{\psi} \end{bmatrix} = \begin{bmatrix} 1 & \sin(\phi) * \dfrac{\sin(\theta)}{\cos(\theta)} & \cos(\phi) * \dfrac{\sin(\theta)}{\cos(\theta)} \\ 0 & \cos(\phi) & -\sin(\phi) \\ 0 & \sin(\phi) * \dfrac{1}{\cos(\theta)} & \cos(\phi) * \dfrac{1}{\cos(\theta)} \end{bmatrix} * \begin{bmatrix} p \\ q \\ r \end{bmatrix} \tag{7.4}$$

$$\begin{bmatrix} \dot{x} \\ \dot{y} \\ \dot{z} \end{bmatrix} = \boldsymbol{R'_{bn}} * \begin{bmatrix} u \\ v \\ w \end{bmatrix} \tag{7.5}$$

Where:

- "m" is the overall system mass:

$$m = m_{payload} + m_{parafoil} + m_{suspension\ lines} \tag{7.6}$$

- "$\boldsymbol{M_f}$" is the hang glider apparent mass tensor.
- "$\boldsymbol{I_f}$" is the hang glider apparent inertia tensor.
- "**W**" is the wind vector expressed in the navigation frame{n}.

$$\boldsymbol{V_{ground}} = \boldsymbol{V_{airspeed}} - \boldsymbol{W} \tag{7.7}$$

- "$\boldsymbol{S}(\boldsymbol{r_{BM}})$" is the skew-symmetric matrix that replace the vector product "$\boldsymbol{r_{BM}} \times$ "

$$S(r_{BM}) = \begin{bmatrix} 0 & -z_{BM} & y_{BM} \\ z_{BM} & 0 & -x_{BM} \\ -y_{BM} & x_{BM} & 0 \end{bmatrix} \quad (7.8)$$

Where $\boldsymbol{r_{BM}}$ is the vector that points from the origin of the body reference frame to the glider center of gravity. In our model it is evaluated as:

$$\boldsymbol{r_{BM}} = [\,x_{BM}\ \ y_{BM}\ \ z_{BM}] \quad (7.9)$$

$$x_{BM} = x_{BM_{steady\ state}} + \delta_x * \frac{z_{BS}}{z_{BM}}\ \ ; y_{BM} = \delta_y * \frac{z_{BS}}{z_{BM}} \quad (7.10)$$

The δ_x *and* δ_y are the payload displacements that change the position of the system center of mass. Therefore, they are needed to find the position vector from body reference frame {b} to {p}. If you change the load position, the system C.G. will shift [4].

- "$\boldsymbol{S(r_{BS})}$" is the skew-symmetric matrix that replace the vector product $\boldsymbol{r_{BS}}\times$:

$$\boldsymbol{S(r_{BS})} = \begin{bmatrix} 0 & -z_{BS} & y_{BS} \\ z_{BS} & 0 & -x_{BS} \\ -y_{BS} & x_{BS} & 0 \end{bmatrix} \quad (7.10)$$

Where $\boldsymbol{r_{BS}}$ is the vector that points from the origin of the body reference frame to the payload mass center. In our model it is evaluated as:

$$\boldsymbol{r_{BS}} = [\delta_x + x_{BS}\ \ \delta_y\ \ \ z_{BS}] \quad (7.11)$$

- "δ_x" is the payload longitudinal displacement used for control.
- "δ_y" is the payload lateral displacement used for control.
- "$S(\boldsymbol{\omega})$" is the skew-symmetric matrix of the system rates:

$$\boldsymbol{S(\omega)} = \begin{bmatrix} 0 & -r & q \\ r & 0 & -p \\ -q & p & 0 \end{bmatrix} \quad (7.12)$$

- "$\boldsymbol{F_a^g}$" is the hang glider aerodynamic force vector expressed as:

$$\boldsymbol{F_a^g} = \frac{1}{2} * \rho * V_{ag}^2 * S_g * \boldsymbol{R_{gw}} * \begin{bmatrix} -(CL_0 + CL_{alpha} * \alpha + CL_{ds} * \overline{\delta_s}) \\ CY_{beta} * \beta \\ -(CD_0 + CD_{a2} * \alpha^2 + CD_{ds} * \overline{\delta_s}) \end{bmatrix} \quad (7.13)$$

Where

➢ "$\boldsymbol{R_{pw}}$" is the rotation matrix between the wind frame {w} and hang glider frame {p}. The matrix is expressed in terms of angle of attach, α, and sideslip angle, β.

$$\boldsymbol{R_{pw}} = \boldsymbol{R_{\alpha}} * \boldsymbol{R_{\beta}} = \begin{bmatrix} \cos(\alpha) & 0 & -\sin(\alpha) \\ 0 & 1 & 0 \\ \sin(\alpha) & 0 & \cos(\alpha) \end{bmatrix} * \begin{bmatrix} \cos(\beta) & \sin(\beta) & 0 \\ -\sin(\beta) & \cos(\beta) & 0 \\ 0 & 0 & 1 \end{bmatrix} \tag{7.14}$$

$$\alpha = \tan^{-1}\left(\frac{w_g}{u_g}\right) \tag{7.15}$$

$$\beta = \tan^{-1}\left(\frac{v_g}{\sqrt{u_g^2 + w_g^2}}\right) \tag{7.16}$$

$$\begin{aligned} \boldsymbol{V_{ag}} &= \left(\begin{bmatrix} u \\ v \\ w \end{bmatrix} + \boldsymbol{S(\omega)} * \boldsymbol{r_{BM}} - \boldsymbol{R_{bn}} * \boldsymbol{W}\right) \\ &= (\boldsymbol{V} + \boldsymbol{S(\omega)} * \boldsymbol{r_{BM}} - \boldsymbol{R_{bn}} * \boldsymbol{W}) \end{aligned} \tag{7.17}$$

$$V_{ag} = \sqrt{u_g^2 + v_g^2 + w_g^2} \tag{7.18}$$

- "$\boldsymbol{M_a^g}$" is the hang glider aerodynamic moment vector expressed as:

$$\boldsymbol{M_a^g} = \frac{1}{2} * \rho * V_{ag}^2 * S_g * \begin{bmatrix} b(C_{l\beta} * \beta + \frac{b}{2 * V_a} * C_{lr} * r + \frac{b}{2 * V_a} * C_{lp} * p + C_{l\delta_a} * \overline{\delta_a}) \\ \bar{c} * (C_{m0} + C_{m\alpha} * \alpha + \frac{b}{2 * V_a} * C_{mq} * q) \\ b(C_{n\beta} * \beta + \frac{b}{2 * V_a} * C_{np} * p + \frac{b}{2 * V_a} * C_{nr} * r + C_{n\delta_a} * \overline{\delta_a} \end{bmatrix} \tag{7.19}$$

- "$\boldsymbol{F_a^s}$" is the payload aerodynamic force vector expressed as:

$$\boldsymbol{F_a^s} = \frac{1}{2} * \rho * V_{as}^2 * S_s * \boldsymbol{R_{sw}} * \begin{bmatrix} -CD_s \\ 0 \\ 0 \end{bmatrix} \tag{7.20}$$

Where

➢ "$\boldsymbol{R_{sw}}$" is the rotation matrix between the wind frame {w} and payload body frame {s}. The matrix has the same expression as the one for the parafoil.

$$\boldsymbol{V_s} = \left(\begin{bmatrix} u \\ v \\ w \end{bmatrix} + \boldsymbol{S}(\boldsymbol{\omega}) * \boldsymbol{r_{BC}} - \boldsymbol{R_{bn}} * \boldsymbol{W} \right) \tag{7.21}$$

$$V_{as} = \sqrt{u_s^2 + v_s^2 + w_s^2} \tag{7.22}$$

The aerodynamic moment of the payload is usually neglected: however, if the payload has some lifting characteristics, we should include it in the computation.

- "$\boldsymbol{F_g^g}$" is the glider weight force expressed in body frame as:

$$\boldsymbol{F_g^g} = \left(m_{glider}\right) * \begin{bmatrix} -\sin(\theta) \\ \cos(\theta) * \sin(\phi) \\ \cos(\theta) * \cos(\phi) \end{bmatrix} \tag{7.23}$$

- "$\boldsymbol{F_g^g}$" is the payload weight force expressed in body frame as:

$$\boldsymbol{F_g^s} = \left(m_{payload}\right) * \begin{bmatrix} -\sin(\theta) \\ \cos(\theta) * \sin(\phi) \\ \cos(\theta) * \cos(\phi) \end{bmatrix} \tag{7.24}$$

- The apparent masses and inertias generate a set of forces and moments that can be expressed as:

$$\begin{aligned} \boldsymbol{F_{app}} = -\Bigg\{ & \left[\boldsymbol{M_f} * \left(\begin{bmatrix} \dot{u} \\ \dot{v} \\ \dot{w} \end{bmatrix} - \boldsymbol{S}(\boldsymbol{r_{BM}}) * \begin{bmatrix} \dot{p} \\ \dot{q} \\ \dot{r} \end{bmatrix} \right) \right] \\ & + \left[\boldsymbol{S}(\boldsymbol{\omega}) * \boldsymbol{M_f} * \left(\begin{bmatrix} u \\ v \\ w \end{bmatrix} - \boldsymbol{S}(\boldsymbol{r_{BM}}) * \begin{bmatrix} p \\ q \\ r \end{bmatrix} - \boldsymbol{R_{bn}} * \boldsymbol{W} \right) \right] \Bigg\} \end{aligned} \tag{7.25}$$

$$\boldsymbol{M_{app}} = -\left(\boldsymbol{M_f} * \begin{bmatrix} \dot{p} \\ \dot{q} \\ \dot{r} \end{bmatrix} + \boldsymbol{S}(\boldsymbol{\omega}) * \boldsymbol{M_f} * \boldsymbol{R_{pb}} * \begin{bmatrix} p \\ q \\ r \end{bmatrix} \right) + \boldsymbol{S}(\boldsymbol{r_{BM}}) * \boldsymbol{F_{app}} \tag{7.26}$$

7.2 GEOMETRICAL CHARACTERISTICS OF THE HANG GLIDER

The geometry of the problem is different from the parafoil. However, the same concerns on the reliability of the aerodynamics and the geometrical guesses rise even in this case.

The initial parameters used are recall in Table 11 (the payload parameters are the same use in section 3.2 for the parafoil). The latero-directional aerodynamics is modelled with aerodynamic coefficients from [20], the longitudinal aerodynamics is derived from plots from [23] for a [20] similar hang glider.

Table 11: Hang Glider geometrical inputs.

$b = 15\ m$	Hang Glider wing span
$AR = 7$	Hang Glider wing aspect ratio
$c_{mean} = \frac{b}{AR} = 1.43\ m$	Hang Glider wing mean aerodynamic chord
$t = 0.14\ m$	Hang Glider wing mean thickness
$S = b * c_{mean} = 14.3\ m^2$	Hang Glider wing surface
$R = 0.12 * b = 1.2\ m$	Hang Glider hang straps length
$\sigma = 1.5$	Hang Glider wing aerial density
$l_{gp} = 0.143\ m$	Hang Glider distance between the wing mass center and the payload hang point in the XY-plane.
$m_g =$	Hang Glider Mass

Table 12: Latero-directional aerodynamic coefficients

$C_{Y_\beta} = 0.037$	$C_{Y_p} = 0.23$	$C_{Y_r} = 0.015$
$C_{l_\beta} = -0.137$	$C_{l_p} = -0.84$	$C_{l_r} = 0.072$
$C_{n_\beta} = 0.034$	$C_{n_p} = -0.370$	$C_{n_r} = -0.027$
$C_{D_{payload}} = 0.4$		

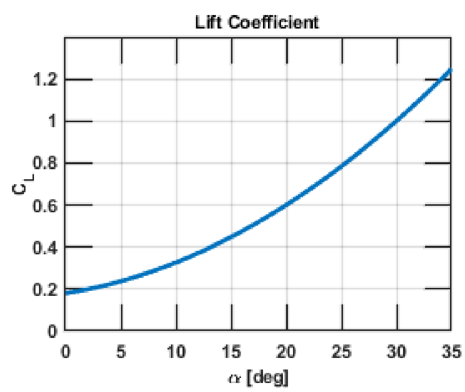

Figure 119: Hang Glider lift coefficient.

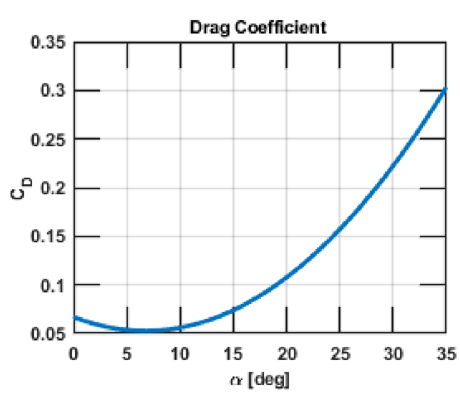

Figure 120: Hang Glider drag coefficient.

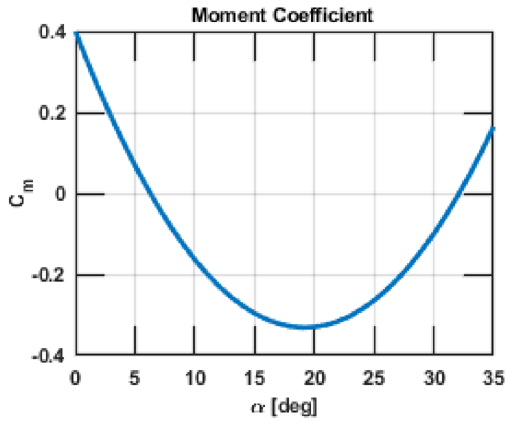

Figure 121: Hang Glider moment coefficient.

The inertia of the payload can be written as in section 3.2.1 for the hang glider the formulas are similar:

$$I_{x_{hg}} = \frac{m_g}{12} * (b^2 + t^2) \tag{7.27}$$

$$I_{y_{hg}} = \frac{m_g}{12} * (c^2 + t^2) \tag{7.28}$$

$$I_{z_{hg}} = \frac{m_g}{12} * (b^2 + c^2) \tag{7.29}$$

The system inertia used in the equation of motion can be written as:

$$I_x = I_{x_{hg}} + I_{xs} + m_g * r_{zhg}^2 + m_s * r_{zs}^2 \tag{7.30}$$

$$I_y = I_{y_{hg}} + I_{ys} + m_g * r_{zhg}^2 + m_s * r_{zs}^2 + m_g * r_{xhg}^2 + m_s * r_{xs}^2 \tag{7.31}$$

$$I_z = I_{z_{hg}} + I_{zs} + m_g * r_{zhg}^2 + m_s * r_{zs}^2 + m_g * r_{xhg}^2 + m_s * r_{xs}^2 \tag{7.32}$$

Where the distance along z of the glider and the payload is:

$$l_z = \frac{z_s}{2} + R + \frac{t}{2} \tag{7.33}$$

The distance along z between the glider center of mass and the system C.G and between the payload center of mass and the system C.G are formulated as:

$$r_{zs} = l_z * \left(\frac{m_g}{m_g + m_s}\right) \tag{7.34}$$

$$r_{zhg} = r_{zg} - l_z \tag{7.35}$$

The distance along x between the glider center of mass and the system C.G and between the payload center of mass and the system C.G are formulated as:

$$r_{xs} = -l_{gs} * \left(\frac{m_g}{m_g + m_s}\right) \tag{7.36}$$

$$r_{xhg} = l_{gs} * |r_{xs}| \tag{7.37}$$

7.3 STEADY STATE SIMULATIONS

The hang glider is a high efficiency system $\left(\frac{L}{D} = 4 \div 5\right)$ that seems to benefit the high-density Titan atmosphere: however, at high altitude (≈ 40 km) some oscillations of small amplitude are experienced. The steady state simulations are performed for a deployment of the hang glide at 40 km with an airspeed velocity of $V_a = 11\ m/s$ to decrease the overall oscillation period: the higher is the deployment velocity the longer will be the time needed to stabilize the system at that altitude.

The overall angle of attack is smaller than the parafoil case study. Nevertheless, the efficiency and the gliding performances are increased. The main issue of the hang-glider could be the complexity of the system deployment after the aeroshell entry. The parafoil can be easily folded: folding a hang-glider imply an accurate study on the shape and deployment of the system.

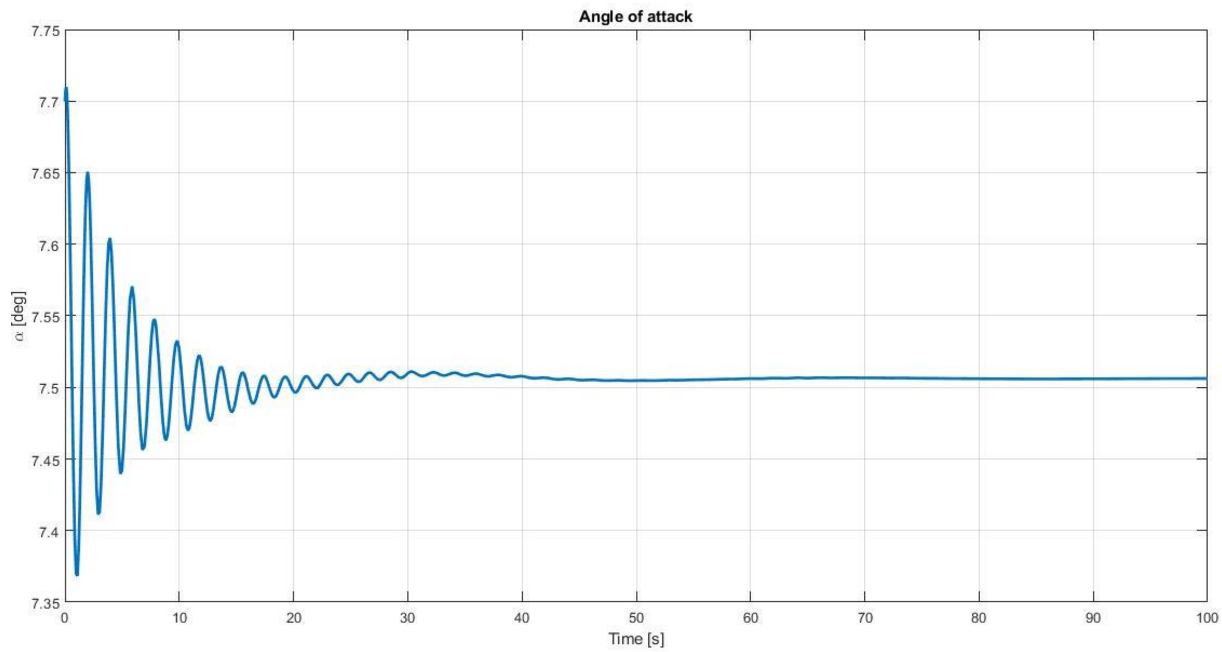

Figure 122: Angle of attack hang glider.

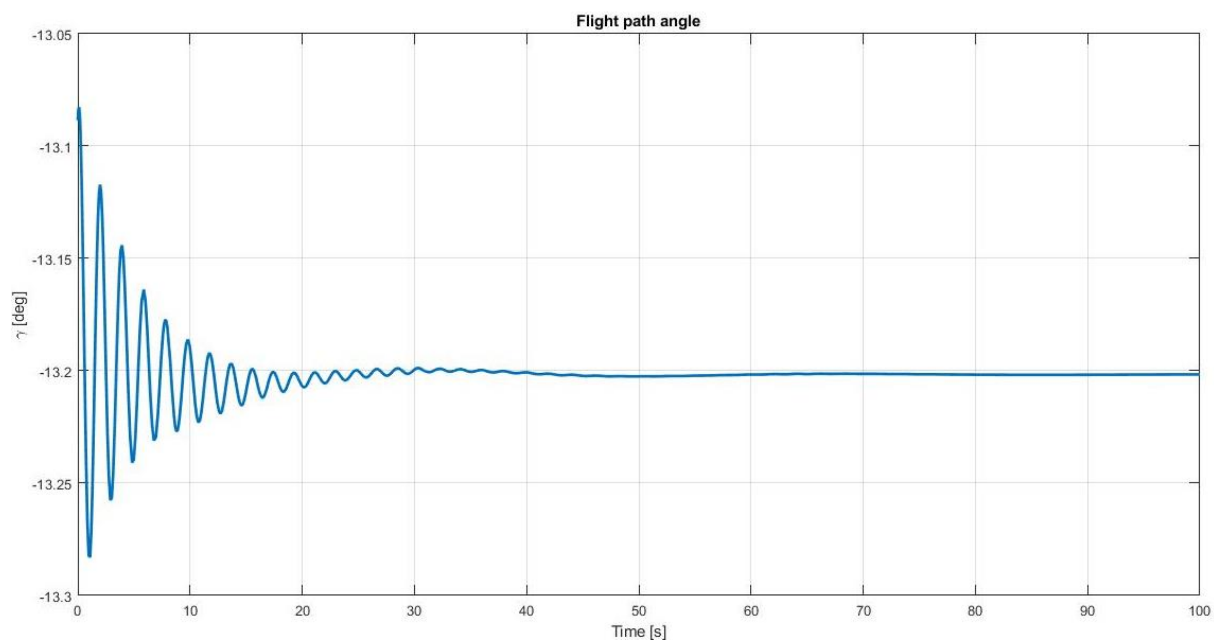

Figure 123: Flightpath angle hang glider.

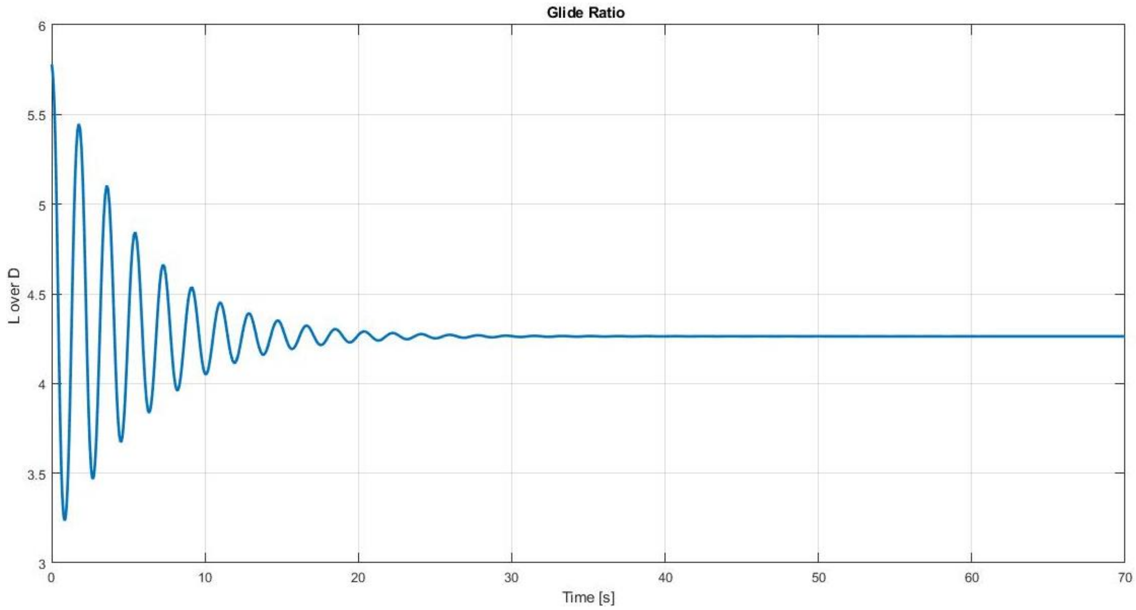

Figure 124: Efficiency of the hang glider.

7.4 ASYMMETRIC DEFLECTION SIMULATION

Both a spiral maneuver and an S-maneuver have been simulated to study the capability of the system: that results show that a small shift of the lift (around the tens of centimeters) can accommodate a stable maneuver. The S-maneuver is performed at 40 km with a $V_a = 11\ m/s$ and will be presented in this section.

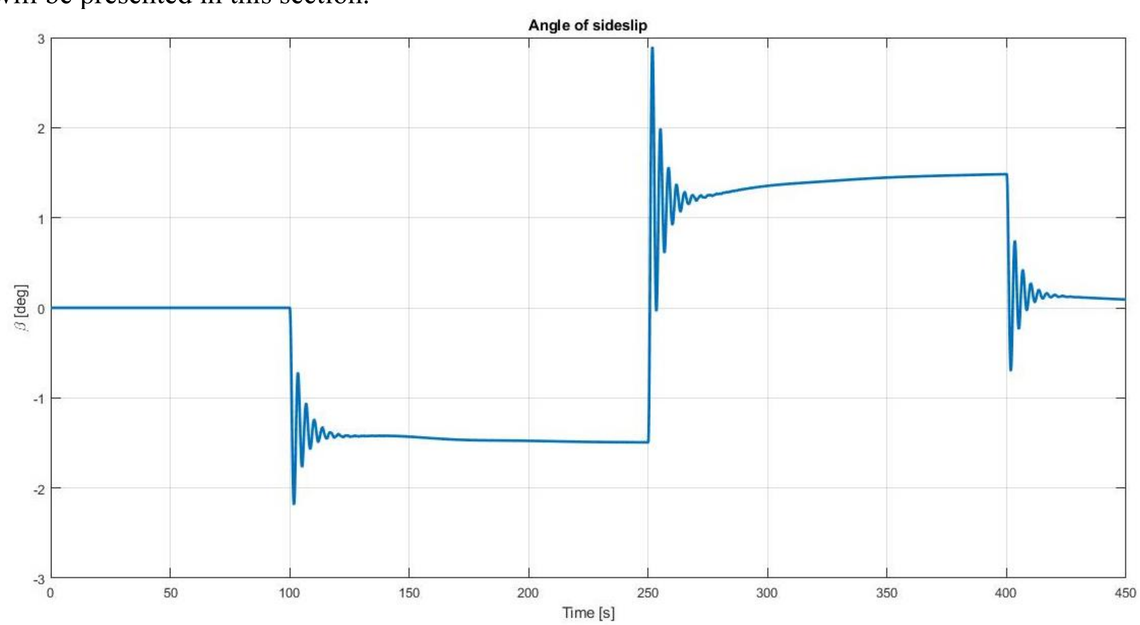

Figure 125: Sideslip angle S-maneuver.

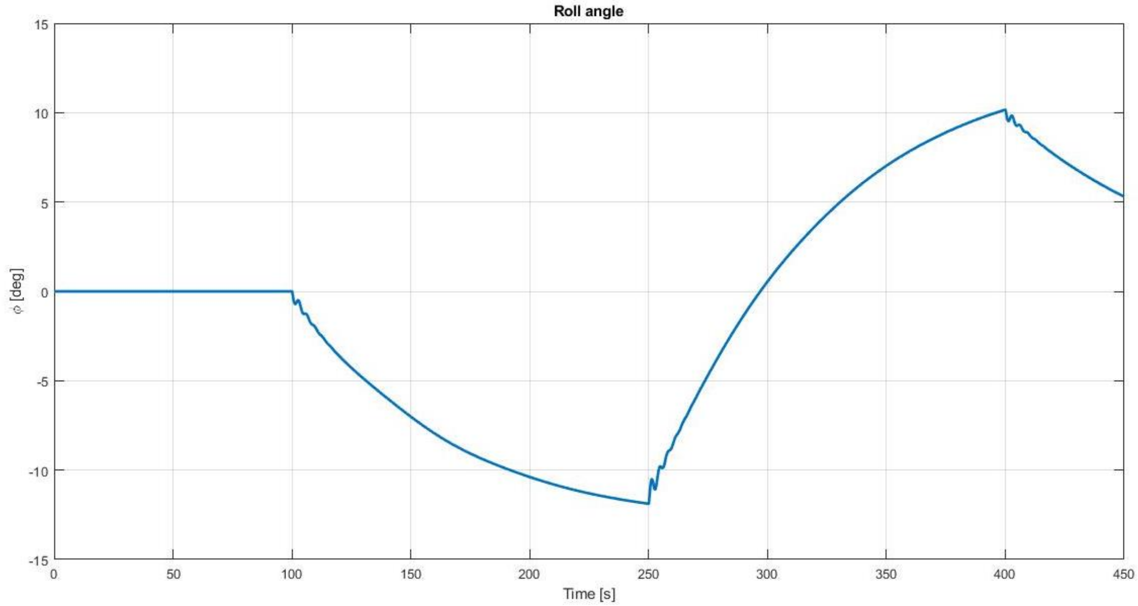

Figure 126: Roll angle S-maneuver.

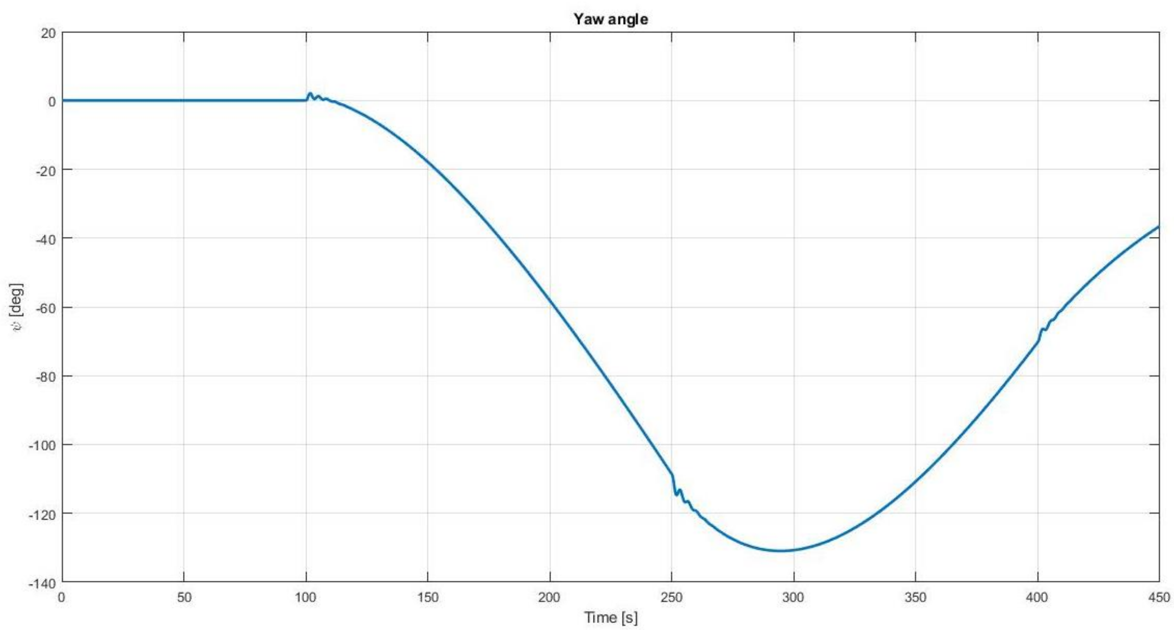

Figure 127: Yaw angle S-maneuver.

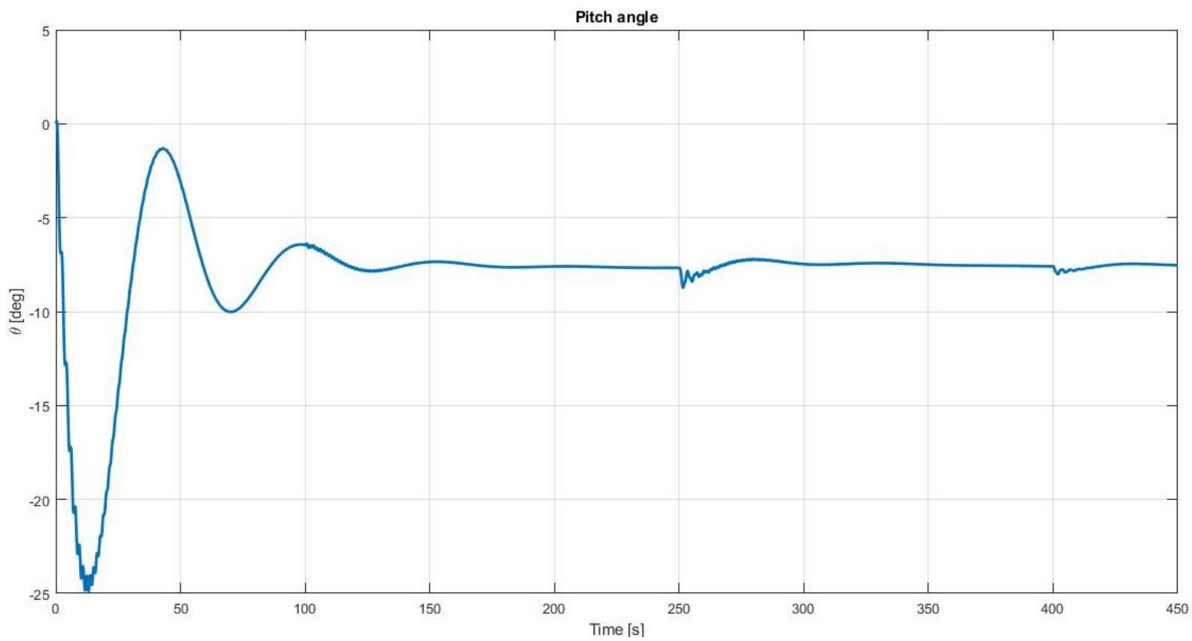

Figure 128: Pitch angle S-maneuver.

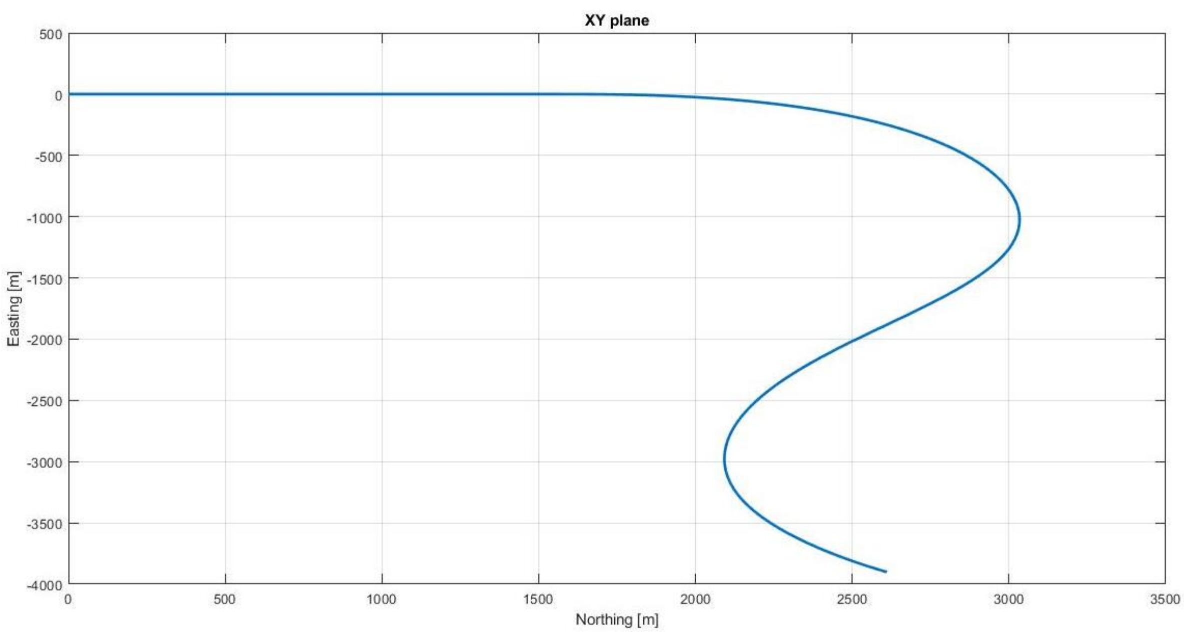

Figure 129: XY-plane S-maneuver.

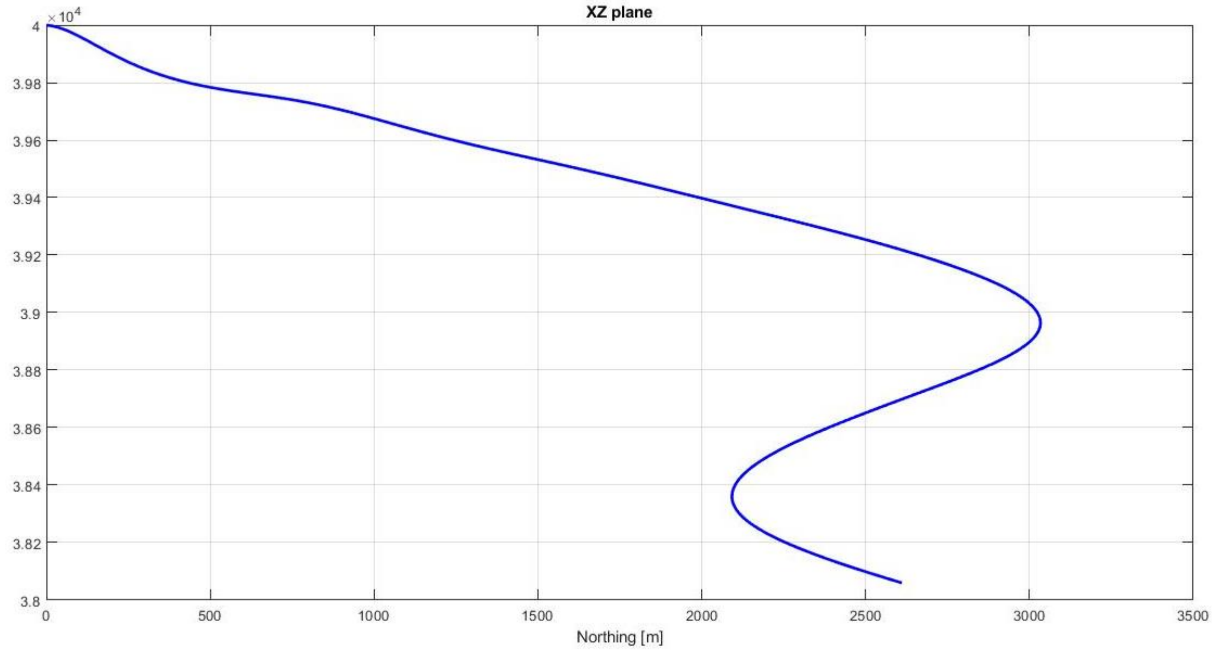

Figure 130: XZ-plane S-maneuver.

8 PAYLOAD WINGSUIT LOW FIDELITY MODEL: 6 DOF

The wingsuit was first thought as a possible alternative to merge the hang glider characteristic with the parafoil simple deployments for a large payload. The simulations show that the solution is not the most feasible choice: however, for small payload we can not only exploit the wingsuit simple deployment but even land "vertically" in a fashion similar to that of a flying squirrel (used as the main model to study this dynamic system [24]). In this section will be analyzed this solution for small payloads. The model needs still development: for other missions with different requirements, targeting the surface of Titan with small gliding sessions the solution start to be very interesting.

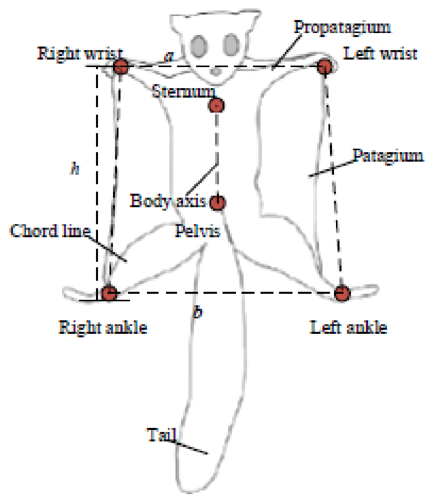

Figure 131: Flying squirrel configuration. The mammal usually increase its performance during flight modifying its paw configuration.

8.1 EQUATIONS OF MOTION

The wingsuit model is composed of a 3 DOF model to size the wingsuit dimensions: fixed the C_L *and* C_D for a rectangular wing of AR of 2, we can find the required wingsuit area to obtain a stable flight based on the payload weight. Than the parameters are inserted in a 6 DOF model. The simulation is performed taking into account a small tail to attach at the payload: the "tail" is needed to stabilize the vehicle. The wingsuit is unstable in low angle/low velocities regimes: to have a stable flight we must trim the system with a tail. The horizontal stabilizer dimensions should be computed case by case thinking about the performances we would like to have and the glider capabilities.

The mathematical expressions for the wingsuit are easier than in the previous cases: they detach the apparent masses effect, the force expressions are simple and straightforward. The only difficult point is to find how to size the tail.

$$\begin{bmatrix} (m+m_e)*\boldsymbol{I_{3x3}} & \boldsymbol{0_{3x3}} \\ \boldsymbol{0_{3x3}} & \boldsymbol{I} \end{bmatrix} * \begin{bmatrix} \dot{u} \\ \dot{v} \\ \dot{w} \\ \dot{p} \\ \dot{q} \\ \dot{r} \end{bmatrix} = \begin{bmatrix} \boldsymbol{F} \\ \boldsymbol{M} \end{bmatrix} \tag{8.1}$$

$$\boldsymbol{F} = \boldsymbol{F_a^{ws}} + \boldsymbol{F_g}$$

$$\boldsymbol{F_a^{ws}} = \frac{1}{2} * \rho * V_{ap}^2 * S_p * \begin{bmatrix} -(CL_0 + CL_{alpha} * \alpha + CL_{ds} * \overline{\delta_s}) \\ CY_{beta} * \beta \\ -(CD_0 + CD_{a2} * \alpha^2 + CD_{ds} * \overline{\delta_s}) \end{bmatrix} \tag{8.2}$$

$$\boldsymbol{F_g} = \left(m_{parafoil} + m_e + m_{payload}\right) * g * \begin{bmatrix} -\sin(\theta) \\ \cos(\theta) * \sin(\phi) \\ \cos(\theta) * \cos(\phi) \end{bmatrix}$$

$$\boldsymbol{M} = \boldsymbol{M_a} - \boldsymbol{S(\omega)} * \boldsymbol{I} * \begin{bmatrix} p \\ q \\ r \end{bmatrix} - \boldsymbol{S(\omega)} * \boldsymbol{I_f'} * \begin{bmatrix} p \\ q \\ r \end{bmatrix} + \boldsymbol{F_{a_{tail}}} * (\boldsymbol{c_{p_{ws}}} - \boldsymbol{c_{p_{tail}}})$$

$$\boldsymbol{M_a^p} = \frac{1}{2} * \rho * V_{ap}^2 * S_p * \begin{bmatrix} b(C_{l\beta} * \beta + \frac{b}{2 * V_a} * C_{lr} * r + \frac{b}{2 * V_a} * C_{lp} * p) \\ \bar{c} * (C_{m0} + C_{m\alpha} * \alpha + \frac{b}{2 * V_a} * C_{mq} * q) \\ b(C_{n\beta} * \beta + \frac{b}{2 * V_a} * C_{np} * p + \frac{b}{2 * V_a} * C_{nr} * r \end{bmatrix} \tag{8.3}$$

$$\begin{bmatrix} \dot{\phi} \\ \dot{\theta} \\ \dot{\psi} \end{bmatrix} = \begin{bmatrix} 1 & \sin(\phi) * \frac{\sin(\theta)}{\cos(\theta)} & \cos(\phi) * \frac{\sin(\theta)}{\cos(\theta)} \\ 0 & \cos(\phi) & -\sin(\phi) \\ 0 & \sin(\phi) * \frac{1}{\cos(\theta)} & \cos(\phi) * \frac{1}{\cos(\theta)} \end{bmatrix} * \begin{bmatrix} p \\ q \\ r \end{bmatrix} \tag{8.4}$$

$$\begin{bmatrix} \dot{x} \\ \dot{y} \\ \dot{z} \end{bmatrix} = \boldsymbol{R'_{bn}} * \begin{bmatrix} u \\ v \\ w \end{bmatrix} \tag{8.5}$$

The maneuvering is performed shifting the "tail" to side or up and down: the contribute of the tail will mainly affect the overall moment. "$(\boldsymbol{c_{p_{ws}}} - \boldsymbol{c_{p_{tail}}})$" is the distance between the center of pressure of the wing and the center of pressure of the wingsuit tail.

8.2 STEADY STATE SIMULATIONS

Some initial steady state simulations have been performed for the wingsuit to understand its capabilities to land vertically.

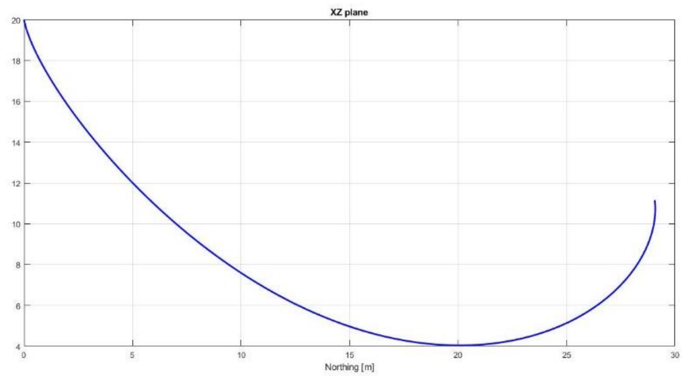

Figure 132: Vertical landing small robot wingsuit model.

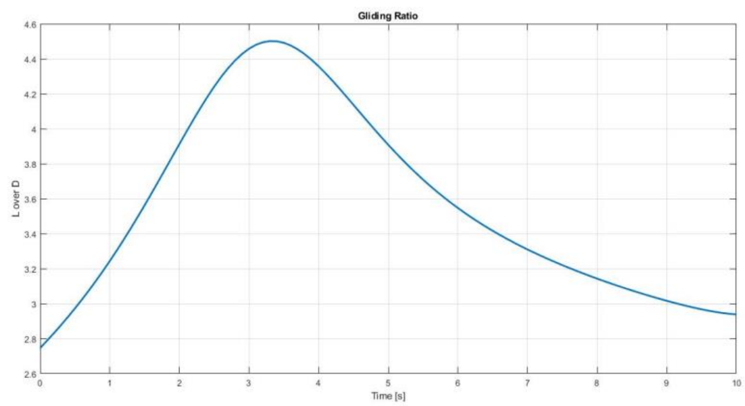

Figure 133: Gliding ratio small robot wingsuit model.

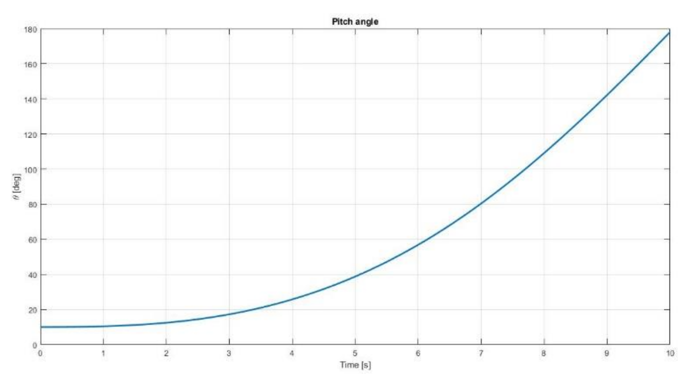

Figure 134: Pitch angle small robot wingsuit model.

9 PADs GUIDANCE, NAVIGATION AND CONTROL

Part of this research was to develop models for a high precision delivery system on Titan environment, the other part is focused on how to use those models in a possible flight scenario in which Titan winds will make the parafoil drift away from target and some maneuvering will be required to land on spot. In this section a guidance navigation and control system will be analyzed for prove the capability of the models in plausible operational conditions and to lay the foundation of this kind on analysis.

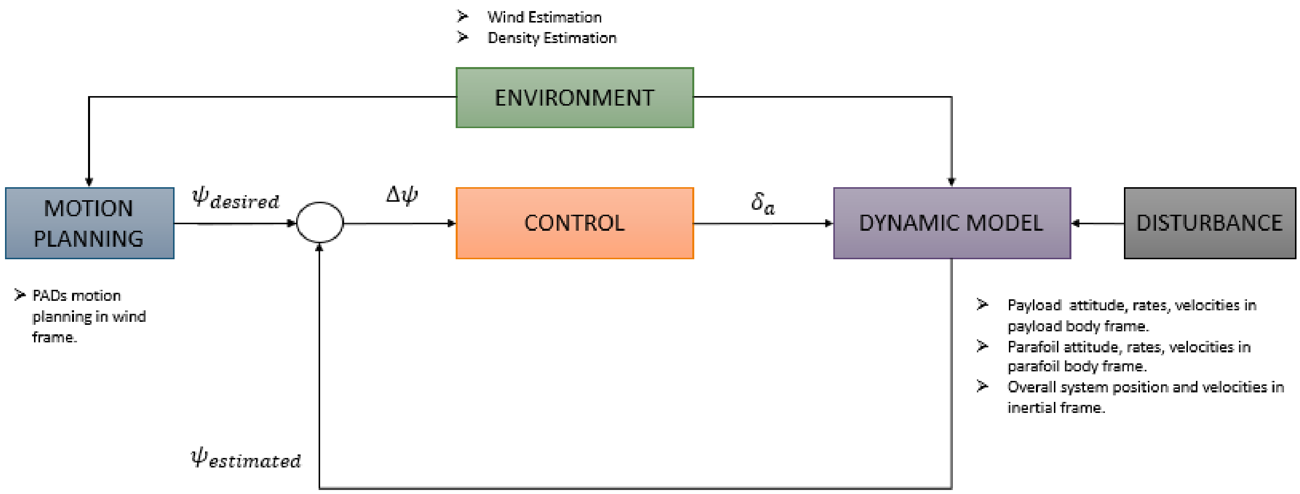

Figure 135: GNC model for the parafoil.

In PADs GNC some important assumptions are made to simplify the equation and the approach of the trajectory definition:

- The sideslip angle β is small so that we can confound heading angle and yaw angle $\chi_{wind\ ref\ frame} \cong \psi_{NED}$.
- The wind is usually considered consistent only along the x-axis.
- The PADs should land against the wind (downwind). This will prevent payload roll-over, will decrease the landing speed and will permit a flare maneuver.

9.1 WIND ESTIMATOR

The environmental conditions should affect the planned trajectory and the parafoil performance during descent. The true guidance system should re-plane the trajectory every interval of time to take into account the strong wing uncertainties during descent.

During flight the wind can be estimated from the airspeed lecture of the Pitot and the IMU (Inertial Measurement Unit) will give the system linear velocities as output.

$$\boldsymbol{W} = \boldsymbol{V_{NED}} - \boldsymbol{V_{airspeed}}$$

These lectures are affected by a noisy environments and errors: the values must be filtered to find a reliable quantity to use to plane the needed corrective maneuver.

Table 13: Noisy uncertainties used for the wind estimation [25].

$\sigma_{airspeed} \cong 0.2\ m/s$	Uncertainty on airspeed lecture
$\sigma_{NED} \cong 0.1\ m/s$	Uncertainty on ground speed lecture
$\sigma_{flightpath} \cong 1\ deg$	Uncertainty on flightpath angle (from TRN)
$\sigma_{heading} \cong 1\ deg$	Uncertainty on heading angle (from TRN)

$$
\begin{gathered}
\dot{x}_m = \dot{x}_{dynamic\ model} + \sigma_{\dot{x}} * p_{\dot{x}} \\
\dot{y}_m = \dot{y}_{dynamic\ model} + \sigma_{\dot{y}} * p_{\dot{y}} \\
\dot{z}_m = \dot{z}_{dynamic\ model} + \sigma_{\dot{z}} * p_{\dot{z}} \\
V_{am} = V_{airspeed} + \sigma_{airspeed} * p_{aispeed} \\
\gamma_{am} = \gamma_a + \sigma_{flightpath} * p_{flightpath} \\
\chi_{am} = \chi_a + \sigma_{heading} * p_{heading}
\end{gathered}
$$

The $\{p_{\dot{x}}, p_{\dot{y}}, p_{\dot{z}},\ p_{aispeed}, p_{flightpath}, p_{heading}\}$ are random number normally distributed: with this expedient we can simulate the noisy measurements while descending in Titan atmosphere with our software.

From those measurements affected by error we can estimate the wind that need to be filtered.

$$
\begin{gathered}
w_{x_m} = \dot{x}_m - V_{am} * \cos(\chi_{am}) * \cos(\gamma_{am}) \\
w_{ym} = \dot{y}_m - V_{am} * \sin(\chi_{am}) * \cos(\gamma_{am}) \\
w_{z_m} = \dot{z}_m - V_{am} * \sin(\gamma_{am})
\end{gathered}
$$

To filter the wind evaluations, we can use a "recursive mean value estimation", a filter (e.g. Nonlinear Estimation Filter) or a predictive method that propagate the wind profile up to ground level (but it can be quite expensive in terms of computational power).

We chose to use the "recursive mean value estimation": simple formulation, reliable results and works throughout all the GNC simulation.

- Mean Error along all the trajectory between exponential wind profile and estimated wind profile (derived from [1]): 0.002%.
- Max Error along all the trajectory between exponential wind profile and estimated wind profile: 20%
- Wind evaluated every 0.1 s (every GNC step).

The standard "recursive mean value estimation" method is thought for PADs in Earth environment and for far lower altitudes than in Titan case study. The classic formulas are reported in [26].

$$
\begin{gathered}
\bar{\boldsymbol{w}}_{\boldsymbol{x}_{\boldsymbol{k+1}}} = (k * \bar{\boldsymbol{w}}_{\boldsymbol{x}_{\boldsymbol{k}}} + \boldsymbol{w}_{\boldsymbol{x}})/(k+1) \\
\bar{\boldsymbol{w}}_{\boldsymbol{y}_{\boldsymbol{k+1}}} = (k * \bar{\boldsymbol{w}}_{\boldsymbol{y}_{\boldsymbol{k}}} + \boldsymbol{w}_{\boldsymbol{y}})/(k+1)
\end{gathered} \tag{9.1}
$$

The expression (9.1) is useful if the wind environment doesn't change abruptly during the simulated scenario: in our case the longitudinal wind changes in its intensity during the descent from 40 km. An update formulation that takes into account only the previous 100 steps to evaluate the mean wind and detach errors from propagating (9.1).

If $i \leq k_1$

$$
\begin{gathered}
\bar{\boldsymbol{w}}_{\boldsymbol{x}_{\boldsymbol{k+1}}} = (k * \boldsymbol{mean}(\bar{\boldsymbol{w}}_{\boldsymbol{x}_{\boldsymbol{k}}}) + \boldsymbol{w}_{\boldsymbol{x}})/(k+1) \\
\bar{\boldsymbol{w}}_{\boldsymbol{y}_{\boldsymbol{k+1}}} = (k * \boldsymbol{mean}(\bar{\boldsymbol{w}}_{\boldsymbol{y}_{\boldsymbol{k}}}) + \boldsymbol{w}_{\boldsymbol{y}})/(k+1)
\end{gathered} \tag{9.2}
$$

If $i > k_1$

$$
\begin{gathered}
\bar{\boldsymbol{w}}_{\boldsymbol{x}_{\boldsymbol{k+1}}} = (k * \boldsymbol{mean}(\bar{\boldsymbol{w}}_{\boldsymbol{x}_{\boldsymbol{k}}}(i-k_1\!:i)) + \boldsymbol{w}_{\boldsymbol{x}})/(k+1) \\
\bar{\boldsymbol{w}}_{\boldsymbol{y}_{\boldsymbol{k+1}}} = (k * \boldsymbol{mean}(\bar{\boldsymbol{w}}_{\boldsymbol{y}_{\boldsymbol{k}}}(i-k_1\!:i)) + \boldsymbol{w}_{\boldsymbol{y}})/(k+1)
\end{gathered}
$$

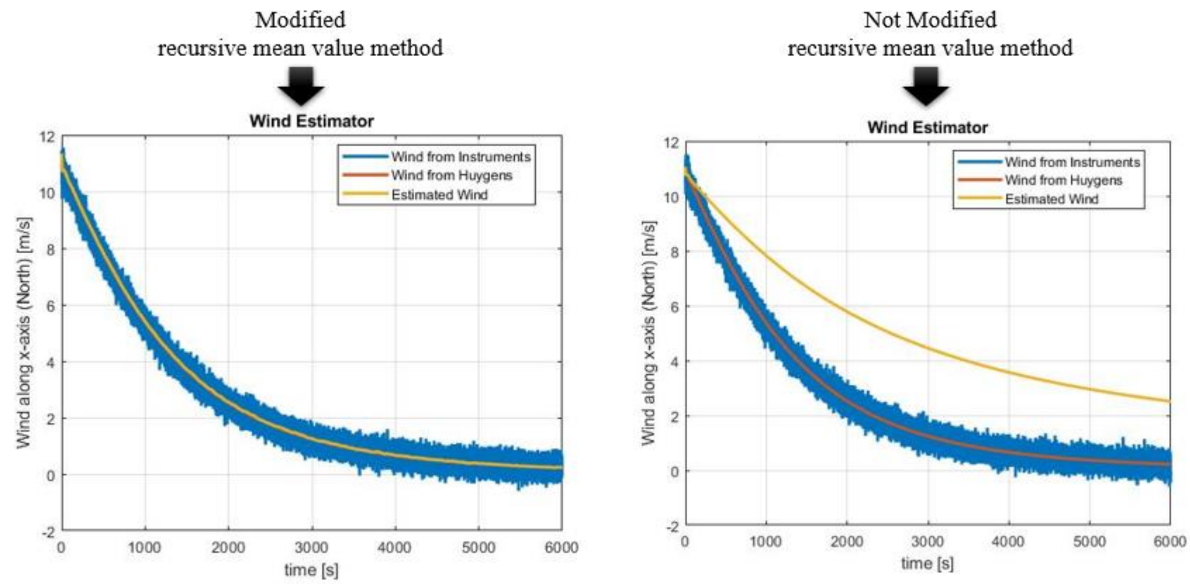

Figure 136:Zonal wind estimation.

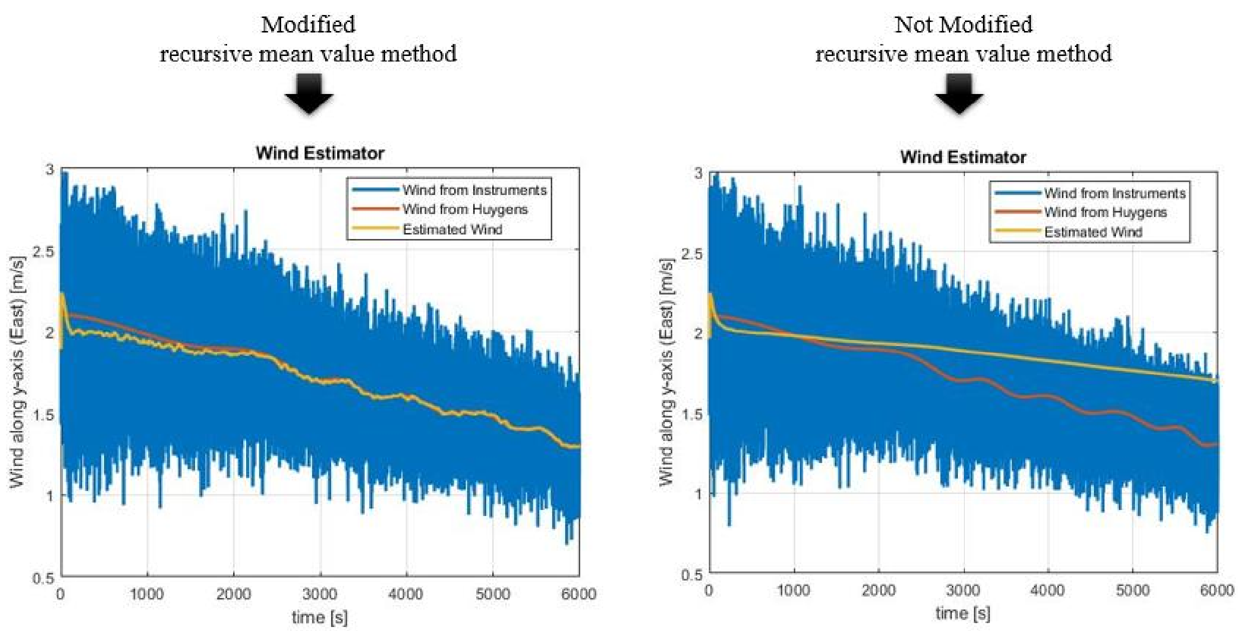

Figure 137: Meridian wind estimation.

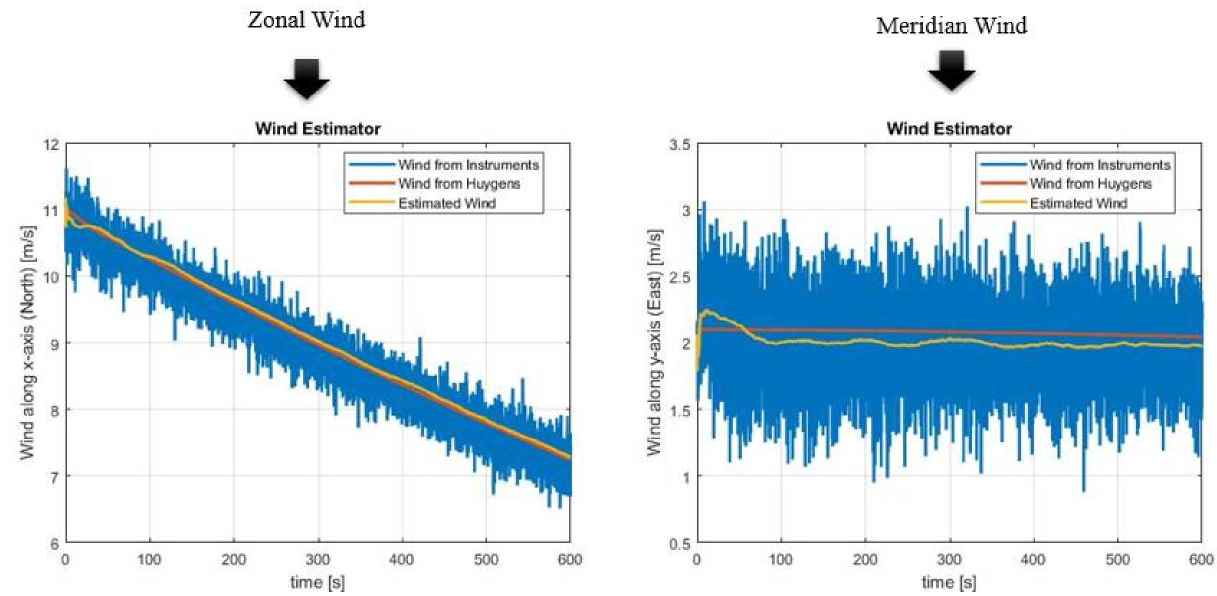

Figure 138: Wind detail for the first 10 minutes of simulations.

9.2 DENSITY ESTIMATOR

During the flight the density will be estimated from the sensors, so we should add some noisy measurements even in that case. The density derives from an exponential formulation that depends on the height [3]:

$$\rho = 5.43 * e^{-0.0512*\frac{h}{1000}} \tag{9.3}$$

To introduce some randomness, we can again think to perturb the airspeed as in the Kalman filter or the height lecture used in (9.3).

The first method is explained in [25] the second is based on the perturbation of the lecture from the radar altimeter. The system uncertainty can be approximated as 2-5% of the indicated height from measurement, we can obtain our value of uncertain density indication.

In the GNC simulations we will use a "fading memory filter": it is a recursive method similar to the linear-polynomial Kalman filter, but with an easiest formulation (less computational burdensome) due to the constant gain value. For a first order filter the gain β is equal to 0.8.

$$\begin{aligned} h_k &= h_{k-1} + (1-\beta) * (h_{measured} - h_{k-1}) \\ h_{measured} &= h_{dynamic\,model} + \sigma_{h_{error}} \\ &= h_{dynamic\,model} * \begin{cases} 1.05\ if\ h > 5000 \\ 1.02\ if\ h < 5000 \end{cases} \\ \rho_k &= \rho_{k-1} + (1-\beta) * (\rho_{exponential\,model} - \rho_{k-1}) \end{aligned} \tag{9.4}$$

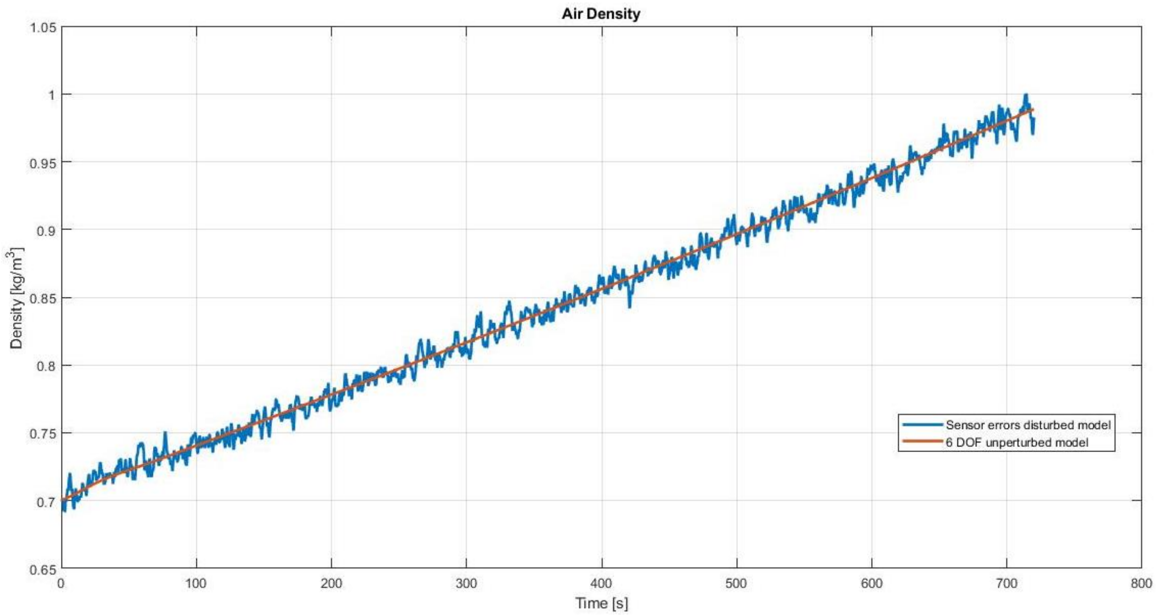

Figure 139: Titan air density estimation.

9.3 Motion Planning

The parafoil trajectory must be planned towards the nearest point of interest (near the entry point): we would need a quick generation of a feasible trajectory. Usually for PADs the trajectory is planned with a 3 DOF model on plane: the variables of interest are $\{x, y, \psi\}$. From the wanted trajectory a series of waypoints is then computed on plane. In our deployment situation (40 km at 22 m/s) we need to take into account a more complex 3 DOF model that consider the sphericity of the planet. The model will generate a trajectory with $\{V_a, \gamma_a . \chi_a\}$ (airspeed, flightpath angle and heading angle) and ϕ_a (bank angle) as a control. From this path we will compute our waypoints identified by a (x, y, z) tern. The final point of the trajectory is $\{x_f, y_f, z_f\}_{NED} = \{0,0,0\}_{NED}$: with this expedient it will be easier to find a simple expression for optimize the trajectory for minimum control or as a Dubin path. During path planning usually only the wind vector is assumed to be $W = \{W_x, 0,0\}$ where the wind component along x is the strongest one. In the true simulated trajectory, the lateral wind and the wind gust will be taken into account. However, the controlled 6 DOF system should be able to contrast those inputs even with a discrete control.

9.3.1 3 DOF Model with Spherical Planet

The mathematical expressions used to define the waypoints are presented shortly in this section. The complete formulation can be found in [27]. In this case the body is modelized as a point mass with lift, drag, lateral force and buoyancy force (L, D, Y, B). The variable are the airspeed and the airspeed related flightpath angle and heading angle, that usually differ from the flightpath angle and heading angle associated to the NED quantities. However, in this formulation the body axis and the wind axis coincide [25]. Throughout all the formulation the wind is accommodated in the control equations (9.14-9.16) as in [26].

$$\dot{V_a} = \left(\frac{B}{m} - g\right) * sin(\gamma_a) - \frac{D}{m} \tag{9.5}$$

$$\dot{\gamma}_a = \frac{V_a}{R_p + h} * \cos(\gamma_a) + \left(\frac{B}{m} - g\right) * \frac{\cos(\gamma_a)}{V_a} + \frac{\mathrm{L} * \cos(\phi_a) + Y * \sin(\phi_a)}{m * V_a} \tag{9.6}$$

$$\dot{\chi}_a = -\frac{V_a}{R_p + h} * \cos(\gamma_a) * \cos(\chi_a) * \tan(\lambda) + \frac{\mathrm{L} * \sin(\phi_a) - \mathrm{Y} * \sin(\phi_a)}{m * V_a} \tag{9.7}$$

$$\dot{r} = V_a * \sin(\gamma_a) = \dot{h} \tag{9.8}$$

$$\dot{\Lambda} = \frac{V_a * \cos(\gamma_a) * \cos(\chi_a)}{r * \cos(\lambda)} \tag{9.9}$$

$$\dot{\lambda} = \frac{V_a * \cos(\gamma_a) * sin(\chi_a)}{r} \tag{9.10}$$

$$\dot{x} = V_a * si\,n(\gamma_a) + w_x \tag{9.11}$$

$$\dot{y} = V_a * \cos(\gamma_a) * \cos(\chi_a) + w_y \tag{9.12}$$

$$\dot{z} = V_a * \cos(\gamma_a) * \sin(\chi_a) + w_z \tag{9.13}$$

$$\tan(\phi_a) = \frac{\dot{\chi}_b * r * Va}{r * g - Va^2} \tag{9.14}$$

$$\dot{\chi}_b = \frac{2 * V_a * \cos(\gamma_a) * \sin(\chi_{desired} - \chi_a)}{L} \tag{9.15}$$

$$L = k * \sqrt{\left(y_{target} - y\right)^2 + \left(x_{target} - x\right)^2} \tag{9.16}$$

L is used to scale the intensity of the heading angle taking into account the distance between target and parafoil. This quantity can be modified with the k parameter: with different k we will obtain different trajectory that keeps into account the wind and that are all potentially feasible. Varying that quantity and the wind environment and the bank angle control, we can shape our path and find different solution to landing site. To automate the process an optimal control with a minimization process is needed. From simulations seems that k should be equal to one in the energy management or terminal guidance phases where the distance between parafoil and target is small but can assume different values to shape the homing phase accordingly to a mission requirement or a scientific task. In the following simulations k is assumed equal to the unity, if not explicitly reported in the plots description.

If we plane to arrive to a point at 30 km of distance from the release point a possible path can be seen in the following figures. The parafoil it's upwind in the homing phase, when the wind intensity decreases below 3 m/s at 10 km the system can perform more intense maneuvers and start to aim more effectively at the landing site and land downwind. Throughout all the trajectory the bank angle is limited in its intensity: we want a feasible trajectory for the system. For small PADs a continuous bank angle over 1 m/s can make the vehicle unstable and the 6 DOF model can experience some problems in following the planned path. To minimize the bank angle and land on point in every different scenario we would need to optimize our trajectory for minimum control.

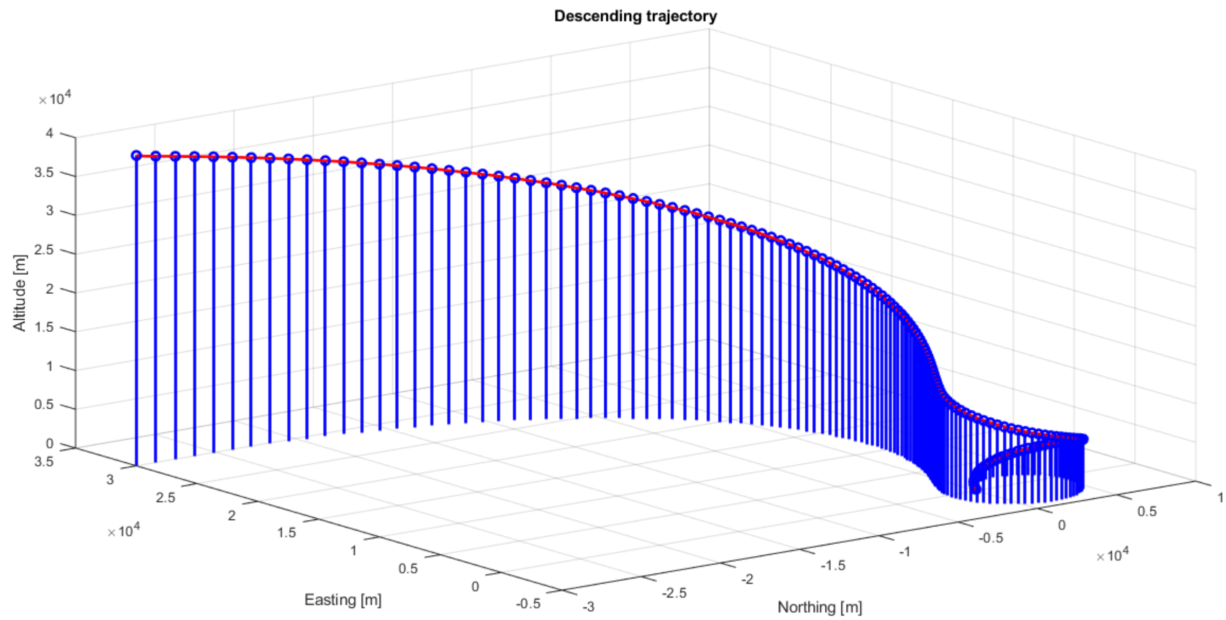

Figure 140: Trajectory from motion planning ($\phi_{a_{max}} = 0.7\ rad/s$)

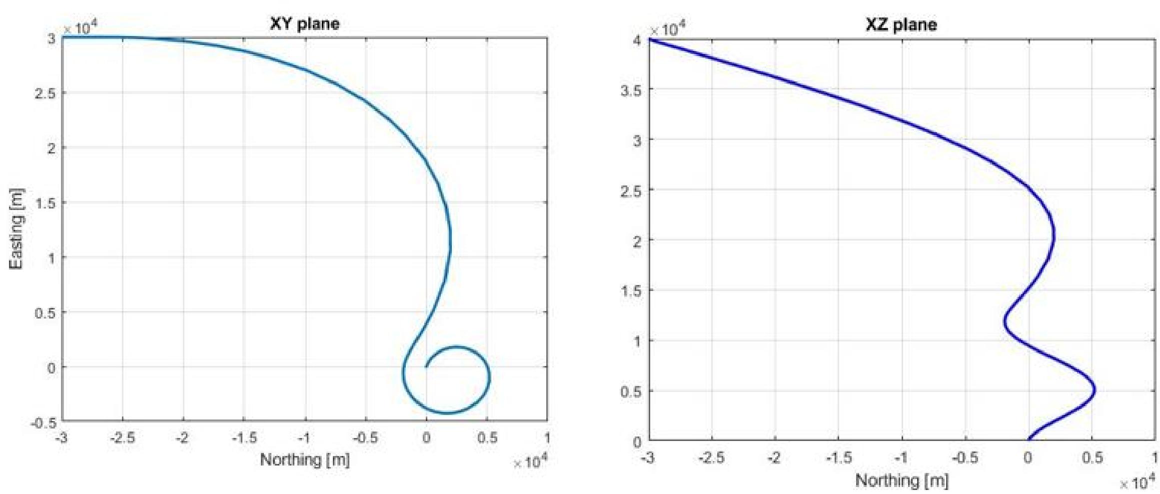

Figure 141: Trajectory from motion planning: tracks on x-y and x-z planes.

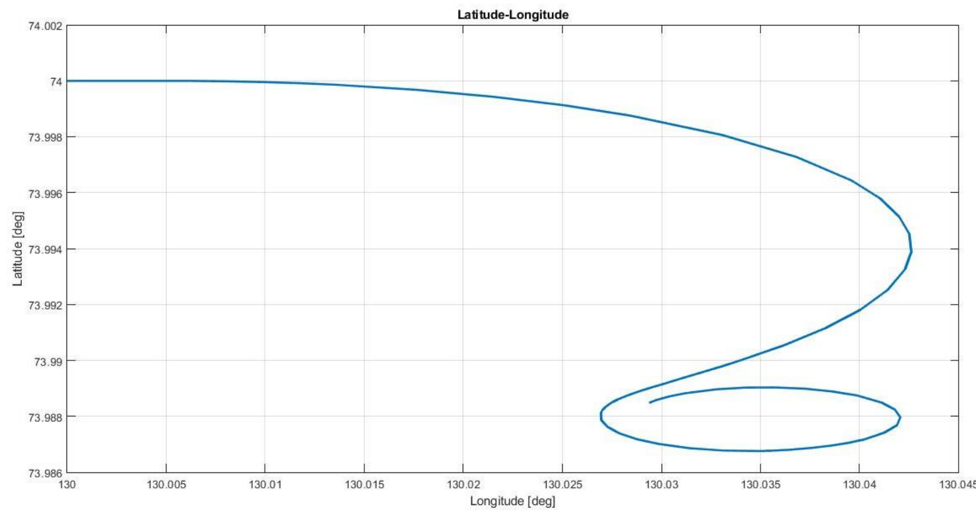

Figure 142: Motion planning reference trajectory latitude and longitude.

The trajectory presented in the previous figures is one possible trajectory with a strong bank angle limitation [28]. The turn maneuver can cause quicker altitude loss and a steep spiral for descent. It can be hard to follow with a discrete control, at least with a simple proportional control in time domain. With a more raffinate control theory we should be able to perform any kind trajectory. If we simulate a series of trajectory with maximum bank angle of $\phi_a = 1.2\ rad/s$, we can obtain different trajectories that lands on our target with different k values (all the other quantities are kept equal for the four paths).

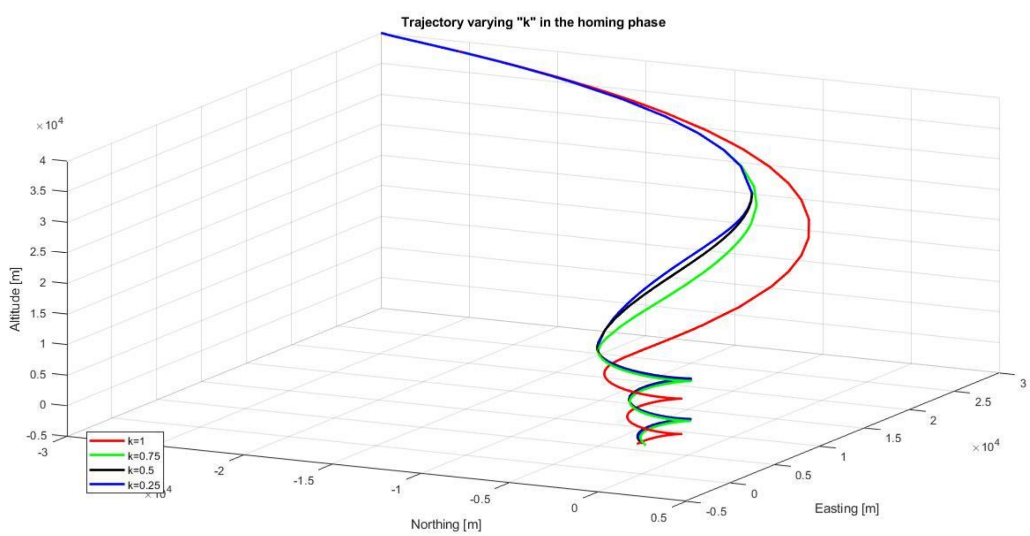

Figure 143: Trajectories obtained varying maximum bank angle and k.

If we change the entry point keeping ($\phi_{a_{max}} = 0.7\ rad/s$), we can plot different trajectories that will try to land at the target $\{x_f, y_f, z_f\} = \{0,0,0\}$ km. The entries point will lie on a circle of radius 5 km around the nominal entry point, $\{x_0, y_0, z_0\} = \{-30,30,40\}$ km. However, without an optimizing tool and with the bank angle limitation the landing spots will can be delimited in an ellipse of major axis of 4 km along x (northing) and a minor axis of 2 km along y (easting). The error in position at the entry point at 40 km will perturb the touchdown point, keeping all the other parameters equal. Future work will expand this analysis into a more detailed Montecarlo analysis.

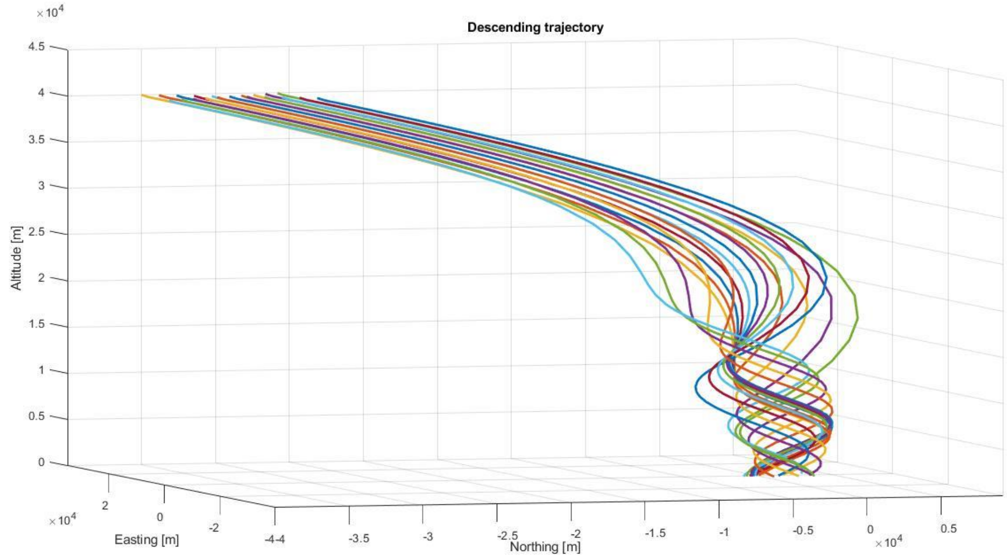

Figure 144: Scattering in the landing site with $\phi_{a_{max}} = 0.7\frac{rad}{s}$

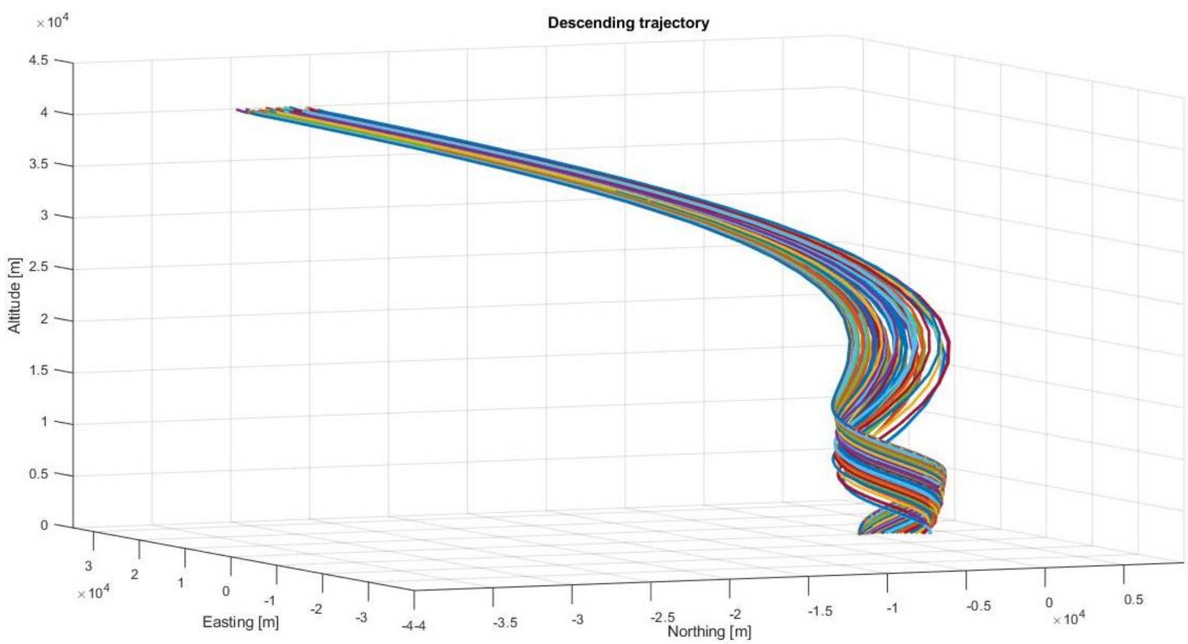

Figure 145: Scattering in the landing site with $\phi_{a_{max}} = 0.7\frac{rad}{s}$ (more complete Montecarlo Analysis)

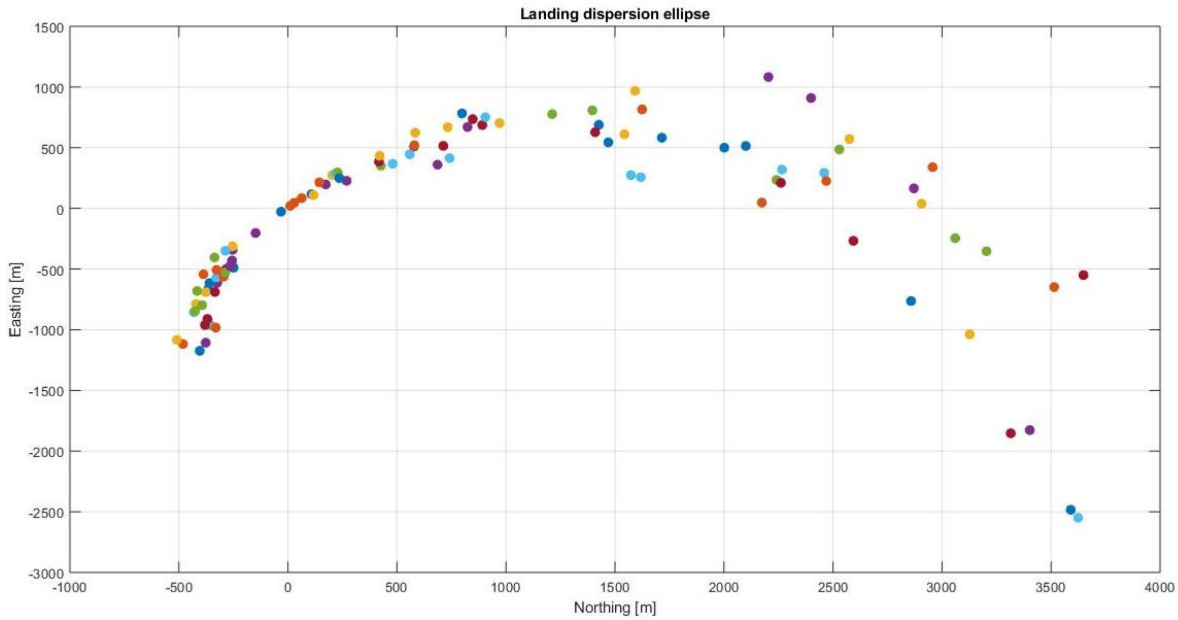

Figure 146: Scattering in the landing site with $\phi_{a_{max}} = 0.7\frac{rad}{s}$ end points..

9.4 PROPORTIONAL CONTROL

The control used in the routine is a simple fixed gain proportional control in time domain. In this preliminary phase we are not focused on the efficiency of the control but how the PADs will behave under some environmental effects, not precise sensor lectures and time-limited actuation.

$$\delta_a = K_{p_1}(t) * \chi_{dot} = K_{p_2}(t) * \Delta\chi = K_{p_2}(t) * (\chi_{waypoint} - \chi_{parafoil}) \quad (9.17)$$

The control will try to follow the on-plane trajectory (North-East). However, some waypoints cannot be reached because the 6 DOF PADs, with a more complex dynamics and various outside environmental effects, seems to lose altitude quicker than when it is modelled as a point mass object. If we follow the on-plane trajectory exactly we can land before our target. To obviate this problem the control algorithm aims always at the nearest waypoint with a lower height than the parafoil actual altitude.

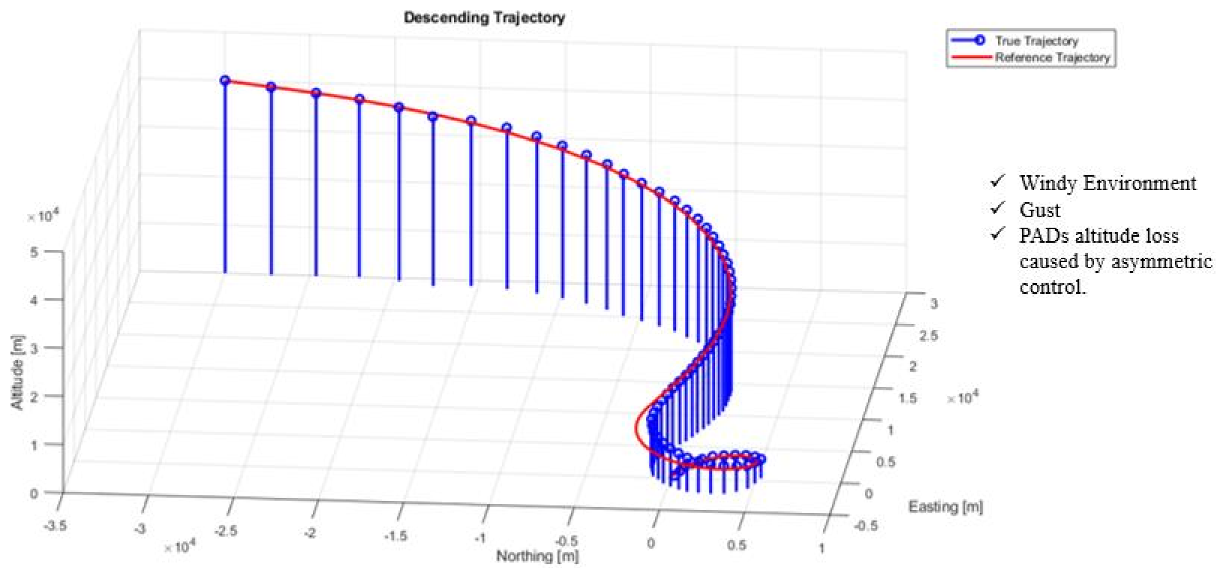

Figure 147: 6 DOF PADs trajectory under control inputs.

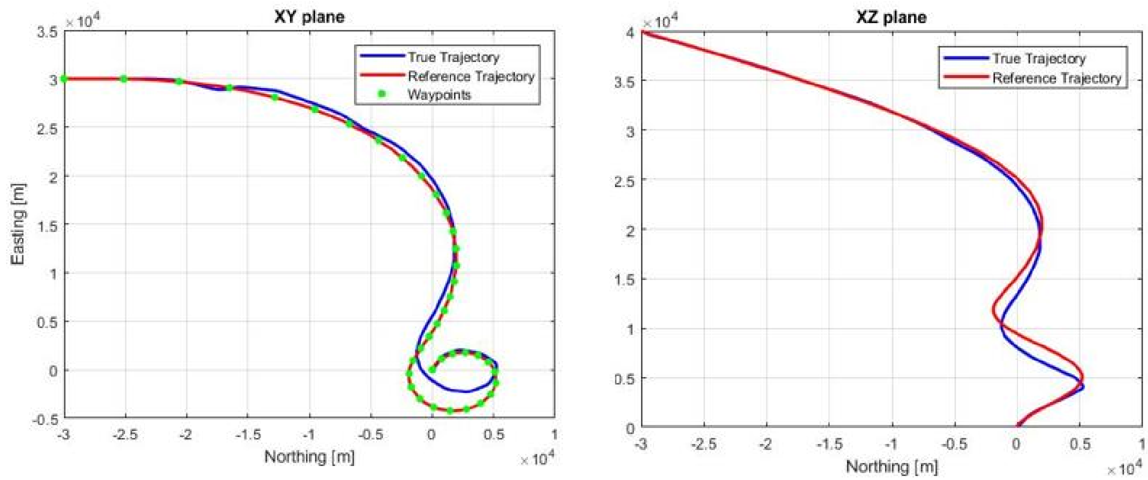

Figure 148: 6 DOF PADs trajectory under control inputs.

9.5 PARAFOIL AND HANG GLIDER: COMPARISON

The hang glider is a system with a higher efficiency than the parafoil, however its deployment from a probe can be tricky. Assuming a greater un-folding complexity, it is natural to ask: which is the advantage in terms of trajectory? If we plan to follow a trajectory similar to that of the parafoil presented in 9.3 the hang glider will have an energy management and will circulate the landing point. That can help us to analyze more accurately our landing spot and, if it is the case, change it a little. Or we can aim to further targets with the efficiency benefits: we can have more than 60 km of possible exploration radius even accommodating wind uncertainties. The hang glider is a potential good solution for planetary exploration due to its maneuverability and agility.

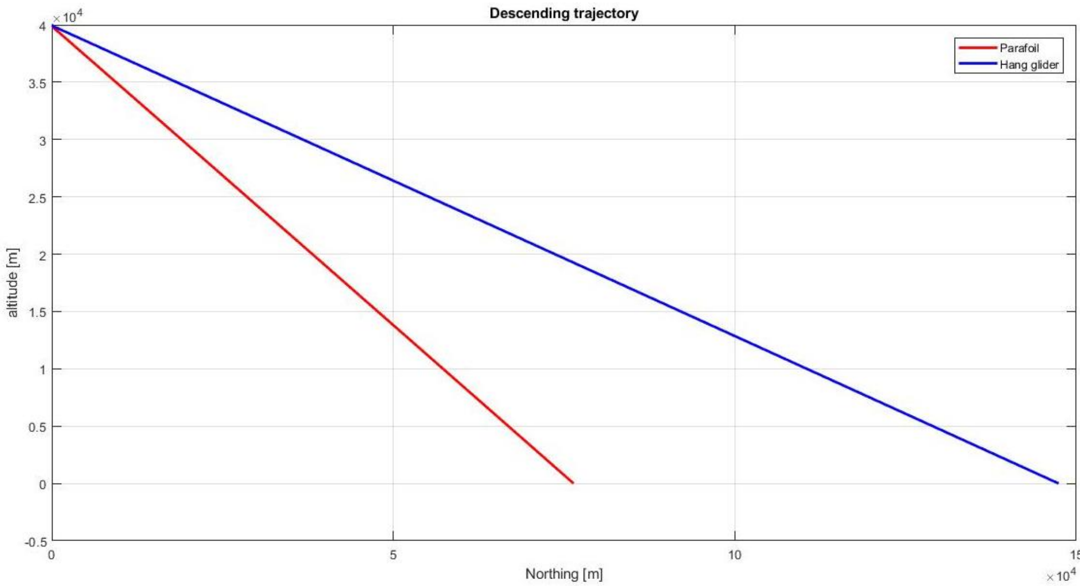

Figure 149: Titan steady state descent for parafoil and hang-glider.

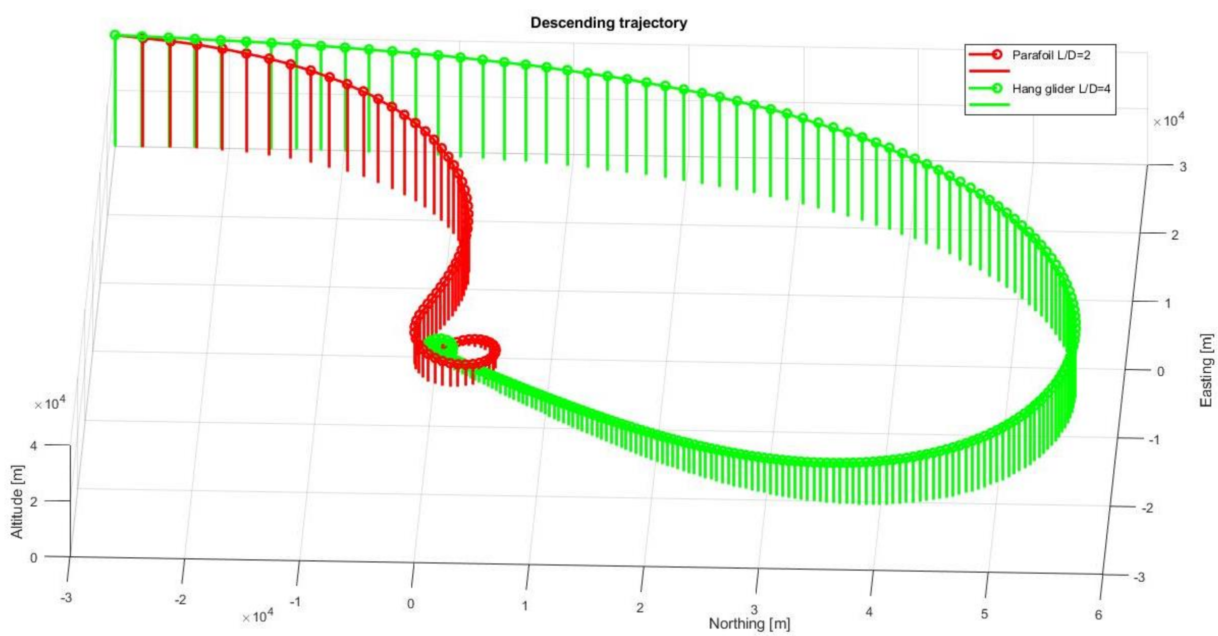

Figure 150: Titan descent for parafoil and hang-glider with maneuvering (2).

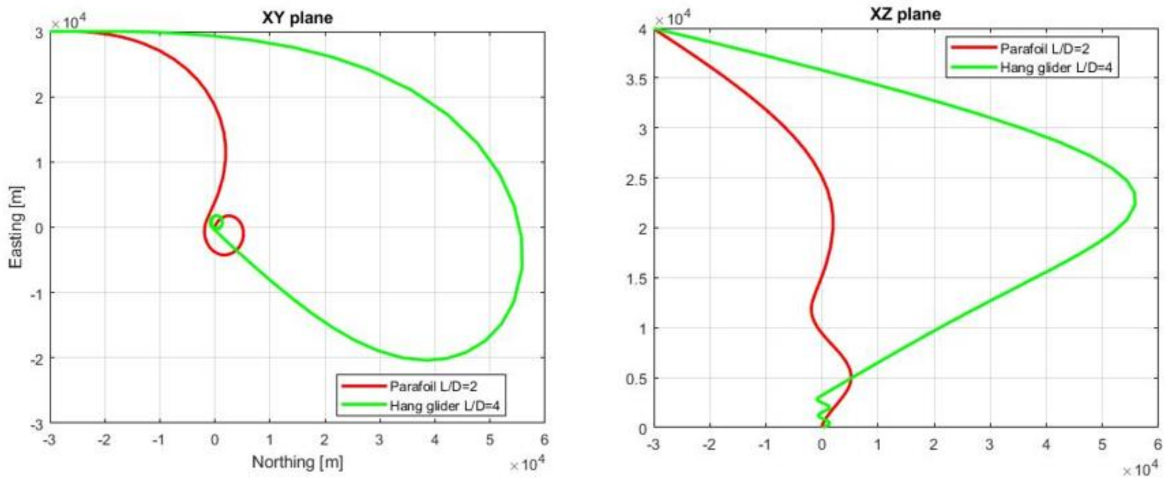

Figure 151: Titan descent for parafoil and hang-glider with maneuvering (1).
For the hang glider k=0.5.

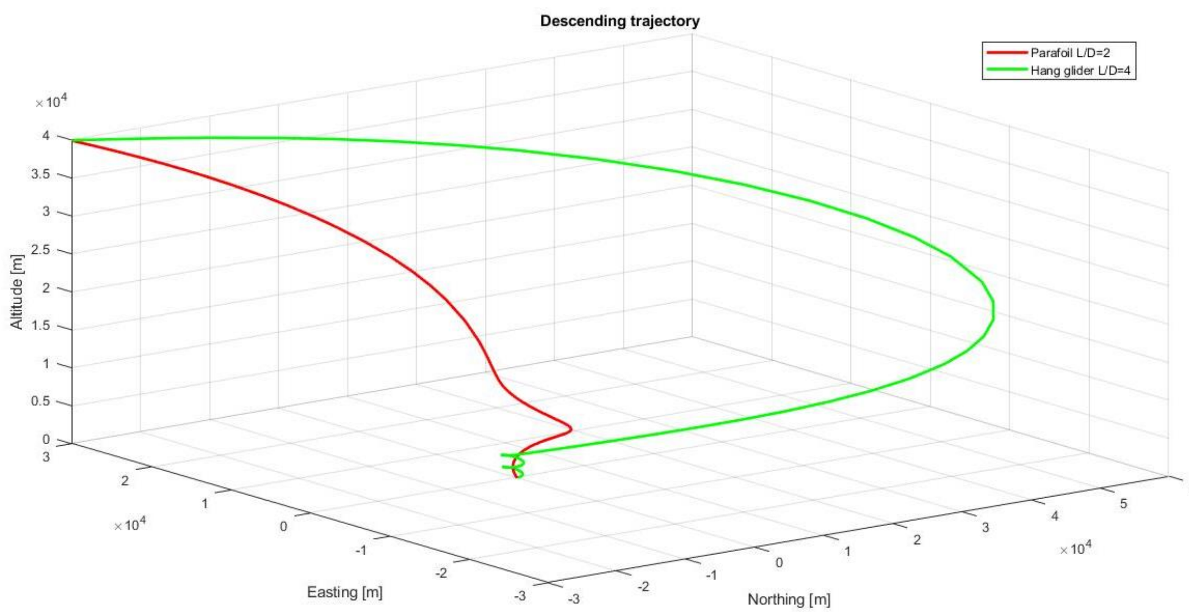

Figure 152:Titan descent for parafoil and hang-glider with maneuvering (3).

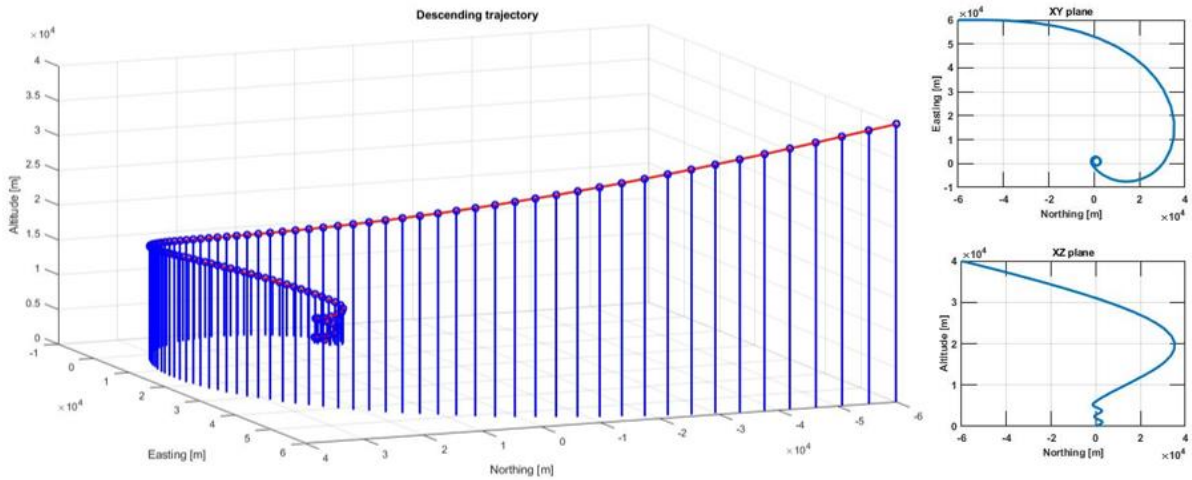

Figure 153: Titan hang-glider descent with 60 km range.

10 CONCLUSIONS AND FUTURE DEVELOPMENTS

In this thesis, I presented a summary of the work performed in five months at the JPL (Jet Propulsion Laboratory) on the dynamics of autonomous parafoils and other autonomous flight solutions.

The analysis of high-efficiency gliding systems (i.e., high lift over drag systems) can identify new and more efficient solutions for terminal descent. The present work follows this trend by studying the advantages of a parafoil for autonomous precision delivery of a probe in the Titan environment. The previous successful mission to Titan, the Huygens probe, used a series of drag-only parachutes to drop the payload (low lift to drag parachute). However, this solution provides a limited maneuverability to negotiate the not well-known environmental conditions (air density and winds) and the possibility of targeting different landing sites of scientific interest, shaping the trajectory accordingly. With a ram-air system (a parafoil) one can fly over different interesting sites, map them ahead of time, and even allow the re-planning of the trajectory to land near the most desirable sites.

To analyze all these possibilities, dynamics models of the PADs (Precision Aerial Delivery System), with different degrees of freedom, had to be developed and tested. Three degree-of-freedom models focused on the trajectory development. Six degree-of-freedom models were needed to evaluate the parafoil-payload system overall system behavior. Seven to nine degree-of-freedom models were needed to determine the payload-canopy interaction. These models were tested those in the relevant environmental conditions on Titan, from the aerodynamics to the wind effect to a noisy sensor reading. As a consequence, the performance of the system trying to follow a trajectory in the uncertain atmosphere was evaluated.

To realize these tasks, we relied on the methodologies derived from dynamics system modelling for the related equations of motion, from the aerodynamics to investigate the effect of the forces that enable the descent on Titan, from the GN&C (Guidance, Navigation and Control) to determine the requirements posed by autonomy. Consequently, the aim of this work was to provide a system modeling and simulation framework to ultimately allow the development of a complete GN&C system that will lead to a feasible system design, and which advantages these high lift solutions can bring to future missions to Titan.

Specifically, the work was carried out along the following topics:

- <u>Modeling and simulation of the dynamics and control of the parafoil and probe system during terminal descent:</u> We have developed several parafoil dynamics models. The 6 DOF (degrees-of-freedom) model is a comprehensive model of all the possible parafoil-payload link fashions. The model encloses all the principal characteristic of the system and it is usually used to build and test the GN&C system. The 7 DOF model, which allows a mechanical constraint between parafoil and payload, facilitates the payload stabilization. In this project the control unit was arranged to lay on the load. Also, strong oscillations can make the TRN (Terrain Relative Navigation) system imprecise, thereby requiring a careful stability analysis. The 8 DOF model gives the payload the freedom to oscillate both in pitch and yaw, and it is the most used model for Earth delivery systems. The only drawback was the uncontrolled pitch oscillation. The 9 DOF model enabled all the rotations of the parafoil relative to the payload. Nevertheless, this system can be a good solution for a spinning load: the mechanical constraint separates the parafoil and payloads dynamics. For this very initial phase of the project with still little information on the possible aspect of the parafoil, considering a 6 DOF model was determined to be the best solution to analyze the problem. For all models we tested S-turn and spiral maneuvers and validated our results with previously published results. Unfortunately, it is difficult to find the exact initial conditions on published results, so in some cases we limited ourselves to match the overall trend.
- <u>Modeling and simulation of the dynamics of hang-glider</u>: The hang glider can be an effective solution to deploy a payload with a range around 80km from the entry point and

with wide maneuverability. The folding and deployment of a hang-glider and the rotating load can be an issue. However, we explored its capabilities and compared it to the parafoil.

- Modeling and simulation of the dynamics of wing-suit: We felt that a wingsuit was a trade-off solution between the high hang glider efficiency and an easy deployment. The obstacle lays in the intrinsic instability of the system and its difficult control and in the payload-wing aerodynamics interaction. The wingsuit is usually stable for high angle of attack at high speeds and this stability windows is small and identifiable only using CFD (Computational Fluid Dynamics) analysis. Moreover, the payload with a possible biconical shape and a huge mass makes the modelling difficult. However, the wingsuit is more appropriate for small payloads (like CubeSat) or with systems that should "land vertically" on a wall or similar.
- Aerodynamics modeling: Another complication in this preliminary project phase, with few information from past mission is how should we model the aerodynamics of our systems? If we cannot use a CFD code in which upload the information of Titan atmosphere obtained from Cassini-Huygens mission, can we find an initial aerodynamics estimation tool to acquire data for the simulations? To answer these questions, we compared the results from the lifting-line theory and the panel method on Earth environment and then attempted to extrapolate the aerodynamics on Titan based on the Reynolds number. It is still a rough estimation, but it can help us to evaluate the initial aerodynamics performance on Titan.
- Guidance, Navigation, and Control (GN&C): We began to develop a guidance, navigation and control tool in order to enable trajectory generation with a quick optimization tool. In this thesis we presented a preliminary trajectory design, an estimation method for wind and density, and a proportional control scheme. The work needs still maturation but can be a good starting point. Furthermore, from this preliminary GN&C we are able to evaluate the capabilities of the parafoil on Titan environment in various stressing conditions.

As a next step, future work should focus on:

- An accurate analysis of the aerodynamics on Titan atmosphere, better if using CFD codes. The Reynolds number on Titan is generally higher than on Earth (from Huygens data), that means less drag but probable anticipated stall and flux break on the airfoil that leads to less lift.
- Building a guidance scheme that can adjust itself during the descent to take into account a consistent and unsettling variation in the wind environment or in other parameters that will need a re-planning of the trajectory.
- Optimizing the trajectory to insert the motion planning in the integration loop of the GN&C: in the computer program developed for this thesis the path is planned before the navigation and control loop. If we can optimize the trajectory control to land exactly on target by changing the inputs at each step, we can solve the more complex problem of the trajectory re-planning.
- Defining a more elegant and efficient control, possibly in frequency domain, to shape the six DOF trajectory. The control should take into account the different flight regimes, the actuator dynamics to shape the on-off actuation timing, the flare maneuvers and the asymmetric deflections.
- Develop a full Montecarlo analysis that will consider the entire entry trajectory from the atmospheric entry interface at 170 km to the touchdown performed with a parafoil.

REFERENCES

[1] R. D. Lorentz and e. al, "Formulation of a wind specification for Titan late polar summer exploration.," in *Planeary and Space Science*, Elvesier, 2012, pp. 73-83.

[2] J. Hartwig, A. Colozza, R. Lorenz, S. Oleson, G. Landis, P. Schmitz, M. Paul and J. Walsh, "Exploring the depths of Kraken Mare – Power, thermal analysis, and ballast control for the Saturn Titan submarine," *Cryogenic,* no. 74, pp. 31-46, 2016.

[3] R. Yelle, D. Strobell, E. Lellouch and D. Gaultier, "Engineering Models for Titan's Atmosphere".

[4] J. Lebreton and D. L. Matson, "The Huygens Probe: Science, Payload and Mission Overview," *SPace Science Reviews,* 202.

[5] "airborne-sys.com," [Online]. Available: https://airborne-sys.com/product/firefly-military-cargo-delivery-parachute/. [Accessed 31 July 2018].

[6] M. Spottiswoode and C. M. V., "Modelling the flight dynamics of the hang glider," in *The Aeronautical Journal*, January 2006.

[7] J. W. Bahlman, S. M. Swartz, D. K. Riskin and K. S. Breuer, "Glide performance and aerodynamics of non-equilibrium glides in northern flying non-equilibrium glides in northern flying," *Journal of The Royal Society Interface,* 2013.

[8] O. A. Yakimenko, Precision Aerial Delivery Systems: Modeling, Dynamics and Control, vol. Volume 248 Progress in Astronautics and Aeronautics, AIAA, 2015.

[9] T. Melin, *USER's GUIDE TORNADO 1.0,* Royal Institute of Technology (KTH), 2001.

[10] M. A. Mohammadi and H. Johari, "Computation of Flow over a High Performance Parafoil," in *AIAA Aerodynamic Decelerator Systems Technology Conference and Seminar*, Seattle, 2009.

[11] P. Lissaman and G. Brown, *Apparent mass effects on parafoil dynamics,* AIAA-93-1236, 1998.

[12] W. Gockel, "Case study 1: Computer Based Modeling and Analysis of a parafoil-load vehicle," in *14th AIAA Aerodynamic Decelerator Systems for Technology Conference & Seminar*, San Francisco, June, 1997.

[13] F. Quagliotti, *Notes from the Atmopsheric Flight Mechanics Course,* Torino: Politecnico di Torino, 2015.

[14] C. Toglia and M. Venditelli, "Modeling and motion analysis of autibomous paragliders," Roma, January 2010.

[15] N. Slegers and M. Costello, "Comparison of measured and simulated motion of a controllable parafoil and payload system," in *Atmospheric Flight Mechanics Conference and Exhibit.*, Austin, Texas, 2003.

[16] N. J. Slegers and C. M. Gorman, "Comparison and Analysis of Multi-body Parafoil Models WIth Varying Degrees of Freedom," in *American Institute of Aeronautics and Astronautics*, 2011.

[17] N. Ananthkrishnan and P. Om, "Modeling and Simulation of 9 DOF Parafoil-Payload System Flight Dynamics," in *AIAA Atmospheric Flight Mechanics Conference and Exhibit*, Keystone, Colorado, August 2006.

[18] N. Slegers and M. Costello, "COMPARISON OF MEASURED AND SIMULATED MOTION OF A CONTROLLABLE PARAFOIL AND PAYLOAD SYSTEM," in *AIAA Atmospheric Flight Mechanics Conference and Exhibit*, Austin, Texas, Augsut 2003.

[19] G. De Matteis, "Dynamics of Hang Gliders," *Jornal of Guidance,* vol. 14, no. 16, Novembre 1991.

[20] G. De Matteis, "Dynamics and Control of Hang-Glider," in *American Institute of Aeronautics and Astronautics*, 1989.

[21] Y. Ochi, "Modeling of Fligh Dynamics and Pilot's Handling of a Hang Gliders," in *AIAA Modeling and Simulation Technologies Conference*, Grapevine, Texas, January 2017.

[22] Y. Ochi, "Pilot's CG location and Attitude Control for Lateral Maneuver of A Hang Glider," in *30th Congress of the International Coucil of the Aeronautical Sciences*, Daejeon, Korea, September 2016.

[23] I. M. Kroo, "Aerodynamics, Aeroelasticity, and Stability of Hang Gliders - Experimental Results," NASA Technical Memorandum, April 1981.

[24] X. Li, W. Wang, S. Wu and P. W. L. Zhu, "A Research on Air Posture Adjustment of Flying Squirrel Inspired Gliding Robot," in *IEEE*, Qingdau, 2016.

[25] L. Ermolli, *Flight Maneuvering for Planetary,* Milano: Politecnico di Torino, 2017.

[26] T. Jann, "Advanced Features for Autonomous Parafoil Guidance, Navigation and Control.," in *AIAA Aerodynamic Decelerator Systems Technology Conference and Seminar*, 2005.

[27] A. A. B. Quadrelli Marco B, "Planetary Aeromanuevering for precision landing.," in *Advances in the Astronautical Sciences*, 2005.

[28] M. Nitin and e. al, "Guidance of Parafoil using Line of Sight and Optimal Control," in *Third International Conference on advances in Control and Optimization of Dynamics Systems*, Kampur, 2014.